THE UNIVERSITY
of EDINBURGH

A light Activated Approach for Large Gap Peripheral Nerve Repair

A thesis submitted for the degree of Doctor of Medicine (MD)

University of Edinburgh, Scotland

Neil G Fairbairn

BSc Hon, MBChB

May 2015

Supervision:

Professor Stephen J Wigmore, Hepatobiliary-Pancreatic Surgical Services and Edinburgh Transplant Unit, Royal Infirmary of Edinburgh, Edinburgh, Scotland

Dr Robert Redmond, Wellman Centre for Photomedicine, The Massachusetts General Hospital, Harvard Medical School, Boston, Massachusetts, USA

Dr Jonathan Winograd, Division of Plastic and Reconstructive Surgery, Department of Surgery, The Massachusetts General Hospital, Harvard Medical School, Boston, Massachusetts, USA

Index of contents

Index of sub-headings

Index of figures

Index of Tables

Abbreviations

ACURO	Animal Care and Use Regulatory Office
ADSCs	Adipose Derived Stem Cells
AFDSCs	Amniotic Fluid Derived Stem Cells
ANA	Acellular Nerve Allograft
ANOVA	Analysis of variance
BBI	Brain Body Interface
BDNF	Brian Derived Neurotrophic Factor
bFGF	Basic Fibroblast Growth Factor
BME	Beta Mercaptoethanol
BMI	Brain Machine Interface
BMSCs	Bone Marrow Derived Stem Cells
CD	Cluster of Differentiation
CMAPS	Compound Muscle Action Potentials
CMV	Cytomegalovirus
CNS	Central Nervous System
CNTF	Ciliary Neurotrophic Factor
CI	Confidence interval

CSPG	Chondroitin Sulphate Proteoglycan
DMEM	Dulbecco's Modified Eagle's Medium
DOF	Degrees of Freedom
DPSCs	Dental Pulp Derived Stem Cells
DRG	Dorsal Root Ganglion
ECM	Extracellular Matrix
EDC	1-ethyl-3-(3-dimethylamionopropyl) carbodiimide hydrochloride
EEG	Electroencephalogram
EGF	Epidermal Growth Factor
EMG	Electromyography
ESC	Embryonic Stem Cell
FBS	Fetal Bovine Serum
FDA	US Food and Drug Administration
FES	Functional Electrical Stimulation
fMRI	Functional Magnetic Resonance Imaging
FSK	Forskolin
GDNF	Glial Cell Derived Neurotrophic Factor
GFAP	Glial Fibrillary Acidic Protein
GM-CSF	Granulocyte Macrophage Colony Stimulating Factor

HAM	Human Amniotic Membrane
HFSCs	Hair Follicle Derived Stem Cells
HGF	Hepatocyte growth factor
HGFR	Hepatocyte Growth Factor Receptor
HIV	Human Immunodeficiency Virus
HLA	Human Leucocyte Antigen
HRG	Heregulin beta-1
HTLV	Human T-Cell Lymphotrophic Virus
IACUC	Institutional Animal Care and Use Committee
ICAM	Intracellular Adhesion Molecule
IGF-1	Insulin-like Growth Factor-1
IL	Interleukin
iPSCs	Induced Pluripotential Stem Cells
KGF	Keratinocyte Growth Factor
KGFR	Keratinocyte Growth Factor Receptor
KTP	Potassium Titanyl Phosphate
LIF	Leukaemia Inhibitory Factor
M-CSF	Macrophage Colony Stimulating Factor
MES	2-(N-morpholino) ethanesulfonic acid

MGC	N-Methacrylate Glycol Chitosan
MHC	Major Histocompatibility Complex
mm	Millimeter
mM	Milimolar
MMP	Matrix Metalloproteinase
MPa	Megapascals
MRI	Magnetic Resonance Imaging
MSC	Mesenchymal Stem Cell
N	Newton
$NaBO_4$	Sodium Borate
NGF	Nerve Growth Factor
NHP	Non-human primate
nm	Nanometer
NMJ	Neuromuscular Junction
NSC	Nerve Stem Cell
NT-3	Neurotrophin-3
OCT	Optical Coherence Tomography
OFDI	Optical Frequency Domain Imaging
PBS	Phosphate Buffered Saline

PDGF	Platelet Derived Growth Factor
PEG	Polyethylene Glycol
PGA	Polyglycolic Acid
PHB	Poly-3-hydroxybutyrate
PLCL	Poly-DL-lactide-caprolactone
PSN	Penicillin-Streptomycin-Neomycin
PTB	Photochemical Tissue Bonding
PTFE	Polytetrafluoroethylene
PVA	Polyvinyl Alcohol
NHS	N-Hydroxysuccinimide
RA	All-trans Retinoic acid
RAG	Regeneration-Associated Gene
RB	Rose Bengal
RNA	Ribonucleic Acid
SC	Schwann Cell
SDF-1α	Stromal Cell Derived Factor-1α
SFI	Sciatic Function Index
SKPs	Skin Derived Precursors
SIS	Swine Intestinal Submucosa

TDT	Tucker-Davies Technologies
TGF-β	Transforming Growth Factor- β
Th	T-Helper Cell
TIMP	Tissue Inhibitor of Metalloproteinase
TNF-α	Tumour Necrosis Factor-α
UC-MSCs	Umblical Cord Derived Mesenchymal Stem Cells
USAMRC	United States Army Medical Research and Command
VCS	Vascular Closure Staples
VEGF	Vascular Endothelial Derived Growth Factor
WJMSCs	Wharton's Jelly Derived Mesenchymal Stem Cells
xHAM	Crosslinked Human Amniotic Membrane
xSIS	Crosslinked Swine Intestinal Submucosa
μm	Micrometer

Acknowledgements

Name	Institute
Dr Robert Redmond (PhD)	The Wellman Centre for Photomedicine
Dr Jonanthan Winograd (MD)	The Massachusetts General Hospital
Mr Mark Randolph	The Massachusetts General Hospital
Dr Joanna Ng-Glazier (MD)	The Massachusetts General Hospital
Ms Amanda Meppelink	The Massachusetts General Hospital
LCDR Dr Ian Valerio (MD)	Walter Reed National Military Medical Centre
CDR Dr Mark Fleming (MD)	Walter Reed National Military Medical Centre
Dr Robert Ajemian (PhD)	The Massachusetts Institute of Technology
Dr Neelakantan Sunder (MD)	The Massachusetts General Hospital
Ms Ashley Turza	The Massachusetts Institute of Technology
Dr Vittorio Caggiano (PhD)	The Massachusetts Institute of Technology
Prof Emilio Bizzi (MD PhD)	The Massachusetts Institute of Technology
Mr William Farenelli	The Wellman Centre for Photomedicine
Dr Irene Kochevar (PhD)	The Wellman Centre for Photomedicine
Mr Frank Doyle	The Wellman Centre for Photomedicine
Mrs Margaret Sherwood	The Wellman Centre for Photomedicine

Ms Megan Scanlan	The Wellman Centre for Photomedicine
Dr Jenny Zao (MD)	The Wellman Centre for Photomedicine
Dr Benjamin Vakoc (PhD)	The Wellman Centre for Photomedicine
Dr Isabel Chico-Calero (PhD)	The Wellman Centre for Photomedicine
Mr Erick Devinney	AxoGen Inc
Dr Curt Deister (PhD)	AxoGen Inc.
Mrs Jennifer Faleris	AxoGen Inc.
Mrs Cheryl Harrington	HealthPoint Biotherapeutics
Mr Douglas Hayden	Harvard Catalyst Statistics
Dr Rob Elton	University of Edinburgh

Declaration

I declare that this thesis is the outcome of original work performed in the Plastic Surgery Research Laboratory and Wellman Centre for Photomedicine at The Massachusetts General Hospital and in The McGovern Institute for Brain Research at The Massachusetts Institute of Technology. I was the lead surgical fellow for all small animal surgeries contained within and unless stated otherwise, I have contributed to all aspects of data collection and analysis. This work has been submitted for the degree of medical doctorate (MD) at the University of Edinburgh, Scotland and has not been submitted for any other qualification at any other institution.

Signature:

Name: Neil Fairbairn

Abstract

Introduction:

Conventional suture repair of peripheral nerves following injury is associated with several limitations such as technical difficulty, intra- and extra-neural scar formation, axonal escape and the leakage of neurotrophic factors. These limitations are particularly relevant following nerve grafting when regenerating axons must traverse two coaptation sites. Outcomes following suture repair are notoriously poor, providing large impetus for the development of alternative methods. Photochemical tissue bonding (PTB) uses visible light to create sutureless, non-thermal bonds between two closely apposed tissue surfaces stained with a photoactive dye. When used with a human amnion nerve wrap for end-to end nerve repair, this technique results in superior functional and histological outcomes in comparison to conventional epineurial suture. When initially applied to large gap injury and nerve grafting, outcomes were unsuccessful due to proteolytic degradation of amnion and photochemical bonds during extended periods of recovery. Chemical crosslinking of nerve wraps prior to PTB may improve wrap durability and efficacy of technique. This thesis provides a comprehensive three-phase assessment of the efficacy of this novel approach when applied to the repair of large gap injuries with nerve grafts. Phase 1 assesses the *ex vivo* biomechanical properties of nerve wraps and light activated bonds in addition to the *in vivo* performance of photochemically sealed crosslinked nerve wraps against several other clinically relevant fixation methods in a rodent sciatic nerve isograft model. Following major multi-limb injury and amputation, demand for autogenous nerve graft may exceed that which can be supplied by the patient. Acellular nerve allograft (ANA) is an alternative option in these circumstances although outcomes are typically inferior to autograft. Phase 2 assesses the performance of the optimum repair strategy from phase 1 against conventional epineurial suture when applied to

ANA. Most studies investigating the efficacy of novel repair techniques tend to perform repairs immediately following injury, a situation that rarely occurs clinically. Delays of weeks or months are not uncommon and have been shown to have a detrimental effect on regeneration and outcome. Phase 3 assesses the efficacy of PTB when applied to delayed nerve grafting.

Additional work investigating a novel imaging technique for visualizing nerve revascularisation following injury and repair has been included. Optical frequency domain imaging (OFDI) uses low power infrared light to provide real time in vivo imaging of tissue microvasculature and flow characteristics. Originally applied to the study of tumour biology, this technique may prove useful for outcome assessment in preclinical research and eventually for the assessment of nerve viability in the clinical setting.

Experiments investigating the early development of a brain body interface system (BBI) for upper limb reanimation following spinal cord injury (SCI) have also been included. The ultimate aim of this project is to restore autonomous motor control in a non-human primate (NHP) using cortically driven stimulation of peripheral nerves via implantable nerve cuffs. The experiments reported in this thesis detail the development of a selective, reversible paralysis model of elbow flexion in a NHP and demonstrate selective fascicular stimulation using acute and chronically implanted nerve cuffs in rodent and murine models.

Methods:

Phase 1: Three candidate nerve wraps (human amnion (HAM), crosslinked human amnion (xHAM), crosslinked swine intestinal sub-mucosa (xSIS)) and 3 fixation methods (suture, fibrin glue, PTB) were investigated. Crosslinking was performed using (1-ethyl-3-(3-

dimethylaminopropyl) carbodiimide (EDC)/N-hydroxysuccinimide (NHS). Biomechanical tests were performed using a tensiometer. *Ex vivo* wrap durability was assessed using a type-2 collagenase degradation assay. Under isoflurane anaesthesia, 110 inbred male Lewis rats had 15mm left sciatic nerve defects created and repaired with reversed isografts. 9 groups (n=10) had isografts secured by one of the aforementioned wrap/fixation combinations. PTB repairs had nerve wraps and nerve ends stained with photoactive dye (Rose Bengal) and, once nerve ends were apposed and wrapped circumferentially, the interface was illuminated with a 532nm laser. Fibrin repairs had nerve ends apposed, wrapped circumferentially and secured with Tisseel fibrin glue. Suture repairs had nerve ends apposed, wrapped circumferentially and then secured with two 10-0 nylon sutures at each coaptation site (one either side of each repair). Positive and negative control groups (n=10) were repaired with graft+suture (10-0 nylon) and no repair respectively. **Phase 2:** 20 sciatic nerves were harvested from Sprague Dawley rats and sent to AxoGen Inc. for decellularisation. An additional 20 male inbred Lewis rats were randomized into 2 groups (n=10). All rats had 15mm left sciatic nerve defects created and repaired with processed ANA. 1 group had nerves secured using conventional epineurial suture. The remaining group had ANA secured using photochemically sealed amnion wraps. **Phase 3:** 40 inbred male Lewis rats were randomized into 4 groups (n=10). All 40 rats had 15mm left sciatic nerve gaps created and reconstructed with reversed isografts harvested from donor Sprague Dawley rats. In groups 1 and 2, nerve gaps were repaired immediately with either conventional epineurial suture or photochemically sealed amnion wraps, respectively. In groups 3 and 4, repair took place 30-days following injury using either conventional epineurial suture or photochemically sealed amnion wraps, respectively. All outcomes were assessed using walking track analysis and calculation of sciatic function index (SFI). Walking track analysis and SFI was performed pre-operatively, after the 30-day delay (phase 3) and at 30-day intervals following surgery.

Following sacrifice after 5-months, left (experimental) and right (control) gastrocnemius muscles were excised and weighed for calculation of muscle mass retention. Nerves were excised for histomorphometric analysis including axon count, fiber diameter, axon diameter, myelin thickness and G-ratio. For all in vivo experiments, statistical analysis was performed using ANOVA, repeated measures ANOVA and the post hoc Bonferroni test.

Optical Frequency Domain Imaging (OFDI) pilot study: eight rodents were randomized into 4 groups (n=2): (1) crush injury, (2) transection and end-to-end repair, (3) transection and repair of 10mm nerve gap using contralateral autograft, (4) transection and repair of 10mm nerve gap using ANA. Under ketamine/xylazine anaesthesia, all rodents had sciatic nerves exposed through hind limb dorsolateral incisions. Imaging was performed immediately pre-injury, immediately post-injury and on post-operative days 1, 3, 5 and 7. Rodents were secured firmly to polystyrene platforms in order to reduce movement artifact during imaging

Brain-Body Interface (BBI) experiments: In the upper limb of a Rhesus macaque non-human primate, the median nerve branch to brachialis and radial nerve branch to brachioradialis were transected, leaving elbow flexion entirely reliant on the musculocutaneous nerve. The musculocutaneous nerve was transposed into a subcutaneous position. Ultrasound guided nerve block resulted in a highly selective, reversible paralysis of elbow flexion.

Under ketamine/xylazine anaesthesia, Sprague Dawley rats (n=5) and C57 Black 6 mice (n=5) had sciatic nerves exposed through dorsolateral, muscle splitting incisions. 8-channel stimulating cuff electrodes were wrapped around sciatic nerves and connected to a Tucker-

Davies stimulation/recording system. Electromyography (EMG) needle electrodes were inserted into the tibialis anterior (TA) and gastrocnemius (G) muscles to record muscle activity. Single pulses and pulse trains were delivered to each animal whilst pulse parameters were systematically varied. In one survival rat, a stimulating nerve cuff and EMG recording electrodes were implanted chronically to assess equipment biocompatibility and recording stability.

Results:

Phase 1: Optimal tensile strength, photochemical bond strength and resistance to collagenase degradation were achieved using 4mM EDC/1mM NHS. Following sacrifice, crosslinked nerve wraps were still present. Un-crosslinked material was completely degraded. xHAM+PTB repairs recovered greatest mean SFI although this was not statistically significant compared with standard repair (-67.9+/-1.6 vs -71.7+/-1.6 (mean+/-SEM)). xHAM+PTB repairs also recovered greatest muscle mass retention and this was significant in comparison to standard repair (67.3% +/- 1.4 vs 60.0% +/- 1.6; p=0.02). No significant difference in axon diameter existed between treatment groups. Fiber and axon diameter and myelin thickness were all significantly greater in the xHAM+PTB group in comparison to standard repair (6.87μm+/-0.04 vs. 5.47μm+/-0.03, p<0.0001; 4.51μm+/-0.04 vs. 3.50μm+/-0.03, p<0.0001; 2.35μm+/-0.01 vs. 1.96μm+/-0.01, p<0.0001). **Phase 2:** Following sacrifice, all ANAs were in continuity and, on gross observation, showed evidence of regeneration. ANA repaired photochemically had less extraneural scar tissue formation in comparison to standard epineurial suture. SFI did not differ significantly between ANA+suture and ANA+PTB groups after 5-months follow up (-80.3+/-1.3 vs. -78.3+/-1.6 respectively; p=0.3). ANA+suture and ANA+PTB recovered significantly less SFI than corresponding isograft+suture and isograft+PTB. Gastrocnemius muscle mass retention did not differ

significantly between ANA+suture and ANA+PTB groups (53.3%+/-1.8 vs. 55.2%+/-1.6 respectively; p=0.5). ANA+suture and ANA+PTB recovered significantly less muscle mass than isograft+suture and isograft+PTB, respectively. Muscle mass retention was statistically equivalent between ANA+PTB and isograft+suture (55.2+/-1.8% vs. 60+/-1.6%; p=0.22). With the exception of G-ratio, no significant differences existed between ANA+suture and ANA+PTB for any remaining histomorphometric parameter. ANA+PTB was statistically equivalent to isograft+suture for all histomorphometric parameters. **Phase 3:** After 5-months, in both immediate and delayed repairs, PTB resulted in greater mean SFI values but these results were not statistically significant (-72.3+/-1.5 vs. -68.5+/-1.5; p=0.4 and -80.1+/-1.4 vs. -77.3+/-1.5; p=1). Both suture and PTB fixation methods resulted in significantly greater recovery of SFI when performed immediately rather than after a 30-day delay after injury (-72.3+/-1.5 vs. -80.1+/-1.4; p=0.003 and -68.5+/-1.5 vs. -77.3+/-1.5; p=0.002). Significantly greater muscle mass retention occurred following PTB fixation in both immediate and delayed repairs (64.9%+/-1.8 vs. 59.0%+/-1.1; p=0.03 and 60.2%+/-1.4 vs. 54.1%+/-1.7; p=0.04). No significant difference existed between immediate suture and delayed suture, or immediate PTB and delayed PTB groups. Muscle mass retention was not significantly different between immediate suture and delayed PTB (59.0+/-1.1% vs. 60.2+/-1.4%; p=1). No significant differences in axon count or density existed between groups. Fiber diameter, axon diameter, myelin thickness and G-ratio were not significantly different between immediate suture and delayed PTB. With the exception of G-ratio, all other histomorphometric parameter comparisons were significantly different between treatment groups, with immediate PTB achieving greatest recovery and delayed suture being poorest.

OFDI: OFDI successfully provided real time images of nerve microvasculature. Vessels of the mesoneurial and epineurial longitudinal plexus were readily identifiable in uninjured

nerve. Marked tortuosity of these vessels was apparent. Different light scattering properties of muscle and nerve permitted easy differentiation between tissues. Injury sites were easily visible as areas of relative hypovascularity. Following crush injury, the longitudinal intrinsic plexus remained intact. Following end-to-end neurorrhaphy, although initially hypovascular, by post-operative day 7, a florid angiogenic response had occurred at the repair site. Following repair of 10mm autografts, the re-establishment of longitudinal vessels was apparent by day 4. Following repair of 10mm ANA, grafts remained relatively avascular. A predominance of inosculated longitudinal vessels existed with a relatively minor centripetal contribution from the surrounding muscle bed.

BBI: Highly selective, reversible paralysis of non-human primate (NHP) elbow flexion was achieved. Application of nerve cuff electrodes around small animal sciatic nerves was technically simple and permitted muscle stimulation in all animals. Needle EMG electrodes successfully recorded muscle activity in all animals. In 9 animals, selective activation of tibial and common peroneal fascicles was possible, allowing the plotting of muscle recruitment curves as a function of stimulation amplitude. Following 6 months of chronic implantation, the nerve cuff and EMG electrodes were well tolerated and stimulation and recording was still possible.

Conclusions

PTB: Chemical crosslinking of biological nerve wraps improves tensile strength and *in vivo* resistance to biodegradation, whilst preserving the formation of light-activated bonds. Light activated sealing of crosslinked amnion around nerve isograft coaptation sites results in

significant improvements in muscle mass retention and nerve histomorphometry in comparison to conventional suture repair. SIS wraps were unsuitable for bonding around small diameter nerves although when applied to larger caliber nerves, may still be useful. Outcomes following ANA were inferior to those achieved following isograft reconstruction in phase 1. No significant difference was detected between photochemically sealed ANA and sutured ANA although the increase in mean values for muscle mass retention and histomorphometry were comparable to epineurial suture, the current standard of care. Immediate repairs performed significantly better than delayed repairs and light-activated repairs performed significantly better than sutured repairs. Delayed PTB repairs were statistically comparable to immediate suture. Light-activated sealing leads to superior outcomes in comparison to suture when applied to nerve isografts and may improve outcomes following the use of ANA and when repairs occur following a surgical delay.

OFDI provides a real time, *in vivo* imaging modality for the assessment of nerve revascularisation following injury and repair. This has potential applications for pre-clinical outcome assessment in peripheral nerve research and also as a means of assessing peripheral nerve viability in the clinical setting.

BBI: We have shown that selective fascicular stimulation of sub-1mm peripheral nerves can be achieved using implantable cuff electrodes. In combination with a highly selective and reversible paralysis of elbow extension in a non-human primate model, these cuffs will be used to deliver cortically recorded signals directly into upper limb nerves. Through operant conditioning and feedback, this BBI should enable the NHP to regain movement during paralysis.

Lay Summary

Introduction and methods:

The current standard of care for peripheral nerve repair involves re-joining nerve ends with suture. When gaps exist between nerve ends, other non-essential nerves in the injured patient can be used to bridge the gap. Suture repair of these injuries is limited by technical difficulty, scarring and the leakage of beneficial factors from the repair site. These limitations are amplified when gaps require nerve grafts because regenerating nerve fibers must cross two repair sites. Outcomes following suture repairs are notoriously poor, providing large impetus for the development of sutureless methods. Photochemical tissue bonding (PTB) uses visible light to create sutureless bonds between two closely apposed tissue surfaces that have been stained with a light activated dye. When dye-stained nerve ends are apposed and wrapped with dye stained nerve wraps, sutureless repair is possible and has been shown to result in superior outcomes in comparison to nerves that have been sutured. Previous application of this technique to large gap injuries requiring grafts was unsuccessful due to premature degradation of nerve wraps and bonds before nerve fibers reached the site of injury. One proposed solution to this problem is to treat nerve wraps with chemicals in order to make them last longer in the tissues and therefore prolong the strength of the bonds. This thesis tests how effective this approach is when applied to large nerve gap injury. Phase 1 tests how chemical concentration affects wrap strength and durability and whether the chemicals interfere with nerve bonding. In a rat model, the performance of light activated nerve bonding is compared to other nerve repair methods that are commonly used in the clinical setting, such as glue and suture. Following major injury, demand for nerve grafts may exceed that which is available from the patient. In these cases, acellular nerve allografts (ANA) can be used. These nerves are taken from cadaveric donors and are specially treated in order to

remove all cells whilst preserving internal structure. Without cells, ANA can be safely transplanted into different patients without fear of rejection. Unfortunately, ANA do not perform as well as nerves taken from the same patient. Phase 2 assesses the performance of light activated nerve bonding in ANA against conventionally sutured ANA in a rat model. Most studies investigating new repair techniques tend to perform nerve repair immediately following injury, a situation that rarely occurs clinically. Delays of weeks or months are not uncommon and have been shown to have a detrimental effect on outcome. Phase 3 assesses the efficacy of light activated nerve bonding when applied to delayed nerve grafting in a rodent model.

Additional work has been included that investigates a novel imaging technique for visualizing the re-establishment of nerve blood supply in rat models of nerve crush injury, transection and suture, regular nerve grafting and following the use of acellular nerve graft. Optical frequency domain imaging (OFDI) uses infrared light to provide real time images of tissue blood vessels and blood flow. Originally applied to the study of tumours, this technique may prove useful for assessing the success of nerve regeneration in preclinical animal models and may also prove useful in the clinical setting by permitting intraoperative assessment of nerve viability following injury.

Experiments investigating the early development of a brain body interface system (BBI) have also been included. This technology aims to help patients move paralysed limbs following spinal cord injury. Signals from the brain that control limb movement can be recorded and used to directly stimulate nerves and muscles, bypassing the injured spinal cord. The ultimate aim of this project is to demonstrate this in a non-human primate (NHP) model. This thesis reports preliminary experiments including the development of a technique permitting the

reversible paralysis of NHP elbow flexion. The ability of implantable stimulating nerve cuffs to activate very specific areas of rat peripheral nerve and therefore provide selective limb muscle activation is also demonstrated.

Results and Conclusions

Light activated nerve bonding: Chemical treatment of biological nerve wraps improves strength and durability, whilst preserving light activated bonding. Light activated bonding of nerve grafts results in superior outcomes in comparison to sutured grafts. When applied to ANA, no difference between sutured and bonded nerves was identified although outcomes in the bonded ANA group were equivalent to sutured nerve grafts in phase 1, the current standard of care. When performed after a surgical delay, light activated nerve bonding resulted in outcomes that were comparable to repairs that were performed immediately with suture. Overall, light-activated bonding is superior to gold standard suture when applied to conventional nerve grafts and may improve outcomes following the use of ANA and when repairs occur following a surgical delay.

OFDI: This novel imaging modality provides real-time assessment of the re-establishment of nerve blood supply following injury and repair. This has potential applications for pre-clinical outcome assessment in peripheral nerve research and also as a means of assessing peripheral nerve viability in the clinical setting.

BBI: Surgical re-organisation of the NHP upper limb nerves allowed the development of a highly selective, reversible and repeatable paralysis of elbow flexion. Stimulating nerve cuff electrodes can be easily implanted and used to activate very specific areas of a nerve, permitting the selective activation of limb muscles. These techniques will be combined in

order to demonstrate that autonomous control of paralysed limbs using only thoughts is possible.

Section 1: Introduction

1.1 The anatomy and physiology of peripheral nerves

Peripheral nerves are extensions of the central nervous system. They provide motor and sympathetic output to the trunk and extremities and also provide afferent channels facilitating the perception of pain, temperature, pressure and joint position sense. Nerves contain huge collections of neurons, one of the fundamental cells of the nervous system. Such neurons are composed of a centrally located cell body, a peripherally extending axon, and its connection with a peripheral target. For example, cell bodies of motor neurons reside in the ventral horn of the spinal cord whereas sensory cell bodies are located in the dorsal root ganglion. Both project long axons into peripheral nerves that branch extensively until reaching their distal targets. The cell body contains structures consistent with other cells in the body such as a nucleus, mitochondria and endoplasmic reticulum. In common with other cells, RNA is transcribed in the nucleus of the neuron and is translated into protein from messenger RNA in the cytoplasm. In the neuron, the majority of cytoplasm is distributed within the axon where it is referred to as the axoplasm. Whilst some protein products are destined for local use within the cell body, others are required by the axon, often at relatively large distances from their site of synthesis.

Axoplasm is continuously produced and contains multiple cytoskeletal elements such as microtubules that run the entire length of the axon[(1)]. These cytoskeletal elements, in combination with motor proteins such as kinesin and dynein create axoplasmic transport, a bidirectional, fast or slow, transport and signaling mechanism allowing anterograde and retrograde transportation of cellular proteins[(2)]. Anterograde flow transports proteins

manufactured in the cell body towards the periphery and is vital for the integrity of the distal axon. Retrograde transport allows movement of elements back towards the cell body from the periphery. Following injury, interruption of this transport heralds the onset of orthograde Wallerian degeneration. Retrograde transport of cellular debris from the site of injury is destined for lysosomal degradation and the influx of this material at the cell body is believed to form part of a feedback mechanism that upregulates cell body metabolism in preparation for regeneration[2].

Although abundant, axons are only part of the volume of the nerve. The majority of the substance of the nerve is composed of connective tissue and supporting cells that provide the nerve with a high level of structural organization[3]. This connective tissue is presented in layers and, from external to internal, includes (1) mesoneurium, (2) epineurium, (3) perineurium and (4) endoneurium. The mesoneurium is the outermost layer and is composed of loose areolar connective tissue. The mesoneurium carries with it a vascular supply and is believed to help tether nerves to surrounding structures such as muscle and fascia. The epineurium is a tough areolar layer composed of longitudinally orientated collagen and elastin fibers (figure 1)[4]. The epineurium contains a dense network of vessels that form anastomoses with endoneurial vessles via connections that run obliquely through the perineurium. The epineurium extends internally to ensheath fascicles where it is known as the interfascicular epineurium.

The perineurium surrounds the fascicles of the nerve and is composed of oblique, longitudinal and circular collagen fibers, interspersed with perineurial cells (figure 1)[5]. Fascicles vary in size and number depending on the nerve. The existence of tight junctions between perineurial cells creates a blood nerve barrier, preventing the intercellular transport of macromolecules. When injured, the breakdown of this barrier has a deleterious effect on axonal function[6]. Demyelination and a loss of axon diameter can occur, all contributing to a loss of signal conduction. The perineurium also provides tensile strength to the nerve and is responsible for resisting the effects of longitudinal traction. In addition to providing strength, the perineurium also appears to maintain positive intrafascicular pressure. Disruption of this layer results in decompression and herniation of axons out-with the confines of the fascicle. The perineurial layer is the site of anastomotic connections between the epneurial vascular plexus and the endoneurium.

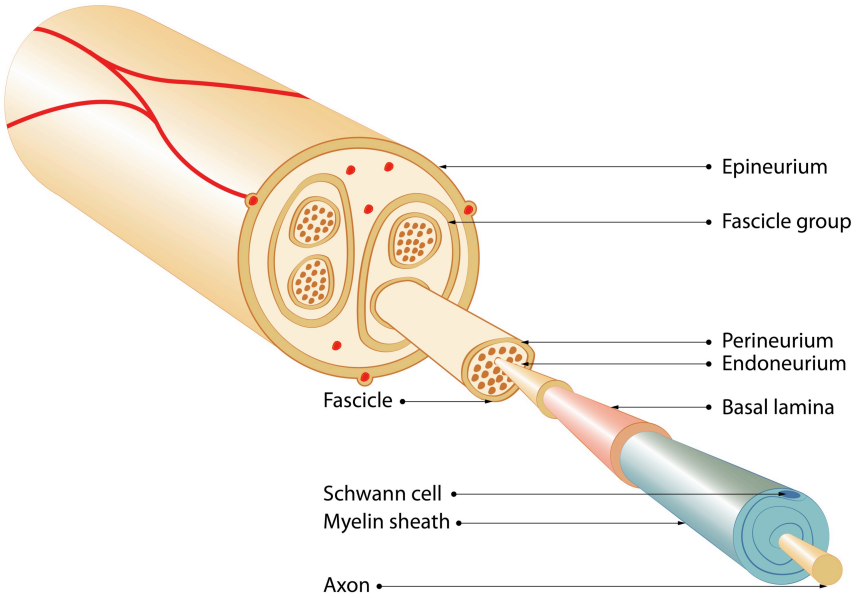

Figure 1. The anatomy of a peripheral nerve. The outermost connective tissue layer is the epineurium. This surrounds and contains fascicular groups. The tissue in between fascicular groups is referred to as the interfascicular epineurium. Individual fascicles contain bundles of axons and are surrounded by the perineurium.

Each axon is surrounded by the endoneurium that, in turn, surrounds basal lamina. All axons are accompanied by Schwann cells that may or may not produce myelin sheaths.

The endoneurium is a matrix of predominantly longitudinally orientated collagen fibers that surround both myelinated and unmyelinated axons (figure 1)[4]. Microvessels permeate the endoneurium and due to tight junctions between the endothelial cells of these vessels, they offer a further blood nerve barrier in addition to that of the perineurium. The permeability of these vessels increases following nerve injury, permitting the influx of inflammatory mediators into the endoneurial environment. The endoneurium also offers protection against longitudinal traction and, similar to the perineurium, also presents a relatively unyielding layer that results in positive pressures surrounding the axons.

The fundamental role of the neuron is to generate and transmit electrical impulses known as action potentials. Action potentials are spikes of electrical activity that arise in excitable cells and play an integral role in cellular communication and the activation of many intracellular processes. As with any other cell, neurons possess a plasma membrane. In the axon, this is referred to as the axolemma. Within the plasma membrane exist many different proteins that serve many different roles. Some of these proteins are channels or carriers that facilitate the effects of diffusion or active transport. The flux of nutritional and waste products across the membrane is tightly regulated and maintains cell integrity in addition to allowing interaction with the surrounding environment. These channels are also responsible for the selective permeability of the membrane to ions. The unequal distribution of sodium (Na^+) and potassium (K^+) ions across the membrane sets up the transmembrane potential, the ionic concentration gradient and electrical charge difference across the cell. Resting membrane

potential varies between excitable cells and tissues but for the neurons, is approximately -75mV. When the transmembrane potential becomes more negative, this is referred to as hyperpolarization. The generation of action potentials is the result of rapid depolarization, brought about by abrupt changes to the transmembrane conductance for Na^+ and K^+ ions through voltage gated ion channels. Following depolarization and action potential firing, the membrane is returned to its resting state through a period of repolarization.

Axons are enveloped with Schwann cells (SCs). In turn, axons and their SCs are surrounded by basal lamina. In large myelinated fibers, SCs produce a lipoprotein rich electrical insulator called myelin that wraps circumferentially around segments of the axon, a feature that distinguishes the SC from other cells in the area. In smaller unmyelinated fibers, axons are surrounded by SCs and basal lamina, but lack myelin typical of larger myelinated fibers. In between adjacent SCs of myelinated fibers, myelin thickness is reduced. These areas of relative myelin thinning, known as nodes of Ranvier, contain an increased density of voltage-gated ion channels in comparison to myelinated, internodal regions that are relatively lacking in ion channels, a finding that may be influenced by the Schwann cell[(7)]. As a result, ion conductance and excitability are greater in these regions.

Like any other electrical signal, action potentials travel down the path of least resistance. In the axon, this involves either continued propagation along the axon or leak through the membrane into the extracellular space. In unmyelinated axons, depolarization of contiguous sections of the membrane results in the activation of localised voltage-gated ion channels resulting in a continuous and complete depolarization of the entire axon membrane as the action potential is conducted away from the site of activation[(8)]. This process is relatively

slow, due to time taken discharging and charging the membrane capacitance and, as a result, conduction velocities are also slow (0.1-2 ms^{-1}). When sodium ions enter a node of Ranvier in a myelinated axon, the reduced capacitance of the myelin sheath ensures that depolarisation spreads rapidly to the next node. This process is referred to as saltatory conduction. It dramatically increases the impulse conduction velocity up to 1000 fold (>100 ms^{-1})[8].

In motor neurons, the arrival of action potentials at the neuromuscular junction results in depolarization of the presynaptic terminal and, through the exocytosis of synaptic vesicles, results in a flood of neurotransmitter release into the synaptic cleft[9, 10]. The neurotransmitter released from the NMJ is acetylcholine (ACh) and, after binding to postsynaptic receptors on the sarcolemma of muscle fibres, results in further depolarisation and activation of muscle contraction. A single motor neuron may synapse with one or many muscle fibres, the combination of which is termed the motor unit[9, 10].

Peripheral nerves are richly vascularized by two integrated but functionally distinct systems. The extrinsic system consists of segmental vessels originating from nearby large arteries and veins. These vessels are tortuous in appearance conveying a large degree of redundancy that allows extensive, unrestricted mobilization during movement. As these vessels approach the nerve, they arborize proximally and distally and run in the distinct, collateral, outermost mesoneurial layer. These nutrient vessels form anastomotic connections with the main longitudinal plexus of vessels situated at the level of the external epineurium and extrafascicular epineurium and marks the transition from extrinsic to intrinsic vascular systems[11]. As previously discussed, epineurial vessels send branches obliquely through the

perineurium and intrafascicularly. These in turn send branches that infiltrate the substance of the endoneurim to supply axons[12]. Although less relevant for uninjured nerve, following injury and repair, the nerve also receives an important vascular supply from the surrounding soft tissues, particularly muscle.

1.2 Nerve injury

1.2.1 The causes of nerve injury

Traumatic nerve injury can occur by many different ways. Injury may be the result of penetrating or non-penetrating trauma, resulting in open or closed wounds respectively. Although open wounds are perceived as being more serious and destructive, in the context of nerve injury, they are often less problematic than closed injuries. Open injuries, with evidence of neurological deficit, warrant immediate intervention, involving decontamination, exploration and subsequent repair of nerves and other tissues. Diagnosis of nerve injury is rapid and plans for definitive reconstruction can be set in motion at an early stage. The freshly and sharply transected nerve following penetrating injury represents the ideal injury for repair and can result in a more predictable and successful functional outcome.

Contrary to expectation however, the majority of penetrating injuries do not result in nerve transection. Instead, the nerve suffers from crushing or traction injury, both of which can result in varying degrees of intraneural damage. In contrast to open wound treatment, the closed, non-penetrating injury is usually managed expectantly, with the patient undergoing regular outpatient follow-up visits to assess and monitor signs of recovery. If after 3-months there are no signs of recovery, then surgical intervention is indicated. Partial transection

injury or a sufficiently severe crush or traction injury will result in intraneural scar tissue formation, a direct obstacle to axonal regeneration and recovery. The forces that a nerve endures during injury are not uniform and as a result, axonal injury tends to be heterogenous and dynamic. Classifying these injuries is useful for standardizing diagnosis, formulating management plans and assessing prognosis.

1.2.2 The classification of nerve injury

Several classification systems of nerve injuries have been proposed. According to all of these systems, nerve injuries fall into one of three general categories: neuropraxia, axonometsis and neurotomesis. This concept was introduced by Seddon[13], developed by Sunderland[14] and has most recently been contributed to by Mackinnon[15]. These descriptive terms represent injuries of increasing severity.

Neuropraxia represents Sunderland's first-degree injury and describes a conduction block across a zone of injury. Although demyelination can occur, axons typically remain intact within their basal lamina tubes and Wallerian degeneration does not occur. Axons find themselves in a state of shock and are temporarily unable to transmit impulses down to distal targets. Conduction block exists exclusively at the site of injury with preserved transmission proximal and distal to the lesion. Larger motor fibers tend to be preferentially affected, in addition to those fibers serving touch and position sense. Smaller fibers including those responsible for the perception of pain can be preserved, explaining why, for some patients, these injuries are painful[16]. Loss of function usually resolves within days although can last for many weeks. Full recovery is expected within 12 weeks. Neuropraxia often arises as a

result of compressive or stretching forces applied to the nerve. A common example is the "Saturday night" palsy which describes the temporary loss of radial nerve function, secondary to prolonged compression of the radial nerve between the arm of a chair and the humerus, typically after a patient falls asleep intoxicated.

Axonotmesis represents Sunderland's second-degree injury and usually occurs as a result of more severe crushing or stretching forces[14]. This injury involves disruption in the continuity of the axon, resulting in Wallerian degeneration and demyelination. EMG recordings show fibrillations and denervation potentials in distal muscle targets. In contrast to neuropraxia, stimulation of the nerve several days after the injury is unable to elicit a muscle contraction. Wallerian degeneration occurs in the distal fiber and also, for a limited extent, in the proximal fiber. Recovery is determined by the success of regeneration and reinnervation. Regeneration occurs slowly and only after an initial period of delay as axons cross the injury site. Once they have negotiated the site of injury, regeneration proceeds distally at a variable rate. Regeneration rate tends to be more rapid, up to 3mm/day in a human, for injuries that are situated more proximally in relation to the cell body. When the level of injury is situated more distal, rates of regeneration of 0.5m/day are more typical[17]. Additional delays also occur when axons reach their targets due to the physical re-establishment of distal connections. As with neuropraxia, the connective tissue layers, including basal lamina tubes, and fascicular architecture are preserved. As a result, axons, guided by SC Bands of Bungner, are able to mostly regenerate down the correct distal pathways. Due to the preservation of connective tissue layers, there is a relative absence of the typical proliferative, fibroplastic response and therefore a lack of disorganized, intervening scar tissue. Consequently, despite the loss of some axons, reinnervation of distal targets by those that survive is accurate,

leading to a relatively high level of functional recovery in comparison to neurotmesis, often obviating the requirement for surgical intervention.

Neurotmesis is the most severe form of injury and encompasses third, fourth and fifth degree injuries in the Sunderland classification[14]. These injuries involve interruption of the axon and various levels of connective tissue elements of the nerve. Neurometsis does not simply refer to transection of the nerve and more often than not, occurs without loss of continuity. Third degree injury involves disruption of the endoneurial layer and to a lesser extent, the perineurium. Part of the external fascicular anatomy is preserved and this remains a predominantly axonotmetic injury with some neurotmetic features. Fourth degree injury involves disruption of the axon, endoneurial and perineurial layers, leading to complete loss of fascicular architecture. The nerve remains in continuity at the epineurial level. A fifth degree injury represents total transection of the nerve. The sixth degree injury, as added by Mackinnon and Dellon, recognizes that injuries often do not fall conveniently into the above classifications and, across the cross section of the nerve, can include a mixture of axonotmetic and neurotmetic injury[15].

The loss of nerve action potentials distal to the site of injury following neurotmesis, in addition to the muscle denervation changes detected by EMG, are consistent with those observed following simple axonotmesis. In contrast to axonotmesis however, the damaged endoneurial and perineurial layers result in a proliferative, fibroplastic response, leading to the formation of disorganized, intervening scar tissue. This, in addition to the loss of fascicular architecture can lead to axons becoming lost in the haphazard injury environment. In fourth degree injuries this may result in the formation of a neuroma in continuity. In fifth

degree, complete transections, failure of surgical intervention results in a proximal end-bulb neuroma. In third and fourth degree injuries, action potentials are unable to conduct through and distal to the injury site. Even if axons are able to negotiate the injury site and reach the distal stump, they are highly unlikely to reinnervate the correct basal lamina tubes. In mixed nerves, this may result in considerable sensory-motor mismatch. In addition, the intervening scar and prolonged denervation of the distal stump can have deleterious effects on axon diameter and myelination, further compromising the likelihood of successful reinnervation and recovery, regardless of whether the regenerating axon reaches their intended peripheral targets. Without surgically re-establishing accurate orientation of completely divided nerve ends, or resecting disorganized intervening scar and neuroma in continuity, successful regeneration and meaningful recovery does not normally occur.

1.2.3 The neurobiology of nerve injury and regeneration

Following nerve transection injury, a complex sequence of neurobiological events occurs in the cell body and in the proximal and distal nerve fiber. The interruption of axonal integrity leads to a rapid influx of ions at the site of injury and an electrophysiological response that propagates back towards the cell body signaling that a lesion has occurred[18]. The retrograde transportation of local factors at the injury site such as leukocyte inhibitory factor (LIF), and the interruption of retrograde transport of neurotrophic factors such as nerve growth factor (NGF) results in chromatolysis[19, 20]. Nissl bodies within the cell body undergo dissolution and the nucleus migrates to the periphery of the cell. Nissl bodies are composed of rough endoplasmic reticulum. The dissolution of this material is a consequence of a reduction in particle size towards the sub-microscopic scale rather than a loss of material. Although many survive, for some cell bodies this process heralds the onset of programmed cell death,

incurring an immediate and permanent loss of regenerative potential for the nerve. The proportion that is lost is believed to be greater in sensory neurons[20]. Surviving cell bodies increase in size, associated with increased levels of RNA, and undergo major cytoskeletal restructuring. Upregulated expression of multiple regeneration-associated genes (RAGs) and protein synthesis prepares the neuron for the increased metabolic demands of regeneration and represents a temporary shift in function from impulse transmission to growth promotion[21-23]. Interestingly, the changes occurring in the cell body are more pronounced with more proximal nerve injuries, implying that cell bodies can in some way detect the extent of regenerative support required for any given level of injury.

The process of degeneration is rapid in most vertebrates, including rats. Within 12-15 hours, NMJs in axotomised rat muscle have begun to degenerate[24]. Within 36 hours, the process of Wallerian degeneration ensues[25, 26]. The activation of calcium dependent proteases results in proteolytic disintegration of axolemma and myelin sheaths, a process that continues to propagate bi-directionally over the following 72 hours[26, 27]. Proximally, this process is usually limited to the first node of Ranvier although can vary depending on the severity of trauma[20]. Denervated SCs in the distal stump undergo a temporary phenotypic transition, upregulating RAGs for growth promotion and down-regulating those genes associated with myelination[7]. Over several days, transformed SCs and circulating myelomonocytic cells that have been recruited to the site of injury, phagocytose axon debris[28]. The persistence of this regeneration-inhibiting material in the zone of injury, and its subsequent clearance, delays the onset of regeneration. Although the axon and its myelin sheath degenerate, basal lamina tubes remain. Within a few days of injury, SCs proliferate, de-differentiate and align themselves within basal lamina tubes where they are referred to as bands of Büngner. These scaffolding

columns form under the influence of neurotrophic factors and guide regenerating axons into distal basal lamina tubes[19, 23, 28, 29].

Regeneration begins at the most distal, intact node of Ranvier and from each proximal axon stump, arise numerous sprouts[20]. Each sprout is enlarged at its tip and gives rise to finger-like projections known as filopodia[30]. The regions in between projecting filopodia are called lamellipodia. Collectively these structures comprise the growth cone[30]. The proteins necessary for growth cone formation and function such as actin, tubulin and growth associated protein-43 (GAP43) are manufactured in the cell body and must be transported to the site of regeneration[31, 32]. The membrane surrounding filopodia contain many receptors and cell adhesion molecules that enable the advancing growth cone to respond to its immediate environment, rapidly changing direction and branching pattern in response to various stimuli[30]. It is through this signaling that axons are attracted towards the distal stump and into basal lamina tubes. For this to be successful, divided nerve ends must be brought back into close apposition. Failure to do so will result in unsuccessful reinnervation of basal lamina tubes, SCs and distal targets. The lack of reinnervation not only has a profoundly detrimental impact on recovery but may also result in troublesome neuroma formation at the proximal stump.

Neurotrophic factors play a key role in axonal regeneration. Several factors have been described such as nerve growth factor NGF, brain derived neurotrophic factor (BDNF), ciliary derived neurotrophic factor (CNTF), and p75[20, 33, 34]. Following injury, the production of these factors is upregulated in both axotomised neuronal cell bodies and from denervated SCs in the distal nerve stump[34]. The increases in production are distinctly different

depending on whether the injured axon is motor or sensory in origin. The period of increased neurotrophic factor production is finite and, after long delays between injury and repair, the number of axotomised neurons that are capable of regeneration and the ability of the distal fiber to support regeneration are reduced, both of which are related to the fall in neurotrophic factor release[35, 36]. Investigators have taken several approaches in an attempt to increase the supply of neurotrophic factors. The injury site has been directly supplemented with neurotrophic factors[37-42]. In addition, undifferentiated stem cells and stem cells that have been pre-differentiated into SC-like cells have also been added in order to augment regenerative support[43-77]. Neurons have also been retrovirally infected in order to try and sustain neurotrophic factor production[78].

Even following technically excellent nerve repair, the accuracy of reinnervation of distal targets is poor. Motor and sensory fibers are unlikely to find their exact basal lamina tubes and, due to extensive disorganization at the repair site, it is possible that sensory fibers inadvertently regenerate down motor pathways or vice versa. Signaling mechanisms can reduce the incidence of this happening and studies have shown that motor axons preferentially reinnervate motor axons in the distal stump[79-81]. Those axons that regenerate down incorrect pathways are often pruned when they fail to form appropriate distal connections[82]. To a certain extent, cortical plasticity can compensate for inappropriate innervation but there are limits to this[83]. The power of cortical plasticity is regularly observed following nerve transfers in brachial plexus patients[84-86]. Transferred nerves can power muscles that previously had non-synergistic or even antagonistic functions prior to injury.

Making the process of regeneration and reinnervation even more challenging is the inevitable formation of scar. Scarring is a natural feature of wound healing and although beneficial in many respects, following nerve injury, the proliferative reaction in epineurial, perineurial and endoneurial connective tissue layers has a detrimental impact on axonal regeneration[20]. These effects tend to be worsened with increasing injury severity, the presence of tension at the repair site, the presence of suture material, and as a result of surgical dissection and manipulation of nerve ends[87]. Importantly, as with healing and regenerative potential, the extent of scar tissue formation following nerve injury varies with animal species and is more pronounced in larger animals and humans in comparison to smaller animal models such as rats[88]. This must be bore in mind when interpreting apparent scar reducing effects of an intervention and its clinical translatability.

The formation of intraneural scar tissue is led by fibroblasts and influenced by a complex array of growth factors and cytokines. The three isoforms of the TGF-beta family of proteins (TGF beta 1, beta 2 and beta3) have a central role[89]. TGF beta 1 is chemotactic to macrophages, stimulates angiogenesis and the formation of granulation tissue, promotes the synthesis of extracellular matrix formation and inhibits its degradation[90]. TGF beta2 may act synergistically with TGF beta 1. In contrast, TGF beta 3, which is primarily synthesized by keratinocytes and fibroblasts, reduces macrophage and monocyte profile, reduces the deposition of fibronectin, collagen 1 and collagen 3, and is believed to be involved in the restoration of normal dermal architecture[90]. All three isoforms of TGF beta have been isolated in SCs from uninjured and injured peripheral nerve. Following nerve injury, the epineurial levels of TGF beta 1 increase whilst those of TGF beta 3 fall[91, 92].

The presence of intraneural scar acts as a physical obstacle to regenerating axons[93]. Axons that are forced to regenerate through this tissue are prone to deflection or complete obstruction. This not only compromises recovery, but also increases the likelihood of neuroma formation. Upon reaching the distal stump, axons have often taken a considerably more haphazard, tortuous and metabolically expensive route than normal and as a result, tend to be smaller in caliber and less myelinated[3, 94].

1.3 Peripheral nerve repair

1.3.1 Basic principles

Traumatic injuries associated with open wounds are initially managed according to basic principles. In order of importance, life is preserved, the patient is stabilized, wounds are decontaminated and debrided and digits, limbs and soft tissues are revascularised, if required. Following on from this, the reconstruction of other tissues such as bone, tendon and nerve are performed. Nerve ends are inspected. If the nerve remains in continuity, management continues as it would for a closed injury. If injured nerves have been severed cleanly, they may only require minimal debridement of ragged ends. In these situations, simple end-to-end repair may be possible. If sections of nerve have been devitalized, this tissue must also be sharply debrided until healthy nerve is visualized. When nerve viability is in question, nerve ends can be tagged together with suture. A delayed procedure can be planned in order to more reliably assess nerve viability. At this point, sections of obviously scarred nerve can be identified, excised and formally reconstructed.

Successful outcome following nerve repair is dependent on multiple factors. Some of these relate to the cause of injury whilst others are specific to the patient and the surgical ability of the surgeon. The severity of injury is perhaps the most obvious of these. Repair of clean, guillotine-type injuries produce more favourable outcomes. Severe crush injuries or blast injuries resulting in loss of large segments of nerve have less favourable outcomes. Proximal injuries present greater regenerative distances and are also more problematic due to the longer periods of denervation of distal SCs and target muscle. Recovery following immediate repair, or repair performed after short delays, tend to outperform those injuries that occur after prolonged delays. This is also related to the duration of denervation, a topic that will be elaborated upon below. Nerve regeneration in elderly patients is less successful than in younger patients. The elderly also have a greater incidence of systemic conditions such as ischaemic heart disease, peripheral vascular disease and diabetes that can also compromise recovery from nerve injury. This demographic also more frequently take multiple medications and some of these, including steroids, can interfere with recovery.

The skill of the operating surgeon is also of paramount importance. The qualified peripheral nerve surgeon has a deep understanding of the anatomy and physiology of nerves, the neurobiology of injury and repair and, with access to modern microsurgical equipment, is able to achieve the best possible results at present for the patient. Some basic principles regarding the approach to peripheral nerve repair must be adhered to.

Thorough clinical examination precedes all other intervention following peripheral nerve injury. Quantitative assessment of motor and sensory function and comparison of these findings with the contralateral uninjured nerve allows the formulation of a differential

diagnosis and determines whether surgical intervention is warranted. This assessment must also be performed post-operatively in order to monitor recovery. As discussed, basic principles of wound management such as decontamination and debridement are essential to optimize the chances of successful regeneration. The use of microsurgical equipment and optical magnification is also essential. If a magnification of x4.0 is unavailable in the form of loupes, an operating microscope should be used. Immediate nerve repair is preferable to repair after a delay. However, in some situations, the patient's condition or the nature of the injury preclude primary nerve repair. For example, when wounds are heavily contaminated and contain devitalized tissue, repair must be delayed so that wound toilet and debridement can occur. In this situation, nerve ends can be tagged or provisionally coapted in order to prevent significant retraction prior to reconstruction.

The existence of tension between coapted nerve ends results in gapping and ischaemia, both of which exacerbate the formation of intraneural scar and have a deleterious effect on regeneration. If tensionless repair is unachievable, some form of bridging technique is indicated. Deciding when excessive tension exists can be difficult. Some have proposed that when nerve ends cannot be satisfactorily coapted with a single 8-0 suture, then excessive tension exists and nerve grafting should be performed. The experienced peripheral nerve surgeon will recognize that positional maneuvers should not be relied upon to reduce tension at the repair site. This practice is not only ineffective but it also introduces the possibility of joint stiffness and contractures. Conservative mobilization of the distal and proximal nerve ends in order to gain extra length is acceptable due to the robust intrinsic blood supply. If tensionless repair is not possible following conservative mobilization, then an interpositional graft should be used. As part of this decision making process, adjacent joints should be flexed and extended under anaesthetic in order to ensure that post-operative mobilization, as part of

a rehabilitation program, can be tolerated. If fascicular topography can be easily re-orientated then a group fascicular repair should be performed. If establishing fascicular orientation is not possible, then epineurial suturing should be performed. This may be due to a lack of specialized equipment or techniques or may be due to the fact that the injury is situated at a level where motor and sensory fibers are still mixed. Fascicular organization varies widely along the course of a nerve. Fascicles situated proximally tend to consist of fibers that serve a wide variety of distal functions. As these fascicles progress distally, a large amount of re-organisation occurs. As a result, distally, fascicles have a high degree of organisation and functional differentiation, thus making group fascicular repair more feasible.

Post-operatively, gentle mobilization should be initiated early in order to prevent the formation of encapsulating scar tissue around the nerve and subsequent traction injury. In addition to mobilization, sensory and motor re-education is also very important. Loss of function following repair is partly due to the reinnervation of different targets by axons. However, due to cortical plasticity, and with the appropriate intervention, the patient can be helped to adapt to the new connections.

1.3.2 Timing of repair

Early investigators postulated that delaying nerve repair until cell bodies had been metabolically primed and distal nerves had been sufficiently cleared of debris would translate into optimized regeneration and recovery. Similarly, others theorized that pre-degeneration of nerve grafts would also result in superior outcomes. Despite early promise, these predictions were not substantiated in animal models[95]. Contemporary studies have highlighted the importance of expeditious nerve repair. Fu and Gordon observed that poor recovery was a

result of the combined effects of chronic axotomy and chronic denervation of the distal nerve and muscle and delineated the relative contributions played by each[35, 36]. These and other studies subsequently confirmed that chronic denervation of the distal nerve and target muscle is the most important[35, 36, 96, 97]. Denervated SCs are less able to support regenerating axons. Denervated muscle undergoes progressive, characteristic histological changes within a few weeks. The muscle atrophies, is less able to recover from this atrophy and has also been shown to impart a retrograde inhibitory influence on regenerating axons, the effects of which worsen with time[97]. Although the effects of denervation atrophy can be reduced by artificial electrical stimulation, stimulation during prolonged denervation is unable to enhance muscle mass, force or motor function once muscles are subsequently reinnervated[98]. With chronic, long-term denervation, particularly in combination with a lack of mobilization, denervated muscles are entirely replaced by fibrotic scar tissue or fat. Delays of up to 2-years can yield some recovery but after this time, the loss of functional muscle mass is often unsalvageable. Following major trauma, prolonged delays prior to the onset of definitive reconstruction are often unavoidable due to the requirement for patient stabilization, wound decontamination, and the presence of proximal injuries and large volume tissue loss. However, the importance of expeditious repair cannot be overemphasized.

Maintaining a permissive regenerative environment following delayed repair may be possible through the supplementation of stem cells and neurotrophic factors[21, 34, 99, 100]. However, delivery of these factors, and their temporal and spatial regulation, is far from being realized clinically. Inappropriately high concentrations of some neurotrophic factors can be inhibitory to regeneration and can even promote cell death[99, 100]. Denervation times can be partially compensated for through external electrical stimulation of nerve repair sites[101, 102]. This has been performed in animal models of immediate and delayed repair[103, 104] and most recently,

has facilitated full reinnervation of thenar muscles in humans with severe carpal tunnel syndrome[105]. This effect has been linked to upregulation of RAG expression and elevated levels of neurotrophic factors[101, 102, 106]. This technique perhaps represents one of the few clinically translatable solutions to date.

1.3.3 End-to-end neurorrhaphy

The use of loupe or microscope magnification is essential. Prior to repair, nerve ends are prepared by sharp transection using either straight scissors or a scalpel blade. The current standard of care for re-anastomosing involves the use of suture. The aim of suture placement is to accurately re-align, with minimum tension, not to create a perfect seal[107]. Overly tight sutures may compromise vascularity and can result in bunching of the axons at the repair site[108]. This leads to distortion of fascicular alignment and can increase the number of axons escaping extra-fascicularly. Herniation of axons out-with the repair site is sometimes unavoidable and in these situations, it is good practice to sharply transect these fibers and allow them to retract back inside the repair[15, 109, 110].

Suture bites can be placed at the level of the epineurium, perineurium or can encompass both connective tissue layers. When nerves are small and monofascicular or when, in larger nerves, fascicular topography cannot be easily discerned and accurately re-established, epineurial suturing is performed. This approach is also preferred when injury occurs at more proximal levels where nerves are more often mono- or oligofascicular and considerable mixing of motor and sensory fibers exist. When fascicular topography can be easily distinguished, group fascicular repair can be performed in order to more accurately align

individual fascicles, reduce the incidence of sensory-motor mismatching and therefore improve outcome. Fascicular re-orientation can be aided by aligning epineurial blood vessels in the proximal and distal stumps. Although evidence exists suggesting a superiority of group fascicular repair over epineurial suturing in rodent models, evidence of this in higher order animals such as non-human primates is lacking[111-113]. No well-controlled clinical trials have been performed. The main disadvantage of group fascicular repair is that the technique requires considerably more tissue handling, dissection and a higher suture burden in the nerve, all of which can lead to increased scar tissue formation and may compromise axonal regeneration. In addition, inadvertently coapting mis-matched fascicles together with perfect technique may be expected to have a more detrimental impact on recovery than a poorly performed epineurial repair.

The identity of fascicles can be established by several techniques. Intraoperative stimulation of proximal and distal nerve stumps, in the case of transection, or along a segment of suspected fourth degree injury, can yield very useful information[114-117]. With the patient awake, and with appropriate regional anaesthesia, stimulation of proximal motor fibers elicits a dull aching sensation whilst stimulation of sensory fibers results in a sharp pain in the distribution of the nerve. Initial dissection is performed under tourniquet although tourniquet time is limited to 30mins in order to avoid a neuropraxic injury that could interfere with stimulation and recording. In the acute setting following injury, if stimulated, the distal nerve stump will continue to produce muscle contractions for approximately 72-hours[107]. Action potentials will also be detectable in sensory fibers for this duration[107]. In cases of fourth degree injury, again with the patient awake, the surgeon can establish the extent of injury by stimulating systematically along the length of the nerve. Stimulation in an area of scarred, non-functioning nerve will obviously elicit no response. As stimulation moves proximally,

when healthy nerve is encountered, a sensory response will be detected. If stimulation occurs out with the critical 72-hour period, fascicles can be identified distally, distal to the point of anatomical segregation, and traced proximally to the point of injury.

Intraoperative conduction studies can also provide information on the viability of injured nerve[107]. Segments of nerve are assessed with stimulating and recording electrodes separated by a length of several centimeters. Stimulation pulses of increasing voltage amplitude are then used until an action potential is triggered. The proximal nerve, injured segment and distal nerve are sequentially evaluated. Lengths of adjacent, normal nerve can be activated and examined as a control and to ensure that the equipment is functioning satisfactorily. If no conduction exists across a segment of injured nerve and in the distal segment, this implies considerable neurotmetic injury and intraneural scar requiring excision and grafting of the involved segment. If high stimulating amplitudes are required for conduction but conduction remains intact, this suggests a first to third degree Sunderland injury. Neurolysis may be all that is required. Poorer conduction may require careful examination of individual fascicles. This technique is of particular relevance when confronted with a sixth degree Mackinnon injury. This pattern of injury is typified by a neuroma-in-continuity and may consist of a spectrum of axonotmetic and neurotmetic injuries. It is recommended in these situations that dissection in the area of scar or neuroma is avoided in order to reduce the chances of injuring healthy, recovering fibers. By considering the information gained from clinical examination and electrical testing, those fascicles that are irreparably damaged are excised and grafted whilst those that are free from scar and have intact conduction are preserved.

Histological methods for distinguishing motor from sensor fascicles have existed for many years[118, 119]. These techniques rely on the detection of cholinesterase enzymes in motor fascicles and carbonic anhydrase in sensory fascicles. Although originally the process took 24-hours, currently results can be returned to the surgeon within one hour. In common with electrical stimulation of the distal nerve stump following injury, staining of enzymes is only possible for 5-days following injury. As a result, in a large proportion of cases, useful topographic information can only be obtained for the proximal stump. Additional limitations are that it requires biopsy of the nerve, is time consuming and it requires a costly, dedicated histology service. Some report superior outcomes but due to the limitations of the technique, it has not been widely adopted.

1.3.4 The nerve gap

A nerve gap is the distance between two injured nerve ends and can result from primary loss of tissue following severe trauma or can result from the surgical resection of nerve. Resection may occur acutely as part of a debridement, sub-acutely after 2-3 weeks when the extent of injury is not immediately apparent, or may be performed following a longer delay for lesions in continuity when it becomes obvious that recovery is not progressing. In the latter two examples, the scarred segments are often different in appearance and consistency in comparison to healthy nerve. Under loupe or microscopic examination, the sectioned nerve end that lies within the area of scar tends to be a homogenous block resembling ground glass with complete loss of fascicular organization. With serial sectioning, the re-appearance of healthy bulging endoneurium and fascicular arrangement becomes apparent[107]. These observations are relied upon, in addition to the electrophysiological techniques previously discussed, in order to accurately determine the amount of nerve that requires removal prior to

reconstruction[107]. Added to the gap caused by loss of actual nerve tissue is the distance that proximal and distal nerve ends retract. This can be substantial, particularly after prolonged periods of delay between injury and reconstruction.

The current standard of care for reconstructing nerve gaps uses autologous nerve as an interpositional graft. However, the use of autografts necessitates the harvest of an "expendable" donor nerve and is associated with prolonged operating time, additional scarring, sensory loss and increased risk of neuroma formation. In cases of major trauma associated with substantial tissue loss, the demand for autograft may exceed that which can be harvested from the patient. Although rare in civilian practice, this scenario has become more frequent in recent years following the return of wounded warfighters from Iraq and Afghanistan who have sustained major nerve injury and limb amputations, often secondary to injuries caused by improvised explosive devices. In these challenging patients, alternative strategies must be employed for nerve reconstruction. Alternatives to nerve autograft include nerve allografts and nerve guidance conduits, although regeneration through these materials has typically been unable to match that of the autograft. As a result, research into improving regeneration through these products has intensified in recent years.

1.3.4.1 Nerve autograft

Although, in theory, any nerve can serve as a donor, a limited few are used routinely. In order to be suitable for use as a donor, nerves must be of sufficiently small caliber in order to ensure that revascularisation is not problematic and they must be "expendable" in the sense that the resulting loss of function is inconsequential for the patient. The commonly used

nerves are all sensory and include the sural nerve, medial and lateral antebrachial cutaneous nerves, the superficial, sensory branch of the radial nerve and the saphenous nerve. Ultimately, the choice is dictated by what nerve has been injured and the extent of the gap that requires bridging. For digital nerves, a reasonable size match can be achieved by using single cables of one of the above nerves. If a smaller caliber nerve is required then branches of the main nerves can also be used. For the reconstruction of larger, multifascicular nerves such as the median and ulnar nerves, several cables may be required. Once the gap length and the number of fascicles that required grafting are known, the length of required donor nerve can be estimated. Once grafts are harvested, they are stored in cool, moist gauze until ready for use. Analogous to blood vessels, nerves branch as they move distally. In order to reduce the proportion of axons that are lost down these branches, nerve grafts are reversed prior to suturing. This essentially creates a funnel of convergence for the axons as they move towards the distal stump. At the distal neurorrhaphy site, the epineurium or perineurium of the distal stump can be sutured so that it overlaps that layer of the graft, further improving axonal capture. The number of sutures used for each cable graft is kept to a minimum, often two or three 9-0 or 10-0 nylon. In order to further reduce the reliance on sutures, the strength of the repair site can be augmented with fibrin glue. Fibrin glue also helps reduce tension and gapping at the repair site, the formation of which results in the deposition of scar[120].

In light of the aforementioned centripetal vascular supply of nerve grafts, it would seem logical that the use of vascularized nerve grafts would be preferable to conventional, non-vascularized grafts. This would be of particular relevance in severely scarred, poorly vascularized wound beds. Initially, vascularized grafts included an axial vessel with the nerve. More recently, the use of pedicled nerve grafts has largely been supplanted by microsurgical techniques[121]. Many preclinical comparisons between vascularized and non-

vascularized grafts have been performed and have provided support for[122-126] and against[127-130] vascularization. In spite of these reports, there is a dearth of well-designed, randomized controlled trials showing a clear clinical benefit. In addition, very few studies have investigated the efficacy of these grafts in poorly vascularized, clinically relevant scenarios. Clinically, the use of non-vascularized grafts is limited to small caliber sensory nerves as previously discussed. If indicated, the use of larger, motor nerves requires vascularization in order to avoid central avascular necrosis.

1.3.4.2 Nerve allograft

Nerve allografts provide the most accurate representation of intraneural architecture and axonal guidance. Initially, allografts were fresh and cellularized, requiring immunosuppression to overcome rejection and preserve donor SC viability over the course of recovery. Early experiments in immunosuppressed rats and non-human primates produced outcomes that were comparable to autograft[131-135]. These observations were partly related to the pro-regenerative effect of immunosuppressant therapy. However, due to the risk of infective and neoplastic disease, this approach has been disfavored and has driven the development of decellularization protocols and the use of acellular nerve allograft (ANA). Initial attempts at decellularization involved thermal and chemical processing and, although technically successful, produced poor regenerative outcomes as a result of inadequate preservation of extracellular matrix (ECM) components and insufficient removal of cellular debris [136, 137]. In 2004, Hudson et al described an optimized detergent-based protocol that resulted in superior histological outcomes in comparison to those previously described methods [138]. In 2007, human ANA (Avance, AxoGen Inc), processed by a modified detergent-based method, was approved for clinical use [139].

Although obviating the requirement and risks of immunosuppression, decellularization removes SCs and other pro-regenerative components. The detrimental impact this has on the extent and rate of regeneration in comparison to conventional autograft has been consistently demonstrated in animal models of large gap injury [136, 140]. This long-standing impasse has prevented widespread clinical acceptance of ANA. Leaders in the field reserve ANA for small diameter, non-critical sensory nerve defects of less than 4cm, for restoring autograft donor site sensation, for nerve supercharging and for end-to-side nerve transfers in the hand. The use of ANA for the reconstruction of motor nerves, large diameter nerves, critical sensory nerves and sensory nerves greater than 4cm in length has been discouraged[141]. This practice has been based on the scarcity of good quality clinical evidence and the fact that existing evidence is often compounded by small sample sizes, the inclusion of sensory nerves only, small nerve gaps and the lack of autograft control groups [142-144]. However, in 2012, Brooks et al published results from the first comprehensive multi-centre trial and showed that Avance was safe and resulted in "meaningful" recovery in 87% of those cases recording quantitative outcomes [139]. Cho et al have also reported results from the RANGER study and conclude that, for gaps between 5-50mm, ANAs can produce motor and sensory outcomes that are comparable to autograft and superior to hollow conduits [145].

Broadening the clinical application of ANAs and ultimately supplanting autograft provides strong impetus to improve regeneration through ANAs. Recent efforts have focused on the supplementation of ANA with neurotrophic factors, SCs and stem cells. Although conceptually exciting, preclinical experience has been disappointing. Although a tissue engineered or cell-based solution is far from being realized, addressing other, technical aspects of conventional suture coaptation may offer a more simplistic and rapidly translatable solution.

1.3.4.3 Nerve conduits

Nerve conduits can be broadly classified into either natural or synthetic. Natural conduits obtained from autologous sources such as bone, artery, vein, muscle and tendon have been used clinically for well over one hundred years[146, 147]. The use of small superficial veins represents an expendable and widely available autologous source and has been shown by many to result in meaningful recovery of function when used for small gaps involving sensory nerves. Due to the flimsy nature of small veins, luminal collapse and obstruction to regeneration can be problematic. Prevention of this has been attempted by including small amounts of nerve or muscle tissue within the lumen of the vein[148-151]. In addition to physical support, nerve and muscle tissue also provide ECM proteins, SCs and neurotrophic factors that may provide biochemical and architectural support to regenerating axons. Another autogenous material that has shown some efficacy is tendon. As with vein grafts filled with luminal support, tendons consists of parallel arrays of collagen fibrils and ECM proteins that can act as guidance channels supporting axonal regeneration. Several investigators have shown promising results with these materials but none have been shown to be superior to the nerve autograft[152, 153]. The main disincentive with using autogenous material as a nerve conduit is the morbidity of harvest. The harvest of autogenous artery, vein or tendon can involve a second surgical site, compounding the risks of bleeding, infection, abnormal or painful scarring and wound breakdown. These factors have driven the search for a suitable synthetic alternative.

Several different synthetic materials have been used to manufacture guidance channels, some of which are approved for clinical use. Synthetic conduits can be further categorized into either non-absorbable or absorbable. Silicone is perhaps the most well known example of a

non-absorbable conduit material. Although initially popular, these products suffered a high incidence of nerve compression, local immunoreactivity and patient discomfort, necessitating explantation in many cases[154]. Recently, an alternative non-absorbable conduit composed of a biocompatible polyvinyl alcohol (PVA) hydrogel has been FDA approved. Currently, insufficient experience with this product exists to permit robust assessment. It remains to be seen whether this product offers any significant advantage over previous non-absorbable materials or indeed, other absorbable alternatives, or whether it suffers from similar aforementioned limitations of compression and immunoreactivity[155]. As a result of these limitations, the majority of products now FDA approved and clinically available, are composed of absorbable materials. Examples of these include type-I collagen, polyglycolic acid (PGA) and poly-DL-lactide-caprolactone (PLCL). Success with other materials such as fibrin[156, 157], poly-3-hydroxybutyrate (PHB)[158] and chitosan[159] has also been described. Conduits manufactured from components of the ECM such as collagen and fibrin may have superior cell adhesion characteristics and a more predictable, non-toxic degradation in comparison to other artificial conduits. Organic polymers such as polypyrrole or electrically poled poly(vinylidene fluoride) are good electrical conductors. Conduits composed of these materials that are subsequently stimulated with low frequency electrical currents have been shown to improve rates of axonal regeneration[160].

It is generally accepted that the application of inert, hollow nerve conduits is limited to short gaps (<3cm)[161]. Nevertheless, optimizing regeneration through these products has important clinical implications and as a result, huge efforts have been focused on this subject. Researchers have manipulated physical properties such as conduit material, flexibility, strength, permeability, luminal profile, diameter and internal architecture[155]. In recognition of the importance of axonal guidance, the design and manufacture of increasingly elaborate

intraluminal architecture has been attempted to recreate native intraneural conditions[155]. Likewise, conduits have been supplemented with SCs, stem cells, extracellular matrix proteins and neurotrophic factors in an attempt to recreate the optimal biochemical conditions found following simple transection and end-to-end repair[146, 155]. However, the temporal and spatial regulation of cells and biochemical mediators is an incredibly complex and incompletely understood process and, at this time, it is uncertain whether this goal is realistically achievable. Advances in the fields of biotechnology and tissue engineering, and the application of these approaches to the development of "bioartificial" guidance channels, may eventually provide a conduit that can supplant the nerve autograft.

1.3.5 Sutureless approaches to peripheral nerve repair

The use of suture for neurorrhaphy has several well-known limitations. Excessive manipulation of nerve ends and needle passage through tissues results in iatrogenic trauma. Although inert, suture material is inflammatory, resulting in fibrosis and intra and extra-neural scar tissue formation[162]. Scar tissue not only presents a direct obstacle to regenerating axons but can also lead to tethering, traction neuritis and external compression, all of which can compromise outcome. Even under high magnification and with meticulous technique, coaptation sites are imperfect. Leakage of growth promoting factors and mis-guided axons into adjacent tissues further compromises outcome and likely contributes to neuroma formation[163-165]. These effects may be exacerbated in the context of gap injury and nerve grafting when axons must traverse two coaptation sites. Reducing the suture burden at the repair site or, ideally, obviating the requirement for suture completely, is a logical solution to try and improve regeneration and outcomes following repair.

Several sutureless methods of nerve repair have been thoroughly investigated. Fibrin sealants and laser-assisted techniques represent two of the most extensively studied[166-168]. Fibrin sealants rely on the combination of fibrinogen and thrombin to form a fibrin clot. Although originally designed for hemostasis, "off-label" application as an adhesive for peripheral nerve repair dates back to the 1940s[169]. Proponents claim that fibrin glue can be rapidly applied, results in less scar tissue formation, and can improve outcomes[166, 170-174]. In contrast, others have reported excessive fibrosis, inferior bond strength and high rates of dehiscence[175-178]. Introduced in the 1980s, laser welding of peripheral nerves has generally been performed using carbon dioxide and argon lasers[167]. A photothermal reaction at the repair site creates a bond from the coagulum of denatured protein. Proposed advantages include shorter repair times, reduced incidence of inflammation, scarring and neuroma. In one rodent model, laser welding was found to be at least as effective as fibrin glue and epineurial suture[167, 179]. However, due to thermal damage, poor bond strength and high rates of dehiscence, the technique has not been clinically adopted[180-185]. The introduction of biological solder such as fascia or bovine albumin promised to enhance bond strength and limit thermal damage but interest in its potential has largely been abandoned[167, 185, 186].

The role of non-penetrating clips and anastomotic couplers has become commonplace in micro- and macrovascular anastomoses. The application of these techniques to the repair of peripheral nerves has also been investigated[187-189]. Anastomotic couplers rely on the insertion of divided nerve ends through two separate but closely apposed rings connected by a spring-mounted hinge. The opposing sides of each ring possess spikes. Once vessel or nerve ends are inserted through the rings, vessel wall or epineurium is everted over the spikes. As the hinge is closed, the spikes interlock and the coapted nerve or vessel can be detached from the device. Studies have shown that the technique is faster than conventional

suture anastomosis although no clear functional or histological benefit has been demonstrated[190]. One study showed that nerves repaired using a coupler device showed evidence of compression at the repair site due to fibrous tissue ingrowth although this did not appear to have a detrimental impact on outcomes. In the same study, axonal escape from the repair site into the surrounding tissues was considerably less in comparison to suture repairs[189]. Non-penetrating vascular closure staples (VCS) are made from titanium and are inert. They aim to grip and appose only the epineurium and have been shown to be a more rapid method of nerve coaptation than conventional suture. However, as with anastomotic couplers, functional and histological outcomes following the use of these staples have not been shown to be significantly better than suture[187, 188].

Photochemical tissue bonding (PTB) is a recently developed platform technology that offers an additional alternative to conventional suture. The technique differs from laser welding as it uses visible light to create bonds between apposed tissues that have been pre-stained with a non-toxic, photoactive dye. Dye photoactivation results in the liberation of reactive species from tissue proteins, covalent bond formation between amino acid residues and the formation of a protective seal with no thermal damage[191-194]. The absence of collateral thermal damage is a distinct advantage over laser welding. When applied to peripheral nerve repair, this light activated technique can be used to bond transected nerves together. A biological nerve wrap is stained with photoactive dye and is wrapped circumferentially around dye-stained coapted nerve ends. Subsequent illumination of the nerve wrap interface results in bond formation between the epineurium of nerve ends and the bridging wrap. In order to allow light to penetrate through the nerve wrap, the biological material in question must be very thin and transparent. Materials that have shown success include chitosan and human amnion[195, 196].

1.4 Human amnion as a biomaterial

1.4.1 History

Prior to the realization of its medical and surgical applications, human amnion was the focus of myth, legend and superstition[197]. Being born with the fetal membranes or "caul" intact was considered extremely lucky. In addition to good fortune, it was believed children were gifted with life-long happiness, the ability to see spirits, and protection from death by arms and drowning. The magical powers of the caul were not confined to the original bearer and could be transferred by inheritance or by legitimate sale. As a result, the trade of caul amulets became extremely popular, particularly between seafaring men during the 1800s at the time of the Napoleonic War[197]. In the early 1900s, amnion was found to be an effective dressing for wounds of multiple aetiologies[198, 199]. Investigators claimed that time to healing and infections were reduced when using fetal membranes. Over the last 100 years, the therapeutic benefits of amnion have been observed following application for burns, chronic vascular and diabetic ulcers, dural defects, intra-abdominal adhesions, peritoneal reconstruction, genital reconstruction, hip arthroplasty, tendon repair, microvascular repair, corneal repair, intra-oral reconstruction and reconstruction of the nasal lining and tympanic membrane[198, 199]. More recently amnion has been shown to be a viable source of stem cells with a potentially exciting future in regenerative medicine[200-203].

1.4.2 The anatomy and physiology of human amnion

Amnion forms during the transition of the morula into the blastocyst at approximately 7-days following fertilization[204]. The amnion is between 0.02-0.05mm thick and consists of five distinct layers: (1) epithelium, (2) basement membrane, (3) compact layer, (4) fibroblast layer, (5) spongy layer (figure 2). The epithelium is the innermost layer, consists of a single layer of cells and is in direct contact with the amniotic fluid. The free border of the cell is

covered with microvilli. The basement membrane border of the cells contains blunt projections that inter-digitate with similar processes in the basement membrane, forming a densely adherent bond. The basement membrane is a thin layer composed of reticular fibers. The compact, fibroblast and spongy layers are collectively referred to as the amniotic mesenchyme and originate from the primary extra-embryonic mesoderm of the blastocyst. The mesenchyme contains collagen I-VII,

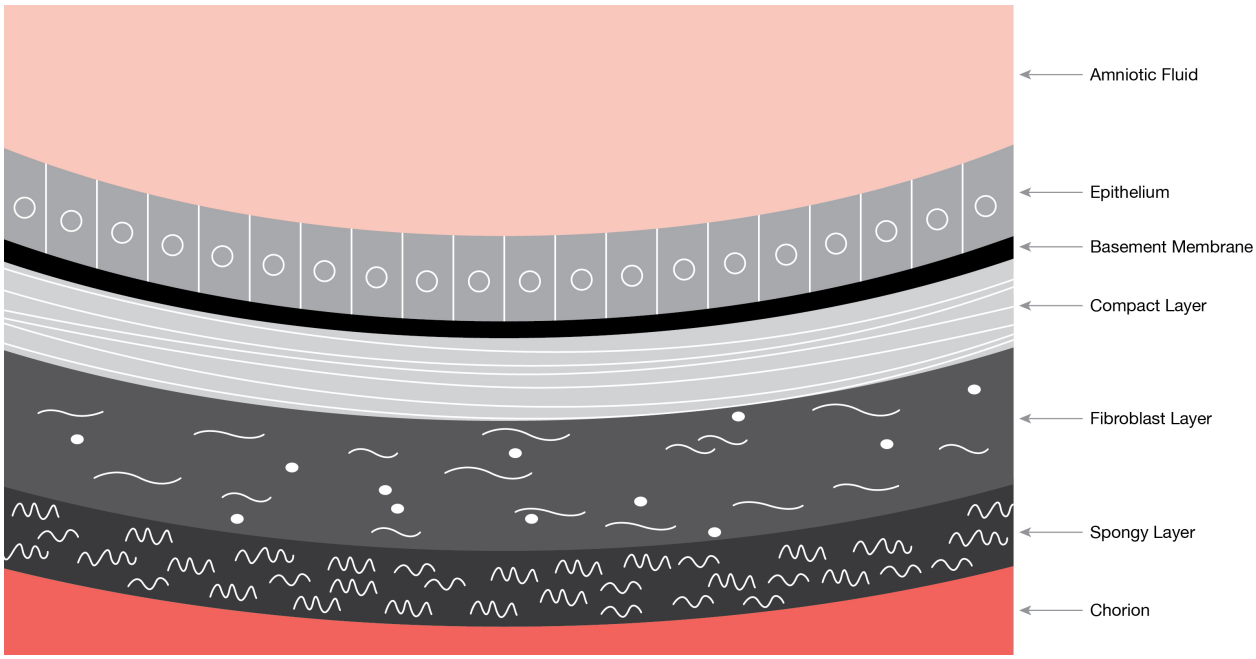

Figure 2. Schematic of the layers of human amniotic membrane. The amniotic epithelium lies adjacent to the amniotic fluid. The histological layers lying external to the epithelium include the basement membrane, compact layer, fibroblast layer and the spongy layer. The compact, fibroblast and spongy layers are collectively referred to as the amniotic mesenchyme and form an interface between the epithelium and the chorion.

elastin, laminin and fibronectin. The compact layer is composed of a dense network of fibers and is almost entirely free from cells. The majority of the tensile strength originates from this layer. The fibroblast layer is the thickest amniotic layer and is composed of a loose fibroblast network within a matrix of reticulin. The outermost spongy layer represents the transitional layer between amnion and chorion and is composed of bundles of reticulin within a

background of mucin. The two layers are loosely adherent, allowing a degree of gliding during gestation and easy separation by blunt dissection during harvest[199]. During the course of gestation, the structure and composition of these layers changes.

The amnion protects the fetus from mechanical stress and desiccation. Uniaxial tensile strength is due to abundant type-1 and 2 collagen and elastin within the mesenchyme. Elasticity is related to type-3 collagen content[205]. The presence of microvilli at the apical surface of amniotic epithelial cells is thought to play an important role in the production and regulation of amniotic fluid homeostasis[198].

Amnion lacks vascularity and receives oxygen and nutrients by diffusion from adjacent amniotic fluid and chorionic vasculature[199]. In spite of this, amnion is metabolically active and is responsible for the production of multiple vasoactive peptides, growth factors and cytokines[205]. The mesenchyme accumulates these growth factors and may act as a reservoir from which the amnion exerts its beneficial effects following transplantation.

Amniotic epithelium has been shown to be a source of prostaglandins, particularly prostaglandin-E2, and is thought to play an important role in the initiation and maintenance of uterine contractions during parturition[206]. The epithelium also contains human chorionic gonadotrophin receptors that have a role in the regulation of prostaglandin production and activity.

1.4.3 Collection, processing and storage of human amnion

Elective cesarean section donors undergo rigorous serological screening for HIV-1/2 (human immunodeficiency virus-1/2), Hepatitis B, Hepatitis C, HTLV (human T-cell lymphotrophic

virus), syphilis, CMV (cytomegalovirus), and TB (tuberculosis)[207]. Following delivery, amnion is separated from the placenta by blunt dissection (figure 3). Once gross contaminants are removed, amnion is usually de-epithelialised to limit immunogenicity, sterilised to reduce risks of disease transmission, and preserved to improve longevity and convenience for storage. Improvements in processing have focused on preserving membrane architecture and growth factor content in order to optimise therapeutic effect[198, 207, 208].

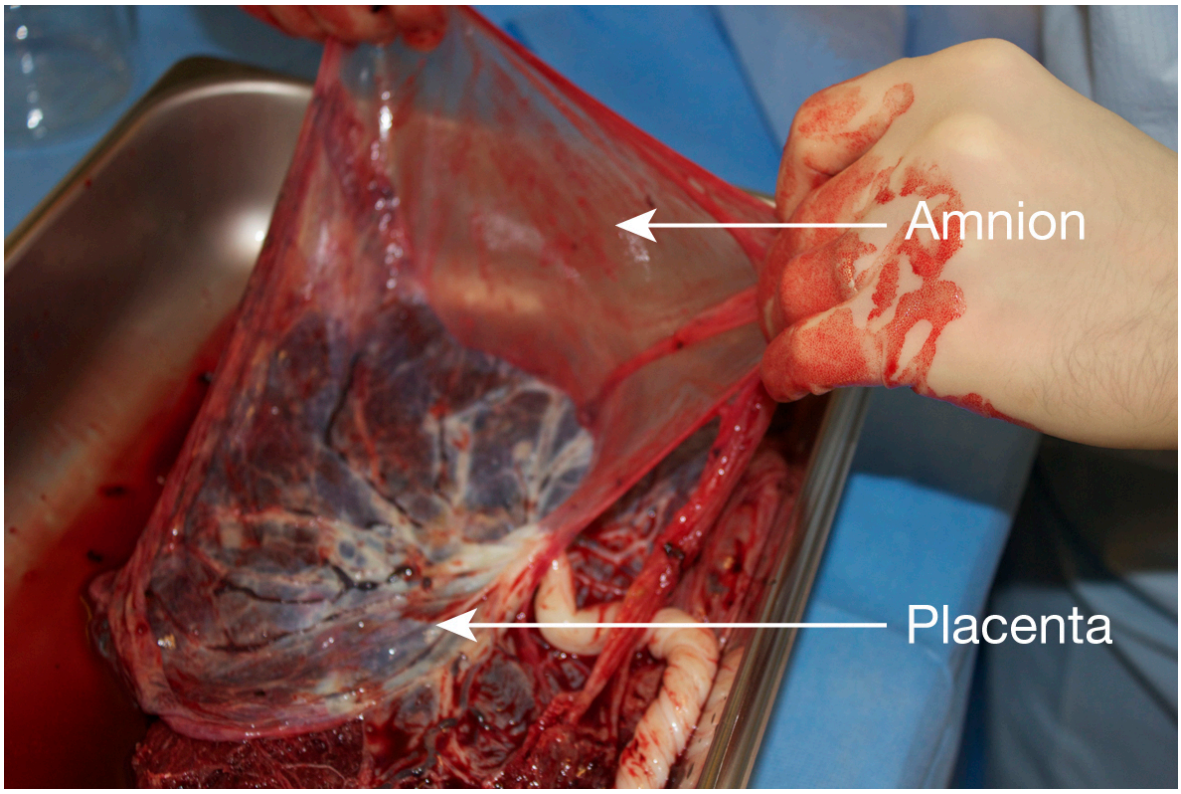

Figure 3. Blunt separation of amniotic membrane from placenta. Using aseptic technique, amniotic membrane is peeled off the placenta. Due to the loose adherence between the amniotic mesenchyme and the chorion, separation is easily achieved using blunt dissection.

De-epithelialisation can be performed by mechanical scraping or exposure to chemicals[207]. It is uncertain how these protocols affect the levels of growth factors and ECM proteins. Koizumi et al showed that, although amnion denuded of its epithelium contained EGF, TGF-α, KGF, HGF, bFGF, TGF-β1, and TGF-β2, protein levels were reduced in comparison to

samples with intact epithelium[209]. Whether this is clinically significant is uncertain. Neurotransmitters, neurotrophic factors and neuropeptides are concentrated in the epithelium and therefore amnion with intact epithelium may be superior when applied to neural injury[210]. In contrast, denuded amnion results in superior cell adhesion, migration and proliferation and therefore may be preferable when applied to acute and chronic wounds[211]. As the majority of clinical applications concern wound healing, the use of denuded amnion has greater representation in the literature.

Developed in the late 1980s, cryopreservation in glycerol is the most widely used preservation technique. Anti-bacterials and anti-fungals are often added before freezing at -80°C. Cells are devitalised although not sterilized[212]. Viable bacteria and viruses can be present following several months of storage[213]. The effect on biological properties is uncertain. Thomasen et al reported no detrimental impact on sterility, histological integrity or the availability of biological mediators. Amnion cryopreserved in 50% glycerol/DMEM (Dulbecco's Modified Eagle's Medium) at -80 degrees for 1-month contained epidermal growth factor (EGF), transforming growth factor-α (TGF-α), TGF-β1, -β2, -β3, keratinocyte growth factor (KGF), hepatocyte growth factor (HGF), basic fibroblast growth factor (bFGF), keratinocyte growth factor receptor (KGFR) and hepatocyte growth factor receptor (HGFR)[208]. Cryopreservation requires expensive equipment that may be unavailable for some institutions, particularly in developing nations.

Lyophilisation is an alternative technique allowing storage of amnion at room temperature, obviating the requirement for deep freeze facilities and increasing surgeon convenience. Lyophilised membranes are commonly sterilised with gamma irradiation. Concerns exist

regarding detrimental changes to membrane architecture and growth factor levels. Nakamura et al reported no significant difference in tensile properties, tissue structure or ECM composition between lyophilised, gamma-irradiated and cryopreserved membrane[214]. Lim et al showed that lyophilisation reduced the levels of several growth factors and ECM proteins although there was no appreciable difference in clinical performance when compared with cryopreserved samples[215]. Other methods of preservation and sterilisation exist although these are less well accepted.

The variation in processing within the literature makes it difficult to draw definitive conclusions on the optimal method. Variation also exists amongst commercially available products. Independent of processing technique, several donor specific factors can influence the biochemical composition of amniotic membrane. Lopez-Valladares et al showed that in fresh, cryopreserved and lyophilised amnion, levels of bFGF, HGF, KGF and TGF-β1 were significantly lower in those membranes of greater gestational and maternal age[216]. Velez et al found significant differences in cytokine profiles between African Americans and Caucasians[217]. Membrane architecture and growth factor profile can also vary depending on what area of amnion a specimen originates from[218]. As a result, standardisation of collection and processing may be essential if consistent therapeutic results are to be achieved. If consistent relationships between donor variables and biochemical profile exist, it may become possible to select certain varieties of amnion for specific clinical situations.

1.4.4 Proposed biotherapeutic effects of amnion on healing and regeneration

1.4.4.1 Non-immunogenicity:

A fundamental requirement of any implantable material is non-immunogenicity. Conflicting reports exist in the literature regarding the presence or absence of human leukocyte antigens (HLA) in human amnion cells. Several investigators conclude that human amniotic epithelial cells and mesenchymal stromal cells lack HLA class A, B, DR and co-stimulatory molecules CD-40, CD-80 and CD-86[219]. In contrast, other studies have shown the presence of class-1 and class-1b antigens in epithelial cells, mesenchymal cells and fibroblasts[220]. Other radiobiological studies have suggested that although amnion cells retain the ability to synthesize HLA, they do not express HLA-A, B, C or DR antigens of β-2 microglobulin on the cell surface[221]. As the widespread technique of cryopreservation in glycerol renders amniotic cells non-viable, this issue is perhaps of little consequence. Regardless of the presence or absence of these antigens, it is widely reported that transplantation into immunocompetent hosts results in a negligible immune response[198, 199]. Mesenchymal stromal cells may also inhibit the maturation of peripheral blood monocytes into antigen-presenting dendritic cells[222].

1.4.4.2 Anti-inflammatory:

Amnion cells have been shown to express a number of anti-inflammatory mediators. Interleukin-10 (IL-10) has been shown to be present in amniotic epithelial cells[223]. IL-10 down-regulates the expression of Th1 cytokines, major histocompatibility complex (MHC) class II antigens and co-stimulatory molecules on macrophages[224]. It also enhances B-cell survival, proliferation and antibody production. IL-10 has also been shown to inhibit the production of pro-inflammatory cytokines such as interferon-γ, IL-2, IL-3, tumour necrosis factor-α (TNF-α), and granulocyte macrophage colony stimulating factor (GM-CSF)

produced by macrophages and regulatory T-cells[224]. Other anti-inflammatory mediators such as IL-1 receptor antagonist and tissue inhibitors of metalloproteinase-1, 2, 3, 4 (TIMPs) have also been found in amnion cells[198, 225-227].

1.4.4.3 Antibacterial

The presence of infection is detrimental to any healing tissue, resulting in an exacerbated inflammatory response and scar tissue formation. Amniotic fluid contains lysozymes and a variety of immunoglobulins[228]. Although it is uncertain whether these factors are retained within amnion cells, many studies have described the antibacterial effect of the amniotic membrane. In vitro experiments have shown reduced viability of group-A and group-B Streptococcus, *Staphylococcus aureus and Staphylococcus saprophyticus* in the presence of amnion[229]. The antibacterial effect is likely mediated by a paracrine-like mechanism rather than cell-cell contact. Amnion has also been shown to produce human-beta-3-defensin, an antimicrobial peptide[230]. Amnion epithelial cells can also be induced to express intercellular adhesion molecule-1 (ICAM-1) by pro-inflammatory cytokines such as tumour necrosis factor-α (TNF-α) and IL-1β[231]. ICAM-1 has a recognized role in the attraction and adhesion of leukocytes and may also have a role in signal transduction in pro-inflammatory pathways resulting in the recruitment of inflammatory mediators such as macrophages and granulocytes[232].

1.4.4.4 Inhibition of fibrosis and scar:

TGF-β1, β2, β3 are partially responsible for the proliferation of fibroblasts and thus the synthesis and deposition of extracellular matrix proteins by increasing the generation of protease inhibitors, cellular adhesion molecules and by inhibiting the production of matrix degrading proteases[233]. Hyaluronic acid within the amniotic mesenchymal layer may inhibit

TGF- β and therefore the over-activity of fibroblasts, their conversion into myofibroblasts and ultimately the generation of fibrosis and excessive scar[209]. The inhibition of intraneural and extraneural scar tissue formation could result in greater numbers of axons regenerating across the repair site and also reduced rates of post-operative tethering and traction neuritis respectively.

1.4.4.5 Regulation of angiogenesis:

Early reports attributed the beneficial effects of amnion on wound healing to a promotion of angiogenesis[234]. The presence of platelet derived growth factor (PDGF) and vascular endothelial derived growth factor (VEGF) are suggestive of a pro-angiogenic role[235]. In addition, bFGF has been shown to have an even greater pro-angiogenic influence than PDGF and VEGF and is responsible for the proliferation of fibroblasts forming granulation tissue[235]. The presence and supplementation of pro-angiogenic factors during nerve regeneration, particularly when using de-vascularised nerve grafts, could potentially result in expedited and improved regeneration and therefore outcomes following repair.

1.4.5 The application of human amnion to the repair of peripheral nerves

Amnion is very thin and transparent and has zero inherent elastic memory. These features make it a potentially favourable material for use as a nerve wrap. Even when applied to very small nerves with a diameter of 1mm or less, amnion readily wraps circumferentially and is adherent upon itself. As with other nerve wraps amnion is believed to provide a protective barrier at the neurorrhaphy site. In one study, amnion was used to wrap autografts following the repair of 10mm sciatic nerve gaps. Amnion treated nerves had reduced scar tissue formation, a finding believed to result in reduced obstruction to regenerating axons and the prevention of nerve tethering, traction injury and ischemia[236]. In addition to acting as a

barrier, amnion has also been shown to be useful for the manufacture of nerve conduits[237-240]. In one study, amnion conduits resulted in outcomes that were comparable to autograft and superior to that achieved with silicone conduits[238]. The authors concluded that amnion represented an ideal conduit material based on the fact that it is biodegradable, non-immunogenic, readily available, semi-flexible, is easily manufactured into different lengths and diameters and may contain important neurotrophic factors. The same group also showed that amnion conduits were also suitable for the inclusion of a hyaluronic acid/nerve growth factor media and showed that the combination of media and amnion wrap resulted in superior outcomes in comparison to amnion wraps alone[239]. Although the aforementioned studies report superior outcomes in comparison to conventional nerve autograft at early time points, at the end of follow-up, early advantages were often lost. The demonstration of initial equivalency with autograft was encouraging although the ultimate goal of surpassing outcomes achieved with conventional suture and autograft remain unmet.

It is possible that amnion fixation with suture causes a detrimental impact on regeneration. In recent years, collaborative work between the Plastic Surgery Research Laboratory and the Wellman Centre for Photomedicine at The Massachusetts General Hospital has demonstrated that amnion nerve wraps can be photochemically bonded to the epineurium of nerves. Light-activated sealing of nerve coaptation sites obviates the requirement for suture fixation and has been shown to result in superior functional and histological outcomes in comparison to conventional techniques[240-243]. As has been highlighted in previous studies, it is likely that these observations are related to a reduction in scar tissue formation, the prevention of axonal escape, and the presence of growth promoting and anti-fibrotic factors within amniotic membrane. Unique to the process of photochemical bonding, it is believed that the creation of

a protective seal may enclose and prevent the leakage of beneficial neuro-regenerative factors.

Photochemical bonding has also been used to seal amnion conduits and has been shown to support regeneration across short nerve gaps[240]. Despite early success with rodent models of end-to-end nerve repair, subsequent application of this technique in a rabbit model of large gap injury led to high rates of dehiscence at the distal coaptation sites. These observations were thought to be a consequence of proteolytic degradation of amnion nerve wraps, and light-activated bonds, prior to the arrival of regenerating axons during long periods of recovery (unpublished results, Plastic Surgery Research Laboratory, The Massachusetts General Hospital, Boston). Studies specifically investigating the *in vivo* degradation of human amnion are lacking. Rapid proteolytic degradation within one week has been observed when untreated amnion is applied to the treatment of corneal ulcers[244]. Glutaraldehyde treated human amnion microvascular interposition grafts were still present after 4 weeks of implantation in a rodent model[245]. Untreated human amnion nerve conduits were completely degraded after four months in a rodent model of sciatic nerve repair[238]. In another similar study, amnion conduits were still present after three months, although these had been photo-crosslinked prior to implantation[240]. It is uncertain from these reports exactly how long amnion persists *in vivo* although it is possible that, with pre-implantation crosslinking, the material can survive for several months.

Cross-linking of biomaterials reduces enzymatic degradation and improved durability and can be readily applied to the collagen matrix of amnion. Chemicals such as glutaraldehyde and physical methods such as gamma and electron beam irradiation are common crosslinking

methods but are limited in this application by toxicity issues and inconsistent cross-linking density respectively[246-250]. The water soluble carbodiimide, 1-ethyl-3-(3-dimethylamionopropyl) carbodiimide hydrochloride (EDC), is an alternative non-toxic agent resulting in carboxyl-to-amine cross-linking between proteins. Often used in combination with N-hydroxysuccinimide (NHS), EDC has been successfully used to improve biomechanical strength and resistance to degradation of several collagen-based biomaterials, including amnion[251-255].

1.5 Aims and Hypothesis

The work presented in this thesis aimed at improving outcomes that typically follow large gap peripheral nerve repair. Although, fundamentally, recovery is limited by large regenerative distance and slow rates of regeneration, refinements to the technical aspects of repair have the ability to improve outcomes in comparison to conventional suture repair. Building on previous success with PTB in end-to-end repair, this work assesses efficacy when reconstructing large gaps. This assessment takes place over three phases. In recognition of previous observations that amnion and light activated bonds undergo proteolytic degradation over long periods of recovery, phase 1 aimed to show that chemical crosslinking of amnion nerve wraps could improve strength and durability. Several *ex-vivo* biomechanical tests exploring parameters such as maximum load to failure, Young's modulus and photochemical bond strength were performed. To facilitate clinical translation, these tests were also performed on a commercially available swine intestinal submucosa (SIS) that is approved for human implantation and is already used to manufacture nerve wraps. Following on from these tests, a comprehensive assessment of the optimal nerve wrap and fixation method was performed in an *in-vivo* rodent model of large gap injury. Different combinations

of three different nerve wraps (untreated amnion (HAM), crosslinked amnion (xHAM) and crosslnked SIS (xSIS)) and three different fixation methods (suture, fibrin glue and PTB) were used to repair 15mm rat sciatic nerve gaps with isografts and were assessed against positive (epineurial suture) and negative (no repair) controls. An attempt was made to disprove the null hypothesis that photochemical sealing of nerve graft coaptation sites with crosslinked amnion nerve wraps would result in outcomes that were not significantly different than those achieved with conventional epineurial suture.

Phase 2 assessed whether light-activated sealing of crosslinked amnion nerve wraps remains efficacious when applied to ANA. This phase of the study was incorporated due to the fact that following major trauma involving tissue loss and amputation, the demand for autograft may exceed that which can be realistically supplied by the patient. Outcomes following the use of ANA are typically inferior to that of autografts due to the absence of SCs and neurotrophic factors. Improving the performance of these grafts has the potential to improve outcomes following these challenging injuries and may avoid the morbidity associated with autologous harvest. In an identical animal model to phase 1, ANAs were used to reconstruct 15mm rat sciatic nerve gaps. Light activated sealing of ANA using crosslinked amnion was assessed against gold standard sutured ANA. This phase aimed to disprove the null hypothesis that light activated sealing offers no significant advantage over conventional suture when applied to ANA.

Previous studies and the initial two phases of this thesis assessed the performance of light activated sealing for nerve repair performed immediately following injury. This rarely occurs clinically, with repairs occurring days, weeks, months and even years following injury.

Unavoidable delays may simply be due to timing of patient presentation although are often enforced due to the nature of the injury or the clinical condition of the patient. Significant delays between injury and repair have a detrimental impact on regeneration, distal target reinnervation and recovery and as a result, the third and final aim of this thesis was to assess the efficacy of light activated sealing following a clinically relevant delay in repair. Isografts were repaired with photochemically sealed crosslinked amnion or gold standard epineurial suture either immediately or following a 30-day delay. This phase aimed to disprove the null hypothesis that light activated sealing offers no significant advantage over conventional suture when performed after a delay.

Section 2: Methods

2.1 Generic Methods

2.1.1 Nerve wrap biomaterials

2.1.1.1 Human amniotic membrane (HAM) harvest and processing

HAM was obtained from elective caesarean section patients who had been screened serologically for HIV-1/2, Hepatitis B, Hepatitis C, HTLV, syphilis, CMV, and TB. Following delivery, amnion was bluntly removed from the placenta and washed liberally with phosphate buffered saline (PBS; Sigma-Aldrich, Co., St Louis, Mo). Membranes were mechanically de-epithelialized using a cell scraper, cut into strips, wrapped around nitrocellulose paper and placed in a storage solution containing a 1:1 mix of 100% sterile glycerol and Dulbeccos modified Eagles medium (DMEM; Gibco, Grand Island, NY), penicillin-streptomycin-neomycin (PSN; Gibco, Grand Island, NY) and amphotericin B (figure 4). HAM was stored at -80°C until required. Following thawing, HAM was mounted onto nitrocellulose paper before being dried and cut into 1cm x 1cm sections (figure 5).

2.1.1.2 Commercially available nerve wraps

Prior to the use of SIS nerve wraps for in-vivo studies, several commercially available nerve wraps and biomaterials were investigated. Collagen based products included: NeuraGen (Integra), NeuraWrap (Integra), Tenoglide (Integra), NeuraMend (Stryker), Neuromatrix (Stryker), Colafilm (Innacol), AmnioFix (MiMedx), and SurgiMend (TEI Biosciences). SIS

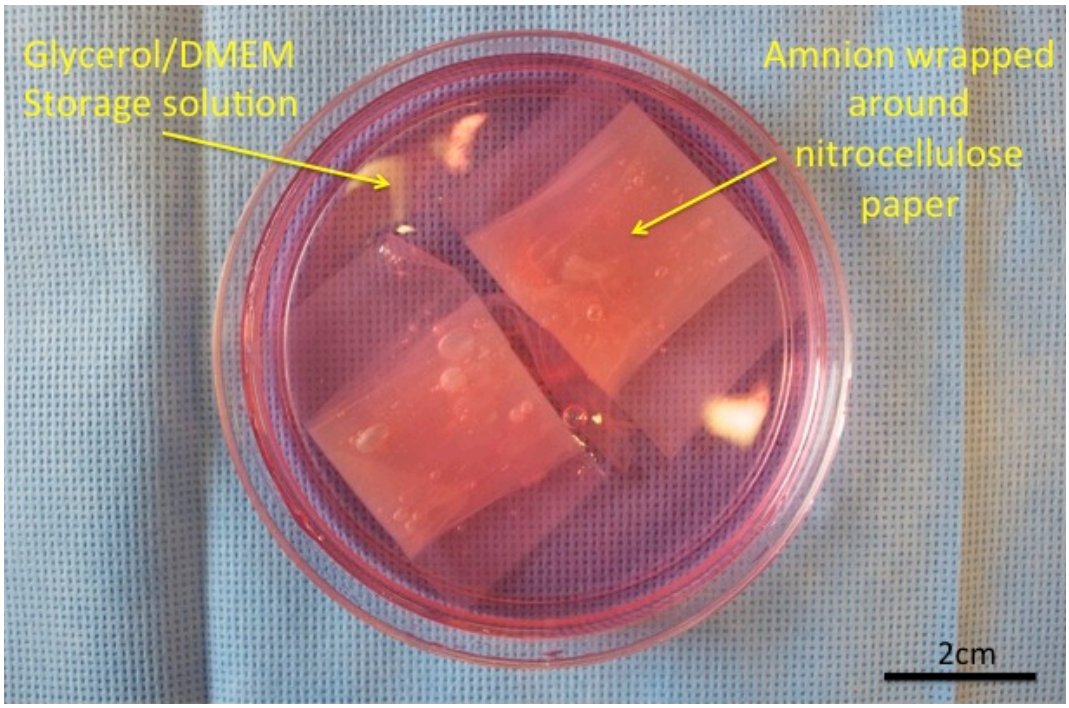

Figure 4. De-epithelialised amnion wrapped around nitrocellulose paper. Amnion is immersed in a storage medium consisting of a 1:1 mix of 100% sterile glycerol and DMEM, penicillin-streptomycin-neomycin and amphotericin B. Amnion is frozen at -80°C and thawed prior to use.

materials included a mutli-layer product (AxoGuard by AxoGen) and a single layer product (Oasis wound dressing by HealthPoint Biotherapeutics). All products were studied under the operating microscope to assess their suitability for photochemical bonding and use in the *in vivo* phase of the study. Particular attention was paid to the assessment of material thickness, material stiffness, memory and the ability to wrap around the small diameter rodent sciatic nerve, and the transparency of the material. In order to ensure close apposition between wrap and nerve, the material had to be extremely thin and lack any inherent memory preventing circumferential wrapping. The material also needed to be transparent to allow light penetration for bonding. Any materials not satisfying these strict inclusion criteria were

dismissed from further assessment. A thorough biomechanical assessment was performed only on those materials selected for *in vivo* experiments.

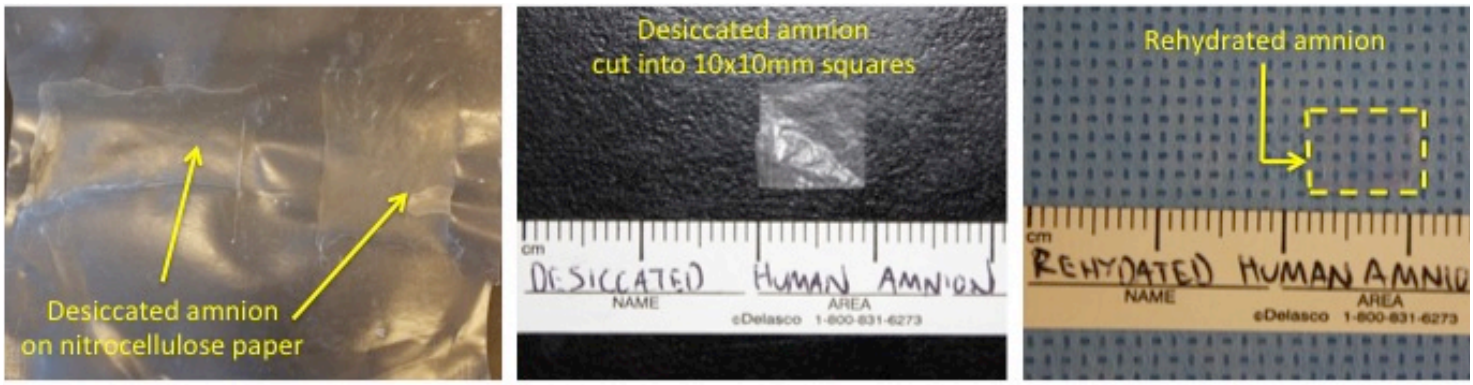

Figure 5. Desiccated and rehydrated amnion wraps. Once thawed, amnion was spread out onto nitrocellulose paper and allowed to dry. Once dry, amnion was cut into 10x10mm squares. Amnion wraps were stored in the refrigerator until required. Note the transparency following rehydration.

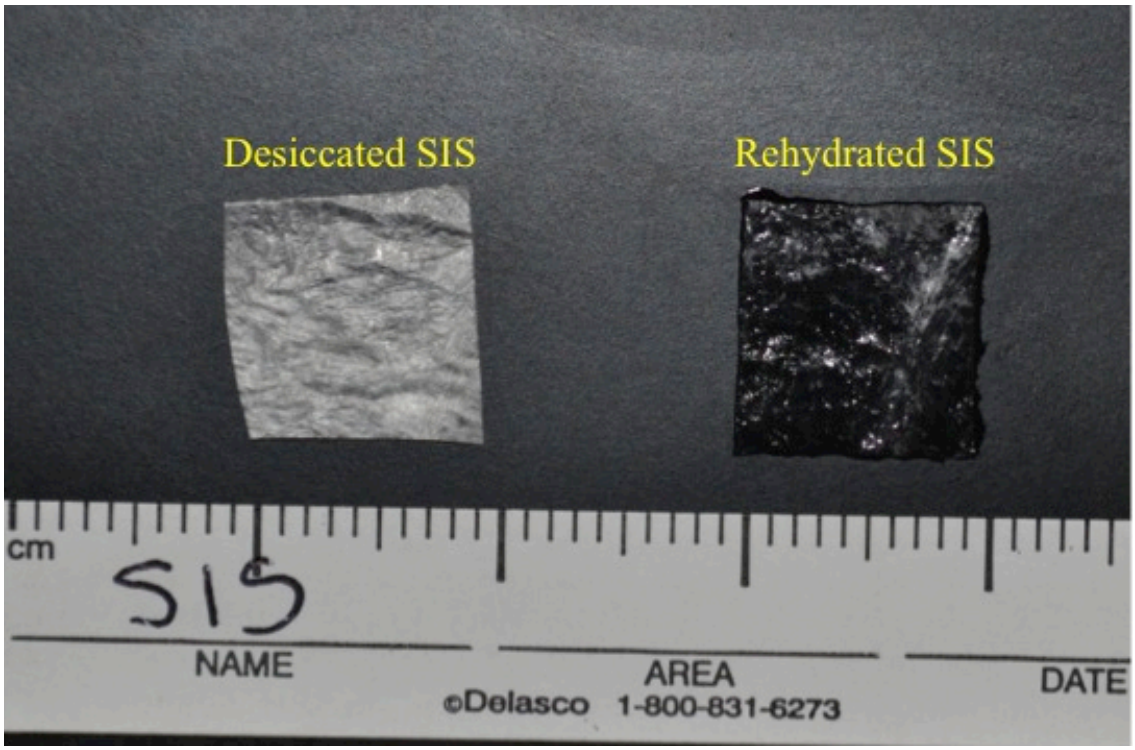

Figure 6. Desiccated and rehydrated SIS wraps. SIS was taken directly from sealed packet and cut into 10x10mm squares. As with amnion, note the transparency of the material following rehydration, an important characteristic facilitating light penetration.

2.1.1.3 Swine intestinal submucosa (SIS)

Single layer SIS material was obtained from HealthPoint Biotherapeutics Ltd. (Fort Worth, TX). This dehydrated material was removed from packaging and cut into 1x1cm sections prior to use (figure 6).

2.1.2 Nerve wrap crosslinking

A 0.05M stock solution of 2-(N-morpholino) ethanesulfonic acid (MES; Sigma-Aldrich, Co., St Louis, Mo) buffer was made by adding 9.76g of MES to 1L distilled water. To this buffer, EDC EDC (1-ethyl-3-(3-dimethylaminopropyl) carbodiimide/NHS (N-hydroxysuccinimide)) (Sigma-Aldrich, Co., St Louis, Mo) and NHS (Sigma-Aldrich, Co., St Louis, Mo) were added to arrive at four different crosslinker concentrations: 1mM EDC/0.25mM NHS, 2mM EDC/0.5mM NHS, 4mM EDC/1mM NHS, 8mM EDC/1mM NHS. Thawed amnion was washed thoroughly as described above in order to remove all trace of storage medium. Segments of amnion were added to separate petri dishes containing each crosslinking solution and were left on a platform shaker for 1-hour. Following crosslinking, the segments of amnion were washed three times with PBS and placed onto nitrocellulose paper to dry (figure 7). Once dry, the crosslinked amnion was cut into 1x1cm squares in preparation for biomechanical testing. The process was repeated for 1x1cm squares of SIS material.

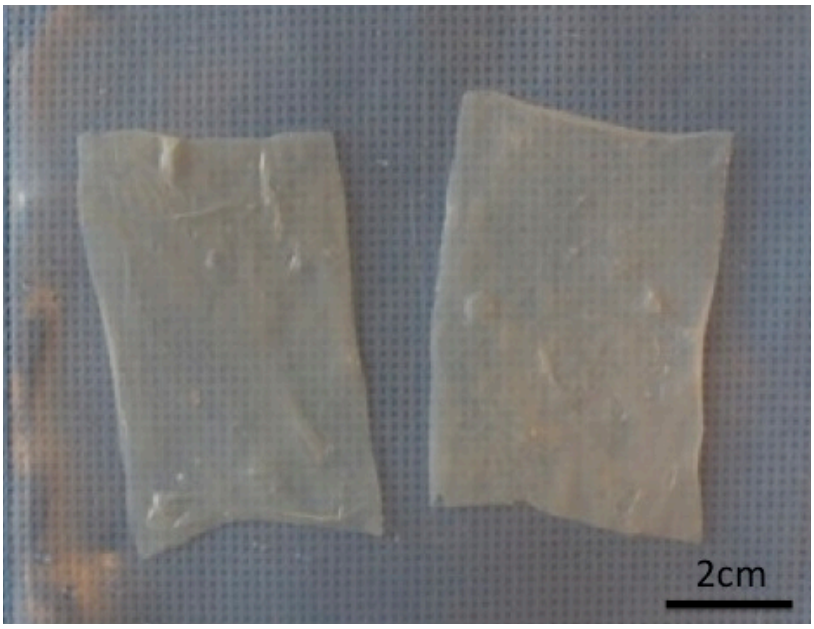

Figure 7. Crosslinked amniotic membrane. After immersion in EDC/NHS, amnion was grossly different. Amnion became more opaque and on palpation, the material felt stronger than untreated, rehydrated amnion.

2.1.3 In vivo rodent sciatic nerve injury and reconstruction

The Institutional Animal Care and Use Committee (IACUC) at the Massachusetts General Hospital and the Animal Care and Use Review Office (ACURO) at the United States Army Medical Research and Command (USAMRC) approved all procedures. Male, inbred Lewis rats weighing 250-300g were used for all experiments. This breed was selected in order to permit immunotolerant isograft exchange between rodents for nerve gap reconstruction. Induction and maintenance anesthesia was achieved using isoflurane (Baxter Healthcare Corp. Deerfield IL; 5% induction/2-3% maintenance). Two surgeons performed all procedures together. The lead surgeon (N.G.F) was a senior plastic surgery trainee experienced in microsurgical technique. The second surgeon was a general surgical trainee (J.N.G) who received microsurgical training prior to rodent surgeries. A dorsolateral, muscle-splitting incision was made on the left hindquarter of each animal. Under the operating microscope, the sciatic nerve was mobilized along its length and marked 5mm proximal to

the trifurcation. Using digital calipers, nerve grafts measuring 15mm proximal to this mark were excised, reversed and exchanged between two simultaneously anesthetized animals (figure 8).

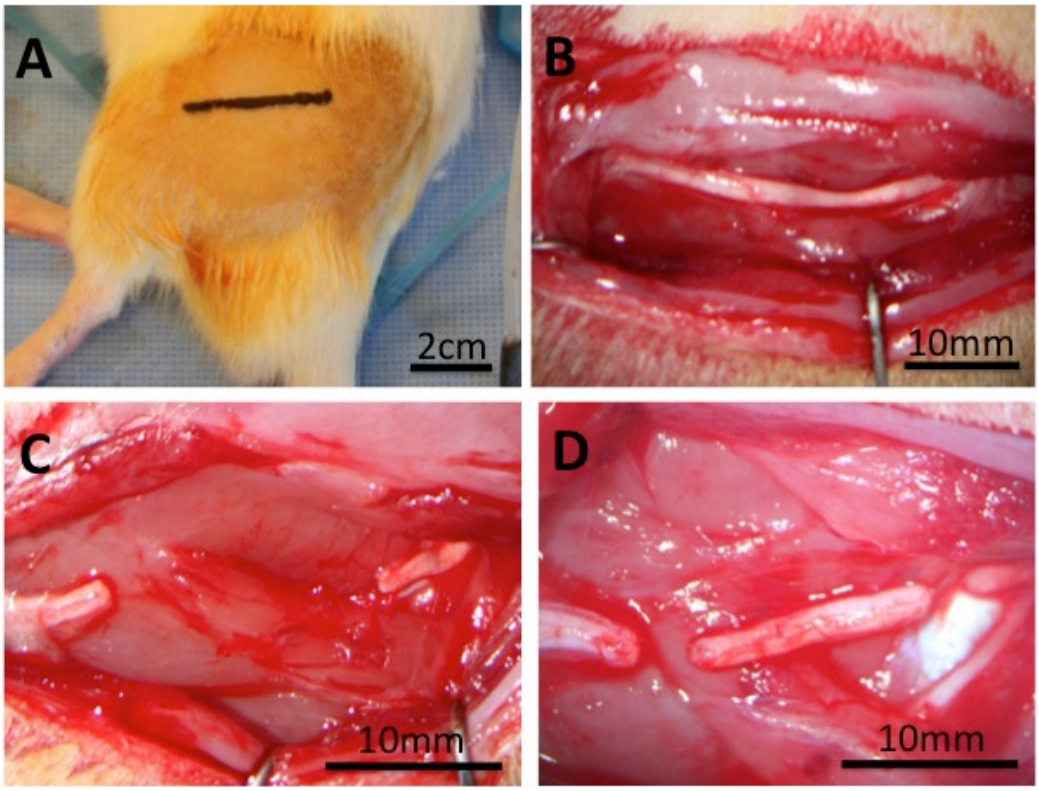

Figure 8. Rodent sciatic nerve exposure and exchange of nerve grafts. (A) Dorsolateral incision on hindlimb of rodent. (B) Muscle splitting incision and freeing of sciatic nerve from investing connective tissue. (C) Excison of 15mm length of sciatic nerve from a point 5mm proximal to trifurcation of nerve. (D) reversal of nerve harvested nerve graft and transfer into wound of adjacent simultaneously anaesthetised rodent.

For reconstructions using ANA, sections of excised sciatic nerve were simply discarded. For experiments involving delayed reconstruction, sections of nerve were discarded and proximal nerve ends buried into adjacent muscle. In these cases, reconstruction following surgical delay was performed using freshly harvested donor sciatic nerves from Sprague Dawley rats. All wounds were closed with 4.0 vicryl (muscle and deep dermal) and 4.0 monocryl

(subcuticular). Topical antibacterial ointment was applied to wounds in order to reduce the incidence of post-operative infection and bitter apple sprayed onto ipsilateral feet to reduce the incidence of automutilation. Rodents were housed in the Massachusetts General Hospital small animal facility and had access to food and water ad libitum.

2.2 Experiment specific Methods

2.2.1 Experiment 1: Ex vivo biomechanical assessment of nerve wrap biomaterials

Maximum load to failure and Young's modulus of amnion was measured using a horizontal tensiometer (MTESTQuattro, ADMET, Norwood Ma) equipped with a 10N load cell (figure 9). 10x10mm sections of untreated and crosslinked amnion (n=5) and SIS were rehydrated and secured between tensiometer crossheads. Crossheads consisted of parallel grips mounted with sandpaper to aid nerve wrap gripping. Crossheads were separated at a rate of 2mm per minute until material failure occurred. Material thickness was assumed to be 50μm for amnion and 100μm for SIS. This information was entered into tensiometer data fields in order to allow MTEST Quattro software to calculate material cross-sectional area, stress, strain and Youngs modulus. During testing, hydration of samples was maintained by aerosolized sterile water. All testing took place at room temperature.

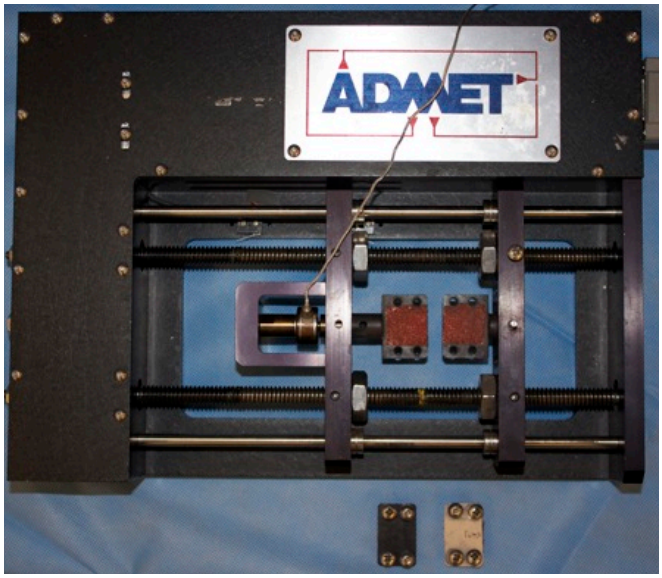

Figure 9. ADMET MTESTQuattro tensiometer. Biological wraps and photochemically bonded nerve/wrap interfaces were placed in between opposing crossheads. One crosshead was mounted to a 10N load cell. Tissues were secured using mounted plates screwed in placed. Emery paper provided additional traction.

2.2.2 Experiment 2: Type-2 collagenase degradation of nerve wrap biomaterials

2.2.2.1 Gross degradation test

Samples of crosslinked amnion and SIS material of uniform weight were prepared and digested in 15mls 0.1% type-2 (Clostridium histolyticum) collagenase (Worthington Biochemical Corp., Lakewood, NJ). Samples were grossly observed every 15 minutes until complete digestion had occurred or it became apparent that digestion was not going to occur within 24 hours.

2.2.2.2 Fluorescamine degradation assay

Samples of crosslinked amnion and SIS of uniform weight were prepared and digested in 0.1% type 2 (Clostridium histolyticum) collagenase (Worthington Biochemical Corp., Lakewood, NJ). At sequential predetermined time points, 100µL of each sample solution was

diluted to 1:100. 50µL of each diluted digestion solution was then added to wells on a 96 well plate. To each well was added 160µL of 10mM $NaBO_4$. After the addition of 90µL of 0.25% fluorescamine (in acetonitrile), sample excitation was achieved by irradiating each well with a 405nm light source. Fluorescence intensity was detected in a plate reader at 470nm. From this data, micromolar mass of liberated protein per 1mg of amnion and SIS was calculated by computer software associated with the plate reader. Untreated samples were not investigated by fluorescamine degradation due to the very rapid degradation identified on gross observation tests.

2.2.3 Experiment 3: Ex vivo uniaxial bond strength between rat sciatic nerve and candidate nerve wraps

Rat sciatic nerves were harvested from 300g adult male Sprague Dawley rats (Charles River Laboratories, Wilmington Ma). Nerves were cut into 1cm sections. 1x1cm sections of candidate nerve wraps were stained with 0.1% (w/v) Rose Bengal (RB) (Sigma-Aldrich, Co., St Louis, Mo) for 60 seconds. Under 3.2x loupe magnification, RB-stained wraps were wrapped circumferentially around RB-stained rat sciatic nerves ensuring that a minimum of 5mm overlap existed (figure 10). The area of overlap was irradiated for 1 minute using a 532nm KTP laser (Laserscope, Orchard Dr, San Jose, Ca) at an irradiance of $0.5W/cm^2$ (figure 11A). After 60 seconds, the nerve/wrap overlap was rotated 180° in order to irradiate the back wall for an additional 60 seconds. Following irradiation, nerve/wrap specimens were placed between tensiometer crossheads and distracted until bond failure, as described above (figure 11B). Load to failure was also assessed for uninjured rat sciatic nerves and also for nerves that had undergone clinically relevant repairs using fibrin glue and epineurial suturing using both four and six 10-0 ethilon sutures.

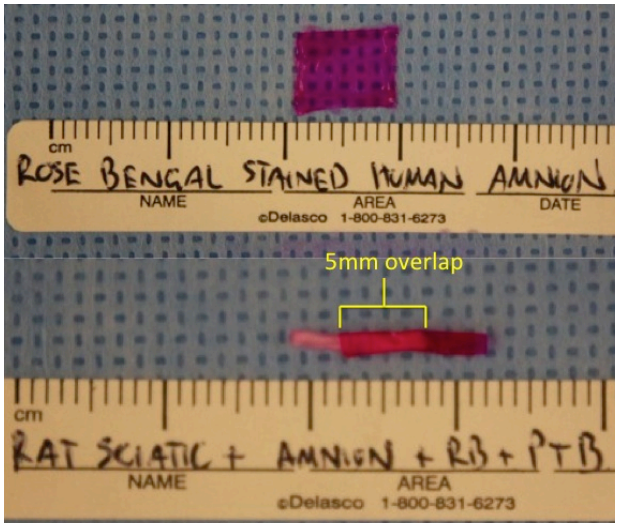

Figure 10. RB-stained amnion wrap and circumferential wrapping around RB-stained rat sciatic nerve

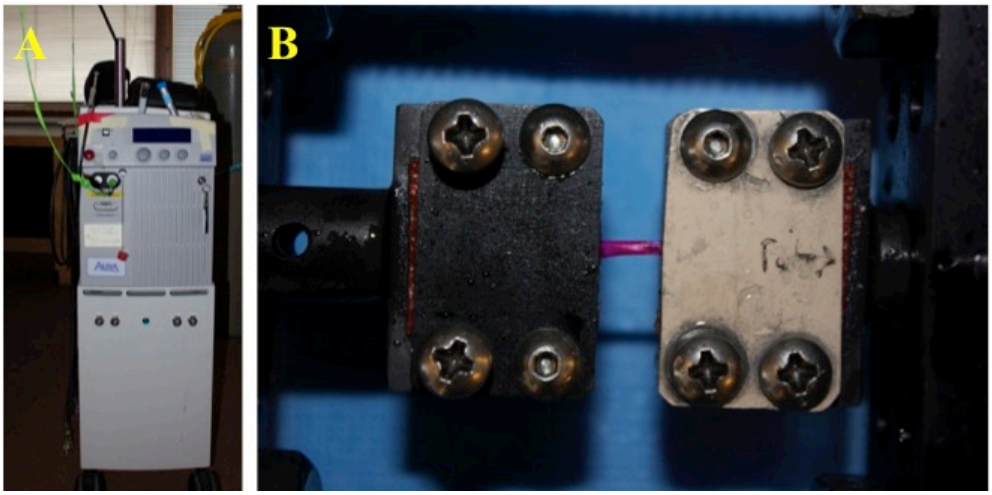

Figure 11. KTP laser unit and assessment of uniaxial bond strength of nerve/wrap bonds. (A) Light was delivered from the laser unit through an optical fiber. Power output was manually set on the laser unit and the actual output from the fiber measured by a power meter. Periodically, the optical fiber had its external cladding stripped and was cut in order to ensure that a uniform beam of light was emitted. (B) Following light activated sealing, the nerve/wrap preparation was placed in between tensiometer crossheads and was distracted as described above.

2.2.4 Experiment 4: The effects of amniotic membrane surface (epithelial or chorionic surface) on photochemical bonding

Rodent sciatic nerves and amnion were prepared as described above. Under loupe magnification, two groups of nerves (n=5) had amnion bonded either with the epithelial surface or the chorionic surface. The nerve/wrap interface was illuminated using the parameters described above and bond strengths were assessed by distraction in the tensiometer.

2.2.5 Experiment 5: Assessment of laser fluence dose response on photochemical bonding

Rodent sciatic nerves and amnion wraps were prepared as described above. Under loupe magnification, amnion was wrapped circumferentially around nerves and was illuminated as described above. Four groups of nerves (n=5) were bonded using a laser fluence of 0, 30, 60, 120 and 240 J/cm^2. Bond strength was evaluated by distracting each repair in the tensiometer as described above. A fluence of zero (no illumination) was tested with and without RB staining.

2.2.6 Experiment 6: In vivo evaluation of optimal nerve wrap and fixation method for reconstruction of large gap rodent sciatic nerve repair

Nerve wrap biomaterials were prepared as described. 110 rodents were randomized into 11 groups (n=10). Two groups served as positive (6-epineurial sutures) and negative (no repair) controls. The remaining nine groups had nerves reconstructed using different combinations of the three different nerve wraps and three different fixation methods (figure 12).

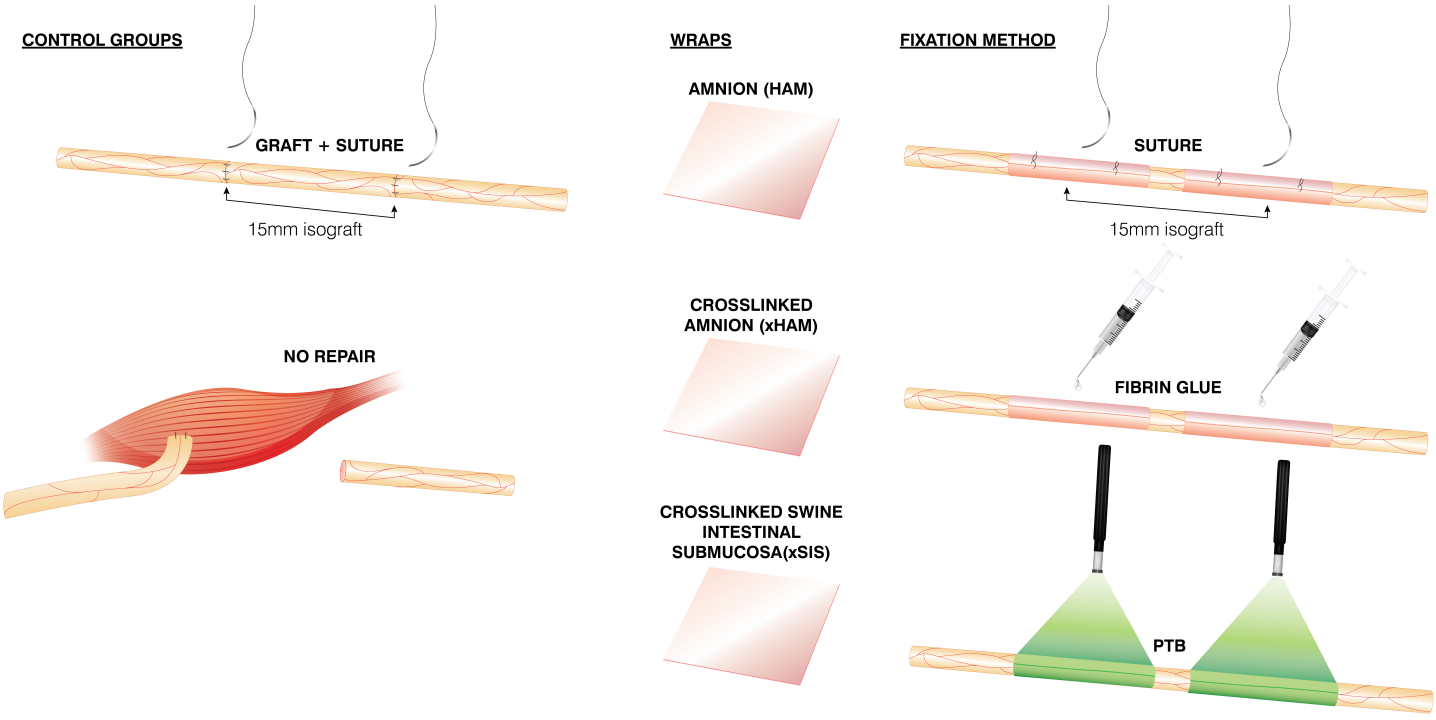

Figure 12. Schematic of treatment groups for in vivo isograft phase. Positive controls had 15mm nerve isografts repaired using conventional 10-0 epineurial suture. Negative controls had nerve sections excised and proximal ends buried into muscle. Distal ends were left free. The remaining nine treatment groups had isografts secured using different combinations of the three different nerve wraps and three different fixation methods.

2.2.6.1 Group 1: Negative control (n=10)

Following the creation of nerve defects, a small incision was made in adjacent muscle. Proximal nerve ends were sutured into muscle pockets using two 10.0 Ethilon sutures (Ethicon, Sommerville, NJ). Distal nerve ends were left free (figure 13).

2.2.6.2 Group 2: Positive control (n=10)

Following nerve exchange, grafts were secured with six 10.0 epineurial sutures at each neurorrhaphy site. Following repair, any axons protruding from the repair site were trimmed (figure 13).

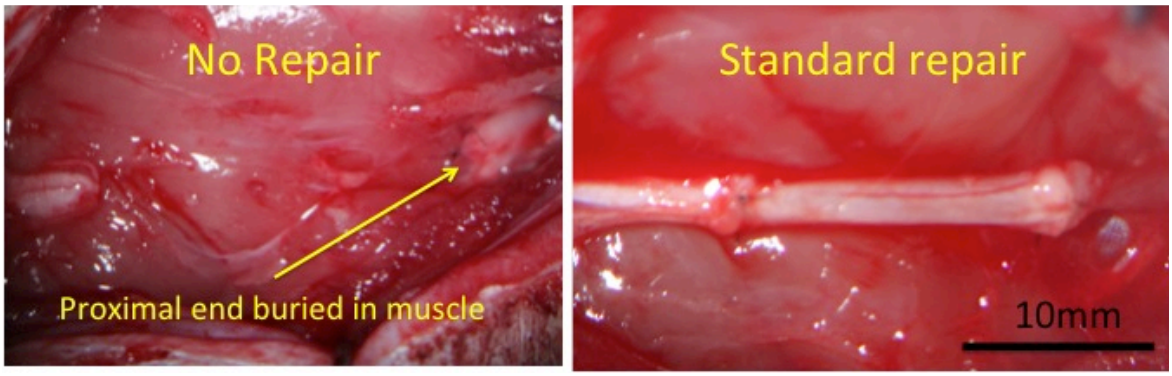

Figure 13. Control groups. Negative control group had nerve sections excised and proximal ends buried into adjacent muscle. Positive control group had 15mm reversed isografts secured with six 10-0 epineurial sutures.

2.2.6.3 Suture fixation (n=10) – groups 3, 4, 5

Candidate nerve wraps were prepared as described. Following nerve graft exchange, each graft was secured into the defect using two 10.0 nylon sutures at each end. Nerve wraps were rehydrated for 60 seconds in PBS before being removed from nitrocellulose paper and transferred into the surgical field. Once applied circumferentially at each repair site, wraps were secured with one proximal and one distal 10.0 suture (figure 14). Great care was taken to include only the wrap and the underlying epineurium in each bite.

2.2.6.4 Fibrin glue fixation (n=10) – groups 6, 7, 8

Wraps were prepared and nerve grafts tacked into place as described above. Following wrap application, Tisseel fibrin glue (Baxter Healthcare Corp. Deerfield IL) was applied to each nerve wrap interface, ensuring that the entire wrap was covered in glue (figure 14).

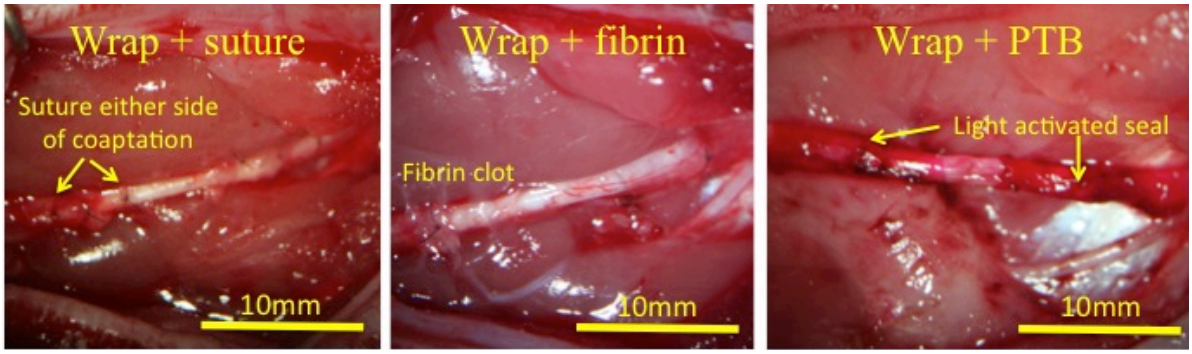

Figure 14. Methods of nerve wrap fixation. Wraps secured with suture had two tacking sutures placed either side of each coaptation site. Wraps secured with fibrin had glue applied all around coaptation sites, ensuring that the entire wrap was covered. Bonded wraps had amnion wrapped and sealed as described in the text

2.2.6.5 PTB fixation (n=10) – groups 9, 10, 11

Wraps were prepared and nerve grafts tacked into place as described above. Prior to transfer into the surgical field, wraps and neurorrhaphy sites were stained with 0.1% (w/v) RB for 60 seconds. After 60 seconds, excess dye was removed. RB-stained wraps were removed from nitrocellulose paper and wrapped circumferentially around sciatic nerves, ensuring that a minimum of 5mm overlap existed (figure 14 and 15). The area of overlap was irradiated for 60-seconds using the same laser parameters as previously described. The nerve/wrap was then rotated 180° in order to irradiate the back wall in the same manner for an additional 60-seconds.

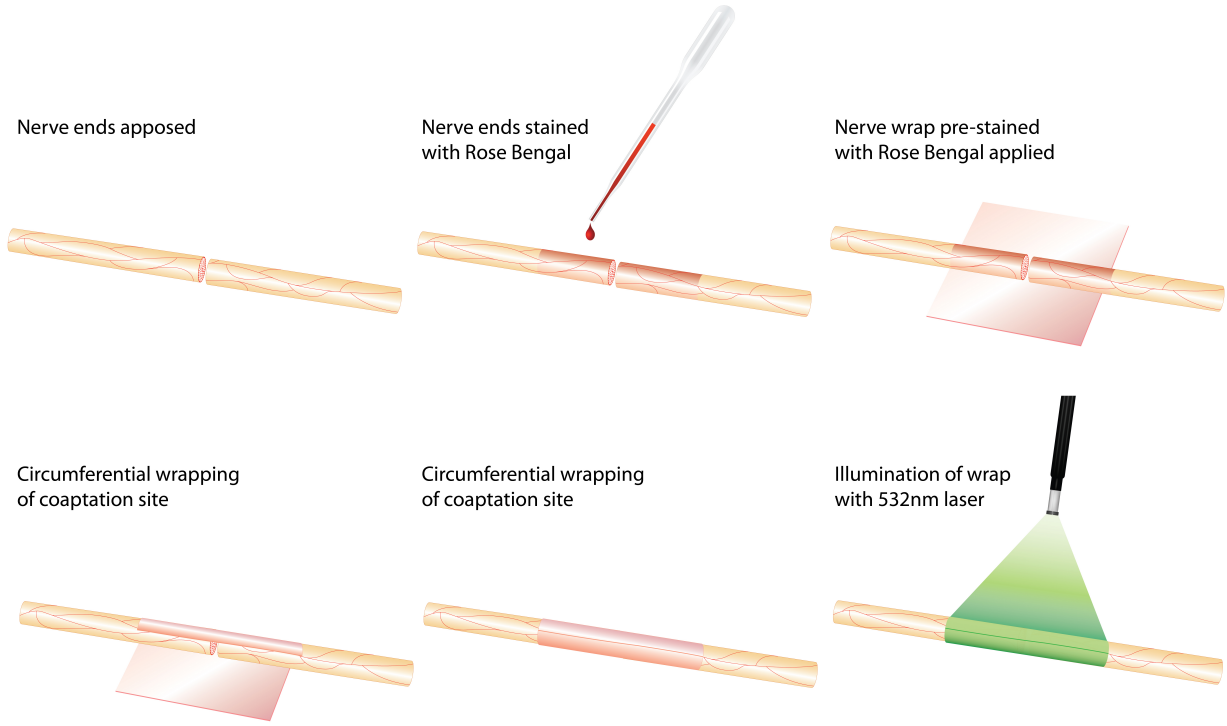

Figure 15. Schematic of light-activated sealing technique. Transected nerve ends are apposed. Two 10-0 tacking sutures are used to overcome any tension between nerve ends. Nerve ends are stained with RB photoactive dye for 60 seconds. 10x10mm nerve wrap is also stained with RB for 60 seconds. Circumferential wrapping of biomaterial is followed by illumination with 532nm KTP laser. Once the anterior wall has been illuminated for 60 seconds, the nerve is rotated 180° and the posterior wall is illuminated for 60 seconds.

2.2.7 Experiment 7: In vivo light-activated sealing of nerve graft coaptation sites using acellular nerve allograft (ANA)

2.2.7.1 Nerve allograft preparation

Sprague Dawley rats provided donor sciatic nerves. The entire length of nerve from sciatic notch to distal trifurcation was harvested. Over-dissection of the nerve was avoided to prevent inadvertent structural damage. Following harvest, nerves were cleaned of gross contaminants, placed in PBS and stored at -80°C before being shipped to AxoGen

Laboratories for detergent-based decellularization and sterilization. Once processed, nerves were returned and stored at -80°C until the day of surgery.

2.2.7.2 Sciatic nerve injury and reconstruction

Twenty male inbred Lewis rats weighing 250-300g were randomized into two groups (figure 16). In 1 group (n=10), nerve gaps were repaired using allografts secured with conventional epineurial suture. In the remaining group (n=10), nerves were repaired using allografts secured with photochemically sealed xHAM.

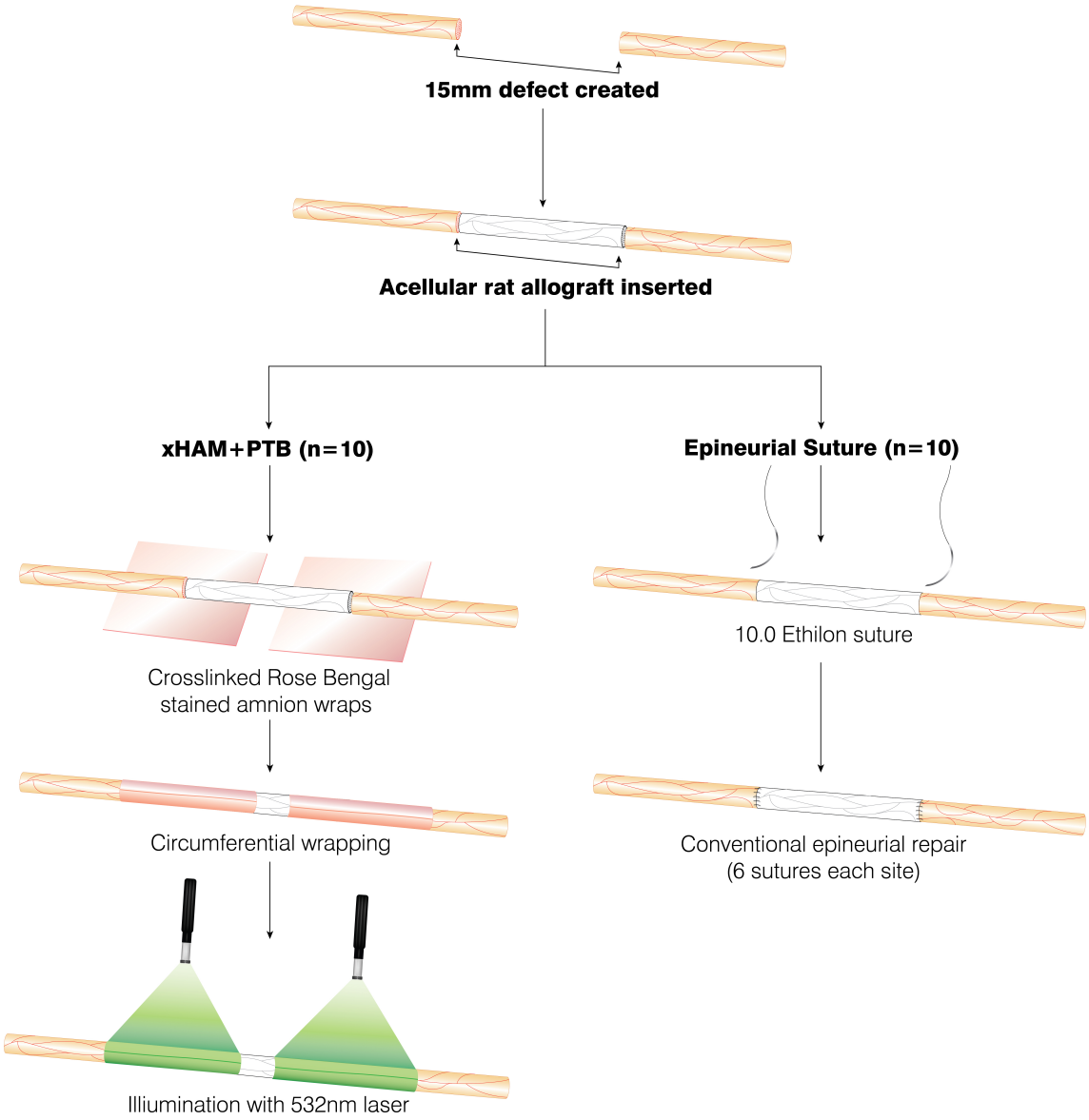

Figure 16. Schematic of treatment groups for in vivo ANA phase. 15mm sections of rat sciatic nerve were excised. These gaps were bridged with 15mm ANA. ANA was secured with either conventional 10-0 epineurial suture or light activated sealing.

2.2.7.3 Group 1- ANA+epineurial suture

Prior to anesthesia, allografts were thawed in a 37°C water bath. Following the excision of 15mm of sciatic nerve, allografts were placed into the field and cut to length. Grafts were secured with six 10.0 epineurial sutures at each site. Following repair, any protruding axons were trimmed and allowed to retract inside the repair (figure 17).

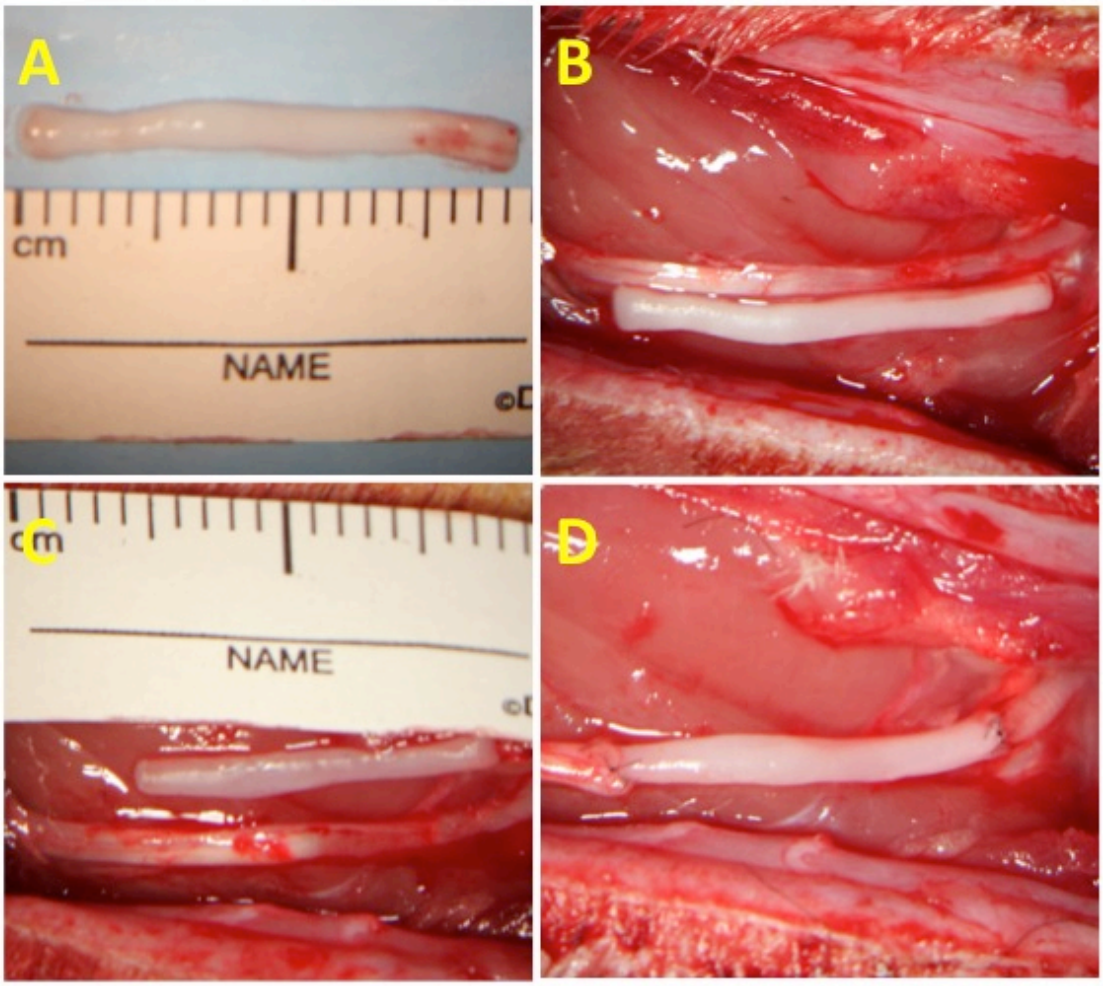

Figure 17 Conventional suture fixation of ANA. (A) ANA was in excess of 15mm. (B) Note the brilliant white appearance of freshly thawed ANA in comparison to normal nerve. (C) ANA trimmed to 15mm. (D) 15mm section of native nerve excised to create gap. Gap bridged with 15mm ANA graft.

2.2.7.4 Group 2 - ANA+PTB

Crosslinked amnion and nerve allografts were prepared as described above. Nerve grafts were tacked into place using two 10.0 epineurial sutures at each coaptation site. Prior to transfer into the surgical field, wraps and coaptation sites were stained with 0.1% RB for 60 seconds. After 60 seconds, excess dye was removed. RB-stained wraps were wrapped circumferentially around sciatic nerves, creating a 5mm overlap either side of the coaptation. The area of overlap was irradiated for 60-seconds using the same light source and parameters previously described. The nerve/wrap was then rotated 180° in order to irradiate the back wall in the same manner for an additional 60-seconds (Figure 18).

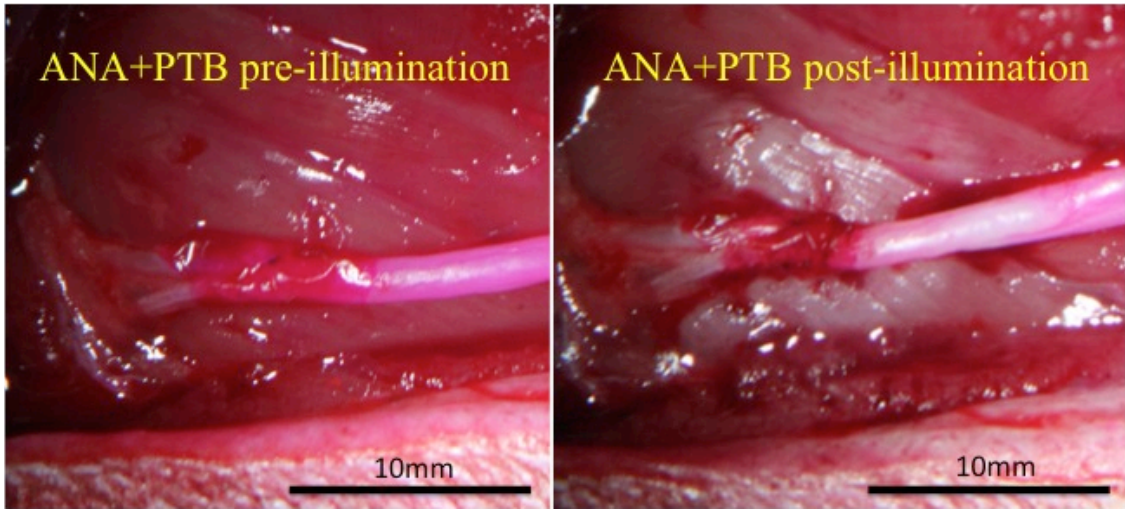

Figure 18. Light activated sealing of ANA with amnion nerve wrap. ANA grafts before and after light activated sealing.

2.2.8 Experiment 8: Immediate versus delayed repair of large gap peripheral nerve injury using light-activated sealing of human amnion nerve wraps around nerve graft coaptation sites

2.2.8.1 Sciatic nerve injury and reconstruction

Forty inbred Lewis rats weighing 250-300g were randomized to one of four experimental groups described below. A further ten Lewis rats were used as isograft donors. Groups 1 and 2 had nerve gaps repaired immediately whereas groups 3 and 4 had nerve gaps repaired following a 30-day delay (figure 19).

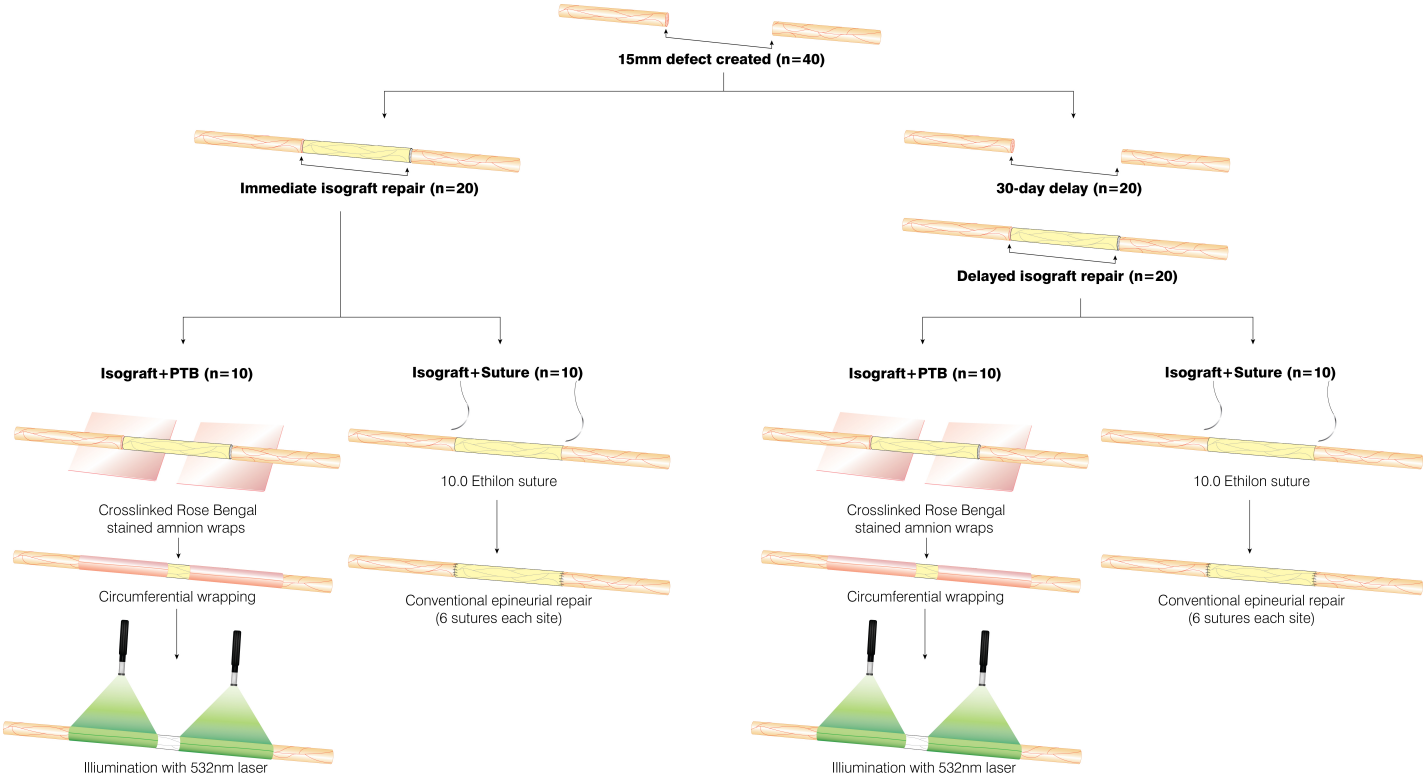

Figure 19. Schematic of treatment groups for immediate versus delayed isograft phase. 15mm gaps were created in rat sciatic nerves. These gaps were repaired using isografts either immediately or after a 30-day delay. Isografts were secured using either conventional 10-0 epineurial suture or light activated sealing

2.2.8.2 Immediate repair: Groups 1 and 2

Two rodents were anaesthetized simultaneously. Following the excision of 15mm segments of sciatic nerve, nerves were reversed and immediately exchanged as isografts between animals. In group 1, isografts were secured using six 10.0 Ethilon suture (Ethicon, Sommerville, NJ), representing the current standard of care. Following repair, any protruding axons were trimmed and allowed to retract within the coaptation site. In Group 2, isografts were secured using photochemical sealing. Amnion nerve wraps were prepared as described above.

2.2.8.3 Delayed Repair: Groups 3 and 4

Following the creation of 15mm sciatic nerve defects, a small incision was made in adjacent muscle and proximal nerve ends were buried and secured using two 10.0 Ethilon sutures. Distal nerve ends were left free. Wounds were closed as described and the animal returned to the animal facility. After 30-days, animals were re-anaesthetised. Wounds were re-opened and nerve ends dissected and mobilized. Simultaneously, fresh isografts were harvested from donor Lewis rats and immediately reversed and transferred into the nerve gap. In group 3, isografts were secured with 10.0 Ethilon suture and in group 4, isografts were sealed photochemically as previously described.

2.3 Outcome assessment

2.3.1 Walking track analysis

Walking track analysis was performed immediately prior to surgery for baseline SFI. Following surgery, walking track analysis was performed at 30-day intervals. After dipping both hind paws in water soluble ink, rats were encouraged to walk up a 10 x 60 cm, partially enclosed ramp lined with white paper and set at an incline of 30° to horizontal. Measurements of print length, toe spread and intermediary toe spread were measured from the resulting prints using digital calipers (figure 20). Mean values from three normal and experimental prints were entered into the SFI formula described by Bain and colleagues[256].

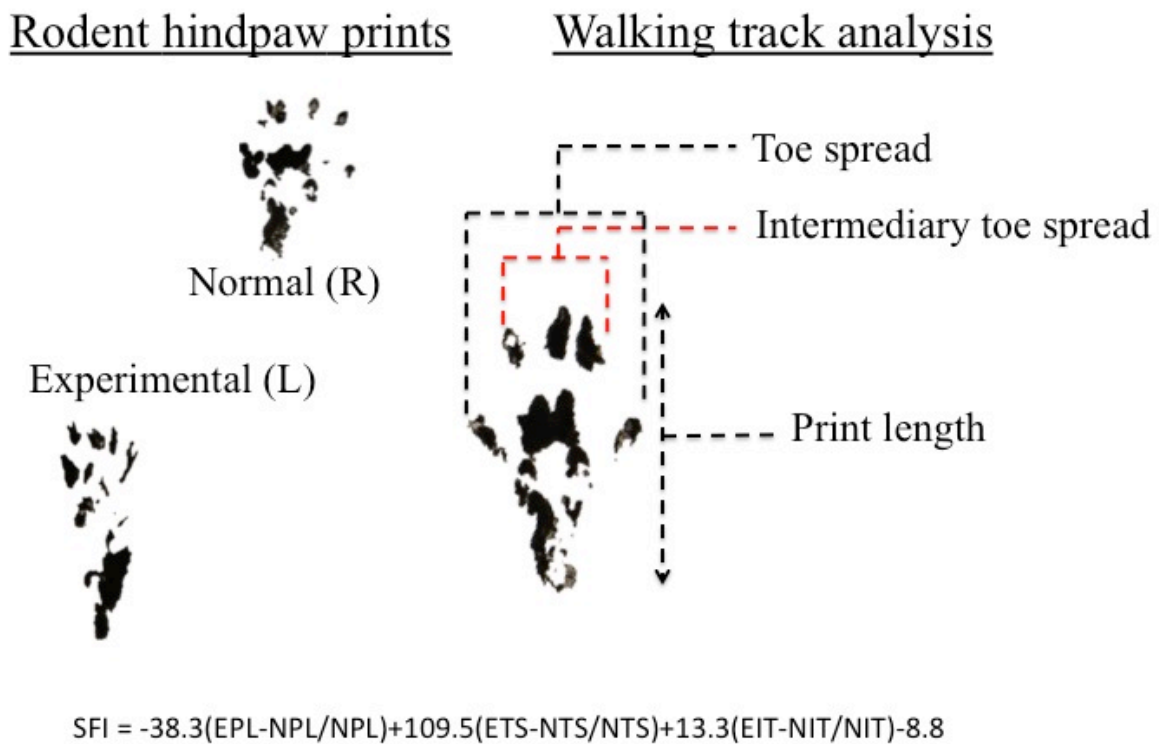

Figure 20. Walking track analysis and calculation of SFI. Rodent hindpaws that have been dipped in indelible ink leave foot prints. Both experimental (E) and normal (N) prints have toe spread (TS), intermediary toe (IT) spread and print length (PL) measured. These values are entered into the above equation to give SFI.

2.3.2 Muscle weight retention

All rodents were sacrificed 150-days post-operatively by carbon dioxide inhalation. Left and right gastrocnemius muscles were harvested. Wet weights were recorded immediately and percentage muscle mass retention calculated (see figure 21).

Figure 21. Gastrocnemius muscle mass retention. Normal right and experimental left-sided gastrocnemius muscles were excised following sacrifice. Muscle weight was measured immediately following harvest and a percentage muscle mass retention calculated. Note the obvious reduced muscle bulk in the left sided gastrocnemius.

2.3.3 Histology and histomorphometric analysis

Following sacrifice, nerves were harvested 5mm proximal and 5mm distal to the graft. In phase 1, contralateral sciatic nerves from one rat in each treatment group (n=11) were

harvested in the same region as distal graft coaptation sites. This permitted interpretation of histomorphometric results in relation to what is “normal”. Nerves were immediately fixed in a mixture of 2% glutaraldehyde/2% paraformaldehyde (Electron Microscopy Sciences, Hatfield, PA). After 48 hours, fixed nerves were washed in sodium cacodylate buffer (0.1M; pH=7.4) and post-fixed in 2% osmium tetroxide (Electron Microscopy Sciences, Hatfield, PA) for 2 hours. Following further washing in sodium cacodylate buffer, specimens were dehydrated in increasing concentrations of ethanol (25%, 50%, 75%, 95%, 100%). Following dehydration, all specimens were washed with propylene oxide (Electron Microscopy Sciences, Hatfield, PA). Specimens were then placed in increasing concentrations of Epoxy resin (DDSA (dodecyl succinic anyhydrides 98+%; Free Acid 2%)/tEPON-812 (Epoxy Resin)/NMA Ultrapure (methyl-5-norbornene-2,3-dicarboxylic anhydride)/DMP-30 (2,4,6-tri (dimethylaminomethyl) phenol (Tousimis Research Corporation, Rockville, MD) before being baked overnight in an oven at 60°C. Using a diamond blade, 1µm sections were cut 5mm distal to the graft. The lead surgeon (N.G.F) and the laboratory technician (A.M) were responsible for all fixation steps and the majority of EPON embedding. Final embedding in 100% EPON, oven baking, microtome cutting, slide mounting and staining were performed by the pathology staff.

Histology slides were digitized using a Hamamatsu NanoZoomer 2.0-HT slide scanner (Meyer Instruments, Houston TX) and read using NDP.com software (Hamamatsu Corp. Bridgewater, NJ). Images were numbered and their identity concealed during analysis. A blinded technician (A.M) manually selected in a random fashion five 400x images from each 40x slide. All 40x and 400x images were converted into JPEGs and imported into Adobe Photoshop (figure 22 and 23). Two blinded researchers (N.G.F and A.M) manually measured nerve cross sectional area from 40x images and counted axons from each 400x image. Total

counts were entered into a randomization website (randomizer.org) in order to obtain 50 random numbers. Numbered axons were then identified on each 400x image, from which fiber diameter and axon diameter were manually measured using the Photoshop measurement tool. These measurements were entered into an excel spreadsheet from which myelin thickness (fibre diameter – axon diameter) and G-ratio (axon diameter/fibre diameter) were calculated from automated formulas. This provided measurements for 250 axons per distal nerve section.

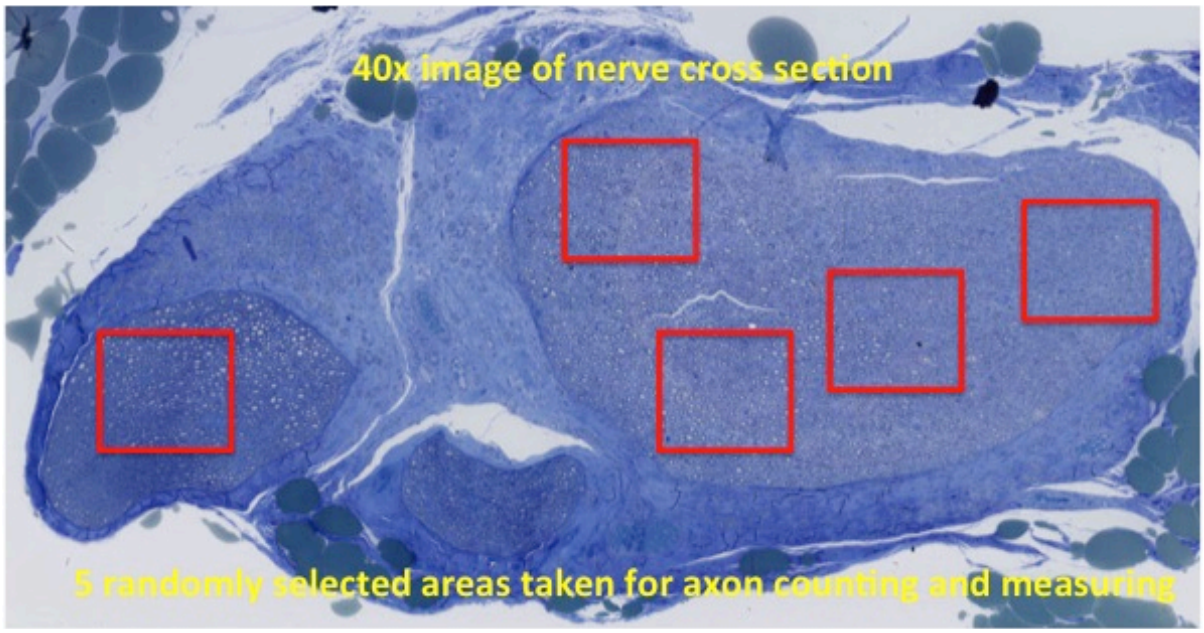

Figure 22. 40x image of isograft cross-section. From these proximal and distal images, total nerve cross sectional area was calculated and five randomly selected 400x images were taken. These images were used for axon counting and measurement of fiber and axon diameter.

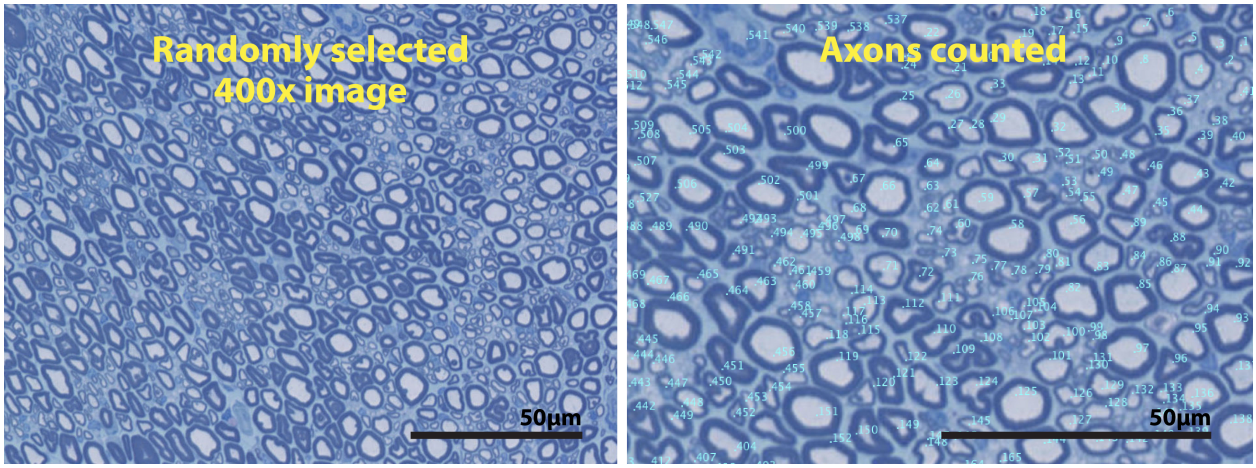

Figure 23. Randomly selected 400x images of isograft cross-sections. Images were imported into Adobe Photoshop. All axons within each image were counted. Fifty randomly selected axons then had fiber (outer diameter) and axon diameters (inner diameter) measured. Myelin thickness was calculated by subtracting axon diameter from fiber diameter.

2.3.4 Statistical analysis

All data has been expressed as mean+/- SEM. Statistical analysis was performed using KaleidaGraph for Windows v4.1 (Synergy Software, Reading, PA). For *ex vivo*, biomechanical data, a regression analysis was used to test for the effect that increasing crosslinker concentration had on maximum load to failure and Youngs modulus. Analysis of variance (ANOVA) was used to assess fluorescamine degradation and photochemical bond strengths. Statistical significance was set at $p<0.05$. For *in vivo* data, repeated measures analysis of variance and the post hoc Bonferroni test was applied to monthly SFI data. Mean values across all time points in each group were compared in order to test for the existence of significant differences over time. ANOVA and post hoc Bonferroni were also used to analyse muscle mass retention and histomorphometric variables. Statistical significance was set at $p<0.05$. In some comparisons, 95% confidence intervals were examined to assess for the

possible existence of type 2 statistical errors. Assistance with the data analysis was provided by Mr. Douglas Hayden (Harvard Catalyst) and Dr Rob Elton (University of Edinburgh).

2.3.4.1 Comparative analysis of ANA vs Isograft

In phase two, the efficacy of light activated sealing when applied to ANA is assessed. In addition to comparing light activated sealing to conventional suture as a method of fixation, a comparison is made between the performance of ANA against gold standard isograft by including data from phase one in the statistical analysis. The inclusion of isograft+PTB (n=10) and isograft+suture (n=10) groups represents historical controls from phase one and helps extend the clinical relevance of this study.

2.4 Acknowledgement

Special thanks go to Jenny Zhao, Margaret Sherwood and Megan Scanlan who very kindly assisted with the processing and preparation of nerve samples for histomorphometric analysis. Special thanks also go to Douglas Hayden and Rob Elton for their statistical advice and for performing some of the data analysis.

Section 3: Results

3.1 Generic results

3.1.1 Selection of commercially available nerve wrap biomaterial

All commercially available nerve wraps (AxoGuard, NeuraGen, NeuraWrap, NeuraMend and NeuraMatrix) were unsuitable for use with the rodent sciatic nerve (figure 24). Likewise, other materials such as TenoGlide (used to wrap tendon repairs), Colafilm, AmnioFix and SurgiMend (acellular collagen matrices used for wound dressings and soft tissue reconstruction) were also unsuitable. Single layer SIS material was found to be the most suitable product for use as a nerve wrap and was selected for *in vivo* experiments as a commercially available alternative to human amnion.

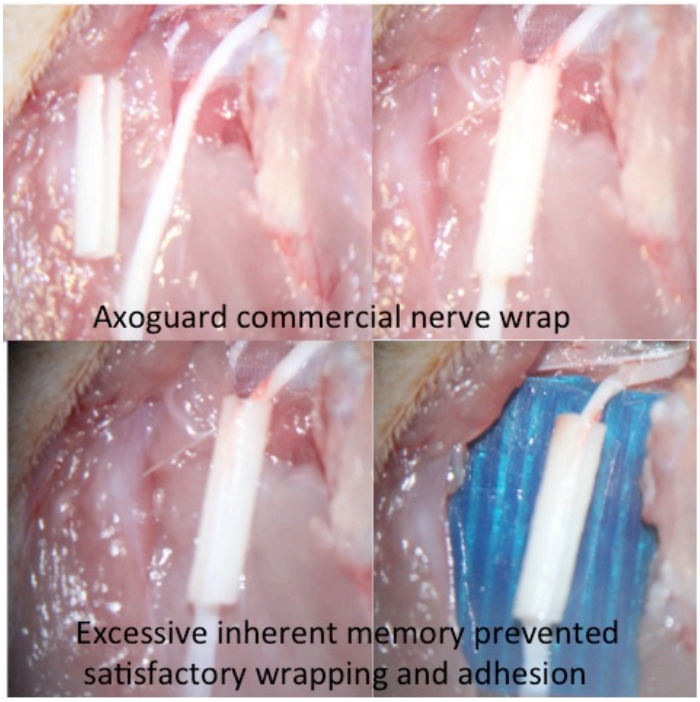

Figure 24. Example of a commercially available nerve wrap (AxoGuard). Excessive thickness, stiffness and elastic memory prevented satisfactory circumferential wrapping.

3.2 Experiment specific results

3.2.1 Experiment 1: Ex vivo biomechanical assessment of nerve wrap biomaterials

Mean maximum load to failure of untreated amnion was 0.46+/-0.05N. Maximum load to failure increased with increasing crosslinker concentration to a maximum of 0.83+/-0.06N and this result was statistically significant on regression analysis (p=0.03; table 1). Maximum load to failure for untreated SIS was 2.80+/-0.21N. With increasing crosslinker concentration, maximum load to failure increased to a maximum of 4.58+/-0.58N. This was not statistically significant on regression analysis (p=0.21; table 1). Mean Youngs modulus for untreated amnion was 4.47+/-0.55MPa and this increased with increasing crosslinker concentration to a maximum of 9.82+/-0.97 MPa. This was statistically significant on regression analysis (p<0.001; table 1). Mean Youngs modulus for untreated SIS was 16.35+/-1.33 MPa. With increasing crosslinker concentration, this increased to a maximum of 31.0+/-3.40 MPa. These results were statistically significant on regression analysis (p=0.006; table 1). No significant differences in photochemical bond strength were observed between untreated, 1mM EDC, 2mM EDC and 4mM EDC treated amnion. When EDC concentration was increased to 8mM, a significant fall in photochemical bond strength was observed (p=0.04; table 1). Due to this finding, a maximum concentration of 4mM was selected for in vivo experiments. Bond strengths using SIS were not significantly different between untreated samples and those that had been crosslinked with 1mM and 4mM EDC (table 1).

	Nerve wrap material									
	HAM					SIS				
Crosslinker conc.(mM)	A	B	C	D	E	A	B	C	D	E
Mean Max load to failure (N)	0.46 +/- 0.05	0.71 +/- 0.09	0.61 +/- 0.09	0.69 +/- 0.15	0.83 +/- 0.06	2.80 +/- 0.21	4.65 +/- 0.85	4.02 +/- 0.95	4.15 +/- 0.66	4.58 +/- 0.58
Mean Young's Modulus (MPa)	4.47 +/- 0.55	6.55 +/- 0.77	6.38 +/- 0.21	7.46 +/- 1.12	9.82 +/- 0.97	16.35 +/- 1.33	16.47 +/- 5.19	22.57 +/- 3.95	23.90 +/- 5.16	31.0 +/- 3.40
Mean Nerve/wrap bond strength (N)	0.61 +/- 0.06	0.54 +/- 0.07	0.52 +/- 0.04	0.61 +/- 0.10	0.34 +/- 0.05*	0.96 +/- 0.04	0.90 +/- 0.09	--------	1.09 +/- 0.09	--------

Table 1. Maximum load to failure, Young's modulus and uniaxial nerve/wrap bond strength for amnion and SIS nerve wraps. Each biomechanical test took place in n=5 rats. All data expressed as mean+/-SEM. A=control sample (uncrosslinked), B=1mM EDC, C=2mM EDC, D=4mM EDC, E=8mM EDC. Assessment of effect of crosslinking on maximum load to failure and Youngs modulus performed using regression analysis. Bond strengths assessed using ANOVA and post hoc Bonferroni test. *statistically significant in comparison to untreated material ($p<0.05$).

3.2.2 Experiment 2: Type-2 collagenase degradation of nerve wrap biomaterials

3.2.2.1 Gross degradation test

Untreated amnion had completely degraded within 30-45 minutes. Untreated SIS had completely degraded within 6hrs 15 minutes. All crosslinked samples were still present after 24 hours. At this point, the gross observation tests were stopped.

3.2.2.2 Fluorescamine degradation assay

Chemical crosslinking of amnion and SIS resulted in significant reductions in type-2 collagenase degradation and protein liberation. Table 2 shows liberated protein concentrations for both amnion and SIS samples following 24 hours digestion. There was no significant difference in degradation between those samples of amnion treated with 4mM EDC/1mM NHS and 8mM EDC/2mM NHS. Significant reductions in degradation were observed at all concentrations of crosslinked SIS (Table 2; figure 25).

Material	EDC (mM)	Liberated protein concentration (μM per 1mg amnion +/- SEM)		
		2hr	4hr	24hr
HAM	1	------	7.44+/-0.30	15.76+/-0.17
	2	------	2.03+/-0.19	6.60+/-0.31
	4	------	1.86+/-0.19	3.00+/-0.36
	8	------	1.33+/-0.30	3.36+/-0.29
SIS	1	1.98+/-0.14	2.95+/-0.12	4.95+/-0.10
	2	1.80+/-0.20	2.64+/-0.01	4.64+/-0.29
	4	1.06+/-0.06	2.04+/-0.02	3.04+/-0.07
	8	0.35+/-0.15	0.62+/-0.03	1.57+/-0.25

Table 2. Protein liberation from amnion and SIS when exposed to increasing concentrations of EDC. increasing EDC concentration from 1mM to 2mM led to a significant reduction in protein liberation ($p<0.0001$). Increasing from 2mM to 4mM also led to a significant reduction in protein liberation ($p<0.0001$). Increasing EDC concentration to 8mM had no further effect on protein liberation. For SIS material, no significant reduction in protein liberation was observed between 1mM and 2mM EDC. Protein liberation was significantly reduced between 2mM and 4mM ($p<0.0001$) and between 4mM and 8mM EDC ($p<0.0001$). ANOVA+post hoc Bonferroni; $p<0.05$.

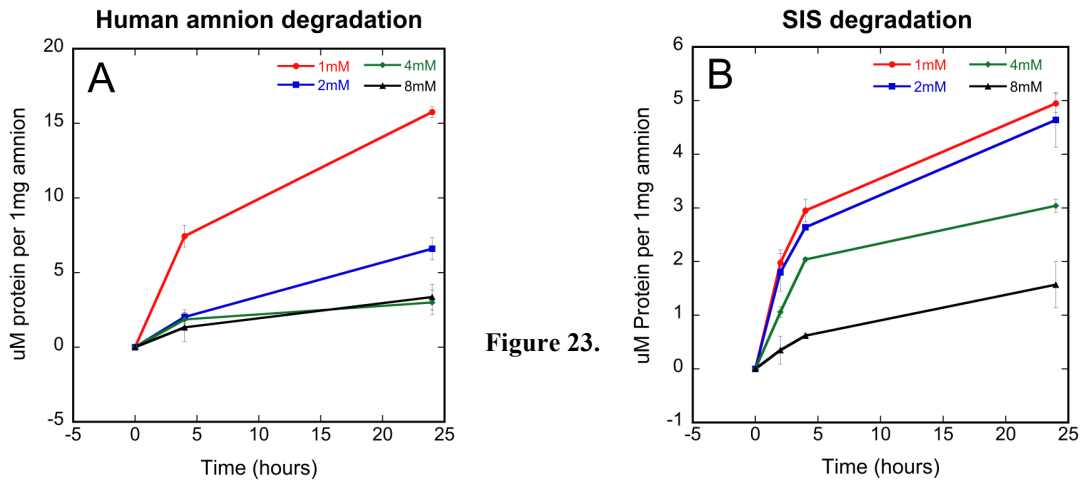

Figure 23.

Fig 25. Fluorescamine degradation assay for amnion and SIS. Different colours in the graphs refer to different concentrations of EDC: red (1mM), blue (2mM), green (4mM), black (8mM). With amnion, increasing EDC concentration from 1mM to 2mM led to a significant reduction in protein liberation ($p<0.0001$). Increasing from 2mM to 4mM also led to a significant reduction in protein liberation ($p<0.0001$). Increasing EDC concentration to 8mM had no further effect on protein liberation. For SIS material, no significant reduction in protein liberation was observed between 1mM and 2mM EDC. Protein liberation was significantly reduced between 2mM and 4mM ($p<0.0001$) and between 4mM and 8mM EDC ($p<0.0001$). Plotted data represent mean+/-SEM. ANOVA + post hoc bonferroni testing used for analysis ($p<0.05$).

3.2.3 Experiment 3: Ex vivo uniaxial bond strength between rat sciatic nerve and candidate nerve wraps

Freshly harvested, uninjured rat sciatic nerves failed under a distractive force of 3.31+/-0.55N. Sciatic nerve transections repaired exclusively with fibrin glue failed at 0.17+/-0.01N. Repairs performed using four and six 10-0 epineurial sutures failed at 0.74+/-0.03N and 1.19+/-0.08N respectively. Maximum load to failure of nerves repaired using photochemically sealed untreated amnion was 0.61+/-0.06N. No significant difference in bond strength existed when amnion was

crosslinked with 1mM, 2mM or 4mM EDC. Bond strength of photochemcially sealed amnion crosslinked with 8mM EDC was 0.34+/-0.05N and this was a significant fall in comparison to those bonds created using untreated amnion (p=0.01). Bond strength of repairs using photochemically sealed untreated SIS were 0.96+/-0.04N. This was significantly higher than bonds created with untreated amnion (p=0.003). No significant difference existed between those performed using SIS wraps crosslinked with 1mM or 4mM EDC. Bond strengths for all light activated bonds tested using amnion or SIS were all significantly poorer than repairs using six 10-0 epineurial sutures, with the exception of 4mM EDC treated SIS which was statistically equivalent (Table 1; figure 26).

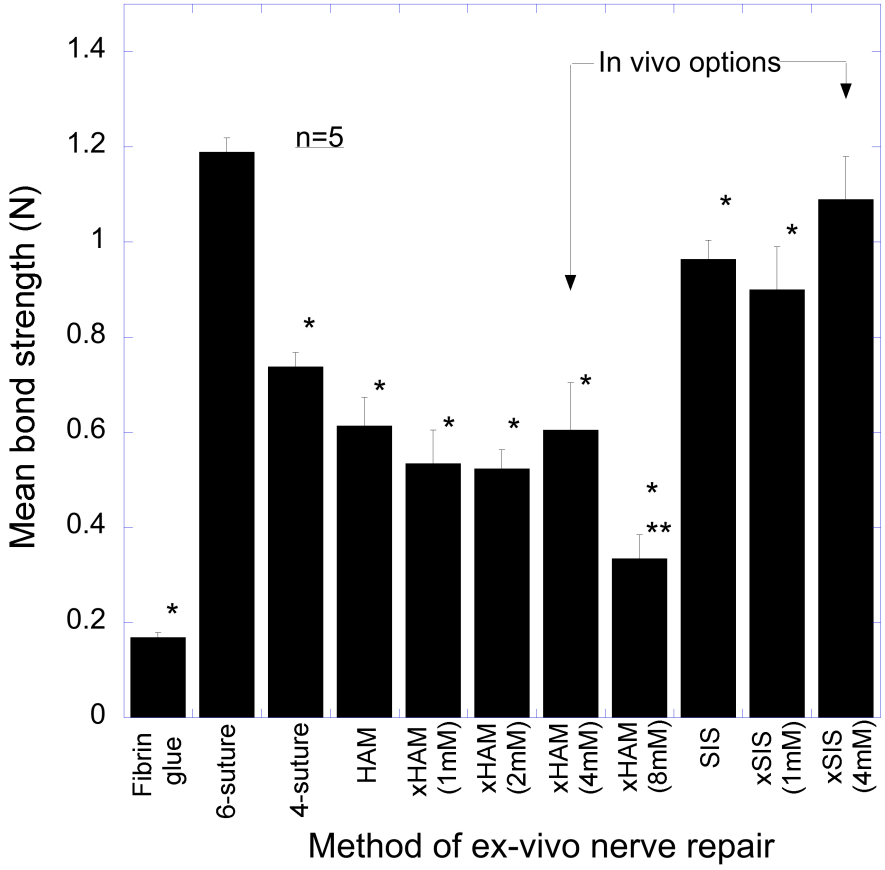

Figure 26. Mean bond strength of experimental and conventional repair methods. Clinically, nerves of 1mm diameter (digital nerves in the fingers) are usually repaired with 4-6 epineurial sutures. In comparison to the tensile strength of suture repairs using six 10-0 epineurial sutures, fibrin glue and all photochemical repairs

using crosslinked amnion resulted in weaker bonds. Bonds created with 4mM crosslinked SIS had bond strengths that were comparable to 6-suture repairs. In comparison to untreated amnion, EDC crosslinking had no significant effect on bond strength up to a maximum concentration of 4mM. Crosslinking with 8mM EDC led to a significant fall in bond strength (p=0.01). Bond strength of untreated SIS was significantly greater than untreated amnion (p=0.04). No significant difference existed between untreated amnion and 1mM xSIS. Bonds using 4mM xSIS were significantly stronger than untreated amnion (p=0.001) and 4mM xHAM (p=0.001). Data presented as mean+/-SEM. *indicates statistical significance in relation to 6-suture repair. **indicates statistical significance in relation to untreated HAM. Analysis performed using ANOVA and post hoc Bonferroni test; p=<0.05.

3.2.4 Experiment 4: The effects of amniotic membrane surface (epithelial or chorionic surface) on photochemical bonding

Mean bond strength when amnion wraps were bonded to sciatic nerve epineurium using the epithelial surface was 0.64+/-0.04N. Mean bond strength when amnion was bonded to epineurium using the chorionic surface was 0.62+/-0.08N. No significant difference existed between the two measurements (figure 27).

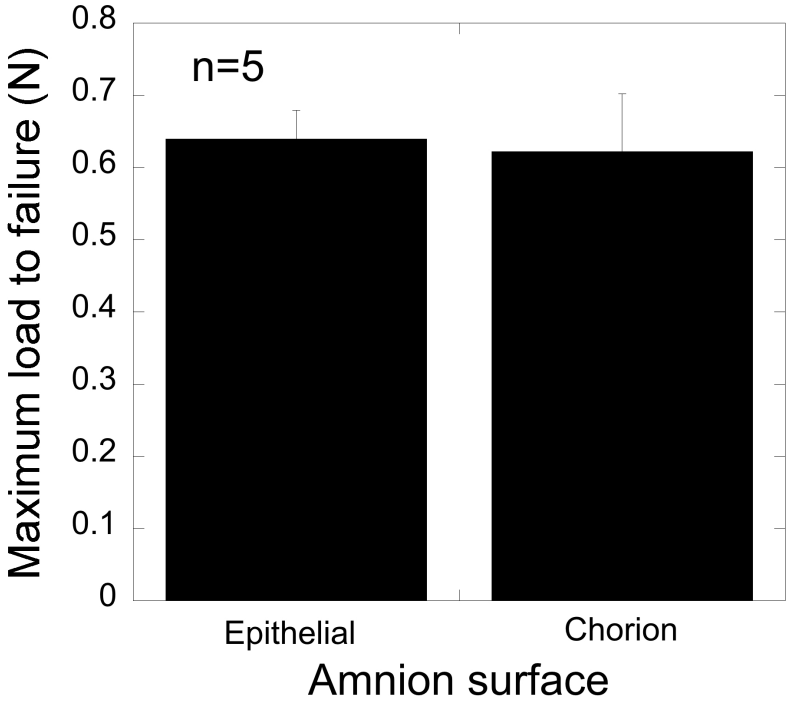

Figure 27. The influence of amnion surface on photochemical bond formation. Sciatic nerves were wrapped with amniotic membrane with either the epithelial (n=5) or chorionic (n=5) surface in apposition with epineurium. Following illumination, uniaxial bond strengths were assessed using the tensiometer. There was no significant difference in bond strength between the two options.

3.2.5 Experiment 5: Assessment of laser fluence dose response on photochemical bonding

When laser fluence is zero, bond formation does not occur. This was confirmed by tensiometer distraction of repairs that were treated with or without RB and were not illuminated with the 532nm light source (0.03+/-0.005N and 0.02+/-0.006N respectively). When laser fluence was 30J/cm^2, maximum load to failure was 0.68+/-0.03N. When fluence was increased to 60J/cm^2, maximum load to failure was 0.92+/-0.08N and this was significantly greater than bond strength obtained with 30J/cm^2 (p=0.04). Further increases of fluence to 120J/cm^2 and 240J/cm^2 had a significantly detrimental impact on the formation of photochemical bonds in comparison to 60J/cm^2 (0.69+/-0.02N (p=0.04) and 0.42+/-0.03N (p=0.002) respectively; figure 28)

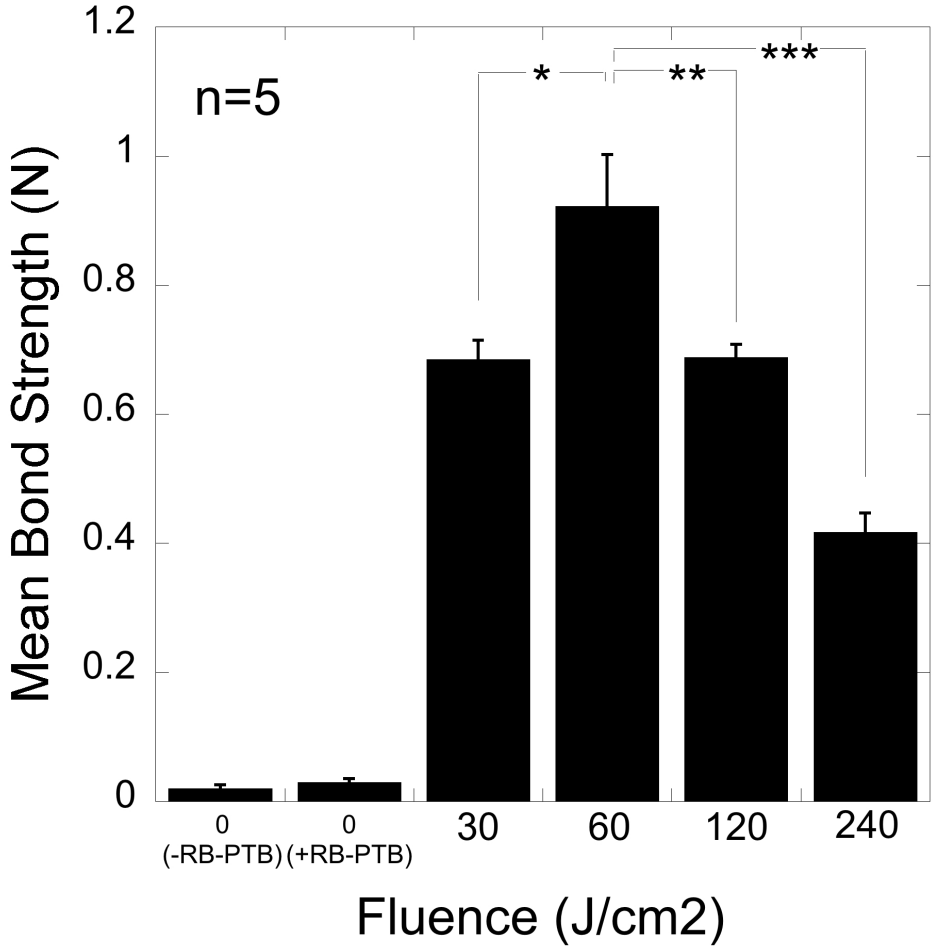

Figure 28. The effect of KTP laser fluence on the formation of photochemical bonds. Bond formation was unsuccessful with a fluence of zero. RB had no effect on the formation of bonds in the absence of illumination. Greatest bond strength was achieved when using a fluence of 60J/cm^2. This was significantly greater than that achieved with 30J/cm^2

3.2.6 Experiment 6: In vivo light-activated sealing of nerve graft coaptation sites improves outcome following large gap peripheral nerve injury.

3.2.6.1 Gross observations following sacrifice

Following sacrifice, two rodents from the xSIS+PTB group were found to have dehisced repairs. All other nerve repairs were intact. Crosslinked amnion and SIS nerve wraps that had

been stained with RB, although not fully intact, were identifiable (figure 29C). No evidence of untreated nerve wraps could be found in any of the fixation groups (figure 29B). Although not quantitatively assessed, those nerves repaired photochemically were found to have considerably less extraneural scar tissue formation in comparison to standard graft+suture (figure 29C vs. 29A respectively)

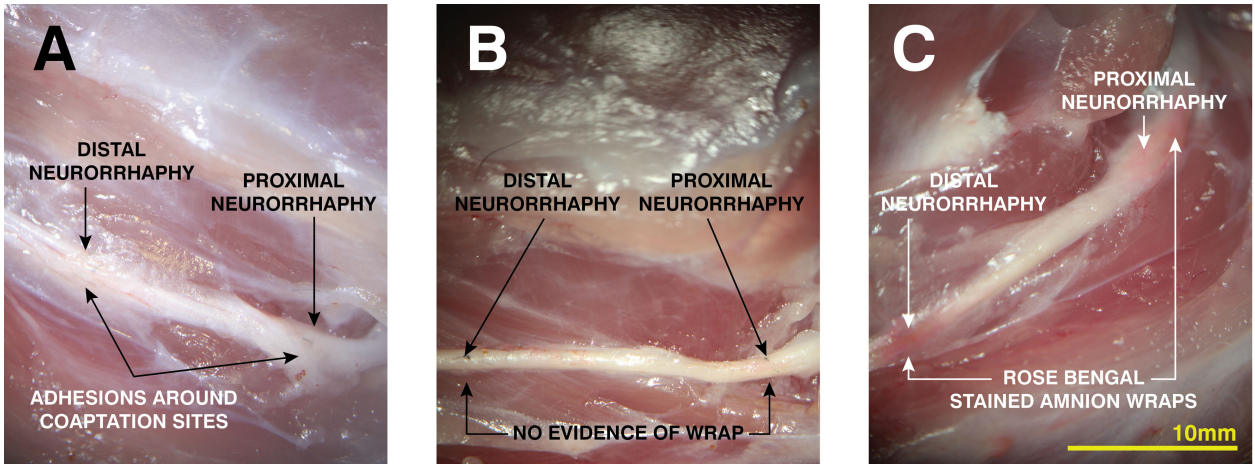

Figure 29. Gross observations of isografts following sacrifice. (A) Typical observation in isograft+suture group. Note the prominent extran-neural adhesions surrounding proximal and distal neurorrhaphy sites. **(B)** Typical result in the HAM+PTB group. No evidence of RB-stained amnion was found. Note the relative absence of extra-neural adhesion formation. **(C)** Typical observation in xHAM+PTB group. RB-stained nerve wraps still intact.

3.2.6.2 Sciatic function Index

All repairs experienced some degree of functional recovery. After 5-months follow-up, nerves repaired with xHAM+PTB showed greatest mean SFI although this was not statistically significant in comparison to graft+suture (-67.9+/-5.1 vs -71.7+/-4.8; table 3, figure 30). SIS+suture and SIS+PTB groups experienced significantly poorer functional recovery in comparison to positive controls (-80.3+/-3.2 and -85.0+/-6.0 vs -71.7+/-4.8

respectively; p<0.01). There were no other significant differences between any of the remaining groups and positive controls.

Experimental group	Mean SFI				
	1-month	**2-month**	**3-month**	**4-month**	**5-month**
No Repair	-89.0+/-1.2	-94.2+/-1.6*	-89.8+/-1.6*	-89.3+/-1.5*	-96.2+/-1.2*Ψ
Standard Graft + Suture	-87.6+/-1.6	-81.1+/-1.4	-71.8+/-2.3	-74.7+/-2.4	-71.7+/-1.6
HAM+suture	-90.3+/-1.6	-85.7+/-3.1	-80.6+/-1.1*	-79.7+/-2.0	-77.9+/-2.2Ψ
HAM+fibrin	-89.2+/-1.3	-81.6+/-1.3	-80.4+/-2.3*	-79.4+/-1.5	-75.2+/-1.6
HAM+PTB	-90.0+/-1.6	-81.2+/-0.8	-72.8+/-1.5	-75.6+/-1.0	-74.5+/-1.4
xHAM+suture	-96.6+/-2.4	-82.4+/-1.5	-80.0+/-1.3*	-81.4+/-1.7	-76.8+/-1.0Ψ
xHAM+fibrin	-90.9+/-1.0	-84.1+/-1.1	-79.8+/-1.1*	-81.2+/-1.0	-75.0+/-1.3Ψ
xHAM+PTB	-88.2+/-1.2	-80.3+/-1.2	-67.2+/-1.1	-71.6+/-1.7	-67.9+/-1.6
xSIS+suture	-94.7+/-1.3	-85.6+/-1.4	-82.5+/-1.4*	-81.4+/-1.6	-80.3+/-1.1*Ψ
xSIS+fibrin	-93.2+/-1.5	-84.7+/-1.6	-82.0+/-1.2*	-81.5+/-1.4	-78.8+/-1.4Ψ
xSIS+PTB	-92.5+/-0.7	-84.7+/-1.6	-84.3+/-1.2*	-85.3+/-2.1*	-85.0+/-1.9*Ψ

Table 3. Monthly mean SFI. After 5-months follow-up, xHAM+PTB recovered greatest SFI although this was not statistically significant in comparison to graft+suture. No repair, xSIS+suture and xSIS+PTB groups performed significantly worse that standard graft+suture, with no significant difference existing between remaining groups. When adjusting for time and, in comparison to standard graft+suture, mean SFI values across the entire 5-months follow-up period were significantly worse in the no repair, HAM+suture, xHAM+fibrin, xSIS+suture, xSIS+fibrin and xSIS+PTB groups. No other significant differences in time-adjusted SFI existed for remaining groups. (*denotes statistically significant at 5-month time point in comparison to standard graft+suture; Ψdenotes statistically significant mean SFI over entire 5-months in comparison to standard graft+suture). Analysis performed using ANOVA, repeated meausures ANOVA (to test for differences across entire period of follow-up) and post hoc Bonferroni test; p<0.05.

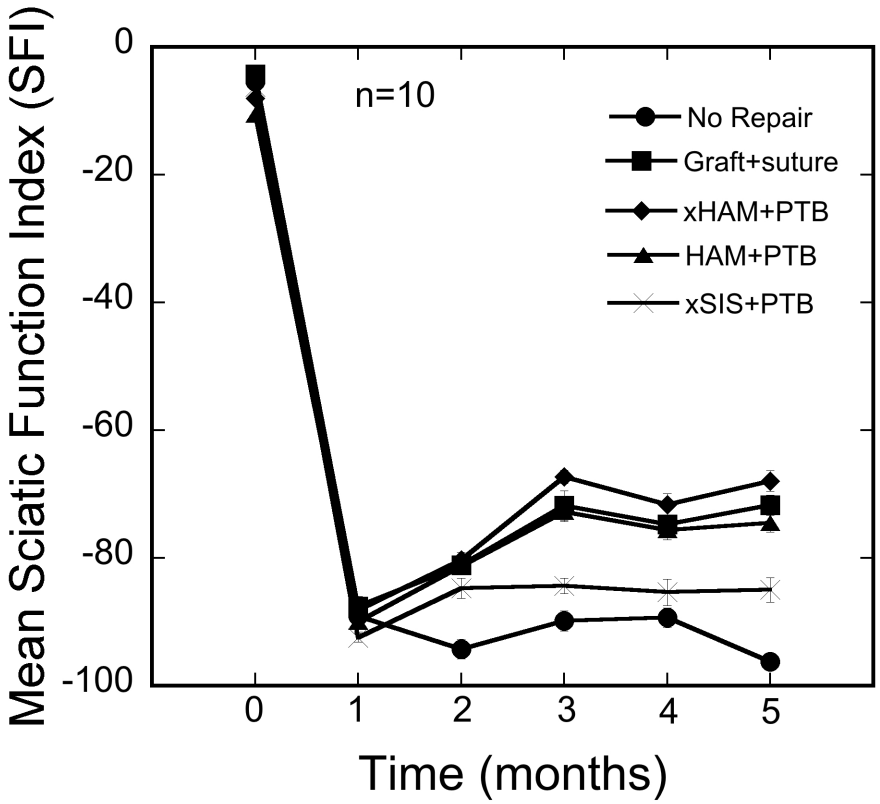

Figure 30. Mean SFI for select treatment groups over 5-month follow-up period. In the interests of clarity, only a select number of treatment groups have been included. Those nerve repaired using xHAM+PTB recovered greatest SFI although this was not statistically significant compared with standard graft+suture (67.9+/-1.6 vs -71.7+/-1.6; mean+/-SEM). Mean SFI in the HAM+PTB was less than xHAM+PTB and standard graft+suture although this was not statistically significant (table 3). xSIS+PTB performed least well out of all treatment groups and was significantly worse than standard repair. Analysis performed using ANOVA, repeated meausures ANOVA (to test for differences across 5-month follow-up) and post hoc Bonferroni test; $p<0.05$.

3.2.6.3 Gastrocnemius muscle mass retention

Nerves repaired with xHAM+PTB experienced a small (<10%) but statistically significant improvement in muscle mass retention compared with graft+suture (67.3%+/-1.4 vs 60.0%+/-1.6; p=0.02). There were no other significant differences between remaining treatment groups and graft+suture controls (table 4; figure 31). Repairs using crosslinked amnion recovered greater mean values than untreated amnion although these were not

significant. Comparisons of HAM+suture vs. xHAM+suture, HAM+fibrin vs. xHAM+fibrin and HAM+PTB vs. xHAM+PTB yielded 95% confidence intervals (CI) of -13.35 to 0.35, -9.75 to 3.95, and -11.65 to 2.05, respectively. These wide ranges contain potentially important effect sizes and as a result, the occurrence of a type-2 statistical error cannot be excluded. Amnion wraps secured with PTB and fibrin glue recovered greater mean muscle mass in comparison to wraps secured with suture (greater suture burden) although these results were not statistically significant. Comparison of HAM+suture vs. HAM+PTB, HAM+suture vs. HAM+fibrin, xHAM+suture vs. xHAM+PTB, and xHAM+suture vs. xHAM+fibrin yielded 95% CI of -13.35 to 0.35, -10.65 to 3.05, -11.65 to 2.05, and -7.05 to 6.65 respectively. As with the aforementioned effect of crosslinking, with the exception of the last comparison, the wide ranges contain potentially important effect sizes and a type-2 error cannot be excluded.

Experimental group	Mean left gastrocnemius muscle mass retention (%)	SEM	P value*
No Repair	9.2	0.3	<0.0001
Standard Graft + Suture	60.0	1.6	1
HAM+suture	56.0	1.8	1
HAM+fibrin	59.8	1.7	1
HAM+PTB	62.5	1.3	1
xHAM+suture	57.7	1.3	1
xHAM+fibrin	62.7	1.4	1
xHAM+PTB	67.3*	1.4	0.02
xSIS+suture	54.9	1.4	0.68
xSIS+fibrin	58.5	1.7	1
xSIS+PTB	54.1	1.1	0.37

Table 4. Left gastrocnemius muscle mass retention. Those nerves repaired using xHAM+PTB recovered greatest gastrocnemius muscle mass retention. This result was statistically significant. Those nerves repaired using xSIS+suture and xSIS+PTB recovered least gastrocnemius muscle mass. *Statistically significant improvement in comparison to standard graft+suture. Analysis performed using ANOVA and post hoc Bonferroni test; $p<0.05$.

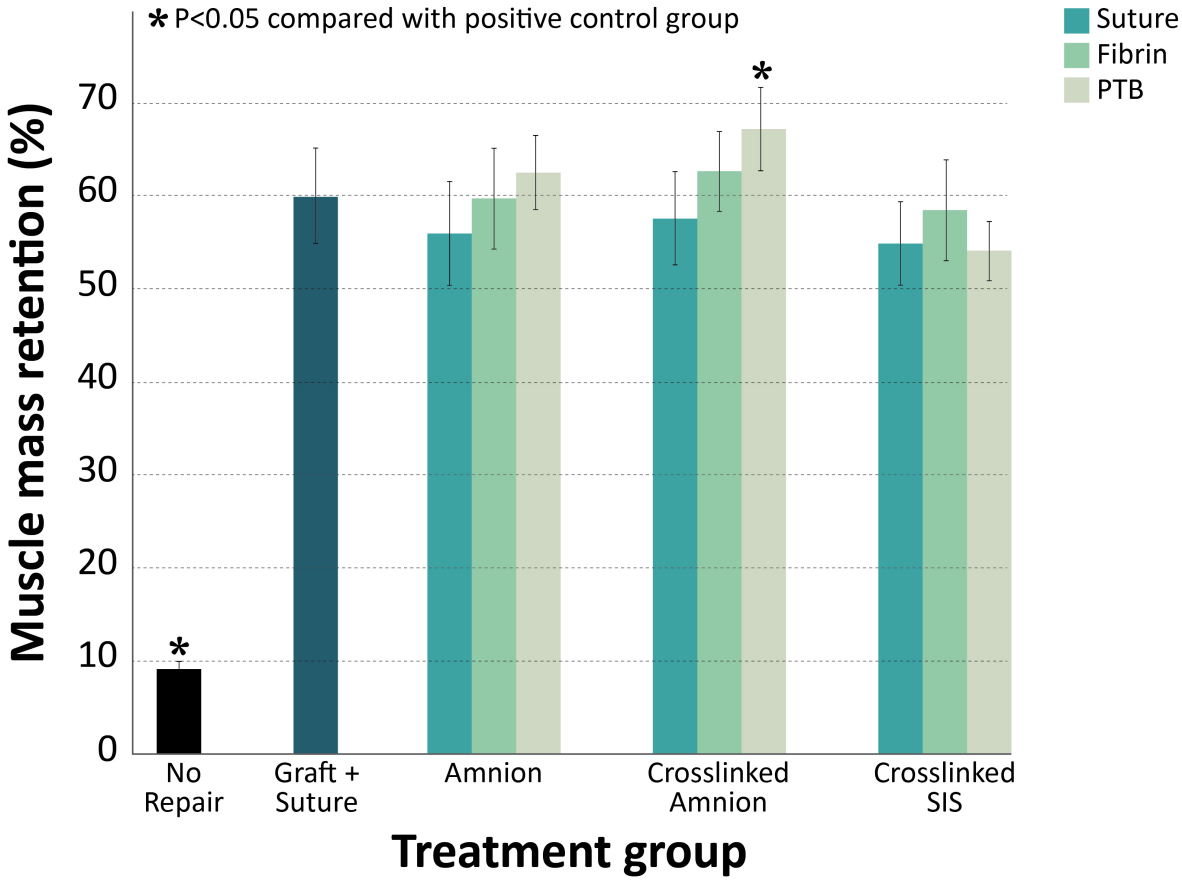

Figure 31. Left gastrocnemius muscle mass retention. All repairs using amnion and SIS resulted in significantly greater recovery in comparison to the no repair group. Nerves repaired using xHAM+PTB resulted in a small (7.3%) but significant improvement in gastrocnemius muscle mass in comparison to graft+suture (67.3+/-1.4 vs 60.0+/-1.6; p=0.02; Mean+/-SEM). Those methods of repair using least suture (PTB and fibrin) recovered greater mean values although, other than that observed for xHAM+PTB, these differences were not significant. This was also observed for crosslinked wraps in comparison to untreated wraps, with the exception of xSIS, which performed least well out of all treatment groups. Photochemically sealed HAM and xHAM both performed significantly better than photochemically sealed SIS (p=0.008 and p<0.0001 respectively). Other

differences between amnion and SIS were marginal. Red line represents graft+suture. Analysis performed using ANOVA and post hoc Bonferroni test; $p<0.05$.

3.2.6.4 Nerve counts and histomorphometry

All distal nerve sections were populated with axons (figure 32). In comparison to uninjured nerve, mean distal axon counts were greater in all treatment groups (with the exception of no repair). This was significant for HAM+suture ($p=0.005$), xHAM+suture ($p=0.02$), HAM+fibrin ($p=0.003$), xHAM+fibrin ($p=0.001$) and xHAM+PTB ($p=0.03$). As expected, axon counts in the no repair group were significantly lower than all repair groups. Distal axon counts in the remaining treatment groups did not differ significantly in comparison to graft+suture (table 5). Nerve fiber diameter, axon diameter and myelin thickness were significantly lower in all treatment groups in comparison to uninjured nerve. xHAM+PTB recovered 80% of uninjured nerve fibre diameter, 81% axon fibre diameter and 78% of myelin thickness. Nerve fiber diameter, axon diameter and myelin thickness were significantly increased in the xHAM+PTB group in comparison to graft+suture repair (table 5; figure 33), translating into improvements of 26%, 29% and 20% respectively.

Histomorphometric parameters 5mm distal to distal isograft coaptation site (Mean+/-SEM)						
Experimental Group	Total axon count (x0.001)	Axon Density (mm^2 x 0.001)	Nerve fiber diameter (μm)	Axon diameter (μm)	Myelin thickness (μm)	G-ratio
Uninjured nerve	**4.66+/-0.50**	**14.11+/-0.39**	**8.55+/-0.04**	**5.55+/-0.03**	**3.00+/-0.01**	**0.64+/-0.01**
No repair	0.04+/-0.02	0.48+/-0.19	4.14+/-0.07	3.13+/-0.07	1.01+/-0.03	0.744+/-0.007
Standard Graft+ Suture	7.61+/-1.08	29.36+/-5.72	5.47+-0.03	3.50+/-0.03	1.96+/-0.01	0.624+/-0.002
HAM+suture	10.41+/-1.33	28.85+/-6.20	5.07+/-0.03	3.44+/-0.03	1.63+/-0.01	0.666+/-0.004
HAM+fibrin	10.42+/-0.49	29.95+/-4.43	5.22+/-0.03	3.44+/-0.03	1.78+/-0.01	0.643+/-0.002
HAM+PTB	9.31+/-1.32	30.70+/-2.83	5.19+/-0.04	3.47+/-0.03	1.72+/-0.01	0.649+/-0.002
xHAM+suture	9.79+/-1.06	27.12+/-2.92	5.14+/-0.03	3.54+/-0.03	1.59+/-0.01	0.673+/-0.002
xHAM+fibrin	10.87+/-1.37	32.12+/-6.41	5.24+/-0.03	3.52+/-0.03	1.72+/-0.01	0.659+/-0.002
xHAM+PTB	9.66+/-0.98	30.73+/-4.66	6.87+/-0.04*	4.51+/-0.04*	2.35+/-0.01*	0.642+/-0.002
xSIS+suture	9.36+/-0.76	30.30+/-5.20	4.83+/-0.03	3.31+/0.03	1.52+/-0.01	0.672+/-0.002
xSIS+fibrin	6.91+/-0.83	31.55+/-4.23	5.18+/-0.03	3.58+/-0.03	1.59+/-0.01	0.684+/-0.002
xSIS+PTB	7.84+/-0.72	30.06+/-4.73	4.81+/-0.03	3.35+/-0.03	1.45+/-0.01	0.684+/-0.002

Table 5 . Histomorphometric analysis of distal nerve sections. Axon count in uninjured nerve was significantly lower than that found in HAM+suture (p=0.005), xHAM+suture (p=0.02), HAM+fibrin (p=0.003), xHAM+fibrin (p=0.001), and xHAM+PTB (p=0.03). Mean axon count did not differ significantly between treatment groups. Fiber diameter, axon diameter and myelin thickness were significantly greater in uninjured nerve in comparison to all treatment groups. Fiber diameter, axon diameter and myelin thickness were significantly greater in those nerves repaired using xHAM+PTB in comparison to graft+suture. All values expressed as mean+/-SEM. *Denotes statistically significant improvement in comparison to standard graft+suture. Analysis performed using ANOVA and post hoc Bonferroni test; $p<0.05$.

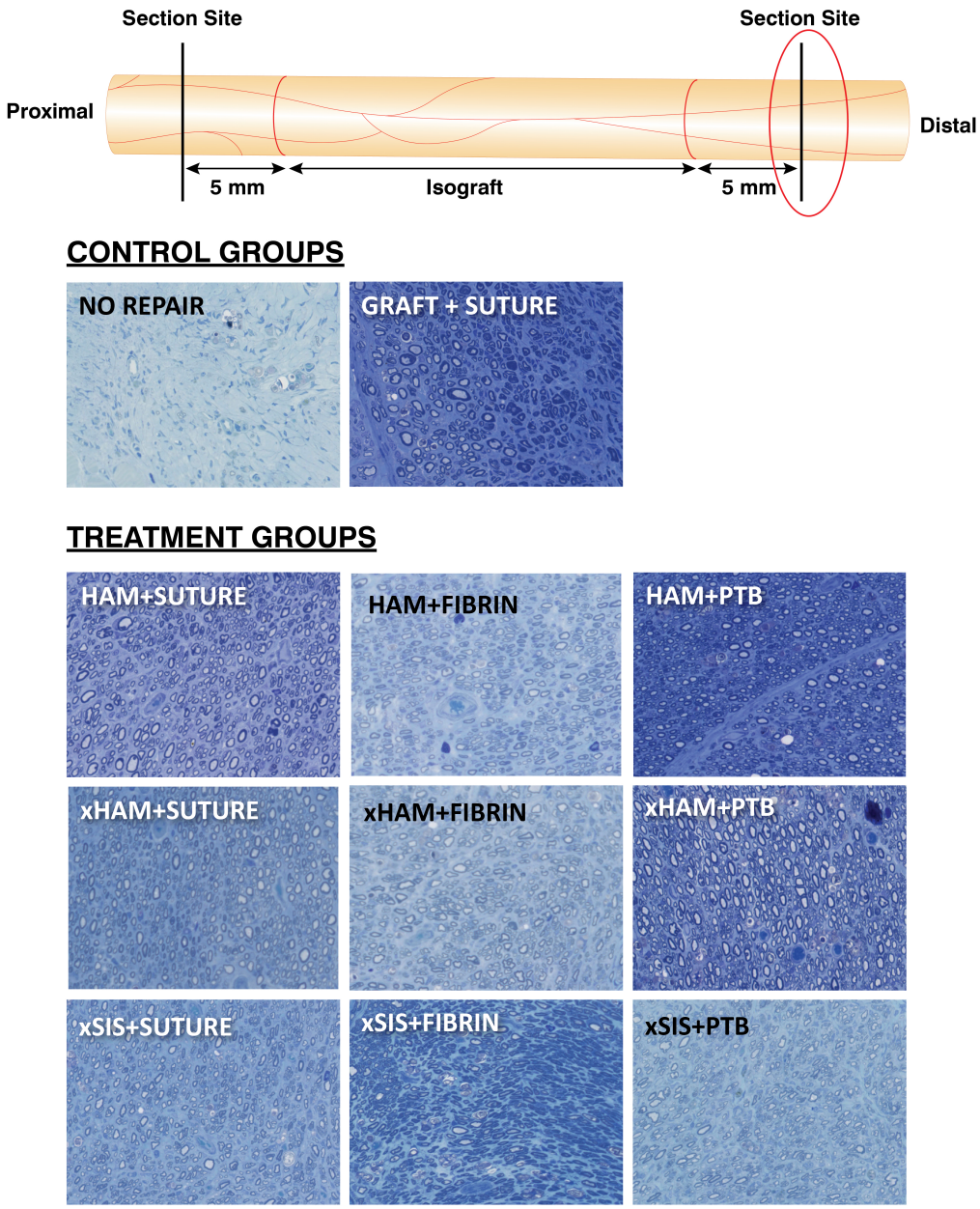

Figure 32. Histology slides from distal isograft section site. Those nerves that were not repaired lacked axons. All treatment groups regenerated axons distal to isografts with the exception of those nerves that dehisced in the xSIS+PTB group. Axons in the xHAM+PTB group had statistically larger fiber diameter, axon diameter and myelin thickness in comparison to graft+suture (see table 5).

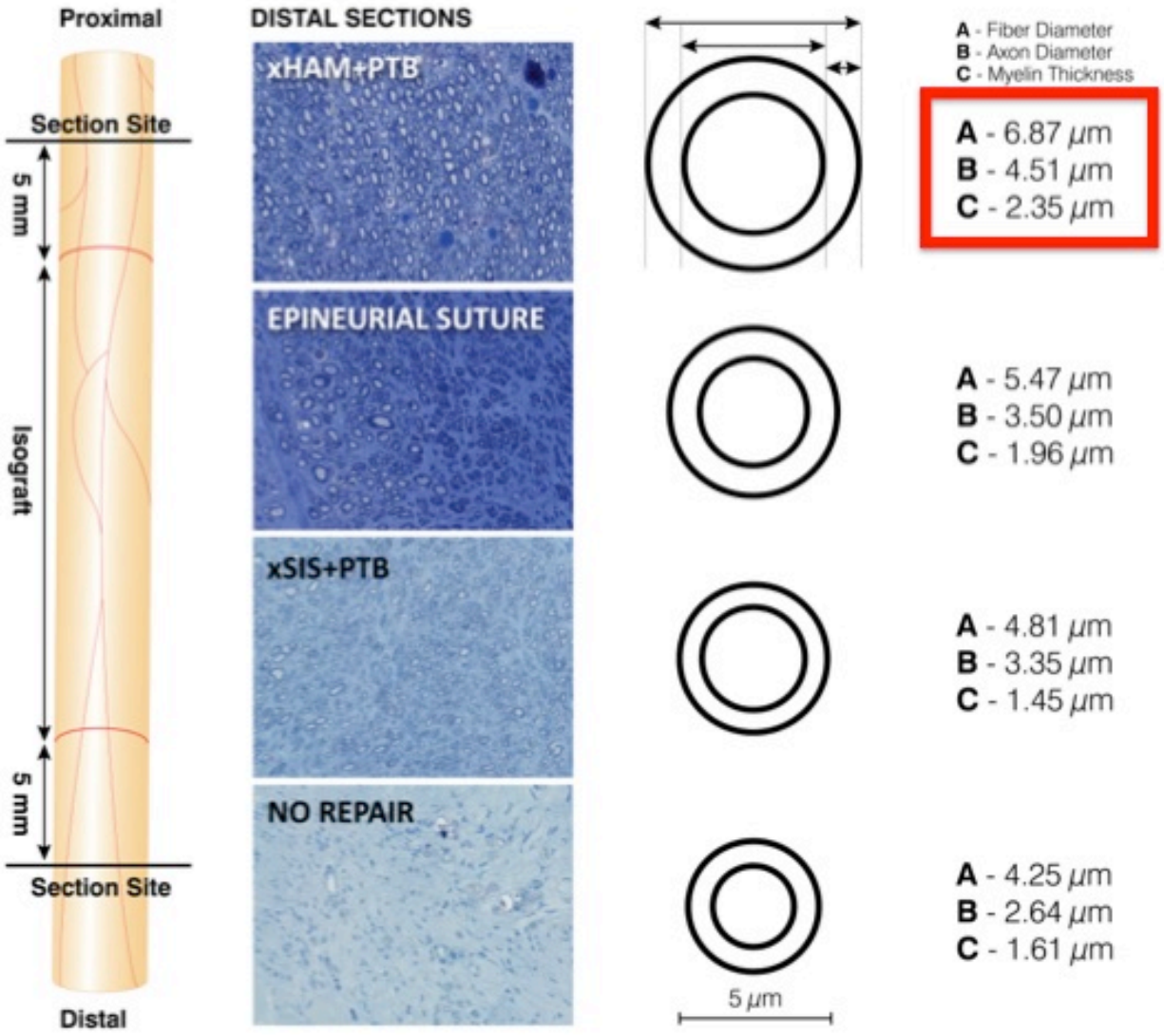

Figure 33. Schematic representation of fibre diameter, axon diameter and myelin thickness for select treatment groups. The data in this schematic represents mean values for fibre diameter, axon diameter and myelin thickness taken from table 5. SEM has been omitted for clarity. The red box highlights the significant increase in diameters in the xHAM+PTB group. Analysis was performed using ANOVA and post hoc Bonferroni; $p<0.05$.

3.2.7 Experiment 7: In vivo light-activated sealing of nerve graft coaptation sites using acellular nerve allograft (ANA)

3.2.7.1 Gross observation following sacrifice

There were no cases of nerve dehiscence in either ANA group and no animals suffered from foot ulceration or automutilation. In those nerves repaired photochemically, remnants of the RB-stained amnion nerve wraps were evident. As with previous studies, extra-neural scar tissue formation was obvious in those nerves repaired using conventional suture and was qualitatively less in photochemically bonded nerves (figure 34). Qualitatively, allografts were of smaller diameter than isografts.

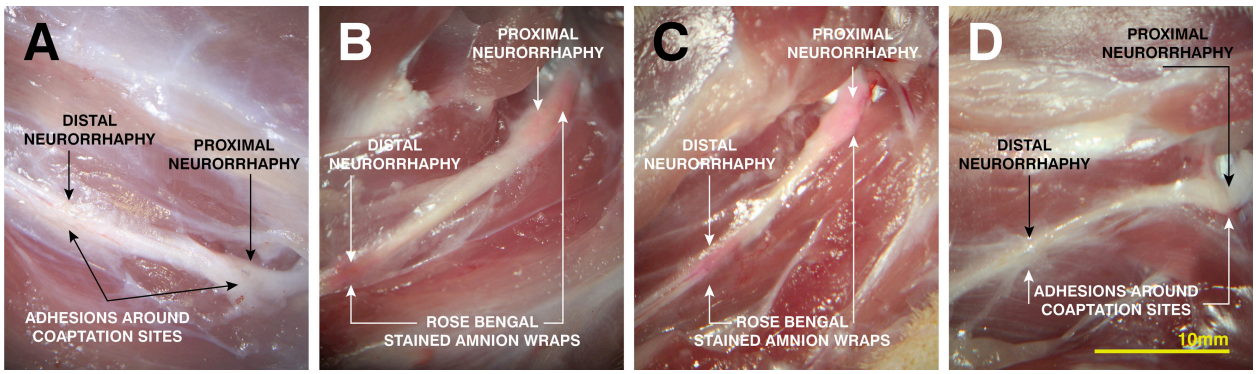

Figure 34. Gross observations of ANA following sacrifice. Nerves from isograft phase have been included for comparison**.** All nerves were found to be intact and showed evidence of regeneration across ANA. Qualitatively, as with sutured isografts (A), sutured ANA (D) had greater adhesion formation around coaptation sites. As with photochemically sealed isografts (B), photochemically sealed ANA (C) showed remnants of RB stained amnion wraps. Qualitatively, sutured ANA diameter was noticeably reduced in comparison to isograft, an observation consistent with their statistically inferior outcome.

3.2.7.2 Sciatic function index

Isograft+PTB from phase 1 recovered greatest mean SFI after 5-months follow-up (table 6; figure 35). This was not statistically significant in comparison to isograft+suture. Likewise, photochemically sealed ANA recovered greater mean SFI values in comparison to sutured ANA although this was not statistically significant (-78.3+/-1.6 vs. -80.3+/-1.3; p=1; 95% CI -8.15 to 3.86; table 6 and 9; Fig 35). ANA+suture performed significantly worse than isograft+suture (-80.3+/-1.3 vs. -71.7+/-1.6; p=0.0019; table 6 and 9). SFI was also statistically less for ANA+PTB in comparison to isograft+suture and isograft+PTB (table 6 and 9).

Experimental group	**Sciatic Function Index (Mean+/-SEM)**				
	1-month	**2-month**	**3-month**	**4-month**	**5-month**
Isograft+suture	-87.6+/-1.6	-81.1+/-1.4	-71.8+/-2.3	-74.7+/-2.4	-71.7+/-1.6
Isograft+PTB	-88.2+/-1.2	-80.3+/-1.2	-67.2+/-1.1	-71.6+/-1.7	-67.9+/-1.6
ANA+suture	-95.4+/-0.79	-90.3+/-3.3	-87.9+/-1.3	-84.1+/-1.0	-80.3+/-1.3*
ANA+PTB	-93.4+/-1.1	-91.1+/-1.7	-88.9+/-1.7	-83.4+/-1.5	-78.3+/-1.6*

Table 6. Mean SFI for all treatment groups (n=10) over 5-month follow-up. At each time point throughout recovery, no significant differences existed within each of the isograft and ANA groups. Recovery of SFI over the entire 5-month follow-up period was statistically poorer for both sutured and photochemically sealed ANA in comparison to sutured and photochemically sealed isografts (*p<0.001). All data expressed as mean+/-SEM. Analysis performed using repeated measures ANOVA and post hoc Bonferroni test.

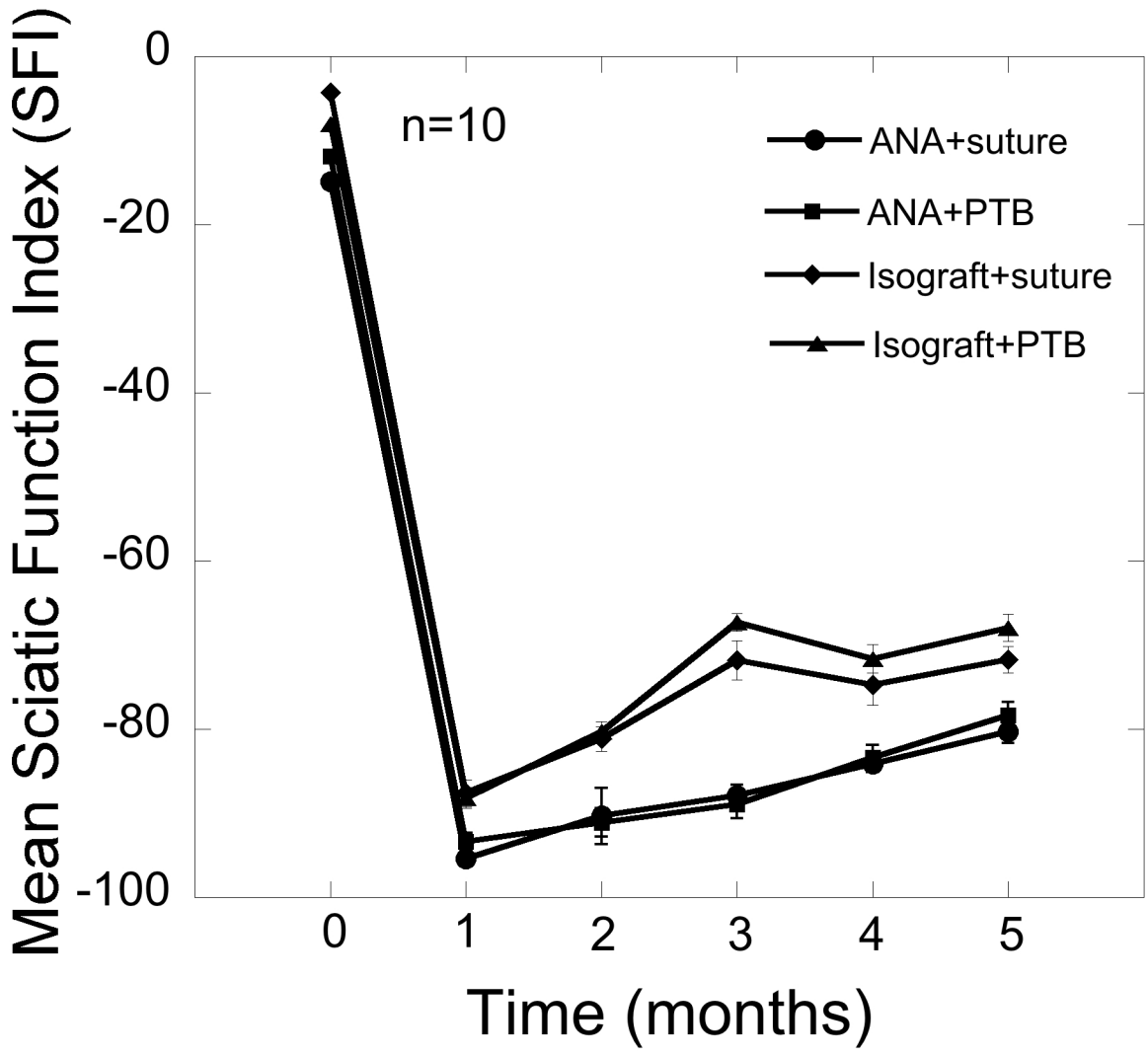

Figure 35. Mean SFI of ANA and isograft treatment groups (n=10). Data points represent mean+/-SEM from table 6. After 5-months follow-up, no significant difference existed within either isograft or ANA groups. ANA+suture and ANA+PTB groups recovered statistically less SFI in comparison to sutured and bonded isografts respectively ($p<0.001$). Analysis performed using repeated measures ANOVA and post hoc Bonferroni test.

3.2.7.3 Gastrocnemius muscle mass retention

Isograft+PTB recovered greatest gastrocnemius muscle mass retention and this was statistically significant in comparison to all other groups (table 7; figure 36). Mean muscle

mass retention values were higher for ANA+PTB but these were not significantly different to ANA+suture (55.2+/-1.8% vs. 52.9+/-1.5%; p=1; 95% CI -8.50 to 3.97; table 7, figure 36). Muscle mass recovery was significantly poorer in ANA+suture group in comparison to isograft+suture group. Likewise, recovery of ANA+PTB was significantly poorer than isograft+PTB. Muscle mass retention in the ANA+PTB group was statistically comparable to that achieved using isograft+suture, the current standard of care.

Experimental group	Mean left gastrocnemius muscle mass retention (%)	SEM	P value
Isograft+suture	60.0	1.6	----
Isograft+PTB	67.3	1.4	0.01
ANA+suture	52.9	1.5	0.02
ANA+PTB	55.2	1.8	0.22

Table 7. Gastrocnemius muscle mass retention for all groups. Isograft+PTB recovered a small but significantly greater muscle mass in comparison to isograft+suture (p=0.01). Muscle mass retention was significantly poorer in the ANA+suture group in comparison to isograft+suture (p=0.02). Retention in the ANA+PTB group was comparable to isograft+suture. P-values are in relation to isograft+suture. Analysis performed using ANOVA and post hoc Bonferroni test.

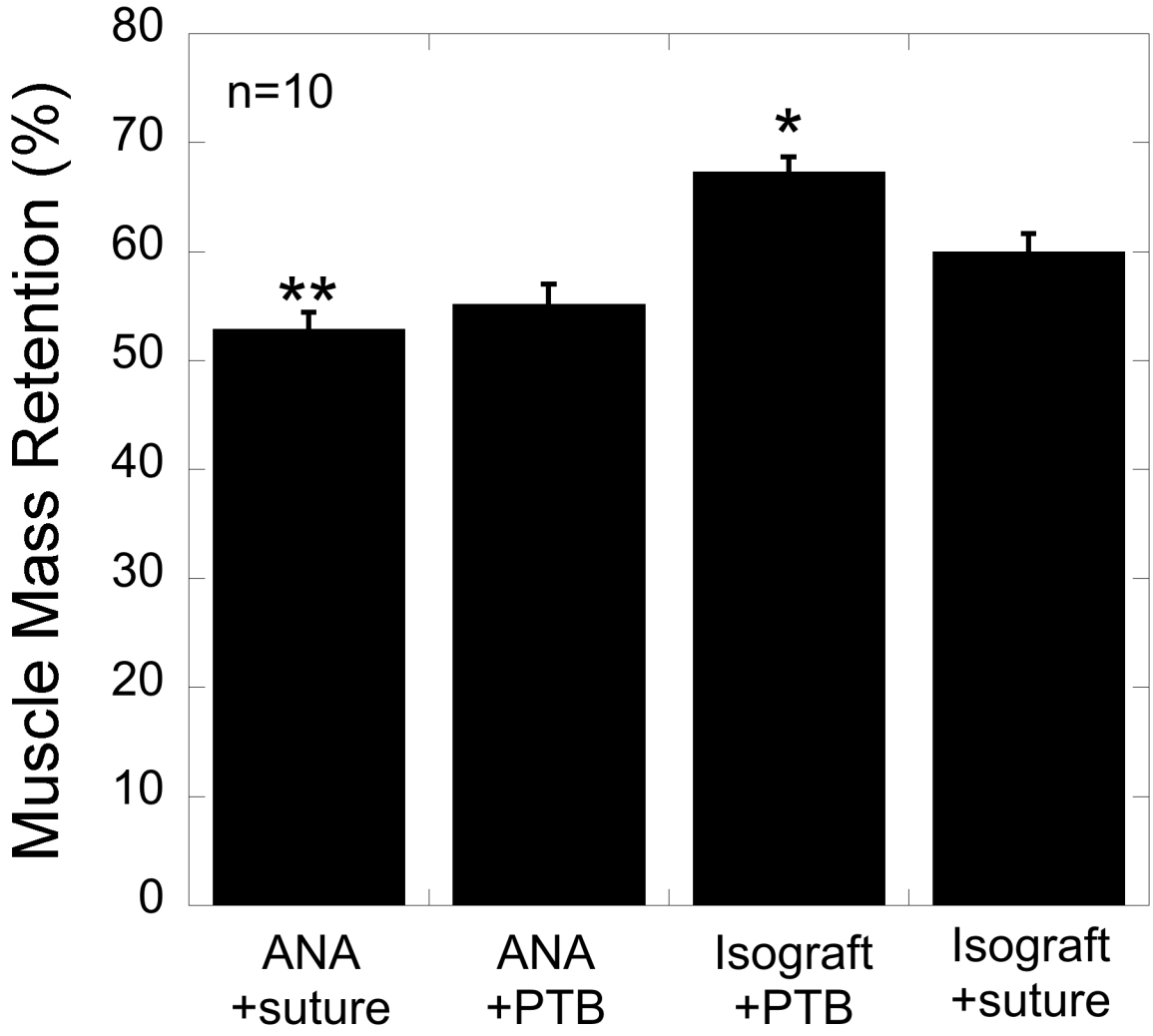

Figure 36. Gastrocnemius Muscle Mass Retention for ANA and isograft treatment groups. Isografts sealed photochemically with crosslinked amnion recovered significantly greater muscle mass than all remaining groups. No significant difference existed between sutured and photochemically sealed ANA. ANA+suture recovered significantly less muscle mass than isograft+suture but there was no significant difference between isograft+suture and ANA+PTB. *Denotes statistically significant improvement in comparison to isograft+suture; p=0.01. **Denotes statistically significant reduction in muscle mass retention in comparison to isograft+suture; p=0.02. Analysis performed using ANOVA and post hoc Bonferroni test.

3.2.7.4 Nerve counts and histomorphometry

Axon counts in the distal nerve stump were significantly greater for isograft+PTB in comparison to ANA+suture. No other significant differences in axon counts or axon density existed between treatment groups. Isograft+PTB recovered the greatest fiber diameter, axon diameter and myelin thickness and this was statistically significant in comparison to all other groups (table 8 and 9; figure 37). Histomorphometric recovery was poorest in the ANA+suture group and this was statistically significant in comparison to isograft+suture and isograft+PTB. Mean values for fiber diameter, axon diameter and myelin thickness were less for ANA+suture in comparison to ANA+PTB but these were not significantly different (5.26+/-0.03 vs. 5.38+/-0.02, p=0.07, 95% CI -0.250 to 0.007; 3.30+/-0.02 vs. 3.41+/-0.02, p=0.06, 95% CI -0.211 to 0.003; 1.95+/-0.01 vs. 1.97+/-0.01, p=1, 95% CI -0065 to 0.030, respectively. There was no significant difference between ANA+PTB and isograft+suture, the current standard of care (table 8 and 9 figure 37)

Histomorphometric parameters 5mm distal from distal graft coaptation site (Mean+/-SD)						
Experimental Group	Total axon count (x0.001)	Axon Density (mm^2 x 0.001)	Nerve fiber diameter (µm)	Axon diameter (µm)	Myelin thickness (µm)	G-ratio
Uninjured nerve	**4.66+/-0.50**	**14.11+/-0.39**	**8.55+/-0.04**	**5.55+/-0.03**	**3.00+/-0.01**	**0.64+/-0.01**
Isograft+Suture	7.61+/-1.08	29.36+/-5.72	5.47+-0.03	3.50+/-0.03	1.96+/-0.01	0.625+/-0.002
Isograft+PTB	9.66+/-0.98	30.73+/-4.66	6.87+/-0.04*	4.51+/-0.04*	2.35+/-0.01*	0.642+/-0.002
ANA+suture	5.04+/-0.86	21.50+/-0.85	5.26+/-0.03	3.30+/-0.02	1.95+/-0.01	0.621+/-0.002
ANA+PTB	6.04+/-1.01	22.03+/-1.63	5.38+/-0.02	3.41+/-0.02	1.97+/0.01	0.631+/-0.002

Table 8. Histomorphometric analysis for all groups. Results from uninjured rat sciatic nerve in phase 1 included for reference**.** Isograft+PTB recovered significantly greater fibre diameter, axon diameter and myelin thickness than all other groups. With the exception of G-ratio, no significant differences existed between

ANA+suture and ANA+PTB. ANA+suture recovered significantly less fibre diameter and axon diameter than isograft+suture. There was no difference in axon count, myelin thickness and G-ratio between these groups. ANA+PTB was statistically comparable to isograft+suture for all histomorphometric parameters (see Bonferroni all-pairs comparison (Table 4)). *Statistically significant improvement in comparison to isograft+suture. Analysis performed using ANOVA and post hoc Bonferroni test ($p<0.05$)

Group Comparison	SFI (5-month)*	Muscle Mass	Axon Count	Fiber Diameter	Axon Diameter	Myelin Thickness	G-ratio
Isograft+suture vs Isograft+PTB	0.22	0.01	0.90	< 0.0001	< 0.0001	< 0.0001	< 0.0001
Isograft+suture vs ANA+suture	<0.001	0.02	0.47	< 0.0001	< 0.0001	1	1
Isograft+suture vs ANA+PTB	<0.001	0.22	1	0.27	0.08	1	0.21
Isograft+PTB vs ANA+suture	< 0.001	< 0.0001	0.02	< 0.0001	< 0.0001	< 0.0001	< 0.0001
Isograft+PTB vs ANA+PTB	<0.001	< 0.0001	0.08	< 0.0001	< 0.0001	< 0.0001	0.0005
ANA+suture vs ANA+PTB	1	1	1	0.07	0.06	1	0.0062

Table 9. Bonferroni all-pairs comparison for all groups. In comparison to isograft +suture, isograft+PTB results in statistically significant improvements in muscle mass retention, fibre diameter, axon diameter and myelin thickness. ANA+suture had significantly poorer recovery of SFI, muscle mass retention, fibre diameter and axon diameter. With the exception of G-ratio, there was no significant difference between ANA+suture and ANA+PTB for any of the outcomes measured. There was no significant difference in muscle mass retention, axon count, fibre diameter, axon diameter, myelin thickness and G-ratio between ANA+PTB and isograft+suture. *Derived from repeated measures ANOVA.

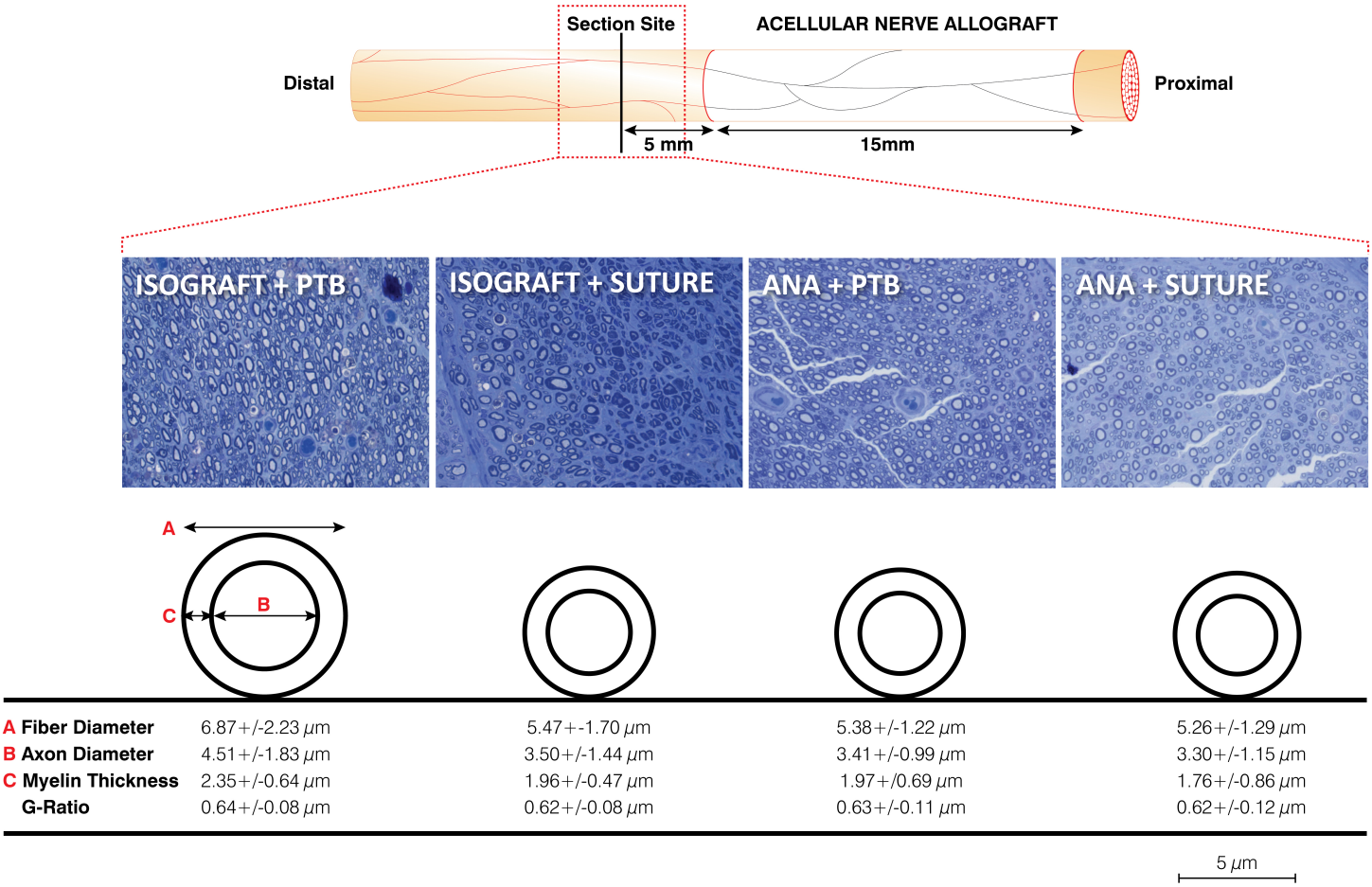

Figure 37. Examples of distal ANA histology and schematic representation of histomorphometric measurements. Isograft+PTB recovered significantly greater fibre diameter, axon diameter and myelin thickness in comparison to remaining groups (see table 9 for Bonferroni all pairs comparison). These outcomes were not significantly different between sutured isografts and photochemically sealed ANA. Analysis was performed using ANOVA and post hoc Bonferroni.

3.2.8 Experiment 8: Immediate versus delayed repair of large gap peripheral nerve injury using light-activated sealing of human amnion nerve wraps around nerve graft coaptation sites

3.2.8.1 Gross observations following sacrifice

Two rodents in the delayed PTB group had to be sacrificed prematurely due to intractable foot ulcers. Unfortunately one of these animals was disposed of before necropsy could be performed. In the remaining rodent, the isograft was found to be in continuity but had experienced considerable atrophy at the mid-portion of the graft (figure 38).

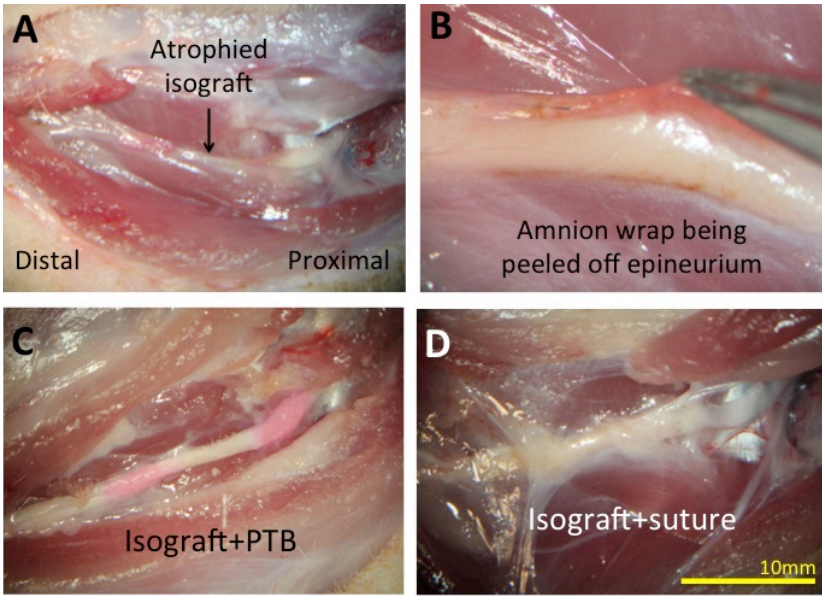

Figure 38. Gross observations of immediate and delayed isograft groups following sacrifice. Two animals in the isograft+PTB group required sacrifice prior to the completion of 150-days follow-up due to intractable foot ulcers. Necropsy of one animal showed intact photochemical bonds but a severely atrophied graft. The remaining animal was disposed of before examination could take place (A). Amnion wraps were found to be present, evidence of successful retardation of proteolytic degradation (B). Qualitatively, isograft+PTB nerves had less extraneural scar tissue formation than isograft+suture groups (C+D).

No other episodes of dehiscence occurred in the remaining groups with all nerves showing evidence of regeneration. Crosslinked amnion nerve wraps were identifiable following

sacrifice in all groups showing that crosslinking protects enzymatic degradation for a minimum of 5-months (figure 38). Extra-neural scarring appeared qualitatively reduced in those nerves repaired photochemically, an observation consistent with previous studies (figure 38).

3.2.8.2 Sciatic Function Index

After 5-months follow-up, greatest recovery of SFI occurred in the immediate PTB group. This result was not statistically significant in comparison to immediate suture although was significantly better than that of the delayed PTB group (-68.5+/-1.5 vs. -72.3+/-1.5; p=0.41 and -68.5+/-1.5 vs. -77.3+/-1.5; p=0.002 respectively). Recovery in the immediate suture group was significantly better than delayed suture, which performed poorest out of all groups (-72.3+/-1.5 vs. -80.1+/-1.4). There was no significant difference between immediate suture and delayed PTB (-72.3+/-1.5 vs. -77.3+/-1.5; table 10 and 13).

3.2.8.3 Gastrocnemius Muscle Mass Retention

Muscle mass retention was greatest in the immediate PTB group and this was statistically significant in comparison to the immediate suture group (64.9+/-1.8% vs. 59.0+/-1.1%; p=0.02). A similar small (<10%) significant improvement was also observed in the delayed PTB group in comparison to delayed suture (60.2+/-1.4% vs. 54.1+/-1.7%; p=0.03). With regards to the surgical delay, no significant difference existed between immediate suture and delayed suture, or immediate PTB and delayed PTB groups. Muscle mass retention was not significantly different between immediate suture and delayed PTB (59.0+/-1.1% vs. 60.2+/-1.4%; p=1; table 11 and 13).

Experimental group	Mean SFI				
	1-month	2-month	3-month	4-month	5-month
Immediate suture	-91.4+/-3.2	-81.4+/-1.3	-78.2+/-1.4	-72.4+/-2.0	-72.3+/-1.5
Immediate PTB	-91.4+/-1.6	-81.3+/-1.1	-74.1+/-1.5	-71.8+/-1.3	-68.5+/-1.5
Delayed suture	-92.9+/-1.4	-84.9+/-2.1	-84.9+/-2.2	-82.8+/-1.7	-80.1+/-1.4
Delayed PTB	-92.4+/-1.1	-84.4+/-2.0	-80.7+/-1.8	-79.7+/-1.9	-77.3+/-1.5

Table 10. Mean SFI for all treatment groups over 5-month follow-up period. All data expressed as mean+/-SEM. Immediate isograft+PTB recovered greatest mean SFI after 5-months although this was not statistically significant in comparison to immediate suture. Similarly, No significant difference existed between delayed PTB and delayed suture. SFI in the immediate suture group was significantly better than the delayed suture group ($p=0.003$). Likewise immediate PTB recovered a significantly greater SFI in comparison to delayed PTB (0.002). Immediate PTB was significantly better than delayed suture, which performed poorest out of all groups ($p<0.0001$). No significant difference existed between immediate suture and delayed PTB. Analysis was performed using repeated measures ANOVA and post hoc Bonferroni test.

Experimental group	Mean left gastroc. muscle mass retention (%)	SEM	P value
Immediate suture	59.0	1.1	-----
Immediate PTB	64.9*	1.8	0.02
Delayed suture	54.1	1.7	0.10
Delayed PTB	60.2	1.4	1

Table 11. Gastrocnemius muscle mass retention for all groups. Groups compared statistically to immediate suture. Immediate PTB group recovered significantly greater muscle mass than immediate suture ($p=0.02$). Delayed suture and delayed PTB did not differ significantly in comparison to immediate suture group. See table

13 for Bonferroni all-pairs comparison. Analysis performed using ANOVA and post hoc Bonferroni test; $p<0.05$.

3.2.8.4 Nerve counts and histomorphometry

No significant differences in axon counts existed between any of the treatment groups. The immediate PTB group recovered significantly greater fiber diameter, axon diameter, myelin thickness and G-ratio in comparison to immediate suture group. This equates to increases in fibre diameter, axon diameter and myelin thickness of 10%, 7% and 11% respectively. Recovery of fibre diameter, axon diameter and myelin thickness in relation to uninjured nerve was 74%, 80% and 62% respectively. With the exception of G-ratio, all measurements were significantly greater in the delayed PTB group in comparison to the delayed suture group. Fibre diameter, axon diameter and myelin thickness were improved by 8%, 9% and 4% respectively. Recovery of these variables in relation to uninjured nerve was 68%, 76% and 53% respectively. With regards to surgical delay, fiber diameter, axon diameter and myelin thickness were significantly greater in the immediate suture group in comparison to the delayed suture group (figure 39). No significant difference in G-ratio was detected. All measurements in the immediate PTB group were significantly better in comparison to the delayed PTB group. No significant difference in any histomorphometric measurement existed between immediate suture and delayed PTB (table 12 and 13; figure 39).

Histomorphometry 5mm distal from distal isograft coaptation site (Mean+/-SD)						
Experimental Group	**Total axon count (x0.001)**	**Axon Density (mm^2 x 0.001)**	**Nerve fiber diameter (µm)**	**Axon diameter (µm)**	**Myelin thickness (µm)**	**G-ratio**
Uninjured nerve	**4.66+/-0.50**	**14.11+/-0.39**	**8.55+/-0.04**	**5.55+/-0.03**	**3.00+/-0.01**	**0.64+/-0.01**
Immediate Suture	7.34+/-1.39	24.83+/-1.34	5.75+/-0.03	4.15+/-0.03	1.60+/-0.01	0.715+/-0.001
Immediate PTB	7.29+/-1.46	23.25+/-0.71	6.30+/-0.03*	4.45+/-0.03*	1.85+/-0.01*	0.703+/-0.001*
Delayed suture	4.04+/-0.45	24.17+/-0.86	5.40+/-0.03	3.88+/-0.02	1.53+/-0.01	0.716+/-0.001
Delayed PTB	5.77+/-0.46	23.00+/-0.84	5.81+/-0.03	4.22+/-0.03	1.59+/-0.01	0.721+/-0.001

Table 12. Histomorphometric analysis for all groups. Results from uninjured nerve in phase 1 included for reference. Although mean axon counts were considerably greater in immediate repair groups, due to large standard deviation, these values were not significantly different. All histomorphometric measurements were greater in the immediate PTB group in comparison to immediate suture (*denotes statistically significant improvement in comparison to immediate suture). Table 13 provides detailed cross-pairs comparison. Analysis was performed using ANOVA and post hoc Bonferroni test; $p<0.05$.

Group Comparison	SFI (5-month)	Muscle Mass	Axon Count	Fiber Diameter	Axon Diameter	Myelin Thickness	G-ratio
Immediate suture vs Immediate PTB	0.41	0.02	1	< 0.0001	< 0.0001	< 0.0001	< 0.0001
Immediate suture vs Delayed suture	0.003	0.10	0.23	< 0.0001	< 0.0001	< 0.0001	1
Immediate suture vs Delayed PTB	0.17	1	1	1	0.35	1	0.06
Immediate PTB vs Delayed suture	< 0.0001	< 0.0001	0.24	< 0.0001	< 0.0001	< 0.0001	< 0.0001
Immediate PTB vs Delayed PTB	0.002	0.16	1	< 0.0001	< 0.0001	< 0.0001	< 0.0001
Delayed suture vs Delayed PTB	1	0.03	1	< 0.0001	< 0.0001	0.001	0.12

Table 13. Bonferroni all-pairs comparison for all groups. No significant differences in SFI were detected between immediate suture and immediate PTB or delayed suture and delayed PTB. Significant differences were detected between immediate and delayed suture and immediate and delayed PTB highlighting the detrimental impact of delay. No significant difference existed between immediate suture and delayed PTB. Muscle mass retention was significantly improved following PTB repair in both immediate and delayed groups. The effects of delay were not significantly different for suture or PTB fixation. As with SFI, immediate suture was not significantly different in comparison to delayed PTB. No significant differences existed in axon count or density existed between groups. Fiber diameter, axon diameter and myelin thickness and G-ratio were not significantly different between immediate suture and delayed PTB. With the exception of G-ratio, all other histomorphometric parameter comparisons were significantly different between treatment groups, with immediate PTB achieving greatest recovery and delayed suture being poorest

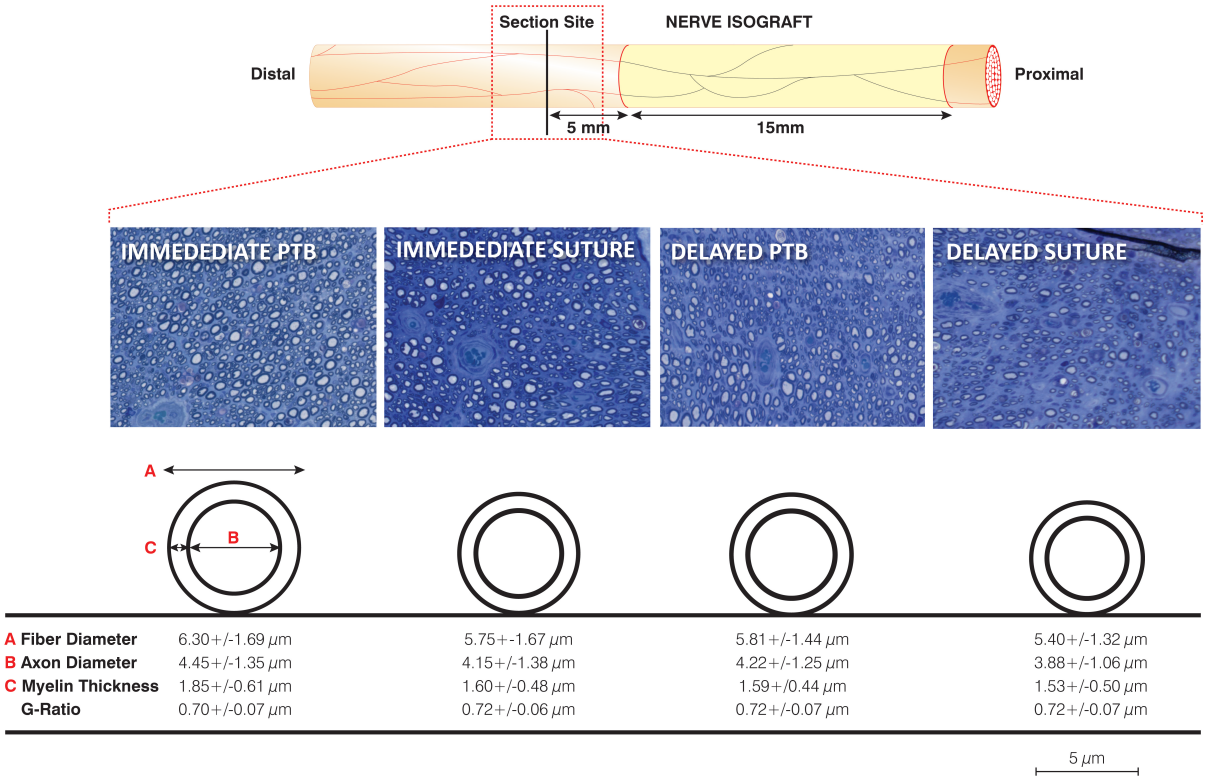

Figure 39. Examples of distal isograft histology and schematic representation of histomorphometric measurements. Sections taken 5mm distal to the distal isograft coaptation site. With the exception of the two rodents that were sacrificed prematurely, all rodents successfully regenerated axons through isografts into the distal nerve stump after 5-months. No significant differences in total axon counts between groups were detected. Histomorphometric measurements were generally greater in immediate repairs versus delayed repairs and in those repairs performed photochemically versus suture. No significant differences existed between immediate suture and delayed PTB groups.

Section 4: Discussion

Main findings

Phase 1 experiments show that photochemical sealing of nerve graft coaptation sites using crosslinked human amnion results in statistically significant improvements in muscle mass retention and histomorphometric outcomes compared with standard graft+suture. With the exception of xSIS groups having significantly poorer SFI, no other significant differences existed between treatment groups. However, mean values for all outcome measures tended to be higher in those groups repaired with crosslinked nerve wraps. The observed 95% confidence intervals cannot exclude the existence of a type-2 statistical error and a larger sample size may have identified a significant correlation. Although *in vivo* nerve wrap degradation was not formally assessed throughout the regenerative period, there was visible evidence of persisting crosslinked RB-stained wraps following sacrifice (figure 29C). In contrast, untreated wraps were completely degraded (figure 29B). The prevention of premature wrap degradation before the arrival of regenerating axons appears to maintain a protective growth permissive seal that lasts longer. Partial degradation of crosslinked material did occur. Although EDC successfully protects against collagenase degradation, it may be unable to offer protection against other proteolytic enzymes.

Likewise, although not significant, mean values for all outcome measures tended to be higher when suture burden was reduced (fibrin glue and PTB). Again, the reported 95% confidence intervals raise the possibility that greater sample sizes may have identified this as a significant effect. These observations are consistent with widely accepted tenets regarding the detrimental, pro-inflammatory effect of suture. Although mean outcome values following photochemical sealing were greater than those achieved using fibrin glue, only those nerves

repaired with photochemically-sealed crosslinked amnion showed significant improvements in muscle mass retention and histomorphometry in comparison to standard graft+suture. This suggests that the effects of reduced suture burden and photochemical sealing may be additive. The lack of significant improvement in those repairs photochemically sealed with untreated amnion supports the claim that sealing of nerve grafts in large deficit injuries is only efficacious if amnion can resist proteolytic degradation over extended periods of recovery. It may be that the added burden of revascularisation, which the graft must undergo to survive, compromises its ability to support axonal re-growth, or it may be that benefits manifest themselves only if photochemical seals are preserved long enough for axons to cross through distal coaptation sites.

In isolation, fibrin glue provides insufficient bond strength for nerve repair although favourable outcomes have been reported when used to augment suture[166, 170-174]. Fibrin bonds have also been shown to degrade within three weeks[257]. As a result, the suitability of fibrin glue for wrap fixation was questionable. In spite of these concerns, no dehiscence occurred in this group and recovery was comparable to standard graft+suture. This verifies that fibrin glue, in combination with epineurial tacking sutures, provides sufficient support and is a useful alternative for repair.

When applied to ANA in phase 2, no significant differences between light-activated sealing and conventional suture were detected. Whilst ANA+suture had significantly poorer outcomes in comparison to isograft+suture, the current standard of care, the improved mean values observed in the ANA+PTB group were statistically equivalent to isograft+suture. When comparing ANA+PTB with ANA+suture, fibre diameter and axon diameter had

narrow 95% CI, not including zero, and p-values that approached significance. Although attenuated, the effect of photochemical sealing when applied to ANA may result in small improvements in regeneration that can rival the current standard of care. This may have important clinical implications in human subjects, who have a limited regenerative capacity, when severe injury, complicated by limb loss, precludes the use of autograft.

Although the presence of basal lamina elements such as fibronectin and laminin in ANA can promote neurite outgrowth and support axonal regeneration in the absence of SCs[258-265], with increasing graft length, successful regeneration is reliant on graft re-population by resident SCs[266, 267]. Studies have shown diminishing regenerative return with increasing graft length[136]. Evidence suggests a finite migratory and proliferative capacity of SCs and shows that repopulation of increasingly long ANAs by recipient SCs can lead to SC senescence[268]. The current study did not assess SC re-population but it is possible that photochemical sealing of the intraneural mileu may augment SC migration and regeneration through ANAs. Assessing SC repopulation in ANAs of varying length may form the basis of future study. Perhaps combining this approach with cell-based therapy may have a synergistic effect.

The method of ANA decellularisation can influence outcome[269]. Comparative analysis between allografts and xenografts from various animal species has also detected significant differences in outcome[270]. Although the use of human cadaveric Avance® would have had greater clinical relevance, investigators have shown that in rodent models, regeneration through Avance® is inferior to rodent ANA[271]. This is believed to be due to a xenograft-induced subclinical inflammatory response. The use of Sprague Dawley ANA in favour of

Avance® in the current study aimed to reduce any detrimental effect of cross species immunoreactivity.

Phase 3 experiments verify that photochemical sealing remains superior to conventional suture, both when performed immediately and after a clinically relevant delay. Although this relationship was not significant for SFI, mean values were greater for photochemical sealing. Both muscle mass retention and nerve histomorphometry were significantly improved in immediate and delayed groups, suggesting that this may be a more sensitive measure than SFI in detecting a difference in regeneration. SFI and histomorphometric outcomes between immediately sutured nerves and delayed, photochemical repairs were not significantly different. This suggests that photochemical sealing may have the ability to ameliorate the poorer outcomes expected following a surgical delay using standard microsurgical repair.

The delay of 30-days in this study had a deleterious impact on recovery, regardless of whether isografts were secured using conventional suture or photochemical sealing. This is consistent with the tenet that increasing periods of axotomy and denervation result in a reduction in regenerating axons, reduced regenerative support in the distal fibre and reduced motor unit reinnervation in muscle targets. Curiously, this effect was not evident from the analysis of muscle mass retention. Gordon et al showed that freshly axotomized axons were able to recover full muscle mass and force of contraction when periods of distal fibre and muscle denervation were less than 50 days[97]. This was also observed when chronically axotomised nerve regenerated down freshly denervated distal nerve and muscle, reflecting compensatory increases in motor unit size[97]. A lack of significant difference in regenerative outcomes with shorter periods of delay has been reported by others[272]. Although mean

muscle mass retention was greater in immediate repair groups in this study, it is possible that the lack of statistical significance reflects an element of compensation through increased innervation ratio. Significant differences in SFI between immediate and delayed groups suggests that compensatory increases in innervation ratio, whilst sufficient to maintain muscle mass of the lower limb, may be unable to compensate for poor reinnervation of intrinsic musculature of the foot and sensory loss, both essential components for coordinated motor control.

The inclusion of histomorphometric data for normal, uninjured nerve allows assessment of recovery of treatment groups not only against the current standard of care for nerve gap repair, but also against that of normal, uninjured nerve. This data was subsequently included in histomorphometric data tables in phase 2 and 3. It was felt unnecessary to repeat sampling of uninjured nerve in these groups as all experiments used 250-300g male Lewis rats. Mean axon counts in the distal nerve fibre were significantly higher in several treatment groups in comparison to uninjured nerve. Wolthers et al showed that after 100 days, the total number of myelinated fibres was almost twice that found in control, uninjured nerve following crush and transection and repair[273]. This may be partly explained by the observation that following injury, transected axons give rise to many daughter axons[274]. These misleadingly high axon numbers do not accurately reflect the number of neurons successfully regenerating and is a major limitation of this outcome measure[275]. Wolthers et al reported a mean fibre diameter of 8.20+/-0.04 in control rat sciatic nerves which is comparable to our results[273]. Mean fibre diameter after transection and repair was 6.70+/-0.05 which, although is also comparable to our results, is following end-to-end repair rather than nerve grafting[273]. Reports of the morphometric outcomes following nerve grafts are less well studied and more conflicting. Axon counts were found to be reduced in distal stumps following regeneration through

mouse sciatic nerve gaps[276]. Declines in axon number in the distal nerve have also been observed in rabbit median nerve grafts[129]. Contrastingly in a monkey median nerve graft model, significant increases in myelinated axon number distal to nerve grafts were reported, in comparison to normal controls. Significant reductions in fibre diameter and increases in G-ratio (less remyelination) were also observed suggesting that regeneration through these grafts was consistent with that observed following end-to-end neurorrhaphy[277].

In phase 3, G-ratio, or the extent of remyelination, was significantly better in the immediate PTB group. This was consistent with the other significantly greater histomorphometric variables in this group, in keeping with this being the optimal method of nerve repair observed in earlier experiments. However, in phase 2, G-ratio was significantly better in isograft+suture in comparison to isograft+PTB and was actually statistically comparable to ANA+suture. These observations imply that re-myelination is less effective following photochemical sealing and is not affected by decellularisation. A similar finding was found in phase 1 where G-ratio was significantly better in the standard isograft+suture group in comparison to xHAM+PTB and other remaining groups. These observations are contrary to the majority of muscle mass retention and histomorphometric data observed throughout this thesis and to the conclusion that light activated sealing is the optimal repair strategy for nerve gap injury. They are also not consistent with the extensive body of literature supporting the conclusion that regeneration through nerve grafts, particularly those that have been decellularised, has a detrimental impact on remyelination. The explanation for these observations is unclear.

The mechanisms behind the observed beneficial effects of light activated sealing are largely unknown. Suture material causes foreign body reaction, granuloma formation and the formation of intraneural scar[87]. The relative absence of suture may lead to a less tumultuous repair environment, expediting the regeneration of axons across coaptation sites. Protection of the repair site may reduce the effects of extraneural scar and may also reduce the escape of axons extra-fascicularly, therefore reducing the formation of neuroma. Those nerves repaired photochemically tended to have less extraneural adhesions in comparison to standard graft+suture (figure 29, 34, 38). Although insufficient data was collected to allow robust assessment of this observation, this is a finding consistent with previous studies[243]. Phototherapy has been shown to inhibit fibroblast and myofibroblast activity and causes massive neurite sprouting and SC proliferation *in vitro*[278-280]. This effect may also explain recently demonstrated reductions in implant capsule formation and capsular contracture by tissues pre-treated with photochemical tissue passivation[281]. Furthermore, the anti-fibrotic effects of transplanted amnion have been well reported[199, 282].

Following injury, neurotrophic rich fluid leaks from nerve ends and can be physically collected[283-285]. Techniques that capture and enclose this fluid at the repair site have resulted in superior outcome[283]. ANA are devoid of SCs and neurotrophic factors. The observation that light activated sealing is less effective when applied to ANA suggests that sealing the repair sites with a durable bond may help contain SCs and fluid and preserve a neurotrophic rich milieu.

Following denervation, SCs in the distal nerve upregulate RAGs and the expression of neurotrophic factors. With increasing denervation time, this expression progressively declines

and SCs become dormant, diminishing their ability to support regeneration[21]. The observation that outcomes using light-activated sealing following a delay can match conventional suture performed immediately suggests that sealing with durable bonds may help maintain neurotrophic levels and may also retard SC dormancy by preventing the loss of mitogenic stimuli released from fresh nerve grafts. The uncertainty surrounding these mechanisms will provide impetus for further study.

Limitations of the study

Rodent animal models are invaluable research tools that have helped facilitate the clinical translation of many peripheral nerve repair techniques that are in use today. Nevertheless, there are several general limitations associated with the use of rats that are also applicable to this thesis. In comparison to humans, rats have a superior ability to regenerate axons. Lunborg et al showed that without any intervention, axons regenerated through a silicone tube, across a 6mm rat sciatic nerve gap, regardless of whether the distal end was included in the conduit[286]. When the gap was increased to 10mm, complete regeneration was possible only if the distal nerve end was included in the conduit. If the distal ends were excluded, little or no axons regenerated. Through 15mm conduits, regeneration was nonexistent, regardless of whether distal ends were included or not. Based on these experiments, the regenerative limit or "critical gap" in rodents was accepted as being 15mm[285-287]. Subsequent studies showed that this upper regenerative limit could be increased to 20mm if conduit lumens were filled with dialysed plasma[288], glycosaminoglycan matrix, laminin, and collagen matrix[289, 290]. Studies by Mackinnon et al suggested that this may be an underestimation. After complete excision of the sciatic nerve at the sciatic notch and 5-months follow-up, regeneration was observed over a mean length of 23.7+/-6.4mm[291]. The critical gap varies

between animal species, being approximately 3cm in rabbits and 4cm in humans[88]. This variation is believed to be due to differences in rates of fibrin cable degradation between proximal and distal nerve ends rather than major differences in rates of regeneration. SCs use these fibrin guidance matrices to form the bands of Büngner[88].

Photochemical bonding required clear access 5mm proximal and distal to the coaptation site. As a result, the maximum achievable nerve gap before sciatic trifurcation was 15mm. Although significant improvements in outcome were detected with the use of photochemically bonded crosslinked amnion in phase 1, these differences were small. It is possible that the use of this "limited" large nerve gap coupled with the superior regenerative ability of rats may have interfered with our ability to detect differences between groups. In other words, regeneration was good regardless of intervention. The lack of significant differences between light-activated sealing and suture when applied to ANA may also reflect this. Whitlock et al reported no significant difference in outcome between isograft and rodent allograft across a 14mm sciatic nerve gap after 12 weeks. However, a significant difference was detected after 16 weeks when the gap was extended to 28mm[292]. Nevertheless, in our experiments, ANA+suture performed significantly poorer than isograft+suture over a 15mm nerve gap. Further studies using larger nerve gaps are planned. It is possible that the small improvements detected will be more pronounced when performed in larger animals and humans.

Although the observations in phase 1, 2 and 3 showed evidence of reduced intraneural and extraneural scarring, this was not objectively tested. Histological assessment and objective, blinded scoring of nerve scarring at sacrifice would have helped substantiate this claim. The

potential scar reducing effects of PTB remains conjecture. A possible confounding factor in the future assessment of nerve scarring and PTB is that, in comparison to humans, rats scar to a much lesser extent[293]. The formation of abnormal scars is very much a human disorder. The presence of the panniculus carnosus in animals such as the rat leads to rapid contraction and minimal scarring following injury to the skin[293]. In light of the increasing propensity for scar tissue formation in humans, it is possible that any real scar reducing effect identified in this thesis could be even more pronounced when applied to human nerve repair.

The performance of light activated sealing was assessed against isograft+suture, the current standard of care. Outcomes in this positive control group are comparable to other studies[292, 294]. However, some have reported more successful outcomes with sutured isografts. Methodological discrepancies between studies commonly exist, making meaningful comparisons difficult. Nonetheless, poorer outcomes may be due to technical aspects of repair and microsurgical experience. The lead surgeon in this study was a senior plastic surgery trainee (N.G.F) with experience in microsurgical repair. It is possible that if repairs had been performed by an "expert" microsurgeon, outcomes following isograft+suture may have been improved, nullifying the observed superiority of light-activated sealing. However the technical demands of microsurgical repair are a fundamental limitation. Expertise and equipment may not be available clinically. An advantage of light-activated sealing is that surgeons without microsurgical training can readily adopt the technique.

Due to the exchange of isografts between rodents, tensionless repair was impossible. The insertion of two tacking sutures at coaptation sites was necessary to permit photochemical sealing. As a result, repairs were not truly "sutureless". A solution to this problem would

have been to use additional rats purely as nerve donors and to simply transect the sciatic nerve prior to nerve graft interposition, rather than excising a length of nerve. However this would have had major financial implications. In the clinical arena, nerve autografts and allografts can be oversized to eliminate tension, obviating the requirement for sutures. Whilst tacking sutures may still be necessary for group fascicular repair and cable grafting, subsequent wrapping of the entire gap still offers the benefit of sealing and containment of neurotrophic-rich fluid.

In phase 2, the use of Isograft+suture and Isograft+PTB groups as historical controls introduced an element of selection bias. An assumption was made that the outcomes in these groups achieved in phase 1 would have been replicated had they been repeated. The use of this data was justified in light of the fact that the same surgeons (N.G.F and J.N.G) performed all experiments, the same methods of repair were used (other than the use of ANA in place of isograft in phase 1), the same researchers were involved in outcome assessment (N.G.F and A.M) and the animals received the same post-operative care by the same animal facility team. The experiments also took place sequentially with very little delay between phases 1 and 2. Although methodologically "cleaner", the inclusion of new isograft groups would have resulted in unnecessary animal morbidity and cost.

In phase 3, the period of surgical delay may have been insufficient. Gordon et al showed that the deleterious effects of prolonged axotomy and denervation were maximal following considerably longer surgical delays than found in this study. However, the exponential decline of motor unit reinnervation was evident with delays of less than 50 days[97]. In addition to surgical delay, denervation time is further extended by slow rates of regeneration.

Although rates are commonly quoted as 1-3mm/day, Brushart et al explained that this referred to only the fastest growing sensory axons[102]. Large numbers of axons can take many days and weeks to traverse coaptation sites. This "staggered regeneration" is the result of the physical obstacle presented by suture repairs, the arborisation of daughter axons and the rationing of raw materials from the cell body, and sensory-motor mismatching leading to pruning[102]. These effects are exacerbated in the context of nerve grafting when axons must negotiate two copatation sites. Gordon et al estimated that regeneration of all motorneurons across an injury site can take 1-month and by extension, regeneration through a 15mm autograft may take in the region of 10 weeks[97, 295]. The deleterious effects of chronic axotomy and denervation are also exacerbated with grafting[35, 36, 97]. Clinically, denervation times may typically exceed that which has been tested in this study. Nevertheless, the 30-day delay led to a deleterious and detectable impact on regeneration and has allowed significant differences to be detected between treatment groups.

The limitations of current functional and histological outcome assessment for peripheral nerve research in rodent models have been well reported[296-299]. The use of walking track analysis and SFI is arguably the most problematic of these. SFI uses inked prints to measure parameters such as print length, toe spread and intermediary toe spread. Entering these values into the validated Bain-Mackinnon-Hunter equation gives results between zero and -100, with -100 representing complete dysfunction and zero representing either a normal, uninjured nerve or a completely recovered nerve[256]. The coefficients associated with print length, toe spread and intermediary toe spread are derived from regression analyses on data from large volumes of rats and represent the significance and weighted contribution of each measurements on the index formula[256]. The importance of narrowed toe spread is reflected by a significantly weighted coefficient.

SFI aims to provide an assessment of integrated motor recovery that is reliant on appropriate sensory and motor target reinnervation and minimization of axonal misdirection. Whilst providing useful information on the success of regeneration, histomorphometry provides little information on the appropriateness of reinnervation. Regenerating axons re-innervate muscles non-selectively and as a result, regeneration, remyelination and reinnervation may be successful but may not translate into successful functional recovery if reinnervated targets are inappropriate. This can account for good recovery of muscle mass and histomorphometry, with relatively poor recovery of SFI, as observed in this thesis. Sensitivity and selectivity of SFI is poorly reported but many have highlighted concerns with the use of SFI. When using SFI to assess recovery across a 1cm nerve gap, Shenaq et al were unable to distinguish between unrepaired nerves and nerves repaired with autograft, amnion conduits and silicone conduits, showing no correlation between SFI and histomorphometry[300]. Urbanchek et al found a lack of correlation between SFI and muscle forces[301], an observation most likely related to abnormal muscle activation patterns during locomotion due to non-selective reinnervation[302]. Others have also suggested that significant cortical re-organisation of sensory-motor maps occurs following nerve injury, further interfering with the reliability of SFI[303]. Other reported limitations of SFI relate to practical issues. Due to non-compliance, often several attempts are required to obtain satisfactory walking tracks to measure from. Some prints may be uninterpretable due to foot dragging, contractures and automutilation. Significant variations in print parameters can occur with changes in velocity and compensatory weight shift to the contralateral limb secondary to the injury[304, 305]. Perhaps most importantly, the act of print measurement is a subjective one. The use of other objective outcome measures, such as electrophysiology and immunohistochemistry would have added depth to this thesis and will be considered for future studies. Despite these limitations,

walking track analysis and SFI provide a non-invasive assessment of integrated motor function.

As has already been discussed, the use of axon counts can be problematic. Transected axons give rise to multiple daughter axons that form part of the regenerating front[274]. As a result, axon counts can be misleadingly high distal to the site of repair and do not necessarily reflect the number of neurons that have successfully regenerated axons[275]. Axon counts were significantly greater than that seen in uninjured sciatic nerve in many treatment groups throughout this thesis. Several others have commented on the inconsistences between distal axon counts and neuron counts[306]. Alternative methods of analysis that can overcome this issue include retrograde labeling of cell bodies[275].

The loss of two animals in the delayed+PTB group and the unsuccessful regeneration in one of these rodents was a concern. It is uncertain what caused this although the excessive delivery of energy from the light source is most likely. The light used in this study was delivered by means of a divergent beam. As a result, small, inadvertent reductions in the distance between nerve and light source during bonding may have resulted in the delivery of excessive energy. Although not apparent at the time of bonding, subtle thermal damage to the internal architecture of nerve stumps and grafts may have compromised axonal regeneration and revascularisation. Collimation of the beam would be a simple, easily achievable solution that would standardise spot size and energy delivery and improve safety for clinical translation.

How the results fit into the current field of peripheral nerve repair

Photochemical sealing of peripheral nerves offers an alternative method of repair to conventional microsuture. In order for the technique to translate clinically, the technique must be safe and the materials involved must be biocompatible and approved for use in humans. Amnion has emerged as a very useful biological membrane that bridges coaptation sites and facilitates the formation of photochemical bonds between nerve ends. Amnion is very thin and has no elastic memory, allowing easy wrapping around the circumference of small diameter nerves. The translucency of the membrane allows easy light penetration, a critical feature during bond formation.

Ex vivo testing confirmed that amnion is strong and elastic with biomechanical properties consistent with those reported in the literature[160]. Amnion bonds to nerve epineurium equally well whether using the chorionic or epithelial surface, a finding consistent with previous studies[307]. Maximum load to failure, Youngs modulus and resistance to collagenase degradation all increased significantly when crosslinked with EDC. Crosslinking up to a maximum concentration of 4mM EDC had no detrimental impact on the formation of photochemical bonds and as a result, this value was selected for *in vivo* testing. Crosslinking beyond 4mM EDC led to a significant fall in uniaxial photochemical bond strength. This may have been related to excessive material stiffness, impaired circumferential wrapping and the presence of microfractures in the material. Chemical crosslinking and photocrosslinking occur by discrete mechanisms and as a result, it is also possible that the observed drop in bond strength at high EDC concentrations may be due to a critical fall in the number of sites that are available for photo-crosslinking and bond formation. *Ex vivo* bond strength between rat sciatic nerve and photochemically bonded crosslinked amnion was comparable to

conventional epineurial suture using four 10-0 ethilon sutures, typically what is used clinically for nerves of this size.

Although several other commercially available nerve wraps were tested, the majority of these products were excessively thick (150-200μm) and stiff, with pre-determined internal diameters. The elastic "memory" could not be overcome and as a result, circumferential wrapping was problematic. The loose fit and lack of adherence between wrap and epineurium made light activated sealing impossible. Based on *ex vivo* tests, single layer SIS (manufactured by Cook Medical and distributed by HealthPoint Biotherapeutics as Oasis® wound dressing) was a suitable alternative. SIS had a thickness of 100μm and once rehydrated, had very little memory, allowing circumferential wrapping, adherence and photochemical bonding. Tensile strength, resistance to collagenase degradation and bond strength were superior to amnion. However, *in vivo* use was problematic. Increased thickness of SIS (100μm vs. 20-50μm for amnion) impaired adherence and circumferential wrapping. As a result, photochemical bonding was sub-optimal leading to two cases of nerve dehiscence in the xSIS+PTB group. Although ineffective in this setting, it is possible this material may still be suitable for larger caliber nerves in humans.

Rose Bengal has been used for several biological applications. Historically, it has perhaps been most commonly used as a conjunctival stain in the field of ophthalmology to diagnose conditions such as kerataconjunctivitis sicca[308]. In addition to its use as a tissue stain it has found several other biological applications due to its photo-reactivity. The mechanism of action of Rose Bengal is still relatively unknown although it is postulated that when activated by 532nm laser light, photons of light absorbed by RB result in the creation of free radical

species. The generation of free radicals is usually synonymous with cellular toxicity and this has been raised as a concern with the use of RB. In keeping with this, RB has been shown to be toxic to corneal epithelial cells and can cause discomfort if not given with topical anaesthesia[308, 309]. As a result, alternatives to RB for this purpose are often preferred. Experimentally, photoactivated RB has been used to deliberately cause tissue damage. Intravenous administration of Bose Bengal and subsequent focal laser activation in the brain is a well-reported technique used to induce photo-thrombotic stroke in animal models[310-312]. It has also been used as a topical agent in photodynamic therapy (PDT) for skin cancer although no toxic effects to the surrounding normal skin were demonstrated[313]. In the context of photochemical bonding, the formation of reactive oxygen species from closely apposed RB-stained tissue surfaces is believed to result in covalent crosslinking between amnion acid residues[242]. As with PDT, when used as a sutureless method of wound closure following surgical excisions, no toxic effects were demonstrated[314]. In the context of peripheral nerve repair, both *in vitro* and *in vivo* experiments have also confirmed a lack of cellular toxicity[314, 315].

Fluence describes the amount of energy delivered per unit area and has the unit joules per centimeter squared (J/cm^2). Irradiance describes the rate of delivery of this energy and is measure in W/cm^2. Dose response experiments performed in this study showed that, with a constant irradiance of $0.5W/cm^2$, optimal bond strength was achieved with a fluence of 60J/cm2. These findings are consistent with previous work[243]. Lower fluences led to inadequate bonding, with higher fluences leading to excessive illumination times and desiccation. These laser settings translate to an illumination time of two minutes which is considerably quicker than conventional suture repair time.

In addition to potential time saving benefits, the technique of light activated sealing relies less on specialist microsurgical equipment, not including the light source. This may make it more accessible to those that do not have access to sophisticated equipment or facilities. Reduced operative time and a reduced requirement on expensive equipment should translate into substantial costs savings for the healthcare provider. The process is technically easier than standard microsurgical techniques and should therefore be readily adopted by surgeons that are less experienced or who lack classic microsurgical training.

Implications for the future of peripheral nerve repair

With refinement, light activated sealing could establish itself as an alternative to suture for the repair of peripheral nerves. Developing a portable hand held light source in addition to a pre-packaged, photo-active dye-stained nerve wrap, may make possible "off-the-shelf" nerve repair kits that could be stocked in operating rooms in a similar way to sutures. The ability to improve regeneration through ANAs may make the use of nerve autografts obsolete, ridding the patient of the morbidity associated with donor nerve harvest. This may have great relevance for military reconstructive surgeons who must often manage devastating injuries in austere, war torn environments.

Very few clinically translatable interventions have been able to improve outcomes following peripheral nerve repair. Electrical stimulation of nerve repair sites may upregulate RAG expression and the production of neurotrophic factors[101, 102]. Improved rates of regeneration have been demonstrated in animal models of immediate and delayed repair[104, 160] and most recently, has facilitated full reinnervation of thenar muscles in humans with severe carpal

tunnel syndrome[105]. The administration of pharmacologics such as acetyl-L-carnitine (ALCAR) or N-acetyl cysteine (NAC), both of which are clinically safe, can offer neuroprotection to the injured nerve by reducing the effects of axotomy-induced apoptosis in the cell body[316]. Clinical trials involving both of these compounds are expected in the near future.

As more is understood about the neurobiology of nerve injury and regeneration, increasing attention is being focused on manipulating the cellular components involved in order to prolong a growth permissive environment. The supplementation of exogenous SCs and neurotrophic factors at the repair site and in the periphery has the potential to improve rates and success of regeneration. However, many pragmatic obstacles exist concerning the delivery of these cells and their temporal and spatial regulation. For example, inappropriately high concentrations of some neurotrophic factors can be inhibitory to regeneration and can even promote cell death[99, 100]. The application of these approaches is exciting but is far from being realised clinically. Contrary to popular opinion, the results presented in this thesis suggest that improvements to the technical aspects of peripheral nerve repair may still be possible. This offers a more simplistic and clinically translatable solution at present. If light activated sealing can be shown to improve the longevity of SCs and neurotrophic factors at the repair site, it is possible that these two approaches may be combined in the future.

Section 5: Conclusions

Photochemical sealing of nerve graft coaptation sites using crosslinked human amnion nerve wraps results in a statistically significant improvement in muscle mass retention and nerve histomorphometry in comparison to conventional graft+suture. This observation may be related to the creation of a protective seal at nerve graft coaptation sites and the improved longevity of this seal as a result of nerve wrap crosslinking. This seal may act to enclose SCs and the growth promoting factors they produce. The lack of suture, the effects of low power laser irradiation and the presence of amnion at the repair site may all contribute to a reduction in inflammation and scar tissue formation. Although unsuitable for small caliber nerves, we are optimistic that SIS may represent a viable, commercially available nerve wrap that may facilitate the rapid clinical translation of photochemical sealing of larger caliber nerves.

The significantly poorer outcomes observed following ANA+suture in comparison to isograft+suture is typical and can be explained by the absence of SCs and their growth promoting influence in these grafts. Outcomes in the ANA+PTB group were not significantly different in comparison to ANA+suture. It is possible that the attenuation of the previously observed photochemical effect is also due to a lack of SCs and neurotrophic factors and the inability to contain these at the repair site. Although not significant, greater mean outcome values in the ANA+PTB group were statistically comparable to isograft+suture, the current standard of care. This could translate into important improvements in peripheral nerve recovery in those cases of severe trauma and limb loss where the use of nerve autograft is not possible. With refinement, photochemical sealing, when used in conjunction with ANA, has the potential to completely supplant the use of autografts following large gap injury.

Outcomes of repair following a 30-day delay are significantly poorer in comparison to those repairs performed immediately. When performed after a delay, light activated sealing of isograft coaptation sites with crosslinked amnion wraps results in significantly better outcomes in comparison to sutured repairs. The use of light activated sealing following delayed repair results in outcomes that are statistically comparable to those achieved with immediate suture. In combination with the potential benefits demonstrated when applied to ANA, these findings may have potentially important clinical implications for the future repair of large gap nerve injury following periods of delay, particularly when the nature of the injury precludes the use of autologous nerve.

Section 6: Additional Work

6.1 Assessing nerve revascularization using Optical Frequency Domain Imaging: a proof of concept pilot study

6.1.1 Introduction

The detrimental effects of hypoperfusion and ischaemia on the structure and function of peripheral nerves is well established. Prolonged periods of ischaemia, regardless of aetiology, result in conduction block and if prolonged, de-myelination and degeneration. Clinical examples of such sequelae include temporary paraesthesia following short periods of limb tourniquet use or weakness and muscle wasting following chronic nerve compression. In addition to the loss of nerve continuity following transection, investigators have shown that stretch and compressive injuries can result in immediate vascular occlusion and latent occlusion secondary to increased microvascular permeability and oedema, long after the injurious event has passed[317]. Due to the rich anastomotic intrinsic vascular system, and the segmental extrinsic supply, vascular compromise following transection and end-to-end repair is unlikely. However, following nerve grafting, particularly when nerve gaps are large, when graft diameter is excessive, when grafts are decellularized, and when the quality of the tissue bed is poor, slow or delayed graft revascularization may have a major impact on the success of regeneration and recovery.

Revascularization of nerve grafts is believed to occur through two mechanisms. Centripetal revascularization refers to neovascularization from surrounding tissues and several

investigators have claimed the predominance of this process[318-321]. In contrast, inosculation describes the process by which the longitudinal plexus of blood vessels lying on and within the connective tissue layers of the nerve are re-established. Others have shown that this process, rather than tissue bed neovascularization, is the primary source of revascularization[322, 323]. With regards to timing, revascularization of nerve grafts has been observed to occur anywhere between 3 days and 3 weeks[323]. The process of centripetal revascularization led to predictions that the use of vascularized grafts would result in superior rates of revascularization and would therefore out-perform conventional, non-vascularized grafts. Although several studies supported this theory[122-126], other investigators were unable to show any significant difference[127-130]. In addition, no significant differences have been observed when comparing nerve autograft with allograft[323, 324].

Several techniques have been used to try and visualize the microvasculature of peripheral nerves. Histological techniques[322, 324] provided useful information of vascularity at specific times and locations but were unable to provide any useful information on the dynamicity of the process. Microangiography using radionuclide labeled microspheres and other washout techniques provided a more comprehensive evaluation of blood flow although these techniques were limited to regional assessments of flow[318-321, 324]. Intravascular tracer (Evans blue bovine albumin) provided more information on individual vessel flow characteristics[323]. The disadvantages of all these approaches is the inability to image in real time, the invasive nature of the techniques and the reliance on contrast media for visualization.

Most recently, novel optical imaging techniques such as orthogonal polarization spectral imaging (OPS) have been applied to peripheral nerves. Emitted light is reflected off

erythrocytes and is captured to produce an image. This imaging modality provides real time evaluation of microcirculatory blood flow and has suggested that revascularisation is primarily through a bi-directional, inosculation-type mechanism[325]. An alternative emerging technology is optical frequency domain imaging (OFDI). OFDI is an optical imaging technique based on very similar principles as its parent technology, optical coherence tomography (OCT)[326]. Using low-power infrared light, OFDI permits visualization of tissue microstructure, allowing in situ image acquisition, precluding the requirement for biopsy. This non-invasive (contact only) imaging has a resolution of up to 1-15μm and a depth penetration of 2-3 mm[327]. OFDI is analogous to ultrasound in that it measures the time-of-flight of launched waves. However, while ultrasound uses sound waves, OFDI uses light waves and has image resolution 1-2 orders of magnitude greater than standard ultrasound[327, 328]. As with ultrasound, OFDI Doppler imaging allows quantitative blood flow measurements. Because the optical properties of soft tissues vary significantly, OFDI provides excellent contrast between soft tissue structures. Importantly, OFDI is safe to deploy in the clinical setting as it operates with near-infrared light and requires no exogenous contrast agents. Current OFDI systems also provide images in real-time. In addition to displaying these images, OFDI systems archive the acquired data for later post-processing. In recent years, our collaborative group at the Wellmen Centre for Photomedicine, The Massachusetts General Hospital, have applied OFDI to the study of *in vivo* tumour biology, providing exquisitely detailed, real time images of tumour lymphangiogenesis and the response to different therapies[329]. Future developments exploring the differences between intratumoral and extratumoral vasculature may lead to novel methods of tumour margin control. In light of the high resolution, non-invasive, real time capabilities of this modality, it is possible that the application of this technology to the study of peripheral nerves may offer important insights into the process of revascularization following injury and repair. It was the

aim of this proof of concept study to test the efficacy of OFDI when used following various different rodent sciatic nerve injuries.

6.1.2 Methods

6.1.2.1 Animal surgery

The Institutional Animal Care and Use Committee (IACUC) at the Massachusetts General Hospital approved all procedures. Eight male Sprague Dawley rats weighing 250-300g were randomized into the following four groups (n=2): (1) crush, (2) transection and end-to-end repair (3) transection and repair of 10mm nerve gap using contralateral autograft, (4) transection and repair of 10mm nerve gap using acellular nerve allograft (ANA). Induction and maintenance anaesthesia was achieved by using ketamine (100mg/kg; Vedco Inc, St Joseph, MO)/xylazine (10mg/kg; Akorn Inc, Decatur, IL). All animals had pre- and postoperative doses of buprenorphine (0.01mg/kg; Reckitt Benckiser, Richmond, VA). Analgesia continued twice daily for 72 hours after surgery or continuously if the interval between surgery was less than 72 hours. All animals had dorso-lateral muscle splitting incisions on the left hindlimb over the distribution of the sciatic nerve. The sciatic nerve was freed from investing connective tissue along the entire length of the nerve from the distal trifurcation to a point approximately 25mm proximal to this (figure 40A). Following mobilization, baseline images were obtained of uninjured nerves. The aforementioned nerve injuries were then created and repaired as described below. All wounds were closed in three layers using 4.0 vicryl (muscle and deep dermal) and 4.0 monocryl (subcuticular). Topical antibacterial ointment was applied to wounds in order to reduce the incidence of post-operative infection. Bitter apple was sprayed onto ipsilateral feet to reduce the incidence of

automutilation. Rodents were housed in The Massachusetts General Hospital small animal facility and had access to food and water as required.

Group 1 – Crush injury

Following exposure, the sciatic nerve was crushed for 10 seconds using a pair of number 4 microsurgery forceps. Crush injuries were performed at a site measuring 10mm proximal from the site of sciatic nerve trifurcation. In order to facilitate sequential nerve imaging at the same site, two Ethilon sutures were inserted into the muscle adjacent to the nerve injury. Images were acquired immediately before and after the injury.

Group 2 – Transection and repair

Following exposure, the sciatic nerve was sharply transected using straight microsurgical scissors at a point measuring 10mm proximal from the sciatic trifurcation. Under loupe magnification, the nerve ends were immediately repaired using six 10-0 Ethilon suture. Images were acquired immediately before and after the repair.

Group 3 – Transection and repair of 10mm nerve gap using contralateral autograft

In order to harvest the autograft, the right sciatic nerve was exposed as described above. A 10mm length of nerve was excised from the mid-portion of the sciatic nerve and was stored in damp gauze until required. Following exposure of the left sciatic nerve as described above, the nerve was sharply transected with straight microsurgery scissors at a point measuring

10mm proximal to the trifurcation. The harvested autograft was reversed and sutured into the gap created by nerve end retraction using six 10-0 Ethilon sutures at each coaptation site.

Group 4 – Transection and repair of 10mm nerve gap using acellular nerve allograft

Following exposure, the left sciatic nerve was sharply transected with straight microsurgery scissors at a point measuring 10mm proximal to the trifurcation. A 10mm length of ANA was reversed and sutured into the gap created by nerve end retraction using six 10-0 Ethilon sutures at each coaptation site.

6.1.2.2 Imaging

OFDI employs a broadband low-coherence light source (beam) that is split to two paths by an optical splitter. One of these two beams is directed to a reflecting mirror in a reference arm. The second beam is directed to the tissue sample. Both the reference arm reflecting mirror and the tissue sample reflect light backward toward the system, and this recollected light from the sample and reflecting mirror are mixed to generate a signal. By analyzing this interfering signal, the optical scattering properties across tissue depth can be measured. By laterally scanning the OFDI beam across the sample, two and three-dimensional OFDI images are acquired. An essential pre-requisite for imaging is tissue/animal stabilization. Movement artifacts greatly interfere with image acquisition. The main movement artifact present in animal preparations is that created and transmitted by respiration. Isolating the sciatic nerve from the tissue bed was one solution that was explored. A platform was designed and 3D printed. This was attached to posts that could be mounted onto the OFDI objective lens. The platform could be slid up or down in the lens tower, allowing regulation

of distance between nerve and lens. The platform also contained a groove to accommodate the nerve (figure 40B, 40C, 41A). Although effective it was felt that repeatedly elevating the nerve out of its tissue bed would be detrimental to healing and neovascularization and as a result, this approach was abandoned.

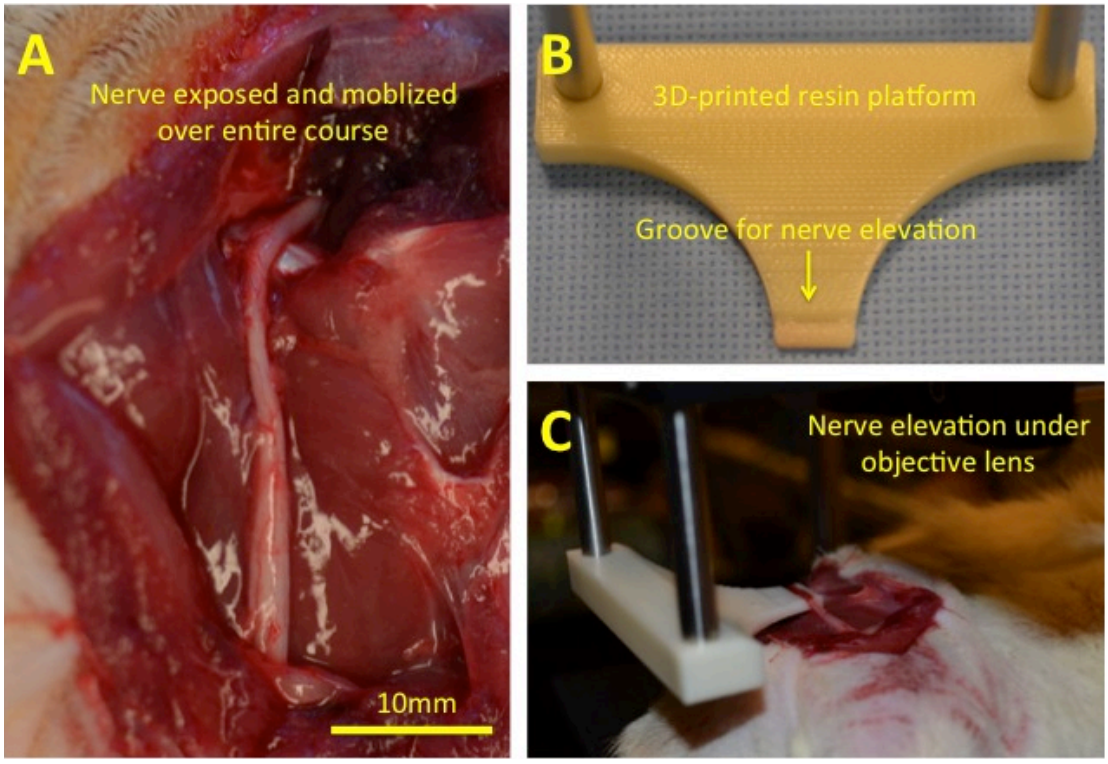

Figure 40. Sciatic nerve exposure and 3D-printed resin platform. (A) Sciatic nerve exposed and mobilized along its length. This length extended from the distal trifurcation to a point approximately 25mm proximal to this. (B) A custom-made, 3D-printed resin platform containing a groove facilitated nerve elevation from the tissue bed. (C) In situ elevation of rodent sciatic nerve from tissue bed.

Instead, following injury and repair, each rodent was firmly secured to a polystyrene platform using a combination of Velcro straps and elastic bands (figure 41B and 41C). It was found that although movement was not completely abolished, it was sufficiently reduced to enable image collection. Image acquisition was obtained immediately pre-injury, immediately post-

repair and on post-operative days 2, 4 and 7. On each post-operative imaging day, rodents were anaesthetized, had nerves exposed and images acquired as described above.

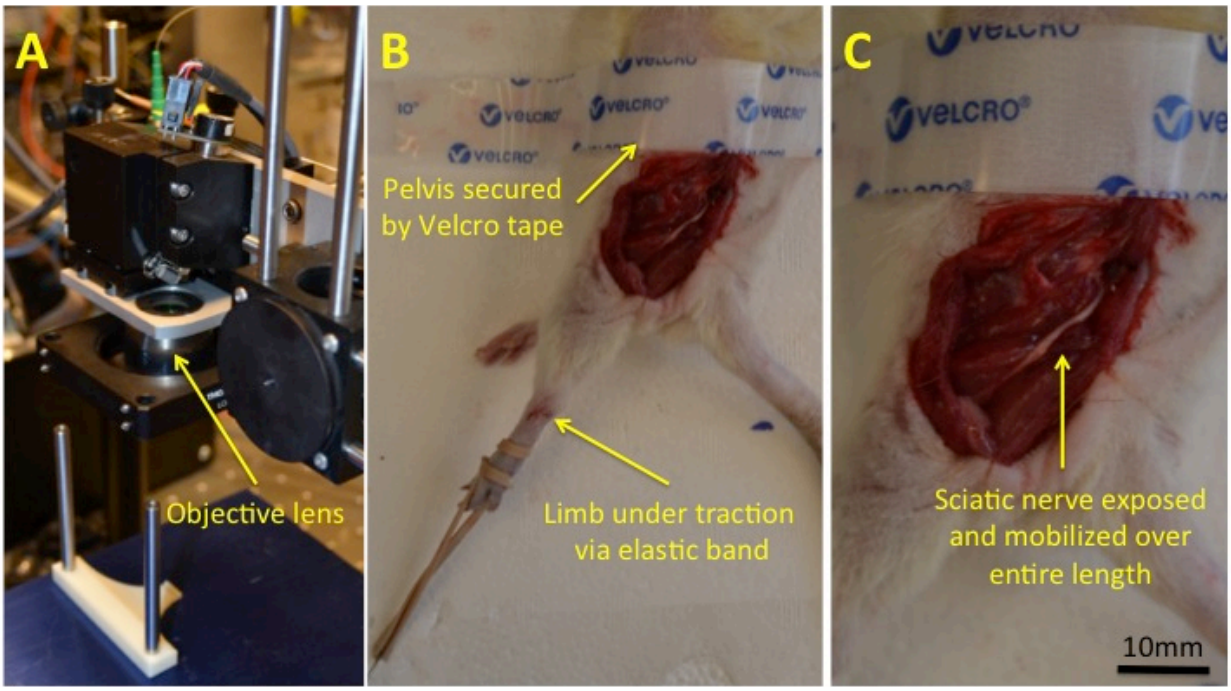

Figure 41. OFDI objective lens tower and rodent stabilization method. (A) Objective lens with rig permitting attachment of 3D printed platform (subsequently not used). (B/C) Rodent placed on polystyrene platform. Left hindlimb placed under traction via elastic band. Rodent pelvis stabilized using Velcro hook-and-loop fastener tape. Preparation successfully limited movement artifact transmitted from respiratory excursion.

6.1.3 Results

Initial image acquisition

Initial images from intact, uninjured nerve showed that, despite some residual movement artifact, nerve microvasculature could be clearly visualized (figure 42).

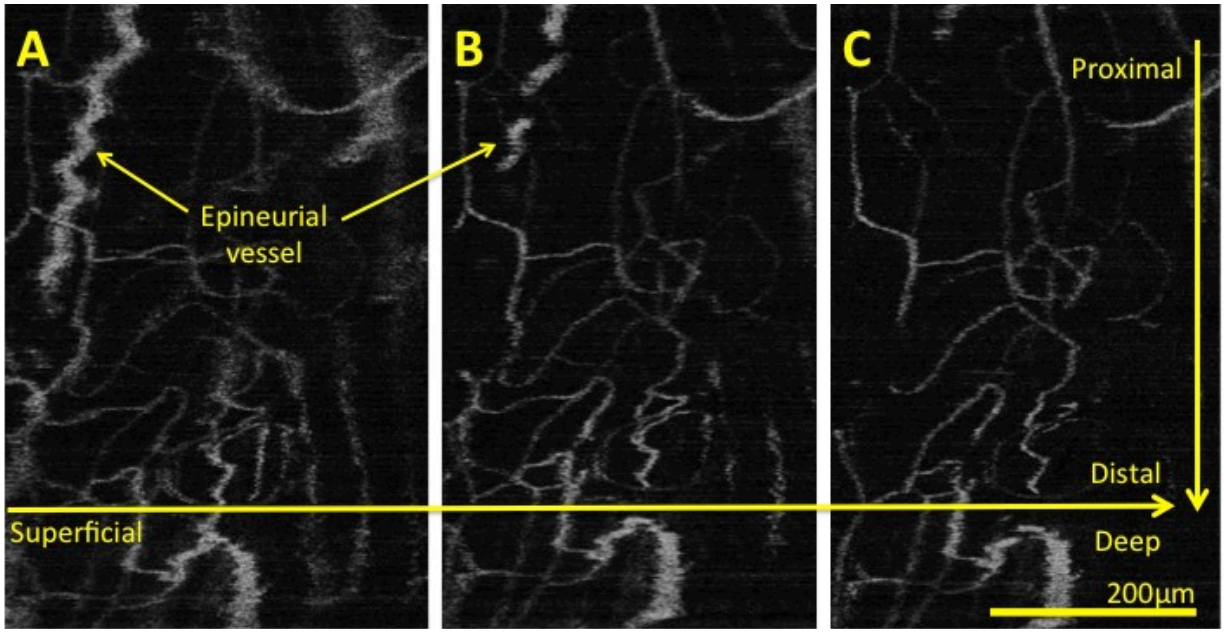

Figure 42. Unprocessed longitudinal images acquired from uninjured nerve. (A) Most superficial image. Note the extensive vasculature lying on the surface of the nerve. These vessels represent part of the mesoneurial and epineurial longitudinal plexus. Note the tortuosity of the vessels, a feature analagous to the bands of Fontana, conveying an accordion-like redundancy protecting the nerve against stretching forces during movement. (B) A deeper image of the same section of nerve. Note the epineurial vessel at the top left hand corner is beginning to disappear out of view. (C) A deeper image showing the complete disappearance of the epineurial vessel at the top left hand corner.

Crush Injury

Following crush injury, the microvasculature at the repair site was clearly visible and interestingly was not interrupted (figure 43).

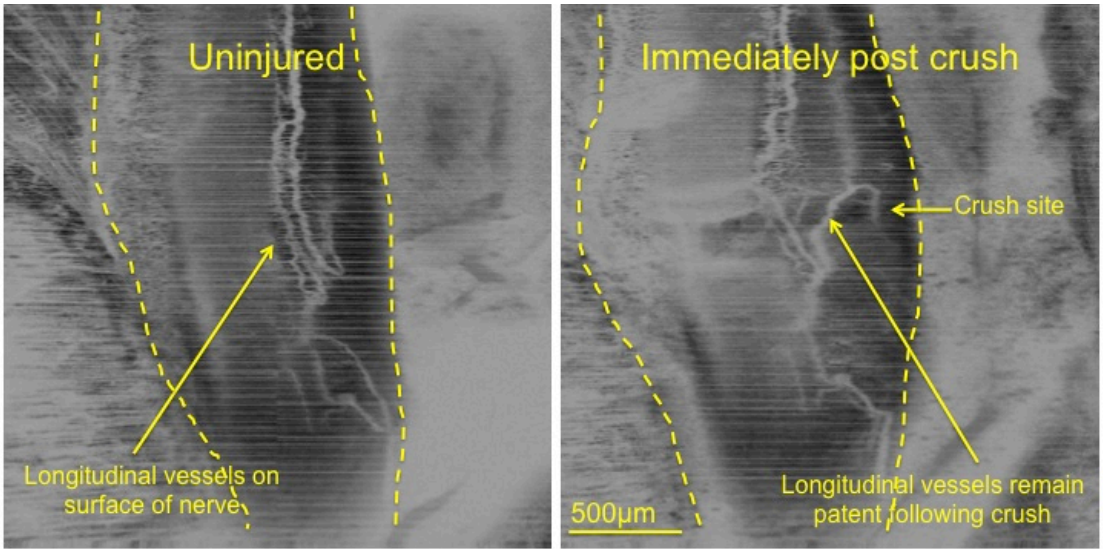

Figure 43. OFDI images of crush injury. Uninjured nerve is easily distinguishable from the surrounding and underlying muscle. Longitudinal vessels on the surface of the epineurium are apparent. A crush injury was administered in the mid-portion of the sciatic nerve using number 5 jewelers forceps. Immediately post-crush, the longitudinal vessels are still patent. The injury site was easily identified.

Transection and suture repair

Images were of reasonable quality. The nerve was easily distinguished from underlying muscle. Microvasculature was easily visible and could be seen running longitudinally along the nerve. At the site of repair, there was an area of relative hypovascularity where the vessels were interrupted (figure 44). After 7 days, a florid angiogenic process had occurred (figure 45). From the images, it appears that this revascularisation is mainly inosculatory in nature rather than from the surrounding tissue bed.

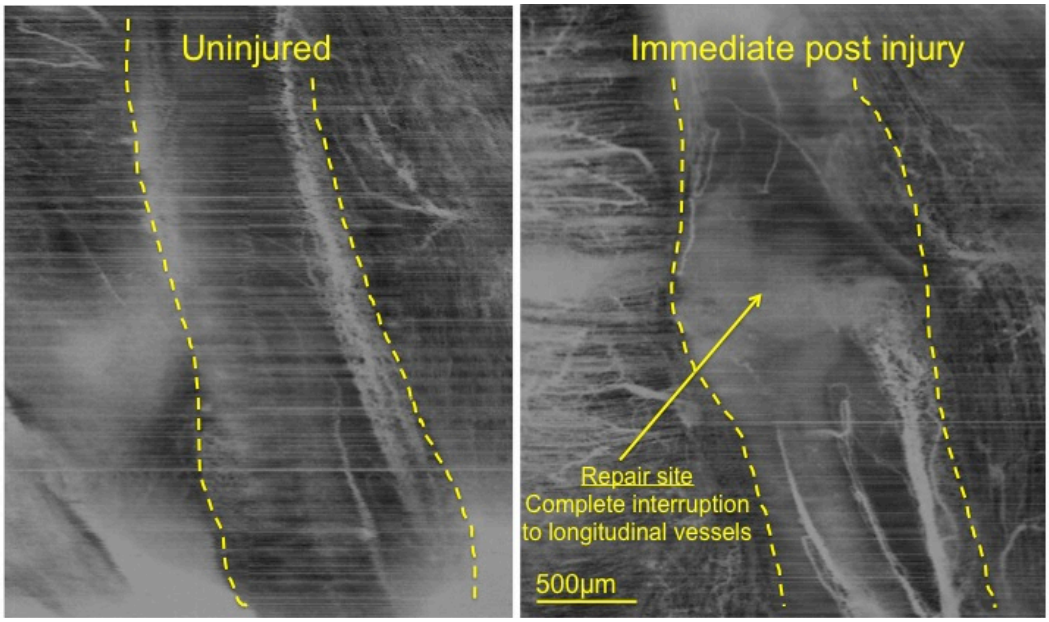

Figure 44. OFDI images of uninjured nerve (left) and immediate neurorrhaphy following transection. The markedly different light scattering properties of different tissues allows easy differentiation between uninjured nerve and the adjacent muscle bed. Longitudinal vessels can be clearly seen lying on the surface of the nerve and on the surface of the muscle. Note the preservation of the longitudinal intrinsic plexus of vessels proximal and distal to the repair site, immediately following epineurial suturing. As expected, the actual neurorrhaphy site represents an area of relative hypovascularity.

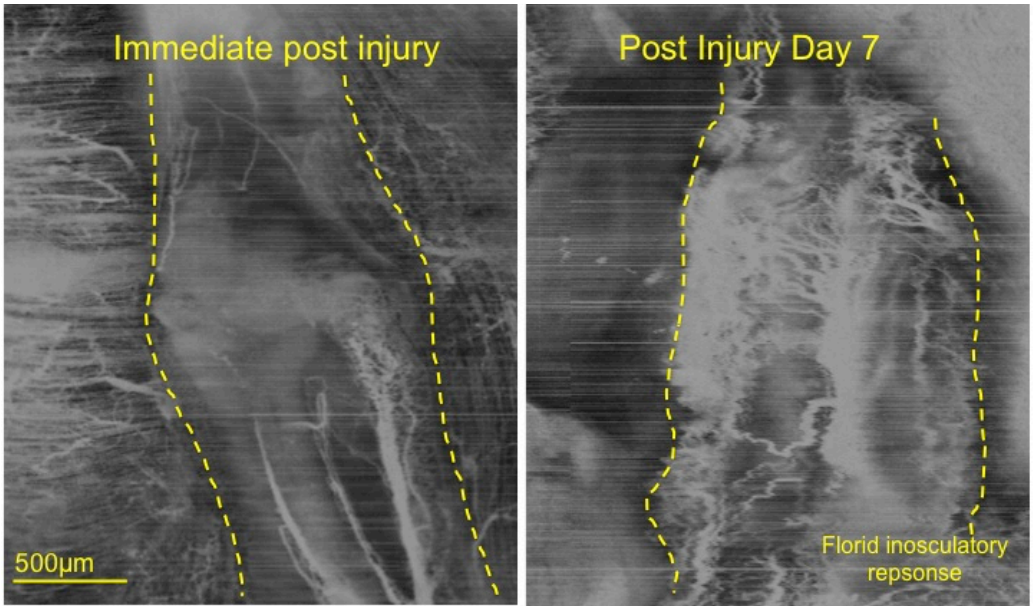

Figure 45. OFDI images of transection and suture repair. The image on the left is immediately post-injury as shown in the previous figure. The image on the right shows the florid angiogenic reaction 7-days after suture neurorrhaphy. The majority of the vessels seem to be from inosculation of the longitudinal plexus.

Repair of a 10mm gap using nerve autograft

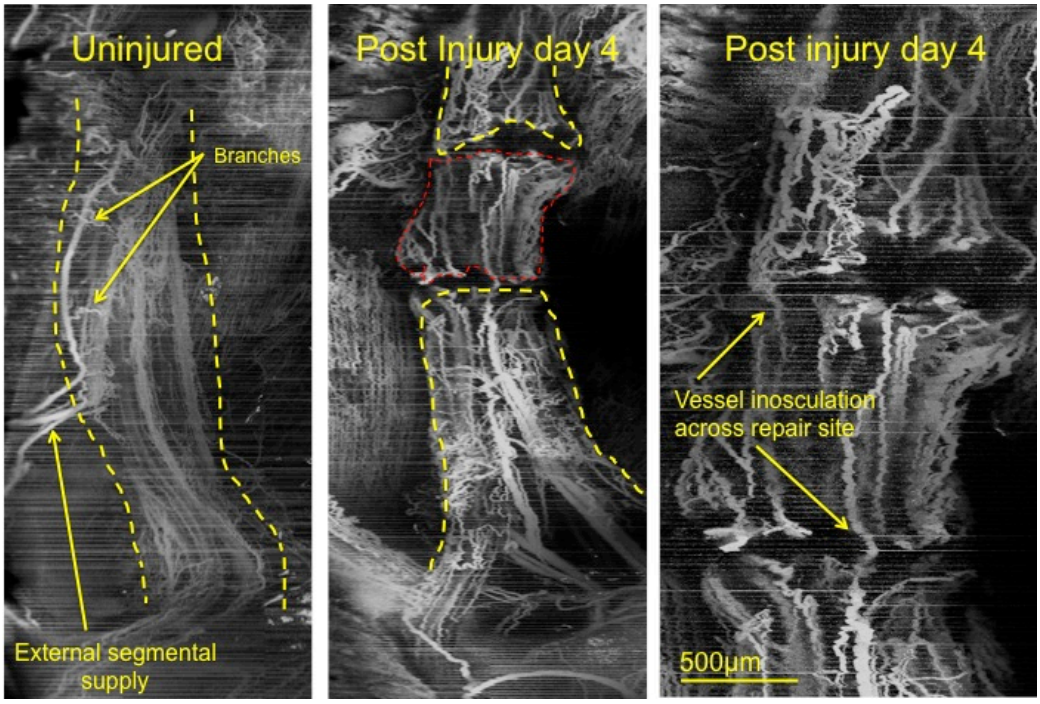

Figure 46. OFDI image of nerve autograft reconstruction of 10mm nerve gap. Note improved image quality in comparison to original images. Pre-injury image shows excellent resolution of intrinsic supply in addition to segmental extrinsic supply. Note the small perpendicular branches penetrating into the core of the nerve forming anastomotic connections between epineurium and perineurial plexi. At day 4 following repair, re-establishment of longitudinal vessels is apparent.

With greater stabilisation, image quality improved. The segmental extrinsic supply and its anastomosis with the intrinsic longitudinal plexi could be easily identified (figure 46). Re-imaging after 4 days showed vessel inosculation across the repair site (figure 46). Some

centripetal contribution could also be seen but the majority vessels were longitudinally orientated.

Repair of a 10mm gap using acellular nerve allograft (ANA)

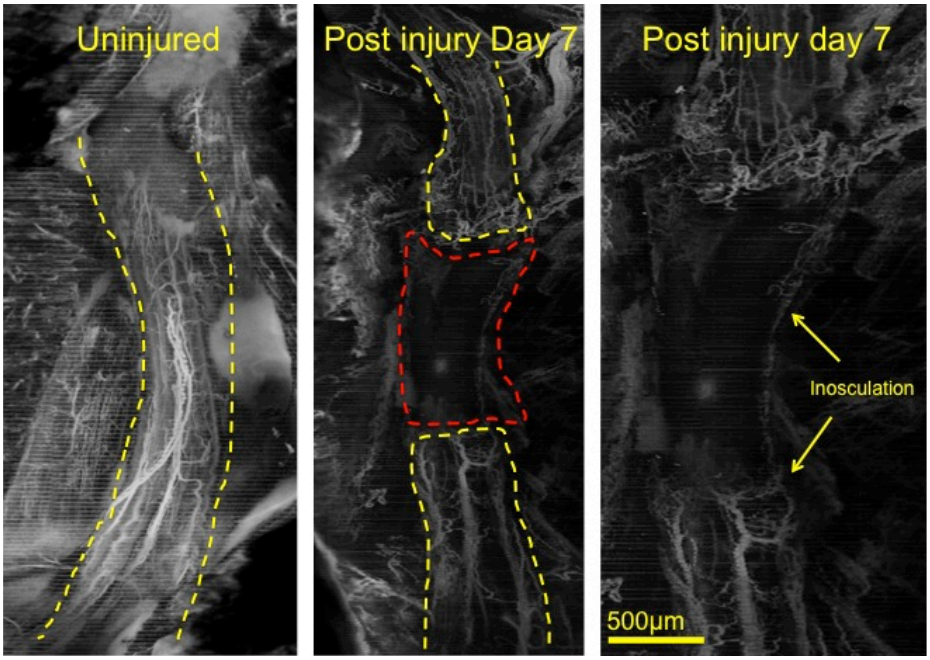

Figure 47. OFDI images of uninjured nerve and nerve gap reconstruction using 10mm ANA. As with the previous autograft images, note the excellent resolution and image quality. Nerve boundaries and longitudinal plexi or vessels are easily visualised in uninjured nerve (left). 7 days after ANA reconstruction of a 10mm nerve gap, little to no revascularistion has occurred. There is perhaps some vessel formation at the periphery of the graft but this is markedly reduced in comparison to the autograft.

As with autograft repair, the quality of OFDI images was excellent. In comparison to autograft, the ANA was hypovascular (figure 47). Very little revascularisation had occurred after 7 days, a longer initial time point than used in the autograft rat (figure 47). These observations are not surprising and partly explain why axonal regeneration through these grafts and the ultimate recovery is inferior to that observed following nerve autograft

reconstruction. Software refinements that will allow quantitative measurement of blood flow are in progress.

6.1.4 Discussion

The results of this pilot study have shown that OFDI has the ability to provide high resolution, real-time images of nerve microvasculature. Images have been successfully acquired from uninjured nerve and in nerves that have been completely transected and microsurgcally repaired. The results of these images imply that inosculation of vessels within the longitudinal plexi of peripheral nerves may be the predominant mechanism of revascularization following injury. These results are consistent with contemporary findings showing that, although centripetal neovascularization contributes to the process of revascularization, it appears to have a minor, accessory role, particularly following nerve grafting[323, 325].

Imaging following autograft and ANA reconstruction, although planned, has not yet been performed. This is due to two main obstacles. Repeated anesthesia every 48 hours was found to have a deleterious effect on the ability of rodents to recover. Incomplete recovery resulted in poor nutritional intake and rehydration to the point where animals were becoming moribund towards the latter time points. As a result, protocol amendments were made in order to increase the periods between imaging sessions and to introduce nutritional supplementation for the rodents. In addition to this, the issue of movement artifact was a continual problem. Although movement was considerably reduced by external fixation, subtle, transmitted vibrations from respiratory excursion were still present. Rather than devise an alternative method of rigid, invasive, skeletal fixation, new software is currently being written. This intends to gate the acquisition of images so that image capture only occurs at

peaks and troughs of respiration. Once these technical and protocol amendments are in place, the remainder of the experiments will be completed.

The limitations of OFDI when applied to peripheral nerve revascularization are generic to all *in vivo* optical imaging techniques. Limited tissue penetration is arguably the most important of these. Maximum light penetration is in the region of 2-3mm and this obviously precludes use of the technique for percutaneous imaging of deep structures. However, the main clinical application of this imaging modality may lie in its ability to provide real time, *in vivo* assessment of nerve vasculature and viability intraoperatively. This would be advantageous following traumatic injuries when the viability of nerve tissue is uncertain. This may also have important applications in the context of chronic injury when intraneural scar tissue obstructs regeneration and recovery. Accurate identification of the extent of these relatively avascular portions of nerve would greatly facilitate excision and repair and the avoidance of iatrogenic injury to healthy tissue.

The experimental applications for peripheral nerve research are also promising. Methods of outcome assessment in peripheral nerve research are notoriously problematic. Several methods are usually employed during any particular study. This combinatory approach acknowledges the limitations of each individual method and aims to reduce subjectivity, bias and error. Common methods include walking track analysis and SFI, muscle weight retention, nerve histomorphometry, electrophysiology, retrograde labeling of cell bodies, immunohistochemistry and fluorescence microscopy. The routine use of imaging techniques to monitor revascularization has not yet been employed although with refinement, it is possible that OFDI may make this feasible. The exact relationship between successful

revascularization, axonal regeneration and functional recovery is uncertain although with further experience, these questions may be answered. The sequential, real-time imaging of autograft and ANA revascularization may also help develop other novel strategies that can augment regeneration and outcome.

6.1.5 Conclusions

OFDI is an emerging technology that has proven efficacious for the study of tumour biology. The application of this technology to the study of peripheral nerves and their regeneration following injury is only now being attempted. This pilot study has confirmed that real-time monitoring of nerve microvasculature and revascularization following injury is possible. With refinement, high-resolution 3D reconstructions and quantitative assessments of blood flow will be possible. This may have useful intraoperative clinical applications when the viability of nerves following injury is questionable and also promises to be of use as an outcome assessment tool in pre-clinical research.

6.2 Development of a Brain-Body Interface system for limb reanimation following high cervical spine injury

6.2.1 Introduction

Background

Annual crude incidence rates of spinal cord injury (SCI) vary between 12.1-57.8 per million[330]. Most SCI show a bimodal age distribution with the first peak arising in young adults between the ages of 15-29 years and the second peak in older adults, mostly over 65 years[330]. Motor vehicle accidents and falls are the commonest mechanisms of injury[330]. SCI has become more prevalent within the ranks of the armed services as a result of the wars in Iraq and Afghanistan. Between 2000-2009, 5928 SCI cases were reported throughout the entire US military population[331]. Among the 7877 combat-wounded from the years 2005 to 2009, 872 were classified as SCI, meaning that more than 1 in 10 injuries sustained in the theatre of war resulted in SCI[332]. During the period from 2001-2009, over 5% of the casualties that required battlefield evacuation (598 out of 10,979) were attributable to spine-related trauma[333]. A significant fraction of SCI injuries sustained in the military occur at the cervical level, leading to severe disability[334].

In cases where spinal cord injury is complete, there is currently very little that can be done to restore lost motor control. The treatment options following these injuries are extremely limited and largely experimental. The majority of focus is placed on rehabilitation and support as the patient accepts and adjusts to their disability. Attempts have been made to repair the damaged cord with cell-based therapy such as stem cells and neurotrophic factors. Despite promising pre-clinical results, this approach has been unsuccessful clinically.

Although patients experience devastating disability, motor intention above and lower motor neurons below the level of the injury are intact. As a result, an alternative approach following these injuries is to bypass the area of damage. Although nerve transfers are an option, the majority of research in this area has focused on neural interface technology.

Neural interface technology aims to restore lost function through the use of neuroprostheses. This concept is by no means novel. Cochlear and retinal implants can be traced back to the 1950s and since then, these devices have helped restore hearing and vision in many patients[335, 336]. The application of this technology for the restoration of movement is more recent. The type of movement restored and the functional gains provided are variable. For example, brain-computer interfaces (BCI) use neural signals to control computer cursors. The ability to point and click facilitates letter selection, spelling, writing and emailing. This has also been linked to various assistive technologies such as light switches and televisions, further extending autonomy of the operator. Brain-machine interfaces (BMI) use neural signals to control devices such as robotic arms. Demonstrations of non-human primates (NHPs) using cortical signals to control computer cursors and robotic arms for reaching and grasping[337-339] were followed by similarly impressive clinical demonstrations in tetraplegics[340-344], generating a huge amount of scientific and public interest. This represents the current limit of BMI capabilities with continued efforts being devoted to increasing degrees of freedom and autonomy. Using paralysed muscles as actuators is a challenging concept that is receiving increasing attention from researchers in the field[345]. Referred to as a brain-body interface (BBI), this represents the ultimate integration of neural interface technology. The type of cortical signals recorded, the method by which they are recorded, and how these signals are processed and delivered to the output actuator are cardinal

variables of these interface systems, and are the major points of focus for researchers in the field[345].

Cortical signal recording

Several types of information-carrying neural signal exist although broadly speaking, these signals are either action potential spikes or field potentials (FP)[346]. Spike rate has emerged as a predominant mode of information transfer and is responsible for coding a huge variety of motor information such as hand velocity, position and joint torques. This activity can be captured from single neurons or from populations of neurons (multi-unit activity (MUA)). Single unit or MUA is detectable only by intraparenchymal electrodes. The high spatial resolution and superior signal-to-noise ratio of these signals is offset by several limitations. Although MUA provides recordings from larger numbers of neurons than single unit activity, representative populations remain small. Insertion of intraparenchymal electrodes is highly invasive and is associated with potentially devastating risks of bleeding and infection. The risk of infection is compounded by the exteriorization of signal recording and transmission hardware on the scalp. In addition, implanted electrodes naturally incite a foreign body reaction. This results in gliosis, scar tissue formation and encapsulation, all of which can have deleterious effects on the function of adjacent cells and the long-term recording ability of electrodes.

Field potentials (FPs) represent summed synaptic currents sampled from large numbers of neurons with large spatial and functional variation. FPs can be sub-classified into slow, medium or fast rhythms or non-rhythm event related potentials (ERPs), all of which have

been used to drive BMIs[343, 347]. FPs can be recorded intraparenchymally as local field potentials (LFPs), from epicortical or epidural locations as electrocorticography (ECoG) signals, or from the surface of the scalp as electrencephalography (EEG) signals [345]. The ability to record FPs extracranially is an advantage over spike recording. However, recording from huge populations of neurons through bone and scalp tissues results in poor signal resolution. In spite of these limitations, EEG driven BMIs have successfully controlled computer cursors in humans[343]. Other non-invasive options such as functional MRI (fMRI) have recently been investigated. Signals can be recorded from the entire brain with high spatial resolution. However, temporal resolution is poor as the signals originate from haemodynamic rather than electrical activity[348].

Whilst recognizing the benefits of non-invasive recording, restoration of complex movement with multiple degrees of freedom requires a degree of signal resolution that, with current technology, can only be provided by invasive methods. Epicortical arrays simply lie on the surface of the dura, reducing the complications associated with intraparenchymal electrodes. The next generation of recording electrodes strives to improve biocompatibility, prolong the duration and reliability of signal recording, allow recording from larger populations of neurons, including those from deeper, currently inaccessible locations of the brain, and will transmit this information wirelessly, obviating the requirement for exteriorized hardware.

Signal processing

Cortical signals can be used to control output actuators in a direct or indirect fashion. Indirect control (figure 48) is the most commonly applied method for BCIs and BMIs, utilizing neural

signals that are not intrinsically related to the intended movement[345]. Recorded signals are correlated with observed movements and this information is used to build a decoder, the purpose of which is to infer movement intention from future recordings. Sophisticated computer algorithms are used to formulate a kinematic plan. Decoded signals are delivered to an encoder, the purpose of which is to convert decoded signals into a language interpretable by the output actuator. The encoded signal may require amplification in order to generate the desired output.

There are several limitations of the indirect approach. Firstly, the brain is not actually in control. All control occurs at the level of the decoder. Although both brain and decoder are adaptable, the two are decoupled. This results in dueling dynamic systems that are unstable and unlikely to converge. Decoding algorithms assign coordinates and variables to neuronal signals and, without re-calibration, these are fixed. When performing pre-registered movements, the system will perform well. However, if asked to perform different movements in response to change, the system performs poorly. This inability to generalize is compounded by a fundamental lack of understanding of exactly how the motor cortex controls hand movement. Understanding has progressed very little since the discovery of the motor strip and the construction of motor maps in the late 1800s[349]. Rather than controlling specific muscles, contemporary opinion is that neurons of the motor cortex encode a state vector representation of the hand, with emphasis on kinetic or force-related aspects of movement such as joint torque, and kinematic variables such as position and velocity of the hand in space[349]. Decoders set coordinates and variables according to this entirely assumed cortical representation and as a result, fully autonomous control is impossible.

.

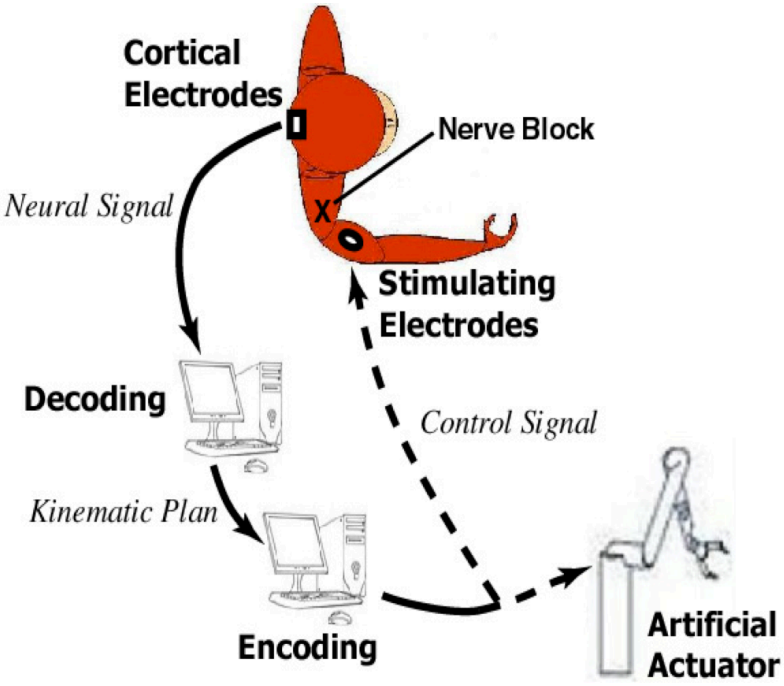

Figure 48. BMI system based on indirect control

Direct control uses neural signals that are responsible for desired movements. Unlike the indirect approach, signals are fed directly into the actuator, without the involvement of a decoder (figure 49). Signals may require amplification to drive the actuator. With this arrangement, all learning and control occurs in the brain. Direct control recognizes that the intricacies of motor control are beyond current understanding. Rather than relying on a decoder that has been constructed around assumed cortical representation, it relies on the vastly superior capacity for learning of the brain. Once the brain and actuator have been linked, synaptic re-wiring and re-learning should

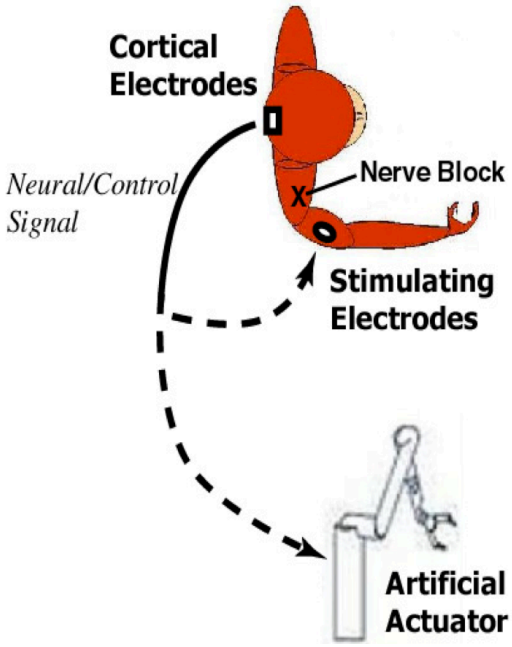

Figure 49. BMI system based on direct control

theoretically enable the subject to achieve autonomous, generalizable control over movement[345]. A disadvantage of this approach is that it may take a prolonged period of time for a subject to re-learn movement. This limitation is not a feature of indirect control where algorithms are used to rapidly infer movement intention.

Neural signal delivery to the output actuator

Once recorded and processed, signals are delivered to the actuator. In BCIs and BMIs, this occurs through external hardware. For BBIs, the successful restoration of autonomous movement following SCI will be largely reliant on establishing a reliable method for delivering signals subcutaneously, directly into muscle. Functional electrical stimulation (FES) is a well established technique that applies electrical currents to neuromuscular tissues in order to restore lost function[350]. Basic components include a power source, control unit, stimulator, lead wires, stimulating electrodes and sensors. Stimulation can be delivered using

skin surface, percutaneous, or implantable electrodes[350]. Surface electrodes are convenient although require repeated replacement, are cosmetically unsightly, are unable to stimulate deep muscles and can be painful due to cutaneous pain receptor activation. Percutaneous electrodes inserted into muscle provide isolated, repeatable activation and are less painful as they do not stimulate cutaneous pain afferents. Longevity of stimulation and tolerance are good although for life long use, are inferior to fully implantable systems[351]. Implantable electrodes can be inserted on the surface of the muscle (epimysial), within the muscle (intramuscular), or at the level of the nerve supplying the muscle in question (nerve cuff).

Stimulation is provided by a pulse of electrical current which varies in frequency, amplitude and duration. At low frequencies, muscle twitching occurs. As the frequency is increased, the fusion threshold is reached where sustained muscle contraction results. Increasing the frequency above the fusion threshold increases the force of contraction although also increases the rate of muscle fatigue. The force of contraction can also be increased by increasing pulse amplitude and duration. Increases in current result in larger electrical fields, area of stimulation and therefore motor unit recruitment[350].

In addition to therapeutic applications such as standing, ambulation, breathing, coughing, bladder and bowel emptying, penile erection and ejaculation, FES has also been successful at restoring reach and grasp movements in paralysed patients[352-354]. Arguably the most well known example is the Freehand system. First generation systems consist of an eight-channel stimulator implanted into a subcutaneous pocket on the chest wall[350, 351]. Epimysial or intramuscular electrodes implanted into flexors and extensors of the fingers allow lateral and palmar grasp. A skin mounted radiofrequency coil overlying the stimulator connects to an

external control unit mounted on the contralateral shoulder. Shoulder movements are detected and transduced in order to drive the stimulator in a patient controlled fashion. FDA approval was granted in 1997 and shortly following this, the system was implanted in excess of 250 tetraplegic patients. In spite of functional improvements, many patients were disappointed with overall performance and subsequently discontinued use. In 2001, the manufacturer withdrew from the market. A second-generation system has since been developed consisting of twelve stimulating electrodes driven by EMG signals from intact muscle and implantable joint sensors situated in the ipsilateral limb. Additional electrodes allow forearm pronation, elbow extension and shoulder movements, in addition to lateral and palmar grasp[351, 352, 354]. The amount of external hardware is reduced and application bilaterally is possible. Although intrinsic muscle activation and grasp is reportedly better, dexterity is still poor.

FES has several general limitations. Artificial stimulation of nerves and muscle results in reverse recruitment of large motor units first. As a result fine motor control is difficult to achieve and the system is susceptible to fatigue. More physiological recruitment has been achieved by applying hyperpolarizing, anodal blocking currents that can selectively block action potential conduction in large fibres. The application of quasitrapezoidal-shaped pulses instead of traditional rectangular pulses has also been showed to recruit small, fatigue-resistant fibers first[355]. Once established, FES performance is fixed with no ability to develop over time. The technology is expensive and availability is limited to specialist units only. The required surgery is extensive. This includes initial hardware implantation, supplementary procedures such as tendon transfers and joint fusions, and also subsequent surgeries for equipment failure. Surgical complexity is exacerbated as electrode number increases. Stimulating proximally at the level of the nerve reduces electrode number and dissection.

Implantable nerve electrodes for FES

Contemporary nerve microelectrodes for use in FES driven neural interface technology aim to provide selective stimulation of nerves and graded muscle contraction. Depending on design, electrodes can be placed adjacent to the nerve (epineurial), around the nerve (cuff) or within the substance of the nerve (intrafascicular and sieve). Cuff electrodes are the most commonly applied and thoroughly investigated electrodes for basic and pre-clinical research[356]. Common designs include the split cylinder and the spiral cuff. The feasibility of a second-generation Freehand system using spiral nerve cuffs has recently been demonstrated in human tetraplegics[353]. Several advantages are associated with cuff electrodes. Stimulation currents are considerably less in comparison to muscle and surface electrodes. Cuffs can be placed precisely on the nerve and, in comparison to intrafascicular and sieve electrodes, are less traumatic. Connecting leads can be carefully orientated in order to reduce mechanical deformation and breakage and excessive traction leading to inadvertent nerve compression or cuff avulsion. This is of particular relevance in the upper limb when elbow and shoulder movements can result in considerable excursion of nerves within the tissues. Compression can also occur secondary to nerve oedema and swelling, particularly following encapsulation. In addition, compression can occur at cuff edges as the nerve enters and exits. Snug fitting cuffs have been shown to result in axonal demyelination and degeneration[357]. As a result, cuffs are designed to be self-sizing, flexible and are deliberately oversized.

Nerve cuffs must be biocompatible. Any substances released from the cuff must be non-toxic and the induced foreign body response must be minor, leading to only mild capsule formation. Cuffs must be mechanically and functionally robust to permit chronic use and the avoidance of implant failure. They must be biologically stable, resisting corrosion and

enzymatic attack. Electrodes must be radiopaque to allow adequate visualization of position. Commonly used conducting materials include stainless steel, platinum, iridium and tungsten. Insulating materials include silicone, polytetrafluoroethylene and polyimide. Polyimide is a flexible polymer and favoured material in precision mechanics due to its suitability for micromachining. It has emerged as an excellent material for the manufacture of nerve cuffs and has been shown in many studies to be biocompatible with minimal foreign body reaction[356, 358]. Silicone remains the material of choice for insulating connecting cables[359].

Stimulating electrodes commonly have a bipolar or tripolar arrangement. The latter consists of a central cathodic pole and two flanking anodes. These arrangements reduce the spread of electrical fields and current, restricting excitation to the vicinity of the cuff[360]. Cuffs with multiple stimulating channels are now available. Once applied, channels are situated around the circumference of the cuff allowing selective fascicular stimulation. The recent development of very small nerve cuffs enables placement around fascicles after they have branched from the main trunk.

6.2.2 Aims

The overarching goal of this work is to demonstrate that fully autonomous, generalizable control of a paralyzed limb can be achieved using a directly controlled brain-body interface (BBI) in a non-human primate model (NHP). The BBI will use ECoG signals to directly re-animate paralyzed muscles rather than an artificial actuator. Neural signals will be delivered to paralyzed muscles by FES using implantable, polyimide nerve cuffs. In order to meet this goal, several specific aims have been set: (1) to train a non-human primate to perform a

simple behavior (elbow flexion) (2) to perform a highly selective reversible paralysis of elbow flexion (3) to demonstrate selective fascicular stimulation of a peripheral nerve using an implantable nerve cuff (4) implant a nerve cuff and a cortical recording array into a NHP (5) activate the cortically driven FES system and, during reversible limb paralysis, establish whether, through operant conditioning and feedback, the NHP can restore movement. The experiments performed as part of this thesis were focused on aim 3 although in order to provide deeper understanding of the project, a summary of the methods and results for aims 1 and 2 has been provided.

6.2.3 Methods

6.2.3.1 Training NHP to perform a simple behaviour

To assess the success of the reversible nerve block, the NHP was required to reliably perform a simple behaviour. The selected task required the NHP to lift a grape up to the mouth and involved a single degree of freedom (elbow flexion), across a single joint, in a vertical plane. It was essential that the motor task in question was as simple as possible in order to reduce the time required for re-learning following paralysis. Two additional tasks were designed although have not yet been imposed on the NHP. The second task is a centre-out pointing exercise where the NHP grips a joystick mounted on a mobile arm, the movement of which is restricted to a single horizontal plane. The joystick moves a cursor on a computer screen towards a moving target. This task involves movement in 2 DOF and requires coordination in 2 DOF (elbow and shoulder). The third task is a crank-turning exercise where the NHP is required to turn a handle attached to a rotating wheel. This involves movement in 1 DOF and requires coordination of 2 DOF (elbow and shoulder). The first and third tasks involve movement in a vertical plane where the effects of gravity alternate between being supportive

and inhibitory at different phases of the tasks. The second task involves movement in a horizontal plane where the effects of gravity are constant. Alternating the task requirements and also the effects of gravity between tasks is a specific design feature permitting the assessment of BBI system generalization.

6.2.3.2 Highly selective reversible paralysis of elbow flexion

In order to thoroughly evaluate the ability of the NHP to assume autonomous control of the paralyzed limb, it was imperative that input from the brain and spinal cord along physiological pathways was blocked during testing. Irreversible paralysis by cord transection or other means in a NHP would almost certainly be declined by an institutional animal care and use committee and would also be disadvantageous for several other pragmatic reasons. As a result, one of the key features of this experimental strategy was to develop a reversible, highly selective, motor paralysis model in the NHP upper limb. Focus was placed on reversibly blocking elbow flexion although ultimately, this technique will also be applied to elbow extension.

Through several cadaveric dissections of Rhesus Macaque monkeys (Macaca mulatta), it was discovered that the neuroanatomy of the upper limb is highly conserved in comparison to humans. Elbow flexion is the product of three different muscles – biceps brachii, brachilais and brachioradilais. Biceps brachii and brachialis muscles are innervated primarily by the musculocutaneous nerve. The brachialis also receives a small contribution from branches of the median nerve. The brachioradialis is innervated by branches of the radial nerve. Under general anaesthetic, the aforementioned muscles and their motor nerves were exposed

through an anteromedial incision in the forelimb. Median nerve branches to the brachialis and the radial nerve branches to the brachioradialis were sharply transected and proximal nerve ends buried into adjacent muscle. As a result, elbow flexion was entirely reliant on the musculocutaneous nerve (figure 50).

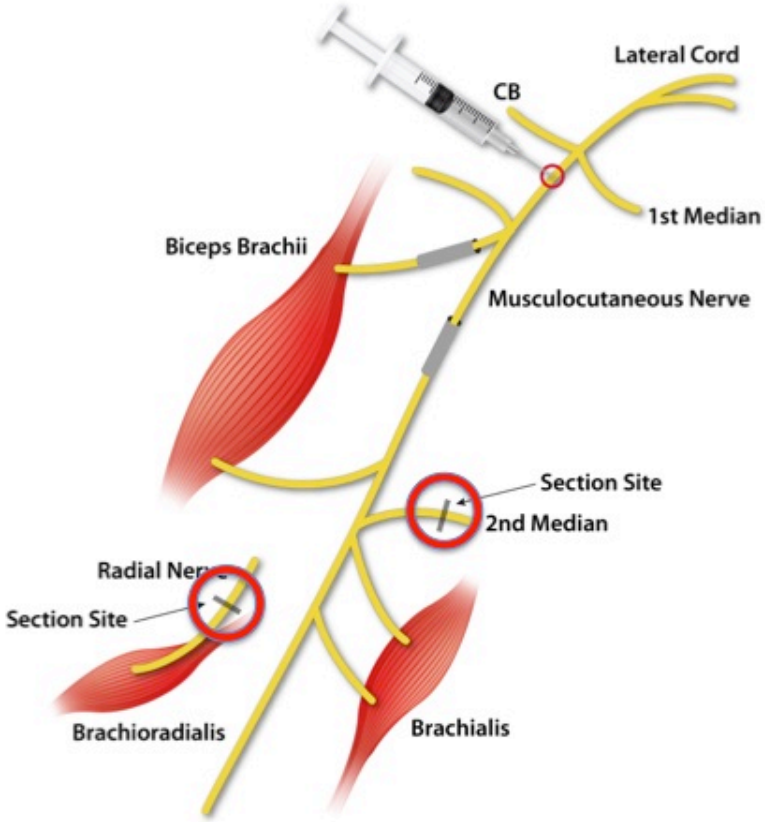

Figure 50. Schematic of neuroanatomy of Rhesus Macaque upper limb and reversible paralysis of elbow flexion

The musculocutaneous nerve was then transposed into a sub-cutaneous position. A metallic ligaclip® was placed adjacent to the nerve at the desired block site to facilitate ultrasound guided local anaesthetic administration. Wounds were closed in layers using deep dermal Vicryl suture and subcuticular Monocryl before returing the animal back to the facility to recover. Two weeks later, the NHP was sedated and, under ultrasound guidance, bupivacaine hydrochloride was used to selectively block this nerve, whilst preserving all other motor and sensory supply. The use of bupivicaine hydrochloride provided sustained paralysis for 6-12

hours. The success of the block was apparent when the NHP was unable to perform the pre-learned task of lifting a grape up to the mouth (figure 51).

Figure 51. Reversible paralysis of NHP elbow flexion. Images A+B and C+D represent two isolated experiments. NHP is unable to flex at the elbow. Note the preservation of hand grasp

The block was confirmed electrophysiologically by the detection of compound muscle action potentials (CMAPS) from relevant muscles before the block compared to a complete absence of CMAPS in the same muscles after the block.

6.2.3.3 Selective fascicular stimulation using implantable nerve cuff - non-survival experiments

The next stage of the study aimed to assess the handling and biocompatibility of an implantable polyimide nerve cuff and its ability to selectively stimulate peripheral nerves. Under ketamine and xylazine anaesthesia, Sprague Dawley rats (n=5) and C57 Black 6 mice (n=5) had dorsolateral incisions made on the thigh. Sciatic nerves were exposed through muscle splitting incisions and mobilized free from their investing connective tissue. Incisions were extended into the leg in order to expose the gastrocnemius (posterior compartment) and tibialis anterior (anterior compartment) muscles. Polyimide nerve cuff electrodes with eight stimulating channels (figure 52; Prof Thomas Stieglitz, Department of Microsystems Engineering, University of Frieberg) were wrapped around the mid-point of the sciatic nerve and were connected to stimulation/recording equipment (Tucker-Davis Technologies (TDT)). Once the self-sizing cuffs were applied, stimulating channels were distributed evenly around the circumference of the nerve (figure 53 and figure 54). A 1.5mm diameter cuff was used for rodent sciatic nerves (approximate nerve diameter 1.2mm) and 1mm cuff for all mouse nerves (approximate nerve diameter 0.65mm). Grounding needle electrodes were inserted into the upper back muscles of each animal and electromyography (EMG) electrodes were inserted into the gastrocnemius and tibialis anterior muscles to record muscle activity (figure 55). Single pulses and pulse trains were

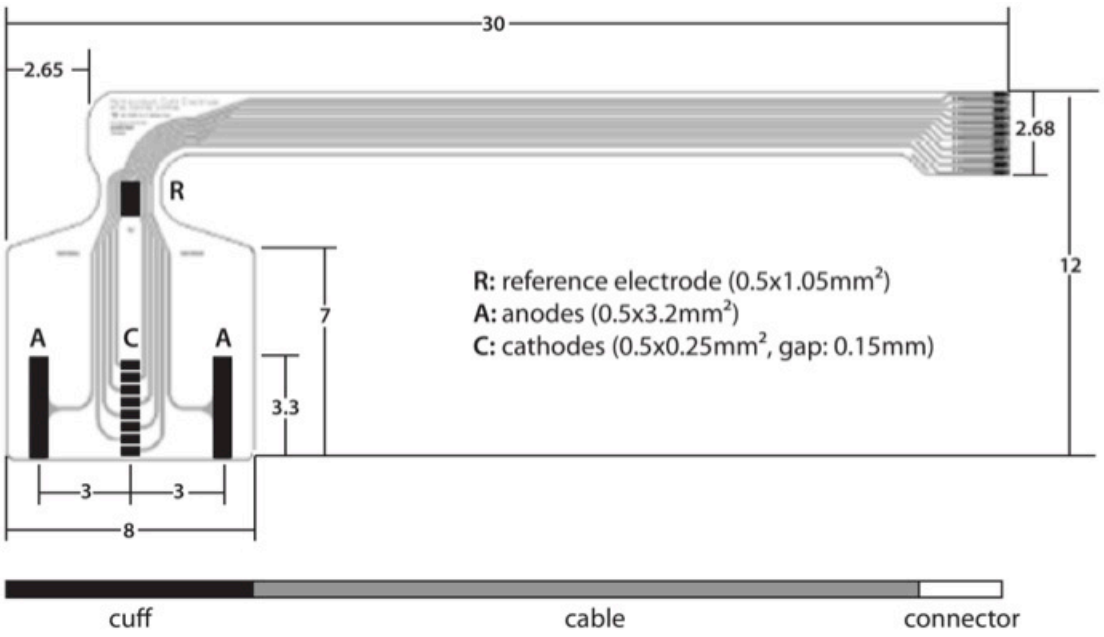

Figure 52. schematic of polyimide nerve cuff electrode. The cuff proper is 8mm in length. The cuff has a natural tendency to furl up upon itself and does so along its 7mm width. The eight stimulating channels lie in the central portion of the cuff and once furled, are distributed evenly around the circumference of the nerve.

delivered to the various nerve cuff channels whilst pulse frequency, amplitude and width were systematically varied. In theory, isolated activation of stimulating channels should allow selective fascicular activation and therefore selective activation of anterior and posterior compartment muscles.

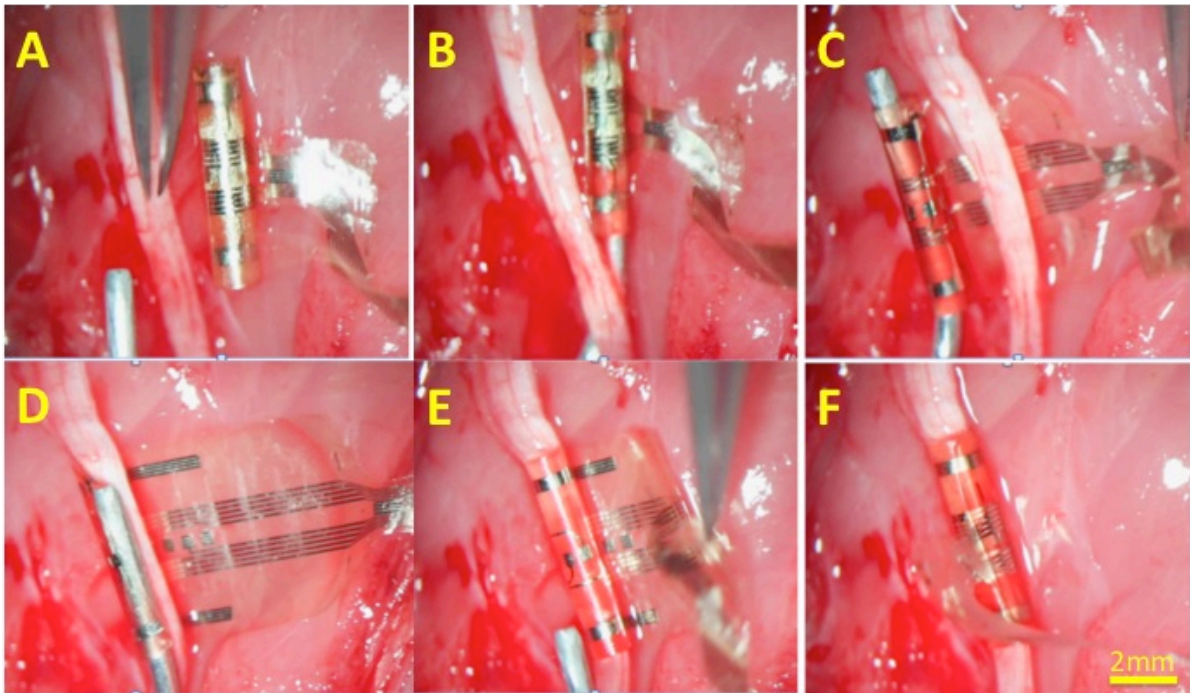

Figure 53. Application of nerve cuff around rat sciatic nerve. (A) Sciatic nerve freed from investing connective tissue and mobilized along length of nerve. Nerve cuff placed into field adjacent to nerve. (B-C) The end of a straightened paper clip was inserted into the furled nerve cuff and by applying light traction, was used to unravel the cuff. (D-F) The unfurled cuff was hooked under the sciatic nerve and was allowed to naturally recoil back around the nerve.

6.2.3.4 Selective fascicular stimulation using implantable nerve cuff - survival experiment

Following successful demonstration of selective fascicular stimulation in non-survival surgeries, stimulating nerve cuff electrodes and EMG recording electrodes were implanted chronically into one rat in order to assess the reliability of the stimulating cuff and recording equipment. The cuff was applied in exactly the same fashion as in the acute, non-survival experiments.

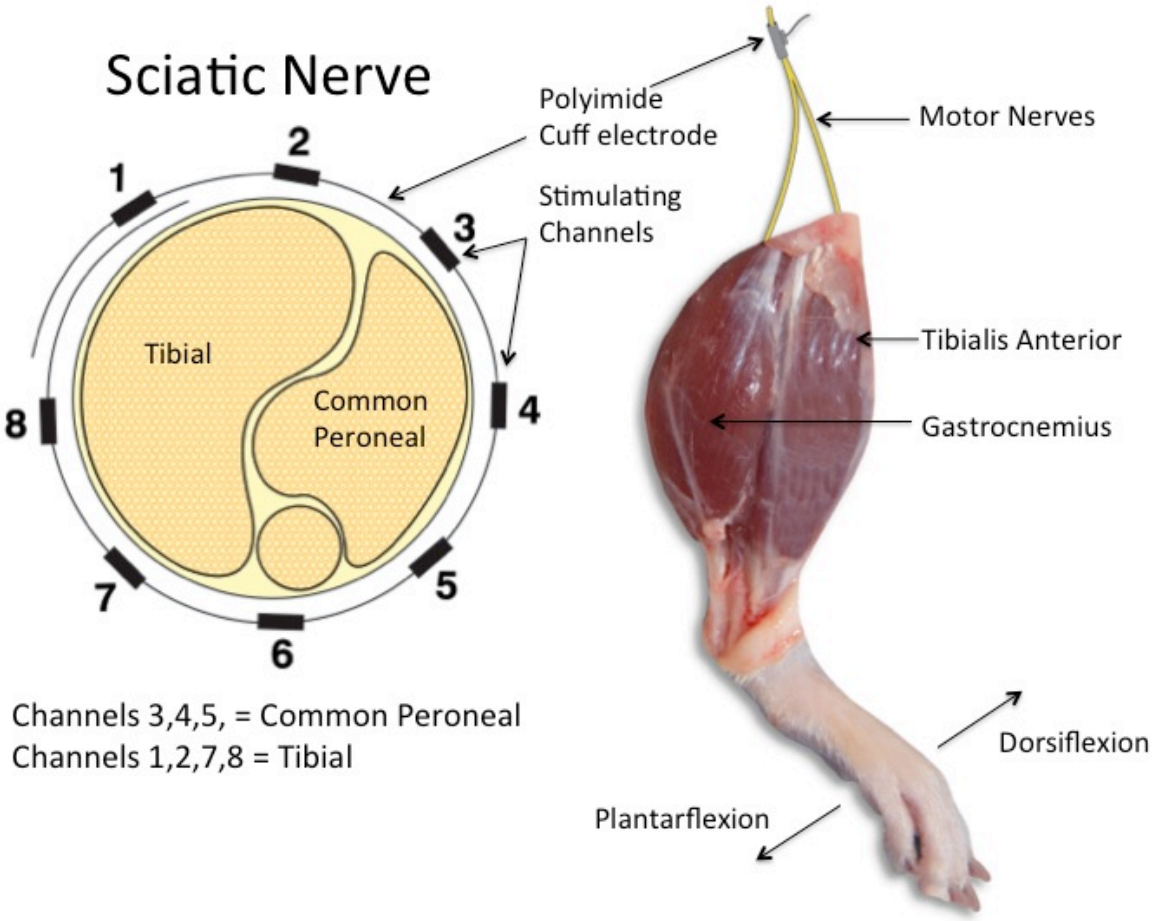

Figure 54. Distribution of stimulating channels around sciatic nerve allowing selective fascicular stimulation. In this schematic, stimulating channels 3, 4 and 5 are distributed over the common peroneal fascicle. Channels 1, 2, 7 and 8 are distributed over the tibial fascicle. In theory, by activating these channels independently, it should be possible to selectively stimulate these fascicles and therefore elicit dorsiflexion and plantarflexion respectively.

Intramuscular wire EMG electrodes were used in place of percutaneous needle electrodes to facilitate secure fixation into the gastrocnemius and tibialis anterior muscles. All wires and connecting cables were buried subcutaneously. Redundant loops were loosely sutured to underlying muscle to reduce the risk of displacement of the cuff or EMG electrodes due to traction. The connecting ports of the stimulating cuff and EMG electrodes were embedded in

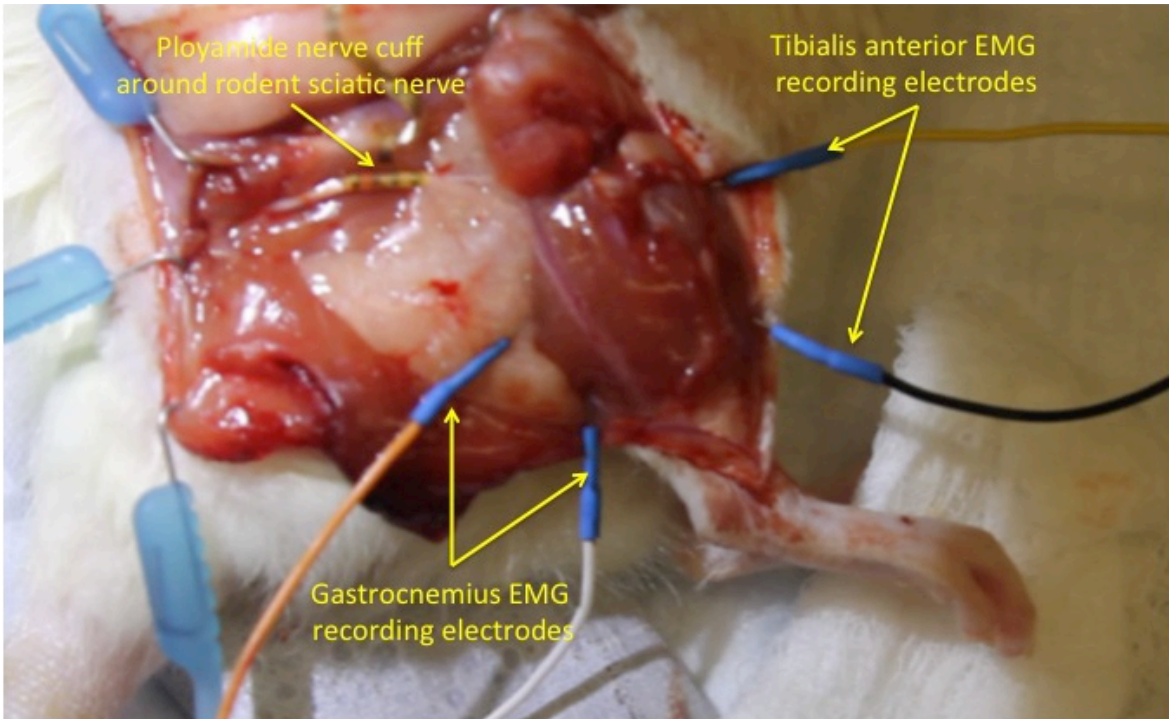

Figure 55. Stimulating nerve cuff in situ with needle EMG recording electrodes inserted into tibilais anterior and gasrocnemius muscles

epoxy resin and mounted on nylon mesh. The mesh was subsequently sutured to the muscles of the back and the skin closed around the resin to exteriorize the ports (figure 56). At the time of implantation, the ports were connected up to the TDT equipment to confirm satisfactory selective fascicular activation. Following this, the animal was allowed to recover before being returned to the animal facility. Stimulation and recording sessions were repeated at weekly intervals for 1-month and then at monthly intervals for up to 6-months. The rat will be kept alive for up to 1 year in order to fully assess biocompatibility and durability of the hardware. The final aim of the study involving the implantation of the nerve cuff and cortical recording electrodes in the NHP are currently in progress.

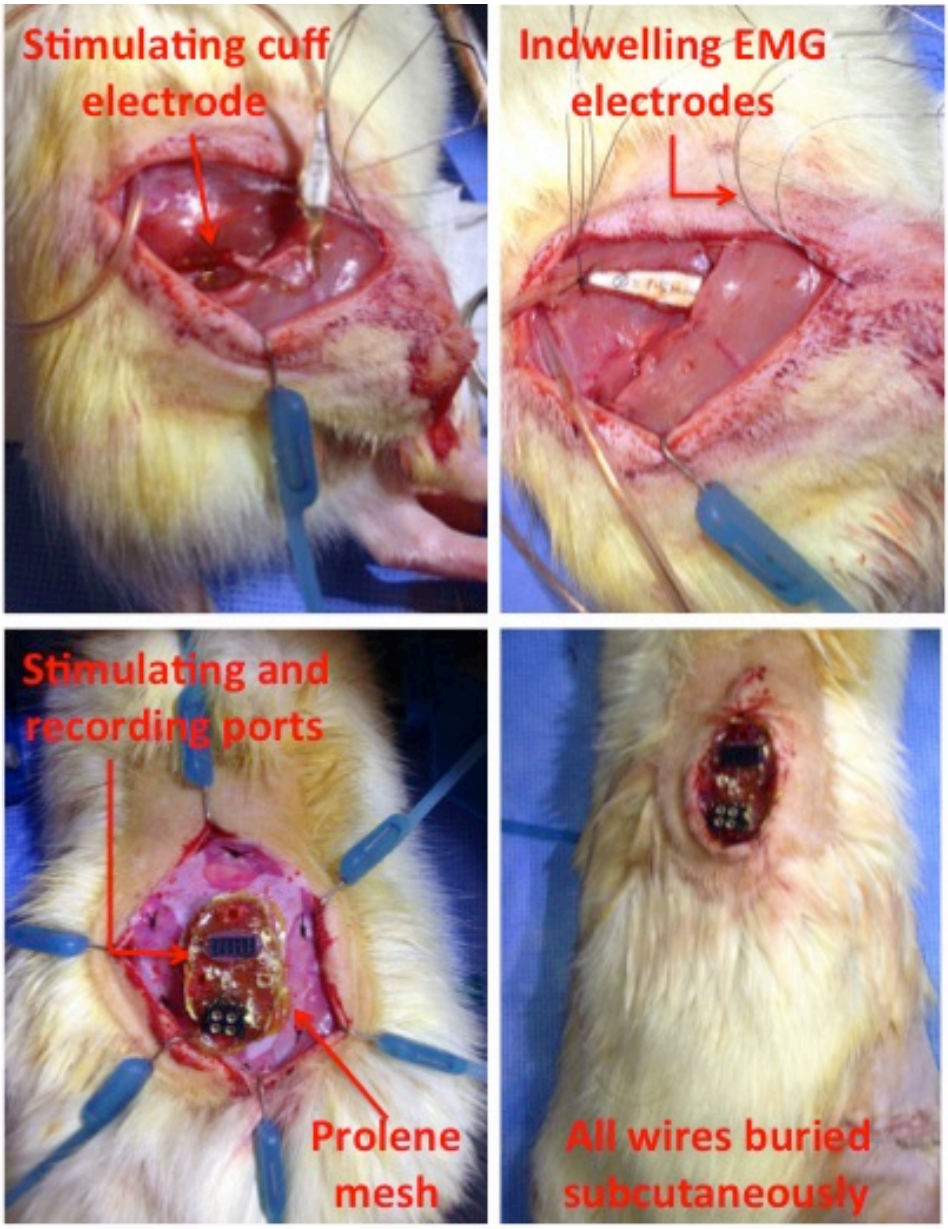

Figure 56. Chronic implantation of polyimide nerve cuff and indwelling EMG electrodes. Once the nerve cuff was applied to the nerve, the silicone coated connecting cable was buried subcutaneously in the back. The cable was connected to stimulation and recording ports that were embedded in epoxy resin and secured to prolene mesh. The ports were exteriorized through the back skin. Mesh was secured to underlying muscle and skin closed around the resin using a purse string suture. EMG electode wires were passed through muscles and tied. All wires were buried subcutaneously.

6.2.4 Results

6.2.4.1 Training NHP to perform a simple behavior

As the movement in question was a natural, instinctive feeding behavior, a small number of sessions within the space of one week were sufficient to ensure that the NHP was comfortable with the task. The sessions were mainly intended to acclimatise the NHP to the experimental environment and the restraints used. The remaining tasks were not imposed upon the NHP during these sessions but are planned to take place once the schedule for ECoG and nerve cuff implantation has been finalized.

6.2.4.2 Highly selective reversible paralysis of elbow flexion

As shown in figure 57, a highly selective, reversible paralysis of elbow flexion was achieved in the NHP. The NHP was unable to flex the elbow in order to bring a grape up to his mouth but importantly, all other motor input and sensory feedback to the limb was preserved. This demonstration highlights the feasibility of this approach and will form the basis of future NHP experiments investigating BBI systems.

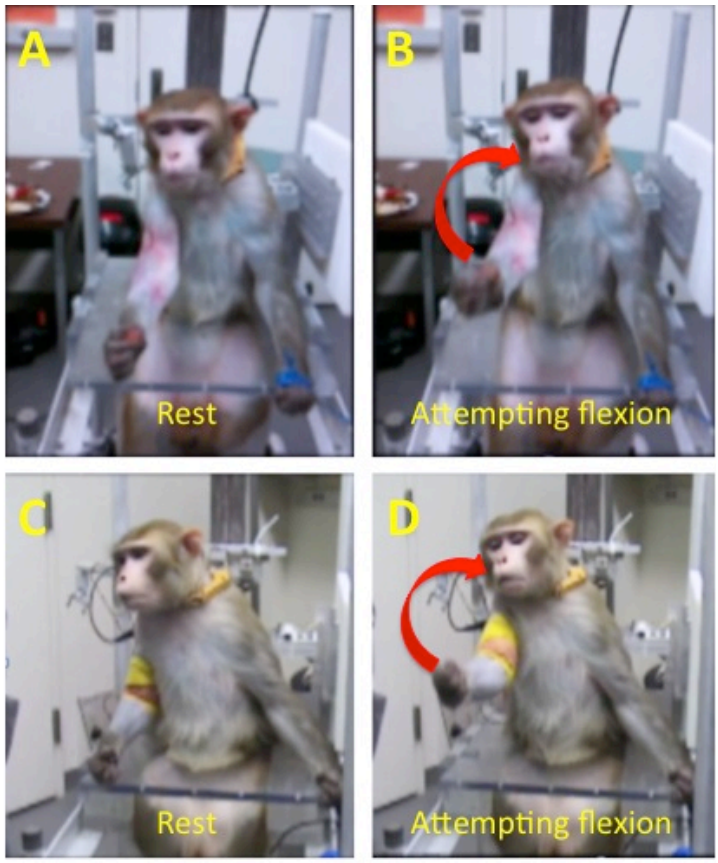

Figure 57. NHP attempting to flex elbow. NHP unable to flex elbow in order to bring grape up to mouth. All remaining motor input and sensory feedback was intact.

6.2.4.3 Selective fascicular stimulation using implantable nerve cuff – non-surivival

Selective activation of nerve cuff channels resulted in muscle activity in all animals. Selective stimulation of common peroneal and posterior tibial fascicles was demonstrated in 9 animals (figure 58 and figure 59). EMG recordings from pulse trains with various different simulation parameters (pulse width, pulse amplitude, pulse frequency) allowed the plotting of muscle recruitment curves (figure 60). Stimulation of channel 2 resulted in the activation of the gastrocnemius muscle with very little EMG signal detected in the tibialis anterior. The reverse was observed in channel 3, with primarily tibialis activation and very little

gastrocnemius activation. Following 6-months of chronic cuff and EMG implantation, successful stimulation and recording was still possible.

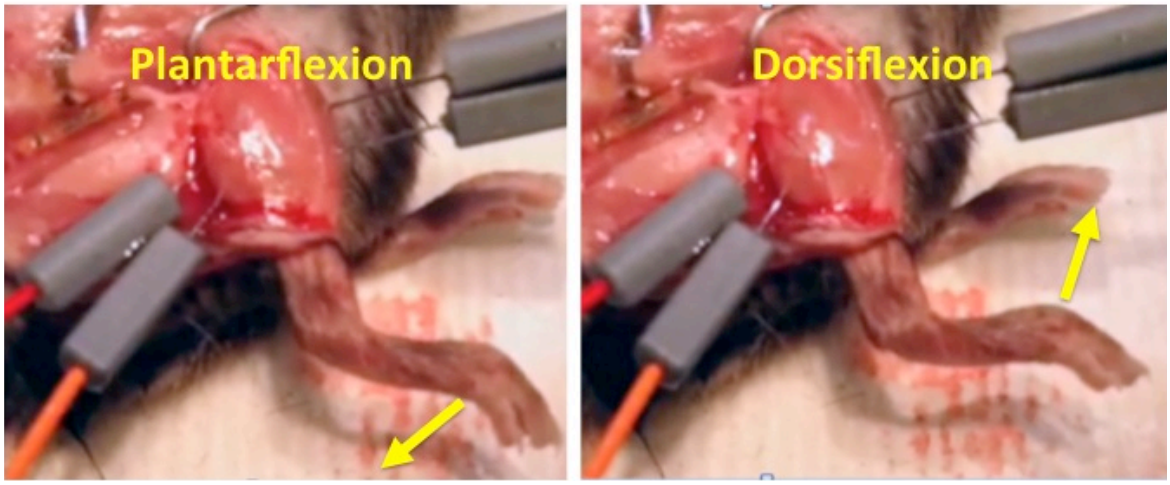

Figure 58. Selective fascicular stimulation in a mouse model. Stimulation of different nerve cuff channels resulted in plantarflexion and dorsiflexion depending on which channels overlay posterior tibial and common peroneal fascicles. Still images obtained from video footage.

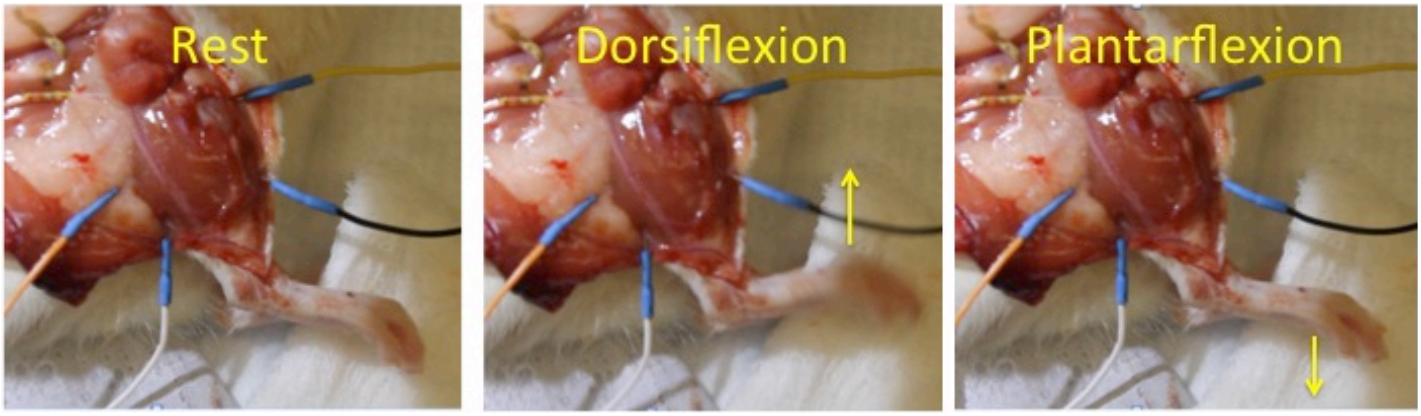

Figure 59. Selective fascicular stimulation in a rodent model. Stimulation of different nerve cuff channels resulted in plantarflexion and dorsiflexion depending on which stimulating channels overlay posterior tibial and common peroneal fascicles. Still images obtained from video footage.

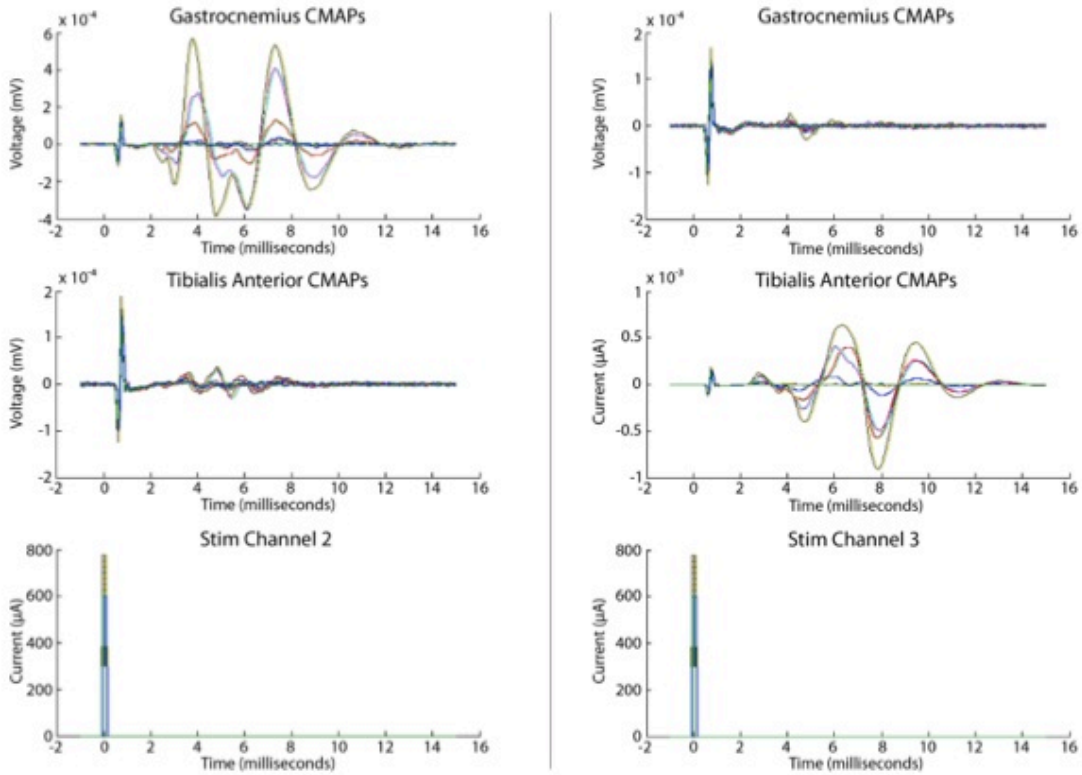

Figure 60. Example of CMAP recruitment curves as a function of stimulation pulse amplitude in a single rodent. Graphs show CMAP recordings from two of the eight stimulating nerve cuff channels. Activation of channel 2 results in the stimulation of the gastrocnemius muscle with very little activity recorded in the tibialis anterior muscle. The reverse pattern is seen with activation of channel 3, with mostly tibialis anterior activation and very little gastrocnemius activity. This suggests that the cuff was situated around the sciatic nerve in such a way that channel 2 overlay the tibial fascicle and channel 3 overlay the common peroneal fascicle.

6.2.4.4 Selective fascicular stimulation using implantable nerve cuff – survival experiment

Stimulation and recording was possible for 6-months following implantation and, as with the non-survival experiments, was successful at showing selective fascicular stimulation. The data collection for this phase of the study took place following the authors departure from the United States and has not yet been analyzed and released by the Bizzi group. Following sacrifice and on gross examination, the sciatic nerve looked healthy with no signs of chronic

inflammatory reaction or infection. Cuff encapsulation with fibrous tissue was apparent and typical of any foreign material. Unfortunately the cuff had become detached from the polyurethane coated wire to which it was attached. This was previously recognized as a potential weak point and may necessitate a different method of implantation or even a re-design of the cuff as the strain will only worsen once implanted into the NHP. Also, when the cuff was unrolled, small fragments of the platinum coated stimulation channels adhered to the nerve. It is uncertain why this occurred and the significance of this finding for long-term recording. There was no evidence of scar tissue between the cuff and the epineurial surface. This information was obtained through verbal communication with one of the lead investigators (R.A).

6.2.5 Discussion

This work represents part of an ongoing, collaborative effort between the Department of Plastic Surgery and Department of Anaesthesiology at The Massachusetts General Hospital and the McGovern Institute for Brain Research at The Massachusetts Institute of Technology. Recent experiments have developed a reversible upper limb paralysis model in a NHP. This important step involved surgically altering the neuroanatomy of the upper limb so that elbow flexion was entirely reliant on the musculocutaneous nerve. Although invasive, the functional deficit to the animal as result of this was minimal. Likewise, the injection of local anaesthetic temporarily paralysed elbow flexion whilst preserving all other motor and sensory supply. This may represent the first description of this highly selective nerve block in a NHP and has made feasible the current and planned experiments developing a BBI. Following successful demonstration of reversible paralysis, the NHP unfortunately developed an inflammatory bowel-type syndrome with associated immunocompromise and thrombocytopaenia. This

condition has recurred on several occasions and has been treated successfully with systemic steroids. It remains uncertain what the exact diagnosis is and how this will influence future implantation of the ECoG recording array and stimulating nerve cuff electrodes.

The experiments performed in mice and rats have demonstrated that polyamide nerve cuffs are biocompatible and are electrophysiologically stable. The chronic, survival rodent has recently been sacrificed although had nerve stimulation and EMG recordings taken successfully up to 6-months post-implantation. Similar studies in the literature have showed that after 6-months, polyimide nerve cuffs were surrounded by a well-vascularized, thin, fibrous capsule[358]. Underlying nerves were grossly normal and free from fibrinous adhesions. No evidence of nerve compression was apparent and on histological evaluation, axon counts, myelination and histomorphomeric measurements were comparable to the contralateral normal nerve. Electron microscopy of the nerve cuff showed no evidence of de-lamination of micro-fracture.

We also identified no gross abnormality with the sciatic nerve following sacrifice. Histological analysis is currently in progress. It was unfortunate that the nerve cuff became detached from the wire but we are confident that this problem can be overcome with a different implantation technique. This was already being contemplated as, following implantation into the NHP, there will need to be considerable “slack” in the connecting wires between the cuff and the exteriorized port to compensate for the wide range of movement at the shoulder girdle. The evidence of de-lamination of the platinum stimulating channels was a surprise and has not yet been observed with this particular cuff. However, the length of

follow-up in this study exceeds other reports. We are uncertain what implications this will have for the future use of this cuff in the NHP.

The feasibility of selective fascicular stimulation, even in sub-1mm diameter murine sciatic nerves, has been confirmed. In future NHP experiments, the BBI system aims to restore elbow flexion only. As a result, selective fascicular stimulation is not entirely necessary at this time. The restoration of autonomous control of only simple movements would still represent a major advance in the field. If this approach proves successful, future attempts to increase movement complexity and degrees of freedom will require selective activation of individual fascicles and muscles. Grading the strength of muscle contraction and providing tactile sensory feedback are additional features that are highly desirable although not a focus of this current work.

The next phase of this work aims to implant a polyimide nerve cuff and epicortical ECoG recording array into the NHP. This will be preceded by a short surgical procedure to ensure that the previously divided median nerve contribution to the musculocutaneous nerve and the radial nerve supply to the brachioradialis remain divided and have not regenerated. This will also ensure that the subcutaneous transposition of the musculcutaneous nerve, facilitating ultrasound-guided block, is still satisfactory. Optimum positioning of the ECoG array over the motor cortex will be achieved by intraoperative stimulation and assessment of motor response. The recording array will be connected to an external power source or amplifier. A nerve cuff, initially placed around the musculocutaneous nerve, and eventually the radial nerve to triceps, will receive the amplified signal from the ECoG array. The silicone encapsulated connecting cable will be buried subcutaneously with ample redundant loops

positioned in the soft tissues to reduce the likelihood of traction injury and cuff avulsion during post-operative limb movements. Once the system is activated during reversible paralysis, it is hoped that, through operant conditioning and feedback, the restoration of autonomous and generalizable control will be possible.

6.2.6 Conclusion

This work reports early experiments aimed at developing a directly controlled BBI system, the ultimate neural interface for the restoration of limb movements following spinal cord injury. Successful demonstration of a reversible, selective upper limb paralysis model in the NHP represents a novel solution to a methodological obstacle that has perhaps limited progress with this approach in the past. Establishing this technique is a fundamental requirement for this experimental approach. With the successful demonstration of selective fascicular stimulation, the polyimide nerve cuffs used in this study appear to provide the ideal interface for the FES of paralyzed muscles. The approach addresses many of the current limitations of indirectly controlled BCIs and BMIs and in our opinion, has the greatest potential to provide fully autonomous and generalizable control.

Section 7: References

1. Lubinska L. AXOPLASMIC STREAMING IN REGENERATING AND IN NORMAL NERVE FIBRES. Progress in brain research. 1964;13:1-71. PubMed PMID: 14302959. Epub 1964/01/01. eng.

2. Maday S, Twelvetrees AE, Moughamian AJ, Holzbaur EL. Axonal Transport: Cargo-Specific Mechanisms of Motility and Regulation. Neuron. 2014 Oct 22;84(2):292-309. PubMed PMID: 25374356. Epub 2014/11/07. Eng.

3. Sunderland S, Bradley KC. The cross-sectional area of peripheral nerve trunks devoted to nerve fibers. Brain : a journal of neurology. 1949 Sep;72(3):428-49. PubMed PMID: 15401756. Epub 1949/09/01. eng.

4. Myers RR. Anatomy and microanatomy of peripheral nerve. Neurosurgery clinics of North America. 1991 Jan;2(1):1-20. PubMed PMID: 1668260. Epub 1991/01/01. eng.

5. Reale E, Luciano L, Spitznas M. Freeze-fracture aspects of the perineurium of spinal ganglia. Journal of neurocytology. 1976 Aug;5(4):385-94. PubMed PMID: 993818. Epub 1976/08/01. eng.

6. Weerasuriya A, Mizisin AP. The blood-nerve barrier: structure and functional significance. Methods in molecular biology. 2011;686:149-73. PubMed PMID: 21082370. Epub 2010/11/18. eng.

7. Arroyo EJ, Scherer SS. On the molecular architecture of myelinated fibers. Histochemistry and cell biology. 2000 Jan;113(1):1-18. PubMed PMID: 10664064. Epub 2000/02/09. eng.

8. Debanne D, Campanac E, Bialowas A, Carlier E, Alcaraz G. Axon physiology. Physiological reviews. 2011 Apr;91(2):555-602. PubMed PMID: 21527732. Epub 2011/04/30. eng.

9. Slater CR. Reliability of neuromuscular transmission and how it is maintained. Handbook of clinical neurology. 2008;91:27-101. PubMed PMID: 18631840. Epub 2008/07/18. eng.

10. Slater CR. The functional organization of motor nerve terminals. Progress in neurobiology. 2015 Oct 9. PubMed PMID: 26439950. Epub 2015/10/07. Eng.

11. Bentley FH, Schlapp W. Experiments on the blood supply of nerves. The Journal of physiology. 1943 Jun 30;102(1):62-71. PubMed PMID: 16991591. Pubmed Central PMCID: PMC1393426. Epub 1943/06/30. eng.

12. Smith JW. Factors influencing nerve repair. I. Blood supply of peripheral nerves. Archives of surgery (Chicago, Ill : 1960). 1966 Aug;93(2):335-41. PubMed PMID: 5913572. Epub 1966/08/01. eng.

13. SEDDON HJ. THREE TYPES OF NERVE INJURY1943 1943-12-01 00:00:00. 237-88 p.

14. SUNDERLAND S. A CLASSIFICATION OF PERIPHERAL NERVE INJURIES PRODUCING LOSS OF FUNCTION1951 1951-12-01 00:00:00. 491-516 p.

15. Mackinnon SE. New directions in peripheral nerve surgery. Annals of plastic surgery. 1989 Mar;22(3):257-73. PubMed PMID: 2660716. Epub 1989/03/01. eng.

16. Strain RE, Olson WH. Selective damage of large diameter peripheral nerve fibers by compression: an application of Laplace's law. Experimental neurology. 1975 Apr;47(1):68-80. PubMed PMID: 1123010. Epub 1975/04/01. eng.

17. Rydevik B, Lundborg G. Permeability of intraneural microvessels and perineurium following acute, graded experimental nerve compression. Scandinavian journal of plastic and reconstructive surgery. 1977;11(3):179-87. PubMed PMID: 609900. Epub 1977/01/01. eng.

18. Mandolesi G, Madeddu F, Bozzi Y, Maffei L, Ratto GM. Acute physiological response of mammalian central neurons to axotomy: ionic regulation and electrical activity. FASEB journal : official publication of the Federation of American Societies for Experimental Biology. 2004 Dec;18(15):1934-6. PubMed PMID: 15451889. Epub 2004/09/29. eng.

19. Burnett MG, Zager EL. Pathophysiology of peripheral nerve injury: a brief review. Neurosurgical focus. 2004 May 15;16(5):E1. PubMed PMID: 15174821. Epub 2004/06/04. eng.

20. Fu SY, Gordon T. The cellular and molecular basis of peripheral nerve regeneration. Molecular neurobiology. 1997 Feb-Apr;14(1-2):67-116. PubMed PMID: 9170101. Epub 1997/02/01. eng.

21. Boyd JG, Gordon T. Neurotrophic factors and their receptors in axonal regeneration and functional recovery after peripheral nerve injury. Molecular neurobiology. 2003 Jun;27(3):277-324. PubMed PMID: 12845152. Epub 2003/07/08. eng.

22. Gordon T, Sulaiman O, Boyd JG. Experimental strategies to promote functional recovery after peripheral nerve injuries. Journal of the peripheral nervous system : JPNS. 2003 Dec;8(4):236-50. PubMed PMID: 14641648. Epub 2003/12/04. eng.

23. Menorca RM, Fussell TS, Elfar JC. Nerve physiology: mechanisms of injury and recovery. Hand clinics. 2013 Aug;29(3):317-30. PubMed PMID: 23895713. Epub 2013/07/31. eng.

24. Gillingwater TH, Thomson D, Mack TG, Soffin EM, Mattison RJ, Coleman MP, et al. Age-dependent synapse withdrawal at axotomised neuromuscular junctions in Wld(s) mutant and Ube4b/Nmnat transgenic mice. The Journal of physiology. 2002 Sep 15;543(Pt 3):739-55. PubMed PMID: 12231635. Pubmed Central PMCID: PMC2290540. Epub 2002/09/17. eng.

25. Beirowski B, Adalbert R, Wagner D, Grumme DS, Addicks K, Ribchester RR, et al. The progressive nature of Wallerian degeneration in wild-type and slow Wallerian degeneration (WldS) nerves. BMC neuroscience. 2005;6:6. PubMed PMID: 15686598. Pubmed Central PMCID: PMC549193. Epub 2005/02/03. eng.

26. Slater CR. Time course of failure of neuromuscular transmission after motor nerve section. Nature. 1966 Jan 15;209(5020):305-6. PubMed PMID: 5915971. Epub 1966/01/15. eng.

27. Conforti L, Gilley J, Coleman MP. Wallerian degeneration: an emerging axon death pathway linking injury and disease. Nature reviews Neuroscience. 2014 Jun;15(6):394-409. PubMed PMID: 24840802. Epub 2014/05/21. eng.

28. Sulaiman W, Gordon T. Neurobiology of peripheral nerve injury, regeneration, and functional recovery: from bench top research to bedside application. The Ochsner journal. 2013 Spring;13(1):100-8. PubMed PMID: 23531634. Pubmed Central PMCID: PMC3603172. Epub 2013/03/28. eng.

29. Wang JT, Medress ZA, Barres BA. Axon degeneration: molecular mechanisms of a self-destruction pathway. The Journal of cell biology. 2012 Jan 9;196(1):7-18. PubMed PMID: 22232700. Pubmed Central PMCID: PMC3255986. Epub 2012/01/11. eng.

30. Tamariz E, Varela-Echavarria A. The discovery of the growth cone and its influence on the study of axon guidance. Frontiers in neuroanatomy. 2015;9:51. PubMed PMID: 26029056. Pubmed Central PMCID: PMC4432662. Epub 2015/06/02. eng.

31. Dent EW, Meiri KF. Distribution of phosphorylated GAP-43 (neuromodulin) in growth cones directly reflects growth cone behavior. Journal of neurobiology. 1998 Jun;35(3):287-99. PubMed PMID: 9622012. Epub 1998/06/11. eng.

32. Meiri KF, Saffell JL, Walsh FS, Doherty P. Neurite outgrowth stimulated by neural cell adhesion molecules requires growth-associated protein-43 (GAP-43) function and is associated with GAP-43 phosphorylation in growth cones. The Journal of neuroscience : the official journal of the Society for Neuroscience. 1998 Dec 15;18(24):10429-37. PubMed PMID: 9852580. Epub 1998/12/16. eng.

33. Abe N, Cavalli V. Nerve injury signaling. Current opinion in neurobiology. 2008 Jun;18(3):276-83. PubMed PMID: 18655834. Pubmed Central PMCID: PMC2633416. Epub 2008/07/29. eng.

34. Gordon T. The role of neurotrophic factors in nerve regeneration. Neurosurgical focus. 2009 Feb;26(2):E3. PubMed PMID: 19228105. Epub 2009/02/21. eng.

35. Fu SY, Gordon T. Contributing factors to poor functional recovery after delayed nerve repair: prolonged denervation. The Journal of neuroscience : the official journal of the Society for Neuroscience. 1995 May;15(5 Pt 2):3886-95. PubMed PMID: 7751953. Epub 1995/05/01. eng.

36. Fu SY, Gordon T. Contributing factors to poor functional recovery after delayed nerve repair: prolonged axotomy. The Journal of neuroscience : the official journal of the Society for Neuroscience. 1995 May;15(5 Pt 2):3876-85. PubMed PMID: 7751952. Epub 1995/05/01. eng.

37. Grothe C, Nikkhah G. The role of basic fibroblast growth factor in peripheral nerve regeneration. Anatomy and embryology. 2001 Sep;204(3):171-7. PubMed PMID: 11681796. Epub 2001/10/30. eng.

38. Lewin SL, Utley DS, Cheng ET, Verity AN, Terris DJ. Simultaneous treatment with BDNF and CNTF after peripheral nerve transection and repair enhances rate of functional recovery compared with BDNF treatment alone. The Laryngoscope. 1997 Jul;107(7):992-9. PubMed PMID: 9217144. Epub 1997/07/01. eng.

39. Meyer M, Matsuoka I, Wetmore C, Olson L, Thoenen H. Enhanced synthesis of brain-derived neurotrophic factor in the lesioned peripheral nerve: different mechanisms are responsible for the regulation of BDNF and NGF mRNA. The Journal of cell biology. 1992 Oct;119(1):45-54. PubMed PMID: 1527172. Pubmed Central PMCID: PMC2289627. Epub 1992/10/01. eng.

40. Midha R, Munro CA, Dalton PD, Tator CH, Shoichet MS. Growth factor enhancement of peripheral nerve regeneration through a novel synthetic hydrogel tube. Journal of neurosurgery. 2003 Sep;99(3):555-65. PubMed PMID: 12959445. Epub 2003/09/10. eng.

41. Moir MS, Wang MZ, To M, Lum J, Terris DJ. Delayed repair of transected nerves: effect of brain-derived neurotrophic factor. Archives of otolaryngology--head & neck surgery. 2000 Apr;126(4):501-5. PubMed PMID: 10772304. Epub 2000/04/20. eng.

42. Novikov L, Novikova L, Kellerth JO. Brain-derived neurotrophic factor promotes axonal regeneration and long-term survival of adult rat spinal motoneurons in vivo. Neuroscience. 1997 Aug;79(3):765-74. PubMed PMID: 9219940. Epub 1997/08/01. eng.

43. Dezawa M, Takahashi I, Esaki M, Takano M, Sawada H. Sciatic nerve regeneration in rats induced by transplantation of in vitro differentiated bone-marrow stromal cells. The

European journal of neuroscience. 2001 Dec;14(11):1771-6. PubMed PMID: 11860471. Epub 2002/02/28. eng.

44. di Summa PG, Kalbermatten DF, Pralong E, Raffoul W, Kingham PJ, Terenghi G. Long-term in vivo regeneration of peripheral nerves through bioengineered nerve grafts. Neuroscience. 2011 May 5;181:278-91. PubMed PMID: 21371534.

45. di Summa PG, Kingham PJ, Raffoul W, Wiberg M, Terenghi G, Kalbermatten DF. Adipose-derived stem cells enhance peripheral nerve regeneration. Journal of plastic, reconstructive & aesthetic surgery : JPRAS. 2010 Sep;63(9):1544-52. PubMed PMID: 19828391.

46. Erba P, Mantovani C, Kalbermatten DF, Pierer G, Terenghi G, Kingham PJ. Regeneration potential and survival of transplanted undifferentiated adipose tissue-derived stem cells in peripheral nerve conduits. Journal of plastic, reconstructive & aesthetic surgery : JPRAS. 2010 Dec;63(12):e811-7. PubMed PMID: 20851070.

47. Ghoreishian M, Rezaei M, Beni BH, Javanmard SH, Attar BM, Zalzali H. Facial nerve repair with Gore-Tex tube and adipose-derived stem cells: an animal study in dogs. Journal of oral and maxillofacial surgery : official journal of the American Association of Oral and Maxillofacial Surgeons. 2013 Mar;71(3):577-87. PubMed PMID: 22868036.

48. Goel RK, Suri V, Suri A, Sarkar C, Mohanty S, Sharma MC, et al. Effect of bone marrow-derived mononuclear cells on nerve regeneration in the transection model of the rat sciatic nerve. Journal of clinical neuroscience : official journal of the Neurosurgical Society of Australasia. 2009 Sep;16(9):1211-7. PubMed PMID: 19596581.

49. Jia H, Wang Y, Tong XJ, Liu GB, Li Q, Zhang LX, et al. Sciatic nerve repair by acellular nerve xenografts implanted with BMSCs in rats xenograft combined with BMSCs. Synapse (New York, NY). 2012 Mar;66(3):256-69. PubMed PMID: 22127791.

50. Keilhoff G, Goihl A, Langnase K, Fansa H, Wolf G. Transdifferentiation of mesenchymal stem cells into Schwann cell-like myelinating cells. European journal of cell biology. 2006 Jan;85(1):11-24. PubMed PMID: 16373171.

51. Keilhoff G, Goihl A, Stang F, Wolf G, Fansa H. Peripheral nerve tissue engineering: autologous Schwann cells vs. transdifferentiated mesenchymal stem cells. Tissue engineering. 2006 Jun;12(6):1451-65. PubMed PMID: 16846343. Epub 2006/07/19. eng.

52. Kingham PJ, Kalbermatten DF, Mahay D, Armstrong SJ, Wiberg M, Terenghi G. Adipose-derived stem cells differentiate into a Schwann cell phenotype and promote neurite outgrowth in vitro. Experimental neurology. 2007 Oct;207(2):267-74. PubMed PMID: 17761164.

53. Ladak A, Olson J, Tredget EE, Gordon T. Differentiation of mesenchymal stem cells to support peripheral nerve regeneration in a rat model. Experimental neurology. 2011 Apr;228(2):242-52. PubMed PMID: 21281630.

54. Liu GB, Cheng YX, Feng YK, Pang CJ, Li Q, Wang Y, et al. Adipose-derived stem cells promote peripheral nerve repair. Archives of medical science : AMS. 2011 Aug;7(4):592-6. PubMed PMID: 22291793. Pubmed Central PMCID: 3258787.

55. Lopatina T, Kalinina N, Karagyaur M, Stambolsky D, Rubina K, Revischin A, et al. Adipose-derived stem cells stimulate regeneration of peripheral nerves: BDNF secreted by these cells promotes nerve healing and axon growth de novo. PloS one. 2011;6(3):e17899. PubMed PMID: 21423756. Pubmed Central PMCID: 3056777.

56. Marconi S, Castiglione G, Turano E, Bissolotti G, Angiari S, Farinazzo A, et al. Human adipose-derived mesenchymal stem cells systemically injected promote peripheral nerve regeneration in the mouse model of sciatic crush. Tissue engineering Part A. 2012 Jun;18(11-12):1264-72. PubMed PMID: 22332955.

57. Mohammadi R, Azizi S, Amini K. Effects of undifferentiated cultured omental adipose-derived stem cells on peripheral nerve regeneration. The Journal of surgical research. 2013 Apr;180(2):e91-7. PubMed PMID: 22560857.

58. Mohammadi R, Azizi S, Delirezh N, Hobbenaghi R, Amini K. Comparison of beneficial effects of undifferentiated cultured bone marrow stromal cells and omental adipose-derived nucleated cell fractions on sciatic nerve regeneration. Muscle & nerve. 2011 Feb;43(2):157-63. PubMed PMID: 21254077.

59. Mohammadi R, Azizi S, Delirezh N, Hobbenaghi R, Amini K, Malekkhetabi P. The use of undifferentiated bone marrow stromal cells for sciatic nerve regeneration in rats. International journal of oral and maxillofacial surgery. 2012 May;41(5):650-6. PubMed PMID: 22154576.

60. Nijhuis TH, Bodar CW, van Neck JW, Walbeehm ET, Siemionow M, Madajka M, et al. Natural conduits for bridging a 15-mm nerve defect: comparison of the vein supported by

muscle and bone marrow stromal cells with a nerve autograft. Journal of plastic, reconstructive & aesthetic surgery : JPRAS. 2013 Feb;66(2):251-9. PubMed PMID: 23063384.

61. Nijhuis TH, Brzezicki G, Klimczak A, Siemionow M. Isogenic venous graft supported with bone marrow stromal cells as a natural conduit for bridging a 20 mm nerve gap. Microsurgery. 2010 Nov;30(8):639-45. PubMed PMID: 20842703.

62. Orbay H, Uysal AC, Hyakusoku H, Mizuno H. Differentiated and undifferentiated adipose-derived stem cells improve function in rats with peripheral nerve gaps. Journal of plastic, reconstructive & aesthetic surgery : JPRAS. 2012 May;65(5):657-64. PubMed PMID: 22137687.

63. Pereira Lopes FR, Camargo de Moura Campos L, Dias Correa J, Jr., Balduino A, Lora S, Langone F, et al. Bone marrow stromal cells and resorbable collagen guidance tubes enhance sciatic nerve regeneration in mice. Experimental neurology. 2006 Apr;198(2):457-68. PubMed PMID: 16487971.

64. Salomone R, Bento RF, Costa HJ, Azzi-Nogueira D, Ovando PC, Da-Silva CF, et al. Bone marrow stem cells in facial nerve regeneration from isolated stumps. Muscle & nerve. 2013 Sep;48(3):423-9. PubMed PMID: 23824709.

65. Santiago LY, Clavijo-Alvarez J, Brayfield C, Rubin JP, Marra KG. Delivery of adipose-derived precursor cells for peripheral nerve repair. Cell transplantation. 2009;18(2):145-58. PubMed PMID: 19499703. Epub 2009/06/09. eng.

66. Shimizu S, Kitada M, Ishikawa H, Itokazu Y, Wakao S, Dezawa M. Peripheral nerve regeneration by the in vitro differentiated-human bone marrow stromal cells with Schwann cell property. Biochemical and biophysical research communications. 2007 Aug 10;359(4):915-20. PubMed PMID: 17573041.

67. Sowa Y, Imura T, Numajiri T, Nishino K, Fushiki S. Adipose-derived stem cells produce factors enhancing peripheral nerve regeneration: influence of age and anatomic site of origin. Stem cells and development. 2012 Jul 20;21(11):1852-62. PubMed PMID: 22150084.

68. Sun F, Zhou K, Mi WJ, Qiu JH. Repair of facial nerve defects with decellularized artery allografts containing autologous adipose-derived stem cells in a rat model. Neuroscience letters. 2011 Jul 20;499(2):104-8. PubMed PMID: 21651959.

69. Tohill M, Mantovani C, Wiberg M, Terenghi G. Rat bone marrow mesenchymal stem cells express glial markers and stimulate nerve regeneration. Neuroscience letters. 2004 May 27;362(3):200-3. PubMed PMID: 15158014.

70. Tomita K, Madura T, Mantovani C, Terenghi G. Differentiated adipose-derived stem cells promote myelination and enhance functional recovery in a rat model of chronic denervation. Journal of neuroscience research. 2012 Jul;90(7):1392-402. PubMed PMID: 22419645.

71. Wakao S, Hayashi T, Kitada M, Kohama M, Matsue D, Teramoto N, et al. Long-term observation of auto-cell transplantation in non-human primate reveals safety and efficiency of

bone marrow stromal cell-derived Schwann cells in peripheral nerve regeneration. Experimental neurology. 2010 Jun;223(2):537-47. PubMed PMID: 20153320.

72. Wang D, Liu XL, Zhu JK, Jiang L, Hu J, Zhang Y, et al. Bridging small-gap peripheral nerve defects using acellular nerve allograft implanted with autologous bone marrow stromal cells in primates. Brain research. 2008 Jan 10;1188:44-53. PubMed PMID: 18061586.

73. Wang Y, Zhao Z, Ren Z, Zhao B, Zhang L, Chen J, et al. Recellularized nerve allografts with differentiated mesenchymal stem cells promote peripheral nerve regeneration. Neuroscience letters. 2012 Apr 11;514(1):96-101. PubMed PMID: 22405891. Epub 2012/03/13. eng.

74. Yang Y, Yuan X, Ding F, Yao D, Gu Y, Liu J, et al. Repair of rat sciatic nerve gap by a silk fibroin-based scaffold added with bone marrow mesenchymal stem cells. Tissue engineering Part A. 2011 Sep;17(17-18):2231-44. PubMed PMID: 21542668.

75. Zarbakhsh S, Bakhtiyari M, Faghihi A, Joghataei MT, Mehdizadeh M, Khoei S, et al. The effects of schwann and bone marrow stromal stem cells on sciatic nerve injury in rat: a comparison of functional recovery. Cell journal. 2012 Spring;14(1):39-46. PubMed PMID: 23626936. Pubmed Central PMCID: PMC3635819. Epub 2013/04/30. eng.

76. Zhang Y, Luo H, Zhang Z, Lu Y, Huang X, Yang L, et al. A nerve graft constructed with xenogeneic acellular nerve matrix and autologous adipose-derived mesenchymal stem cells. Biomaterials. 2010 Jul;31(20):5312-24. PubMed PMID: 20381139.

77. Zheng L, Cui HF. Enhancement of nerve regeneration along a chitosan conduit combined with bone marrow mesenchymal stem cells. Journal of materials science Materials in medicine. 2012 Sep;23(9):2291-302. PubMed PMID: 22661248.

78. Sayers ST, Khan N, Ahmed Y, Shahid R, Khan T. Preparation of brain-derived neurotrophic factor- and neurotrophin-3-secreting Schwann cells by infection with a retroviral vector. Journal of molecular neuroscience : MN. 1998 Apr;10(2):143-60. PubMed PMID: 9699155. Epub 1998/08/12. eng.

79. Brushart TM. Preferential reinnervation of motor nerves by regenerating motor axons. The Journal of neuroscience : the official journal of the Society for Neuroscience. 1988 Mar;8(3):1026-31. PubMed PMID: 3346713. Epub 1988/03/01. eng.

80. Brushart TM. Motor axons preferentially reinnervate motor pathways. The Journal of neuroscience : the official journal of the Society for Neuroscience. 1993 Jun;13(6):2730-8. PubMed PMID: 8501535. Epub 1993/06/01. eng.

81. Brushart TM, Gerber J, Kessens P, Chen YG, Royall RM. Contributions of pathway and neuron to preferential motor reinnervation. The Journal of neuroscience : the official journal of the Society for Neuroscience. 1998 Nov 1;18(21):8674-81. PubMed PMID: 9786974. Epub 1998/10/24. eng.

82. Madison RD, Archibald SJ, Brushart TM. Reinnervation accuracy of the rat femoral nerve by motor and sensory neurons. The Journal of neuroscience : the official journal of the Society for Neuroscience. 1996 Sep 15;16(18):5698-703. PubMed PMID: 8795625. Epub 1996/09/15. eng.

83. Navarro X, Vivo M, Valero-Cabre A. Neural plasticity after peripheral nerve injury and regeneration. Progress in neurobiology. 2007 Jul;82(4):163-201. PubMed PMID: 17643733. Epub 2007/07/24. eng.

84. Fox IK, Davidge KM, Novak CB, Hoben G, Kahn LC, Juknis N, et al. Nerve Transfers to Restore Upper Extremity Function in Cervical Spinal Cord Injury: Update and Preliminary Outcomes. Plastic and reconstructive surgery. 2015 Oct;136(4):780-92. PubMed PMID: 26397252. Epub 2015/09/24. eng.

85. Mackinnon SE, Yee A, Ray WZ. Nerve transfers for the restoration of hand function after spinal cord injury. Journal of neurosurgery. 2012 Jul;117(1):176-85. PubMed PMID: 22587551. Epub 2012/05/17. eng.

86. Midha R. Nerve transfers for severe brachial plexus injuries: a review. Neurosurgical focus. 2004 May 15;16(5):E5. PubMed PMID: 15174825. Epub 2004/06/04. eng.

87. Myles LM, Gilmour JA, Glasby MA. Effects of different methods of peripheral nerve repair on the number and distribution of muscle afferent neurons in rat dorsal root ganglion. Journal of neurosurgery. 1992 Sep;77(3):457-62. PubMed PMID: 1506894. Epub 1992/09/01. eng.

88. Kaplan HM, Mishra P, Kohn J. The overwhelming use of rat models in nerve regeneration research may compromise designs of nerve guidance conduits for humans. Journal of materials science Materials in medicine. 2015 Aug;26(8):226. PubMed PMID: 26296419. Pubmed Central PMCID: PMC4545171. Epub 2015/08/25. eng.

89. O'Kane S, Ferguson MW. Transforming growth factor beta s and wound healing. The international journal of biochemistry & cell biology. 1997 Jan;29(1):63-78. PubMed PMID: 9076942. Epub 1997/01/01. eng.

90. Atkins S, Loescher AR, Boissonade FM, Smith KG, Occleston N, O'Kane S, et al. Interleukin-10 reduces scarring and enhances regeneration at a site of sciatic nerve repair. Journal of the peripheral nervous system : JPNS. 2007 Dec;12(4):269-76. PubMed PMID: 18042137. Epub 2007/11/29. eng.

91. Scherer SS, Kamholz J, Jakowlew SB. Axons modulate the expression of transforming growth factor-betas in Schwann cells. Glia. 1993 Aug;8(4):265-76. PubMed PMID: 8406683. Epub 1993/08/01. eng.

92. Taskinen HS, Ruohonen S, Jagodic M, Khademi M, Olsson T, Roytta M. Distinct expression of TGF-beta1 mRNA in the endo- and epineurium after nerve injury. Journal of neurotrauma. 2004 Jul;21(7):969-75. PubMed PMID: 15307908. Epub 2004/08/17. eng.

93. Mathur A, Merrell JC, Russell RC, Zook EG. A scanning electron microscopy evaluation of peripheral nerve regeneration. Scanning electron microscopy. 1983 (Pt 2):975-81. PubMed PMID: 6635582. Epub 1983/01/01. eng.

94. Sunderland S, Bradley KC. Endoneurial tube shrinkage in the distal segment of a severed nerve. The Journal of comparative neurology. 1950 Dec;93(3):411-20. PubMed PMID: 14803569. Epub 1950/12/01. eng.

95. Ellis JC, McCaffrey TV. Nerve grafting. Functional results after primary vs delayed repair. Archives of otolaryngology (Chicago, Ill : 1960). 1985 Dec;111(12):781-5. PubMed PMID: 4062648. Epub 1985/12/01. eng.

96. Furey MJ, Midha R, Xu QG, Belkas J, Gordon T. Prolonged target deprivation reduces the capacity of injured motoneurons to regenerate. Neurosurgery. 2007 Apr;60(4):723-32; discussion 32-3. PubMed PMID: 17415210. Epub 2007/04/07. eng.

97. Gordon T, Tyreman N, Raji MA. The basis for diminished functional recovery after delayed peripheral nerve repair. The Journal of neuroscience : the official journal of the Society for Neuroscience. 2011 Apr 6;31(14):5325-34. PubMed PMID: 21471367. Epub 2011/04/08. eng.

98. Dow DE, Cederna PS, Hassett CA, Dennis RG, Faulkner JA. Electrical stimulation prior to delayed reinnervation does not enhance recovery in muscles of rats. Restorative neurology and neuroscience. 2007;25(5-6):601-10. PubMed PMID: 18334775. Epub 2008/03/13. eng.

99. Boyd JG, Gordon T. The neurotrophin receptors, trkB and p75, differentially regulate motor axonal regeneration. Journal of neurobiology. 2001 Dec;49(4):314-25. PubMed PMID: 11745667. Epub 2001/12/18. eng.

100. Boyd JG, Gordon T. A dose-dependent facilitation and inhibition of peripheral nerve regeneration by brain-derived neurotrophic factor. The European journal of neuroscience. 2002 Feb;15(4):613-26. PubMed PMID: 11886442. Epub 2002/03/12. eng.

101. Al-Majed AA, Neumann CM, Brushart TM, Gordon T. Brief Electrical Stimulation Promotes the Speed and Accuracy of Motor Axonal Regeneration. The Journal of Neuroscience. 2000 April 1, 2000;20(7):2602-8.

102. Brushart TM, Hoffman PN, Royall RM, Murinson BB, Witzel C, Gordon T. Electrical Stimulation Promotes Motoneuron Regeneration without Increasing Its Speed or Conditioning the Neuron. The Journal of Neuroscience. 2002 August 1, 2002;22(15):6631-8.

103. Huang J, Zhang Y, Lu L, Hu X, Luo Z. Electrical stimulation accelerates nerve regeneration and functional recovery in delayed peripheral nerve injury in rats. The European journal of neuroscience. 2013 Dec;38(12):3691-701. PubMed PMID: 24118464. Epub 2013/10/15. eng.

104. Xu C, Kou Y, Zhang P, Han N, Yin X, Deng J, et al. Electrical Stimulation Promotes Regeneration of Defective Peripheral Nerves after Delayed Repair Intervals Lasting under One Month. PloS one. 2014;9(9):e105045. PubMed PMID: 25181499. Pubmed Central PMCID: PMC4152131. Epub 2014/09/03. eng.

105. Gordon T, Brushart TM, Chan KM. Augmenting nerve regeneration with electrical stimulation. Neurological research. 2008 Dec;30(10):1012-22. PubMed PMID: 19079975. Epub 2008/12/17. eng.

106. Geremia NM, Gordon T, Brushart TM, Al-Majed AA, Verge VM. Electrical stimulation promotes sensory neuron regeneration and growth-associated gene expression. Experimental neurology. 2007 Jun;205(2):347-59. PubMed PMID: 17428474. Epub 2007/04/13. eng.

107. Dvali L, Mackinnon S. Nerve repair, grafting, and nerve transfers. Clinics in plastic surgery. 2003 Apr;30(2):203-21. PubMed PMID: 12737353. Epub 2003/05/10. eng.

108. Harris ME, Tindall SC. Techniques of peripheral nerve repair. Neurosurgery clinics of North America. 1991 Jan;2(1):93-104. PubMed PMID: 1821737. Epub 1991/01/01. eng.

109. Maggi SP, Lowe JB, 3rd, Mackinnon SE. Pathophysiology of nerve injury. Clinics in plastic surgery. 2003 Apr;30(2):109-26. PubMed PMID: 12737347. Epub 2003/05/10. eng.

110. Sunderland S. The anatomy and physiology of nerve injury. Muscle & nerve. 1990 Sep;13(9):771-84. PubMed PMID: 2233864. Epub 1990/09/01. eng.

111. Brushart TM, Tarlov EC, Mesulam MM. Specificity of muscle reinnervation after epineurial and individual fascicular suture of the rat sciatic nerve. The Journal of hand surgery. 1983 May;8(3):248-53. PubMed PMID: 6348148. Epub 1983/05/01. eng.

112. Grabb WC, Bement SL, Koepke GH, Green RA. Comparison of methods of peripheral nerve suturing in monkeys. Plastic and reconstructive surgery. 1970 Jul;46(1):31-8. PubMed PMID: 4988132. Epub 1970/07/01. eng.

113. Tupper JW, Crick JC, Matteck LR. Fascicular nerve repairs. A comparative study of epineurial and fascicular (perineurial) techniques. The Orthopedic clinics of North America. 1988 Jan;19(1):57-69. PubMed PMID: 3275929. Epub 1988/01/01. eng.

114. Hakstian RW. Funicular orientation by direct stimulation. An aid to peripheral nerve repair. The Journal of bone and joint surgery American volume. 1968 Sep;50(6):1178-86. PubMed PMID: 5675401. Epub 1968/09/01. eng.

115. Vandeput J, Tanner JC, Huypens L. Electro-physiological orientation of the cut ends in primary peripheral nerve repair. Plastic and reconstructive surgery. 1969 Oct;44(4):378-82. PubMed PMID: 5809008. Epub 1969/10/01. eng.

116. Gual JS, Jr. Electrical fascicle identification as an adjunct to nerve repair. The Journal of hand surgery. 1983 May;8(3):289-96. PubMed PMID: 6875231. Epub 1983/05/01. eng.

117. Kato H, Minami A, Kobayashi M, Takahara M, Ogino T. Functional results of low median and ulnar nerve repair with intraneural fascicular dissection and electrical fascicular orientation. The Journal of hand surgery. 1998 May;23(3):471-82. PubMed PMID: 9620188. Epub 1998/06/10. eng.

118. Riley DA, Lang DH. Carbonic anhydrase activity of human peripheral nerves: a possible histochemical aid to nerve repair. The Journal of hand surgery. 1984 Jan;9A(1):112-20. PubMed PMID: 6198352. Epub 1984/01/01. eng.

119. Riley DA, Sanger JR, Matloub HS, Yousif NJ, Bain JL, Moore GH. Identifying motor and sensory myelinated axons in rabbit peripheral nerves by histochemical staining for carbonic anhydrase and cholinesterase activities. Brain research. 1988 Jun 21;453(1-2):79-88. PubMed PMID: 3135920. Epub 1988/06/21. eng.

120. Miyamoto Y. Experimental study of results of nerve suture under tension vs. nerve grafting. Plastic and reconstructive surgery. 1979 Oct;64(4):540-9. PubMed PMID: 482439. Epub 1979/10/01. eng.

121. Taylor GI. Free vascularized nerve transfer in the upper extremity. Hand clinics. 1999 Nov;15(4):673-95, ix-x. PubMed PMID: 10563270. Epub 1999/11/24. eng.

122. Kanaya F, Firrell J, Tsai TM, Breidenbach WC. Functional results of vascularized versus nonvascularized nerve grafting. Plastic and reconstructive surgery. 1992 May;89(5):924-30. PubMed PMID: 1561263. Epub 1992/05/01. eng.

123. Karcher H, Kleinert R. Regeneration in vascularized and free nerve grafts. A comparative morphological study in rats. Journal of maxillofacial surgery. 1986 Dec;14(6):341-3. PubMed PMID: 3467003. Epub 1986/12/01. eng.

124. Kawai H, Baudrimont M, Travers V, Sedel L. A comparative experimental study of vascularized and nonvascularized nerve grafts. Journal of reconstructive microsurgery. 1990 Jul;6(3):255-9. PubMed PMID: 2292788. Epub 1990/07/01. eng.

125. Koshima I, Harii K. Experimental study of vascularized nerve grafts: morphometric study of axonal regeneration of nerves transplanted into silicone tubes. Annals of plastic surgery. 1985 Mar;14(3):235-43. PubMed PMID: 3994268. Epub 1985/03/01. eng.

126. Koshima I, Harii K. Experimental study of vascularized nerve grafts: multifactorial analyses of axonal regeneration of nerves transplanted into an acute burn wound. The Journal of hand surgery. 1985 Jan;10(1):64-72. PubMed PMID: 3968406. Epub 1985/01/01. eng.

127. Pho RW, Lee YS, Rujiwetpongstorn V, Pang M. Histological studies of vascularised nerve graft and conventional nerve graft. Journal of hand surgery (Edinburgh, Scotland). 1985 Feb;10(1):45-8. PubMed PMID: 2582074. Epub 1985/02/01. eng.

128. Seckel BR, Ryan SE, Simons JE, Gagne RG, Watkins E, Jr. Vascularized versus nonvascularized nerve grafts: an experimental structural comparison. Plastic and reconstructive surgery. 1986 Aug;78(2):211-20. PubMed PMID: 3725966. Epub 1986/08/01. eng.

129. Shibata M, Tsai TM, Firrell J, Breidenbach WC. Experimental comparison of vascularized and nonvascularized nerve grafting. The Journal of hand surgery. 1988 May;13(3):358-65. PubMed PMID: 3379269. Epub 1988/05/01. eng.

130. Shupeck M, Ward KK, Schmelzer JD, Low PA. Comparison of nerve regeneration in vascularized and conventional grafts: nerve electrophysiology, norepinephrine, prostacyclin, malondialdehyde, and the blood-nerve barrier. Brain research. 1989 Jul 31;493(2):225-30. PubMed PMID: 2670062. Epub 1989/07/31. eng.

131. Bain JR, Mackinnon SE, Hudson AR, Falk RE, Falk JA, Hunter DA. The peripheral nerve allograft: an assessment of regeneration across nerve allografts in rats immunosuppressed with cyclosporin A. Plastic and reconstructive surgery. 1988 Dec;82(6):1052-66. PubMed PMID: 3264409. Epub 1988/12/01. eng.

132. Bain JR, Mackinnon SE, Hudson AR, Wade J, Evans P, Makino A, et al. The peripheral nerve allograft in the primate immunosuppressed with Cyclosporin A: I.

Histologic and electrophysiologic assessment. Plastic and reconstructive surgery. 1992 Dec;90(6):1036-46. PubMed PMID: 1448498. Epub 1992/12/01. eng.

133. Fish JS, Bain JR, McKee N, Mackinnon SE. The peripheral nerve allograft in the primate immunosuppressed with Cyclosporin A: II. Functional evaluation of reinnervated muscle. Plastic and reconstructive surgery. 1992 Dec;90(6):1047-52. PubMed PMID: 1448499. Epub 1992/12/01. eng.

134. Weinzweig N, Grindel S, Gonzalez M, Kuy D, Fang J, Shahani B. Peripheral-nerve allotransplantation in rats immunosuppressed with transient or long-term FK-506. Journal of reconstructive microsurgery. 1996 Oct;12(7):451-9. PubMed PMID: 8905545. Epub 1996/10/01. eng.

135. Midha R, Mackinnon SE, Evans PJ, Best TJ, Hare GM, Hunter DA, et al. Comparison of regeneration across nerve allografts with temporary or continuous cyclosporin A immunosuppression. Journal of neurosurgery. 1993 Jan;78(1):90-100. PubMed PMID: 8416248. Epub 1993/01/01. eng.

136. Gulati AK. Evaluation of acellular and cellular nerve grafts in repair of rat peripheral nerve. Journal of neurosurgery. 1988 Jan;68(1):117-23. PubMed PMID: 3335896. Epub 1988/01/01. eng.

137. Hudson TW, Zawko S, Deister C, Lundy S, Hu CY, Lee K, et al. Optimized acellular nerve graft is immunologically tolerated and supports regeneration. Tissue engineering. 2004 Nov-Dec;10(11-12):1641-51. PubMed PMID: 15684673. Epub 2005/02/03. eng.

138. Hudson TW, Liu SY, Schmidt CE. Engineering an improved acellular nerve graft via optimized chemical processing. Tissue engineering. 2004 Sep-Oct;10(9-10):1346-58. PubMed PMID: 15588395. Epub 2004/12/14. eng.

139. Brooks DN, Weber RV, Chao JD, Rinker BD, Zoldos J, Robichaux MR, et al. Processed nerve allografts for peripheral nerve reconstruction: a multicenter study of utilization and outcomes in sensory, mixed, and motor nerve reconstructions. Microsurgery. 2012 Jan;32(1):1-14. PubMed PMID: 22121093. Epub 2011/11/29. eng.

140. Giusti G, Willems WF, Kremer T, Friedrich PF, Bishop AT, Shin AY. Return of motor function after segmental nerve loss in a rat model: comparison of autogenous nerve graft, collagen conduit, and processed allograft (AxoGen). The Journal of bone and joint surgery American volume. 2012 Mar 7;94(5):410-7. PubMed PMID: 22398734. Epub 2012/03/09. eng.

141. Boyd KU, Nimigan AS, Mackinnon SE. Nerve reconstruction in the hand and upper extremity. Clinics in plastic surgery. 2011 Oct;38(4):643-60. PubMed PMID: 22032591. Epub 2011/10/29. eng.

142. Karabekmez FE, Duymaz A, Moran SL. Early clinical outcomes with the use of decellularized nerve allograft for repair of sensory defects within the hand. Hand (New York, NY). 2009 Sep;4(3):245-9. PubMed PMID: 19412640. Pubmed Central PMCID: PMC2724628. Epub 2009/05/05. eng.

143. Shanti RM, Ziccardi VB. Use of decellularized nerve allograft for inferior alveolar nerve reconstruction: a case report. Journal of oral and maxillofacial surgery : official journal

of the American Association of Oral and Maxillofacial Surgeons. 2011 Feb;69(2):550-3. PubMed PMID: 21145638. Epub 2010/12/15. eng.

144. Gunn S, Cosetti M, Roland JT, Jr. Processed allograft: novel use in facial nerve repair after resection of a rare racial nerve paraganglioma. The Laryngoscope. 2010;120 Suppl 4:S206. PubMed PMID: 21225804. Epub 2011/01/13. eng.

145. Amoh Y, Aki R, Hamada Y, Niiyama S, Eshima K, Kawahara K, et al. Nestin-positive hair follicle pluripotent stem cells can promote regeneration of impinged peripheral nerve injury. The Journal of dermatology. 2012 Jan;39(1):33-8. PubMed PMID: 22098554.

146. Lin MY, Manzano G, Gupta R. Nerve allografts and conduits in peripheral nerve repair. Hand clinics. 2013 Aug;29(3):331-48. PubMed PMID: 23895714. Epub 2013/07/31. eng.

147. Rivlin M, Sheikh E, Isaac R, Beredjiklian PK. The role of nerve allografts and conduits for nerve injuries. Hand clinics. 2010 Aug;26(3):435-46, viii. PubMed PMID: 20670808. Epub 2010/07/31. eng.

148. Tang JB. Group fascicular vein grafts with interposition of nerve slices for long ulnar nerve defects: report of three cases. Microsurgery. 1993;14(6):404-8. PubMed PMID: 8371689. Epub 1993/01/01. eng.

149. Tang JB. Vein conduits with interposition of nerve tissue for peripheral nerve defects. Journal of reconstructive microsurgery. 1995 Jan;11(1):21-6. PubMed PMID: 7714875. Epub 1995/01/01. eng.

150. Brunelli GA, Battiston B, Vigasio A, Brunelli G, Marocolo D. Bridging nerve defects with combined skeletal muscle and vein conduits. Microsurgery. 1993;14(4):247-51. PubMed PMID: 8412634. Epub 1993/01/01. eng.

151. Battiston B, Tos P, Cushway TR, Geuna S. Nerve repair by means of vein filled with muscle grafts I. Clinical results. Microsurgery. 2000;20(1):32-6. PubMed PMID: 10617879. Epub 2000/01/05. eng.

152. Brandt J, Dahlin LB, Lundborg G. Autologous tendons used as grafts for bridging peripheral nerve defects. Journal of hand surgery (Edinburgh, Scotland). 1999 Jun;24(3):284-90. PubMed PMID: 10433437. Epub 1999/08/05. eng.

153. Brandt J, Dahlin LB, Kanje M, Lundborg G. Functional recovery in a tendon autograft used to bridge a peripheral nerve defect. Scandinavian journal of plastic and reconstructive surgery and hand surgery / Nordisk plastikkirurgisk forening [and] Nordisk klubb for handkirurgi. 2002;36(1):2-8. PubMed PMID: 11925824. Epub 2002/04/03. eng.

154. Merle M, Dellon AL, Campbell JN, Chang PS. Complications from silicon-polymer intubulation of nerves. Microsurgery. 1989;10(2):130-3. PubMed PMID: 2770512. Epub 1989/01/01. eng.

155. Pabari A, Lloyd-Hughes H, Seifalian AM, Mosahebi A. Nerve conduits for peripheral nerve surgery. Plastic and reconstructive surgery. 2014 Jun;133(6):1420-30. PubMed PMID: 24867724. Epub 2014/05/29. eng.

156. Kalbermatten DF, Pettersson J, Kingham PJ, Pierer G, Wiberg M, Terenghi G. New fibrin conduit for peripheral nerve repair. Journal of reconstructive microsurgery. 2009 Jan;25(1):27-33. PubMed PMID: 18925549. Epub 2008/10/18. eng.

157. Pettersson J, Kalbermatten D, McGrath A, Novikova LN. Biodegradable fibrin conduit promotes long-term regeneration after peripheral nerve injury in adult rats. Journal of plastic, reconstructive & aesthetic surgery : JPRAS. 2010 Nov;63(11):1893-9. PubMed PMID: 20005193. Epub 2009/12/17. eng.

158. Bian YZ, Wang Y, Aibaidoula G, Chen GQ, Wu Q. Evaluation of poly(3-hydroxybutyrate-co-3-hydroxyhexanoate) conduits for peripheral nerve regeneration. Biomaterials. 2009 Jan;30(2):217-25. PubMed PMID: 18849069. Epub 2008/10/14. eng.

159. Gu J, Hu W, Deng A, Zhao Q, Lu S, Gu X. Surgical repair of a 30 mm long human median nerve defect in the distal forearm by implantation of a chitosan-PGA nerve guidance conduit. Journal of tissue engineering and regenerative medicine. 2012 Feb;6(2):163-8. PubMed PMID: 21370489. Epub 2011/03/04. eng.

160. Huang J, Lu L, Zhang J, Hu X, Zhang Y, Liang W, et al. Electrical stimulation to conductive scaffold promotes axonal regeneration and remyelination in a rat model of large nerve defect. PloS one. 2012;7(6):e39526. PubMed PMID: 22737243. Pubmed Central PMCID: PMC3380893. Epub 2012/06/28. eng.

161. Schlosshauer B, Dreesmann L, Schaller HE, Sinis N. Synthetic nerve guide implants in humans: a comprehensive survey. Neurosurgery. 2006 Oct;59(4):740-7; discussion 7-8. PubMed PMID: 17038939. Epub 2006/10/14. eng.

162. DeLee JC, Smith MT, Green DP. The reaction of nerve tissue to various suture materials: a study in rabbits. The Journal of hand surgery. 1977 Jan;2(1):38-43. PubMed PMID: 839053. Epub 1977/01/01. eng.

163. Lubiatowski P, Unsal FM, Nair D, Ozer K, Siemionow M. The epineural sleeve technique for nerve graft reconstruction enhances nerve recovery. Microsurgery. 2008;28(3):160-7. PubMed PMID: 18286656. Epub 2008/02/21. eng.

164. Siemionow M, Tetik C, Ozer K, Ayhan S, Siemionow K, Browne E. Epineural sleeve neurorrhaphy: surgical technique and functional results--a preliminary report. Annals of plastic surgery. 2002 Mar;48(3):281-5. PubMed PMID: 11862033. Epub 2002/02/28. eng.

165. Tetik C, Ozer K, Ayhan S, Siemionow K, Browne E, Siemionow M. Conventional versus epineural sleeve neurorrhaphy technique: functional and histomorphometric analysis. Annals of plastic surgery. 2002 Oct;49(4):397-403. PubMed PMID: 12370646. Epub 2002/10/09. eng.

166. Menovsky T, Beek JF. Laser, fibrin glue, or suture repair of peripheral nerves: a comparative functional, histological, and morphometric study in the rat sciatic nerve. Journal of neurosurgery. 2001 Oct;95(4):694-9. PubMed PMID: 11596965. Epub 2001/10/13. eng.

167. Menovsky T, Beek JF, Thomsen SL. Laser(-assisted) nerve repair. A review. Neurosurgical review. 1995;18(4):225-35. PubMed PMID: 8927238. Epub 1995/01/01. eng.

168. Sameem M, Wood TJ, Bain JR. A systematic review on the use of fibrin glue for peripheral nerve repair. Plastic and reconstructive surgery. 2011 Jun;127(6):2381-90. PubMed PMID: 21311390. Epub 2011/02/12. eng.

169. Tarlov IM, Benjamin B. AUTOLOGOUS PLASMA CLOT SUTURE OF NERVES. Science. 1942 Mar 6;95(2462):258. PubMed PMID: 17774166. Epub 1942/03/06. eng.

170. Bento RF, Miniti A. Anastomosis of the intratemporal facial nerve using fibrin tissue adhesive. Ear, nose, & throat journal. 1993 Oct;72(10):663. PubMed PMID: 8269873. Epub 1993/10/01. eng.

171. Feldman MD, Sataloff RT, Epstein G, Ballas SK. Autologous fibrin tissue adhesive for peripheral nerve anastomosis. Archives of otolaryngology--head & neck surgery. 1987 Sep;113(9):963-7. PubMed PMID: 3606848. Epub 1987/09/01. eng.

172. Martins RS, Siqueira MG, Da Silva CF, Plese JP. Overall assessment of regeneration in peripheral nerve lesion repair using fibrin glue, suture, or a combination of the 2 techniques in a rat model. Which is the ideal choice? Surgical neurology. 2005;64 Suppl 1:S1:10-6; discussion S1:6. PubMed PMID: 15967220. Epub 2005/06/22. eng.

173. Narakas A. The use of fibrin glue in repair of peripheral nerves. The Orthopedic clinics of North America. 1988 Jan;19(1):187-99. PubMed PMID: 2447544. Epub 1988/01/01. eng.

174. Smahel J, Meyer VE, Bachem U. Glueing of peripheral nerves with fibrin: experimental studies. Journal of reconstructive microsurgery. 1987 Apr;3(3):211-20. PubMed PMID: 2439687. Epub 1987/04/01. eng.

175. Cruz NI, Debs N, Fiol RE. Evaluation of fibrin glue in rat sciatic nerve repairs. Plastic and reconstructive surgery. 1986 Sep;78(3):369-73. PubMed PMID: 3526370. Epub 1986/09/01. eng.

176. Herter T. Problems of fibrin adhesion of the nerves. Neurosurgical review. 1988;11(3-4):249-58. PubMed PMID: 2471944. Epub 1988/01/01. eng.

177. Maragh H, Meyer BS, Davenport D, Gould JD, Terzis JK. Morphofunctional evaluation of fibrin glue versus microsuture nerve repairs. Journal of reconstructive microsurgery. 1990 Oct;6(4):331-7. PubMed PMID: 2269954. Epub 1990/10/01. eng.

178. Sames M, Blahos J, Jr., Rokyta R, Benes V, Jr. Comparison of microsurgical suture with fibrin glue connection of the sciatic nerve in rabbits. Physiological research / Academia Scientiarum Bohemoslovaca. 1997;46(4):303-6. PubMed PMID: 9728497. Epub 1997/01/01. eng.

179. Fischer DW, Beggs JL, Kenshalo DL, Jr., Shetter AG. Comparative study of microepineurial anastomoses with the use of CO2 laser and suture techniques in rat sciatic nerves: Part 1. Surgical technique, nerve action potentials, and morphological studies. Neurosurgery. 1985 Aug;17(2):300-8. PubMed PMID: 3929156. Epub 1985/08/01. eng.

180. Bass LS, Moazami N, Pocsidio J, Oz MC, LoGerfo P, Treat MR. Changes in type I collagen following laser welding. Lasers in surgery and medicine. 1992;12(5):500-5. PubMed PMID: 1406002. Epub 1992/01/01. eng.

181. Dort JC, Wolfensberger M, Felix H. CO2 laser repair of the facial nerve: an experimental study in the rat. The Journal of laryngology and otology. 1994 Jun;108(6):466-9. PubMed PMID: 8027642. Epub 1994/06/01. eng.

182. Eppley BL, Kalenderian E, Winkelmann T, Delfino JJ. Facial nerve graft repair: suture versus laser-assisted anastomosis. International journal of oral and maxillofacial surgery. 1989 Feb;18(1):50-4. PubMed PMID: 2497212. Epub 1989/02/01. eng.

183. Huang TC, Blanks RH, Berns MW, Crumley RL. Laser vs. suture nerve anastomosis. Otolaryngology--head and neck surgery : official journal of American Academy of Otolaryngology-Head and Neck Surgery. 1992 Jul;107(1):14-20. PubMed PMID: 1528597. Epub 1992/07/01. eng.

184. Korff M, Bent SW, Havig MT, Schwaber MK, Ossoff RH, Zealear DL. An investigation of the potential for laser nerve welding. Otolaryngology--head and neck surgery : official journal of American Academy of Otolaryngology-Head and Neck Surgery. 1992 Apr;106(4):345-50. PubMed PMID: 1565483. Epub 1992/04/01. eng.

185. Menovsky T, Beek JF. Carbon dioxide laser-assisted nerve repair: effect of solder and suture material on nerve regeneration in rat sciatic nerve. Microsurgery. 2003;23(2):109-16. PubMed PMID: 12740882. Epub 2003/05/13. eng.

186. Menovsky T, Beek JF, van Gemert MJ. CO2 laser nerve welding: optimal laser parameters and the use of solders in vitro. Microsurgery. 1994;15(1):44-51. PubMed PMID: 8133768. Epub 1994/01/01. eng.

187. Park JW, Lee KS, Kim SK, Park JH, Hong JS, Oh KJ. Rapid neurorrhaphy with titanium clips. Microsurgery. 2002;22(8):386-90. PubMed PMID: 12497577. Epub 2002/12/24. eng.

188. Payne CE, Hunt SP, Lamberty BG. Primary sciatic nerve repair using titanium staples. British journal of plastic surgery. 2002 Jun;55(4):330-4. PubMed PMID: 12160540. Epub 2002/08/06. eng.

189. Lutz BS, Lidman D. Morphological and functional evaluation of leg-muscle reinnervation after coupler coaptation of the divided rat sciatic nerve. Microsurgery. 2005;25(3):235-40. PubMed PMID: 15696517. Epub 2005/02/08. eng.

190. Prevel CD, Eppley BL, McCarty M, Brock C. Mechanical anastomosis of nerves: a histological and functional comparison to conventional suturing. Annals of plastic surgery. 1994 Dec;33(6):600-5. PubMed PMID: 7880049. Epub 1994/12/01. eng.

191. Balasubramanian D, Du X, Zigler JS, Jr. The reaction of singlet oxygen with proteins, with special reference to crystallins. Photochemistry and photobiology. 1990 Oct;52(4):761-8. PubMed PMID: 2089424. Epub 1990/10/01. eng.

192. Chan BP, Hui TY, Chan OC, So KF, Lu W, Cheung KM, et al. Photochemical cross-linking for collagen-based scaffolds: a study on optical properties, mechanical properties,

stability, and hematocompatibility. Tissue engineering. 2007 Jan;13(1):73-85. PubMed PMID: 17518582. Epub 2007/05/24. eng.

193. Kochevar IE, Redmond RW. Photosensitized production of singlet oxygen. Methods in enzymology. 2000;319:20-8. PubMed PMID: 10907495. Epub 2000/07/25. eng.

194. Webster A, Britton D, Apap-Bologna A, Kemp G. A dye-photosensitized reaction that generates stable protein-protein crosslinks. Analytical biochemistry. 1989 May 15;179(1):154-7. PubMed PMID: 2757189. Epub 1989/05/15. eng.

195. Barton M, Morley JW, Stoodley MA, Ng KS, Piller SC, Duong H, et al. Laser-activated adhesive films for sutureless median nerve anastomosis. Journal of biophotonics. 2013 Dec;6(11-12):938-49. PubMed PMID: 23712961. Epub 2013/05/29. eng.

196. Barton MJ, Morley JW, Stoodley MA, Shaikh S, Mahns DA, Lauto A. Long term recovery of median nerve repair using laser-activated chitosan adhesive films. Journal of biophotonics. 2013 Oct 17. PubMed PMID: 24132983. Epub 2013/10/18. Eng.

197. Forbes TR. The social history of the caul. The Yale journal of biology and medicine. 1953 Jun;25(6):495-508. PubMed PMID: 13078640. Pubmed Central PMCID: PMC2599448. Epub 1953/06/01. eng.

198. Dua HS, Gomes JA, King AJ, Maharajan VS. The amniotic membrane in ophthalmology. Survey of ophthalmology. 2004 Jan-Feb;49(1):51-77. PubMed PMID: 14711440. Epub 2004/01/09. eng.

199. Mamede AC, Carvalho MJ, Abrantes AM, Laranjo M, Maia CJ, Botelho MF. Amniotic membrane: from structure and functions to clinical applications. Cell and tissue research. 2012 Aug;349(2):447-58. PubMed PMID: 22592624. Epub 2012/05/18. eng.

200. Diaz-Prado S, Muinos-Lopez E, Hermida-Gomez T, Cicione C, Rendal-Vazquez ME, Fuentes-Boquete I, et al. Human amniotic membrane as an alternative source of stem cells for regenerative medicine. Differentiation; research in biological diversity. 2011 Mar;81(3):162-71. PubMed PMID: 21339039. Epub 2011/02/23. eng.

201. Ilancheran S, Moodley Y, Manuelpillai U. Human fetal membranes: a source of stem cells for tissue regeneration and repair? Placenta. 2009 Jan;30(1):2-10. PubMed PMID: 18995896. Epub 2008/11/11. eng.

202. Parolini O, Alviano F, Bagnara GP, Bilic G, Buhring HJ, Evangelista M, et al. Concise review: isolation and characterization of cells from human term placenta: outcome of the first international Workshop on Placenta Derived Stem Cells. Stem Cells. 2008 Feb;26(2):300-11. PubMed PMID: 17975221. Epub 2007/11/03. eng.

203. Rennie K, Gruslin A, Hengstschlager M, Pei D, Cai J, Nikaido T, et al. Applications of amniotic membrane and fluid in stem cell biology and regenerative medicine. Stem cells international. 2012;2012:721538. PubMed PMID: 23093978. Pubmed Central PMCID: PMC3474290. Epub 2012/10/25. eng.

204. Trelford JD, Anderson DG, Hanson FW, Mendel V, Sawyer RH. Amnion autografts and allografts as a cover for skin defects in sheep. A preliminary report. Journal of medicine. 1972;3(2):81-7. PubMed PMID: 4507072. Epub 1972/01/01. eng.

205. Bourne GL. The microscopic anatomy of the human amnion and chorion. American journal of obstetrics and gynecology. 1960 Jun;79:1070-3. PubMed PMID: 13803349. Epub 1960/06/01. eng.

206. Okazaki T, Casey ML, Okita JR, MacDonald PC, Johnston JM. Initiation of human parturition. XII. Biosynthesis and metabolism of prostaglandins in human fetal membranes and uterine decidua. American journal of obstetrics and gynecology. 1981 Feb 15;139(4):373-81. PubMed PMID: 6781352. Epub 1981/02/15. eng.

207. Riau AK, Beuerman RW, Lim LS, Mehta JS. Preservation, sterilization and de-epithelialization of human amniotic membrane for use in ocular surface reconstruction. Biomaterials. 2010 Jan;31(2):216-25. PubMed PMID: 19781769. Epub 2009/09/29. eng.

208. Thomasen H, Pauklin M, Noelle B, Geerling G, Vetter J, Steven P, et al. The effect of long-term storage on the biological and histological properties of cryopreserved amniotic membrane. Current eye research. 2011 Mar;36(3):247-55. PubMed PMID: 21275517. Epub 2011/02/01. eng.

209. Koizumi NJ, Inatomi TJ, Sotozono CJ, Fullwood NJ, Quantock AJ, Kinoshita S. Growth factor mRNA and protein in preserved human amniotic membrane. Current eye research. 2000 Mar;20(3):173-7. PubMed PMID: 10694891. Epub 2000/03/01. eng.

210. Sakuragawa N, Elwan MA, Uchida S, Fujii T, Kawashima K. Non-neuronal neurotransmitters and neurotrophic factors in amniotic epithelial cells: expression and function in humans and monkey. Japanese journal of pharmacology. 2001 Jan;85(1):20-3. PubMed PMID: 11243569. Epub 2001/03/13. eng.

211. Koizumi N, Rigby H, Fullwood NJ, Kawasaki S, Tanioka H, Koizumi K, et al. Comparison of intact and denuded amniotic membrane as a substrate for cell-suspension culture of human limbal epithelial cells. Graefe's archive for clinical and experimental ophthalmology = Albrecht von Graefes Archiv fur klinische und experimentelle Ophthalmologie. 2007 Jan;245(1):123-34. PubMed PMID: 16612639. Epub 2006/04/14. eng.

212. Hennerbichler S, Reichl B, Pleiner D, Gabriel C, Eibl J, Redl H. The influence of various storage conditions on cell viability in amniotic membrane. Cell and tissue banking. 2007;8(1):1-8. PubMed PMID: 16807768. Epub 2006/06/30. eng.

213. van Baare J, Cameron PU, Vardaxis N, Pagnon J, Reece J, Middelkoop E, et al. The 1998 Lindberg Award. Comparison of glycerol preservation with cryopreservation methods on HIV-1 inactivation. The Journal of burn care & rehabilitation. 1998 Nov-Dec;19(6):494-500. PubMed PMID: 9848039. Epub 1998/12/16. eng.

214. Nakamura T, Yoshitani M, Rigby H, Fullwood NJ, Ito W, Inatomi T, et al. Sterilized, freeze-dried amniotic membrane: a useful substrate for ocular surface reconstruction. Investigative ophthalmology & visual science. 2004 Jan;45(1):93-9. PubMed PMID: 14691159. Epub 2003/12/24. eng.

215. Lim LS, Poh RW, Riau AK, Beuerman RW, Tan D, Mehta JS. Biological and ultrastructural properties of acelagraft, a freeze-dried gamma-irradiated human amniotic membrane. Archives of ophthalmology. 2010 Oct;128(10):1303-10. PubMed PMID: 20938000. Epub 2010/10/13. eng.

216. Lopez-Valladares MJ, Teresa Rodriguez-Ares M, Tourino R, Gude F, Teresa Silva M, Couceiro J. Donor age and gestational age influence on growth factor levels in human amniotic membrane. Acta ophthalmologica. 2010 Sep;88(6):e211-6. PubMed PMID: 20528787. Epub 2010/06/10. eng.

217. Velez DR, Fortunato SJ, Morgan N, Edwards TL, Lombardi SJ, Williams SM, et al. Patterns of cytokine profiles differ with pregnancy outcome and ethnicity. Human reproduction (Oxford, England). 2008 Aug;23(8):1902-9. PubMed PMID: 18487217. Epub 2008/05/20. eng.

218. Gicquel JJ, Dua HS, Brodie A, Mohammed I, Suleman H, Lazutina E, et al. Epidermal growth factor variations in amniotic membrane used for ex vivo tissue constructs. Tissue engineering Part A. 2009 Aug;15(8):1919-27. PubMed PMID: 19196134. Epub 2009/02/07. eng.

219. Bilic G, Zeisberger SM, Mallik AS, Zimmermann R, Zisch AH. Comparative characterization of cultured human term amnion epithelial and mesenchymal stromal cells for application in cell therapy. Cell transplantation. 2008;17(8):955-68. PubMed PMID: 19069637. Epub 2008/12/17. eng.

220. Hammer A, Hutter H, Blaschitz A, Mahnert W, Hartmann M, Uchanska-Ziegler B, et al. Amnion epithelial cells, in contrast to trophoblast cells, express all classical HLA class I molecules together with HLA-G. American journal of reproductive immunology (New York, NY : 1989). 1997 Feb;37(2):161-71. PubMed PMID: 9083612. Epub 1997/02/01. eng.

221. Adinolfi M, Akle CA, McColl I, Fensom AH, Tansley L, Connolly P, et al. Expression of HLA antigens, beta 2-microglobulin and enzymes by human amniotic epithelial cells. Nature. 1982 Jan 28;295(5847):325-7. PubMed PMID: 6173762. Epub 1982/01/28. eng.

222. Magatti M, De Munari S, Vertua E, Nassauto C, Albertini A, Wengler GS, et al. Amniotic mesenchymal tissue cells inhibit dendritic cell differentiation of peripheral blood and amnion resident monocytes. Cell transplantation. 2009;18(8):899-914. PubMed PMID: 19523334. Epub 2009/06/16. eng.

223. Hao Y, Ma DH, Hwang DG, Kim WS, Zhang F. Identification of antiangiogenic and antiinflammatory proteins in human amniotic membrane. Cornea. 2000 May;19(3):348-52. PubMed PMID: 10832697. Epub 2000/06/01. eng.

224. Ouyang W, Rutz S, Crellin NK, Valdez PA, Hymowitz SG. Regulation and functions of the IL-10 family of cytokines in inflammation and disease. Annual review of immunology. 2011;29:71-109. PubMed PMID: 21166540. Epub 2010/12/21. eng.

225. Fidel PL, Jr., Romero R, Ramirez M, Cutright J, Edwin SS, LaMarche S, et al. Interleukin-1 receptor antagonist (IL-1ra) production by human amnion, chorion, and decidua. American journal of reproductive immunology (New York, NY : 1989). 1994 Aug;32(1):1-7. PubMed PMID: 7945810. Epub 1994/08/01. eng.

226. Fortunato SJ, Menon R, Lombardi SJ. Presence of four tissue inhibitors of matrix metalloproteinases (TIMP-1, -2, -3 and -4) in human fetal membranes. American journal of

reproductive immunology (New York, NY : 1989). 1998 Dec;40(6):395-400. PubMed PMID: 9894562. Epub 1999/01/23. eng.

227. Koh JW, Shin YJ, Oh JY, Kim MK, Ko JH, Hwang JM, et al. The expression of TIMPs in cryo-preserved and freeze-dried amniotic membrane. Current eye research. 2007 Jul-Aug;32(7-8):611-6. PubMed PMID: 17852184. Epub 2007/09/14. eng.

228. Thadepalli H, Bach VT, Davidson EC, Jr. Antimicrobial effect of amniotic fluid. Obstetrics and gynecology. 1978 Aug;52(2):198-204. PubMed PMID: 355963. Epub 1978/08/01. eng.

229. Kjaergaard N, Hein M, Hyttel L, Helmig RB, Schonheyder HC, Uldbjerg N, et al. Antibacterial properties of human amnion and chorion in vitro. European journal of obstetrics, gynecology, and reproductive biology. 2001 Feb;94(2):224-9. PubMed PMID: 11165729. Epub 2001/02/13. eng.

230. Buhimschi IA, Jabr M, Buhimschi CS, Petkova AP, Weiner CP, Saed GM. The novel antimicrobial peptide beta3-defensin is produced by the amnion: a possible role of the fetal membranes in innate immunity of the amniotic cavity. American journal of obstetrics and gynecology. 2004 Nov;191(5):1678-87. PubMed PMID: 15547542. Epub 2004/11/18. eng.

231. Marvin KW, Hansen WR, Miller HC, Eykholt RL, Mitchell MD. Amnion-derived cells express intercellular adhesion molecule-1: regulation by cytokines. Journal of molecular endocrinology. 1999 Apr;22(2):193-205. PubMed PMID: 10194522. Epub 1999/04/09. eng.

232. Etienne-Manneville S, Chaverot N, Strosberg AD, Couraud PO. ICAM-1-coupled signaling pathways in astrocytes converge to cyclic AMP response element-binding protein phosphorylation and TNF-alpha secretion. Journal of immunology (Baltimore, Md : 1950). 1999 Jul 15;163(2):668-74. PubMed PMID: 10395656. Epub 1999/07/08. eng.

233. Sporn MB, Roberts AB, Wakefield LM, de Crombrugghe B. Some recent advances in the chemistry and biology of transforming growth factor-beta. The Journal of cell biology. 1987 Sep;105(3):1039-45. PubMed PMID: 3308901. Pubmed Central PMCID: PMC2114801. Epub 1987/09/01. eng.

234. Faulk WP, Matthews R, Stevens PJ, Bennett JP, Burgos H, Hsi BL. Human amnion as an adjunct in wound healing. Lancet. 1980 May 31;1(8179):1156-8. PubMed PMID: 6155575. Epub 1980/05/31. eng.

235. Koob TJ, Lim JJ, Massee M, Zabek N, Rennert R, Gurtner G, et al. Angiogenic properties of dehydrated human amnion/chorion allografts: therapeutic potential for soft tissue repair and regeneration. Vascular cell. 2014;6:10. PubMed PMID: 24817999. Pubmed Central PMCID: PMC4016655. Epub 2014/05/13. eng.

236. Meng H, Li M, You F, Du J, Luo Z. Assessment of processed human amniotic membrane as a protective barrier in rat model of sciatic nerve injury. Neuroscience letters. 2011 May 27;496(1):48-53. PubMed PMID: 21511004. Epub 2011/04/23. eng.

237. Mligiliche N, Endo K, Okamoto K, Fujimoto E, Ide C. Extracellular matrix of human amnion manufactured into tubes as conduits for peripheral nerve regeneration. Journal of

biomedical materials research. 2002;63(5):591-600. PubMed PMID: 12209905. Epub 2002/09/05. eng.

238. Mohammad J, Shenaq J, Rabinovsky E, Shenaq S. Modulation of peripheral nerve regeneration: a tissue-engineering approach. The role of amnion tube nerve conduit across a 1-centimeter nerve gap. Plastic and reconstructive surgery. 2000 Feb;105(2):660-6. PubMed PMID: 10697174. Epub 2000/03/04. eng.

239. Mohammad JA, Warnke PH, Pan YC, Shenaq S. Increased axonal regeneration through a biodegradable amnionic tube nerve conduit: effect of local delivery and incorporation of nerve growth factor/hyaluronic acid media. Annals of plastic surgery. 2000 Jan;44(1):59-64. PubMed PMID: 10651367. Epub 2000/01/29. eng.

240. O'Neill AC, Randolph MA, Bujold KE, Kochevar IE, Redmond RW, Winograd JM. Preparation and integration of human amnion nerve conduits using a light-activated technique. Plastic and reconstructive surgery. 2009 Aug;124(2):428-37. PubMed PMID: 19644257. Epub 2009/08/01. eng.

241. Henry FP, Goyal NA, David WS, Wes D, Bujold KE, Randolph MA, et al. Improving electrophysiologic and histologic outcomes by photochemically sealing amnion to the peripheral nerve repair site. Surgery. 2009 Mar;145(3):313-21. PubMed PMID: 19231584. Epub 2009/02/24. eng.

242. Johnson TS, O'Neill AC, Motarjem PM, Amann C, Nguyen T, Randolph MA, et al. Photochemical tissue bonding: a promising technique for peripheral nerve repair. The Journal

of surgical research. 2007 Dec;143(2):224-9. PubMed PMID: 17543988. Epub 2007/06/05. eng.

243. O'Neill AC, Randolph MA, Bujold KE, Kochevar IE, Redmond RW, Winograd JM. Photochemical sealing improves outcome following peripheral neurorrhaphy. The Journal of surgical research. 2009 Jan;151(1):33-9. PubMed PMID: 18599081. Epub 2008/07/05. eng.

244. Spoerl E, Wollensak G, Reber F, Pillunat L. Cross-linking of human amniotic membrane by glutaraldehyde. Ophthalmic research. 2004 Mar-Apr;36(2):71-7. PubMed PMID: 15017101. Epub 2004/03/16. eng.

245. Gray KJ, Shenaq SM, Engelmann UH, Fishman IJ, Jeraj K, Spira M. Use of human amnion for microvascular interpositional grafts. Plastic and reconstructive surgery. 1987 May;79(5):778-85. PubMed PMID: 3575523. Epub 1987/05/01. eng.

246. Bigi A, Cojazzi G, Panzavolta S, Rubini K, Roveri N. Mechanical and thermal properties of gelatin films at different degrees of glutaraldehyde crosslinking. Biomaterials. 2001 Apr;22(8):763-8. PubMed PMID: 11246944. Epub 2001/03/15. eng.

247. Fujisato T, Tomihata K, Tabata Y, Iwamoto Y, Burczak K, Ikada Y. Cross-linking of amniotic membranes. Journal of biomaterials science Polymer edition. 1999;10(11):1171-81. PubMed PMID: 10606034. Epub 1999/12/22. eng.

248. Guldner NW, Jasmund I, Zimmermann H, Heinlein M, Girndt B, Meier V, et al. Detoxification and endothelialization of glutaraldehyde-fixed bovine pericardium with

titanium coating: a new technology for cardiovascular tissue engineering. Circulation. 2009 Mar 31;119(12):1653-60. PubMed PMID: 19289635. Epub 2009/03/18. eng.

249. Isenburg JC, Simionescu DT, Vyavahare NR. Tannic acid treatment enhances biostability and reduces calcification of glutaraldehyde fixed aortic wall. Biomaterials. 2005 Apr;26(11):1237-45. PubMed PMID: 15475053. Epub 2004/10/12. eng.

250. Spira M, Liu B, Xu Z, Harrell R, Chahadeh H. Human amnion collagen for soft tissue augmentation--biochemical characterizations and animal observations. Journal of biomedical materials research. 1994 Jan;28(1):91-6. PubMed PMID: 8126034. Epub 1994/01/01. eng.

251. Duan X, Sheardown H. Dendrimer crosslinked collagen as a corneal tissue engineering scaffold: mechanical properties and corneal epithelial cell interactions. Biomaterials. 2006 Sep;27(26):4608-17. PubMed PMID: 16713624. Epub 2006/05/23. eng.

252. Liu W, Deng C, McLaughlin CR, Fagerholm P, Lagali NS, Heyne B, et al. Collagen-phosphorylcholine interpenetrating network hydrogels as corneal substitutes. Biomaterials. 2009 Mar;30(8):1551-9. PubMed PMID: 19097643. Epub 2008/12/23. eng.

253. Liu Y, Griffith M, Watsky MA, Forrester JV, Kuffova L, Grant D, et al. Properties of porcine and recombinant human collagen matrices for optically clear tissue engineering applications. Biomacromolecules. 2006 Jun;7(6):1819-28. PubMed PMID: 16768403. Epub 2006/06/14. eng.

254. Ma DH, Lai JY, Cheng HY, Tsai CC, Yeh LK. Carbodiimide cross-linked amniotic membranes for cultivation of limbal epithelial cells. Biomaterials. 2010 Sep;31(25):6647-58. PubMed PMID: 20541801. Epub 2010/06/15. eng.

255. Rafat M, Li F, Fagerholm P, Lagali NS, Watsky MA, Munger R, et al. PEG-stabilized carbodiimide crosslinked collagen-chitosan hydrogels for corneal tissue engineering. Biomaterials. 2008 Oct;29(29):3960-72. PubMed PMID: 18639928. Epub 2008/07/22. eng.

256. Bain JR, Mackinnon SE, Hunter DA. Functional evaluation of complete sciatic, peroneal, and posterior tibial nerve lesions in the rat. Plastic and reconstructive surgery. 1989 Jan;83(1):129-38. PubMed PMID: 2909054. Epub 1989/01/01. eng.

257. Dunn CJ, Goa KL. Fibrin sealant: a review of its use in surgery and endoscopy. Drugs. 1999 Nov;58(5):863-86. PubMed PMID: 10595866. Epub 1999/12/14. eng.

258. Akers RM, Mosher DF, Lilien JE. Promotion of retinal neurite outgrowth by substratum-bound fibronectin. Developmental biology. 1981 Aug;86(1):179-88. PubMed PMID: 7286392. Epub 1981/08/01. eng.

259. Bryan DJ, Miller RA, Costas PD, Wang KK, Seckel BR. Immunocytochemistry of skeletal muscle basal lamina grafts in nerve regeneration. Plastic and reconstructive surgery. 1993 Oct;92(5):927-40. PubMed PMID: 8415975. Epub 1993/10/01. eng.

260. Fawcett JW, Keynes RJ. Muscle basal lamina: a new graft material for peripheral nerve repair. Journal of neurosurgery. 1986 Sep;65(3):354-63. PubMed PMID: 3734886. Epub 1986/09/01. eng.

261. Glasby MA, Gilmour JA, Gschmeissner SE, Hems TE, Myles LM. The repair of large peripheral nerves using skeletal muscle autografts: a comparison with cable grafts in the sheep femoral nerve. British journal of plastic surgery. 1990 Mar;43(2):169-78. PubMed PMID: 2328378. Epub 1990/03/01. eng.

262. Hall SM. Regeneration in cellular and acellular autografts in the peripheral nervous system. Neuropathology and applied neurobiology. 1986 Jan-Feb;12(1):27-46. PubMed PMID: 3703154. Epub 1986/01/01. eng.

263. Ide C. Nerve regeneration and Schwann cell basal lamina: observations of the long-term regeneration. Archivum histologicum Japonicum = Nihon soshikigaku kiroku. 1983 Apr;46(2):243-57. PubMed PMID: 6882155. Epub 1983/04/01. eng.

264. Ide C, Tohyama K, Yokota R, Nitatori T, Onodera S. Schwann cell basal lamina and nerve regeneration. Brain research. 1983 Dec 12;288(1-2):61-75. PubMed PMID: 6661636. Epub 1983/12/12. eng.

265. Keynes RJ, Hopkins WG, Huang LH. Regeneration of mouse peripheral nerves in degenerating skeletal muscle: guidance by residual muscle fibre basement membrane. Brain research. 1984 Mar 19;295(2):275-81. PubMed PMID: 6713188. Epub 1984/03/19. eng.

266. Ray WZ, Mackinnon SE. Management of nerve gaps: autografts, allografts, nerve transfers, and end-to-side neurorrhaphy. Experimental neurology. 2010 May;223(1):77-85. PubMed PMID: 19348799. Pubmed Central PMCID: PMC2849924. Epub 2009/04/08. eng.

267. Siemionow M, Brzezicki G. Chapter 8: Current techniques and concepts in peripheral nerve repair. International review of neurobiology. 2009;87:141-72. PubMed PMID: 19682637. Epub 2009/08/18. eng.

268. Saheb-Al-Zamani M, Yan Y, Farber SJ, Hunter DA, Newton P, Wood MD, et al. Limited regeneration in long acellular nerve allografts is associated with increased Schwann cell senescence. Experimental neurology. 2013 Sep;247:165-77. PubMed PMID: 23644284. Pubmed Central PMCID: PMC3863361. Epub 2013/05/07. eng.

269. Moore AM, MacEwan M, Santosa KB, Chenard KE, Ray WZ, Hunter DA, et al. Acellular nerve allografts in peripheral nerve regeneration: a comparative study. Muscle & nerve. 2011 Aug;44(2):221-34. PubMed PMID: 21660979. Pubmed Central PMCID: PMC3136642. Epub 2011/06/11. eng.

270. Kvist M, Sondell M, Kanje M, Dahlin LB. Regeneration in, and properties of, extracted peripheral nerve allografts and xenografts. Journal of plastic surgery and hand surgery. 2011 Jun;45(3):122-8. PubMed PMID: 21682608. Epub 2011/06/21. eng.

271. Wood MD, Kemp SW, Liu EH, Szynkaruk M, Gordon T, Borschel GH. Rat-derived processed nerve allografts support more axon regeneration in rat than human-derived processed nerve xenografts. Journal of biomedical materials research Part A. 2014 Apr;102(4):1085-91. PubMed PMID: 23630071. Epub 2013/05/01. eng.

272. Miyamoto Y, Sugita T, Higaki T, Ikuta Y, Tsuge K. The duration of denervation and regeneration in nerve grafting. Quantitative histological assessment in the rat. International orthopaedics. 1985;9(4):271-6. PubMed PMID: 4093230. Epub 1985/01/01. eng.

273. Wolthers M, Moldovan M, Binderup T, Schmalbruch H, Krarup C. Comparative electrophysiological, functional, and histological studies of nerve lesions in rats. Microsurgery. 2005;25(6):508-19. PubMed PMID: 16145683. Epub 2005/09/08. eng.

274. Mackinnon SE, Dellon AL, O'Brien JP. Changes in nerve fiber numbers distal to a nerve repair in the rat sciatic nerve model. Muscle & nerve. 1991 Nov;14(11):1116-22. PubMed PMID: 1745287. Epub 1991/11/01. eng.

275. Wood MD, Kemp SW, Weber C, Borschel GH, Gordon T. Outcome measures of peripheral nerve regeneration. Annals of anatomy = Anatomischer Anzeiger : official organ of the Anatomische Gesellschaft. 2011 Jul;193(4):321-33. PubMed PMID: 21640570. Epub 2011/06/07. eng.

276. Gomez N, Cuadras J, Buti M, Navarro X. Histologic assessment of sciatic nerve regeneration following resection and graft or tube repair in the mouse. Restorative neurology and neuroscience. 1996 Jan 1;10(4):187-96. PubMed PMID: 21551519. Epub 1996/01/01. eng.

277. Archibald SJ, Shefner J, Krarup C, Madison RD. Monkey median nerve repaired by nerve graft or collagen nerve guide tube. The Journal of neuroscience : the official journal of the Society for Neuroscience. 1995 May;15(5 Pt 2):4109-23. PubMed PMID: 7751969. Epub 1995/05/01. eng.

278. Rochkind S. Phototherapy in peripheral nerve regeneration: From basic science to clinical study. Neurosurgical focus. 2009 Feb;26(2):E8. PubMed PMID: 19199510. Epub 2009/02/10. eng.

279. Van Breugel HH, Bar PR. He-Ne laser irradiation affects proliferation of cultured rat Schwann cells in a dose-dependent manner. Journal of neurocytology. 1993 Mar;22(3):185-90. PubMed PMID: 8478640. Epub 1993/03/01. eng.

280. Wollman Y, Rochkind S, Simantov R. Low power laser irradiation enhances migration and neurite sprouting of cultured rat embryonal brain cells. Neurological research. 1996 Oct;18(5):467-70. PubMed PMID: 8916064. Epub 1996/10/01. eng.

281. Fernandes JR, Salinas HM, Broelsch GF, McCormack MC, Meppelink AM, Randolph MA, et al. Prevention of capsular contracture with photochemical tissue passivation. Plastic and reconstructive surgery. 2014 Mar;133(3):571-7. PubMed PMID: 24263392. Epub 2013/11/23. eng.

282. Fairbairn NG, Randolph MA, Redmond RW. The clinical applications of human amnion in plastic surgery. Journal of plastic, reconstructive & aesthetic surgery : JPRAS. 2014 May;67(5):662-75. PubMed PMID: 24560801. Epub 2014/02/25. eng.

283. Demirkan F, Snyder CC, Latifoglu O, Siemionow M. A method of enhancing regeneration of conventionally repaired peripheral nerves. Annals of plastic surgery. 1995 Jan;34(1):67-72. PubMed PMID: 7535514. Epub 1995/01/01. eng.

284. Longo FM, Manthorpe M, Skaper SD, Lundborg G, Varon S. Neuronotrophic activities accumulate in vivo within silicone nerve regeneration chambers. Brain research. 1983 Feb 14;261(1):109-16. PubMed PMID: 6839146. Epub 1983/02/14. eng.

285. Lundborg G, Longo FM, Varon S. Nerve regeneration model and trophic factors in vivo. Brain research. 1982 Jan 28;232(1):157-61. PubMed PMID: 7055692. Epub 1982/01/28. eng.

286. Lundborg G, Dahlin LB, Danielsen N, Gelberman RH, Longo FM, Powell HC, et al. Nerve regeneration in silicone chambers: influence of gap length and of distal stump components. Experimental neurology. 1982 May;76(2):361-75. PubMed PMID: 7095058. Epub 1982/05/01. eng.

287. Lundborg G, Dahlin LB, Danielsen N, Hansson HA, Johannesson A, Longo FM, et al. Nerve regeneration across an extended gap: a neurobiological view of nerve repair and the possible involvement of neuronotrophic factors. The Journal of hand surgery. 1982 Nov;7(6):580-7. PubMed PMID: 7175129. Epub 1982/11/01. eng.

288. Mackinnon SE, Dellon AL, Hudson AR, Hunter DA. Nerve regeneration through a pseudosynovial sheath in a primate model. Plastic and reconstructive surgery. 1985 Jun;75(6):833-41. PubMed PMID: 4001203. Epub 1985/06/01. eng.

289. Madison R, da Silva CF, Dikkes P, Chiu TH, Sidman RL. Increased rate of peripheral nerve regeneration using bioresorbable nerve guides and a laminin-containing gel. Experimental neurology. 1985 Jun;88(3):767-72. PubMed PMID: 3996520. Epub 1985/06/01. eng.

290. Madison RD, Da Silva CF, Dikkes P. Entubulation repair with protein additives increases the maximum nerve gap distance successfully bridged with tubular prostheses. Brain research. 1988 May 3;447(2):325-34. PubMed PMID: 3390701. Epub 1988/05/03. eng.

291. Mackinnon SE, Hudson AR, Hunter DA. Histologic assessment of nerve regeneration in the rat. Plastic and reconstructive surgery. 1985 Mar;75(3):384-8. PubMed PMID: 2579408. Epub 1985/03/01. eng.

292. Whitlock EL, Tuffaha SH, Luciano JP, Yan Y, Hunter DA, Magill CK, et al. Processed allografts and type I collagen conduits for repair of peripheral nerve gaps. Muscle & nerve. 2009 Jun;39(6):787-99. PubMed PMID: 19291791. Epub 2009/03/18. eng.

293. Seo BF, Lee JY, Jung SN. Models of abnormal scarring. BioMed research international. 2013;2013:423147. PubMed PMID: 24078916. Pubmed Central PMCID: PMC3775400. Epub 2013/10/01. eng.

294. Fox IK, Brenner MJ, Johnson PJ, Hunter DA, Mackinnon SE. Axonal regeneration and motor neuron survival after microsurgical nerve reconstruction. Microsurgery. 2012 Oct;32(7):552-62. PubMed PMID: 22806696. Pubmed Central PMCID: PMC4142191. Epub 2012/07/19. eng.

295. Gordon T, Sulaiman OA, Ladak A. Chapter 24: Electrical stimulation for improving nerve regeneration: where do we stand? International review of neurobiology. 2009;87:433-44. PubMed PMID: 19682653. Epub 2009/08/18. eng.

296. Boyd JG, Gordon T. Glial cell line-derived neurotrophic factor and brain-derived neurotrophic factor sustain the axonal regeneration of chronically axotomized motoneurons in vivo. Experimental neurology. 2003 Oct;183(2):610-9. PubMed PMID: 14552902. Epub 2003/10/14. eng.

297. Guntinas-Lichius O, Irintchev A, Streppel M, Lenzen M, Grosheva M, Wewetzer K, et al. Factors limiting motor recovery after facial nerve transection in the rat: combined structural and functional analyses. The European journal of neuroscience. 2005 Jan;21(2):391-402. PubMed PMID: 15673438. Epub 2005/01/28. eng.

298. Redett R, Jari R, Crawford T, Chen YG, Rohde C, Brushart TM. Peripheral pathways regulate motoneuron collateral dynamics. The Journal of neuroscience : the official journal of the Society for Neuroscience. 2005 Oct 12;25(41):9406-12. PubMed PMID: 16221849. Epub 2005/10/14. eng.

299. Streppel M, Azzolin N, Dohm S, Guntinas-Lichius O, Haas C, Grothe C, et al. Focal application of neutralizing antibodies to soluble neurotrophic factors reduces collateral axonal branching after peripheral nerve lesion. The European journal of neuroscience. 2002 Apr;15(8):1327-42. PubMed PMID: 11994127. Epub 2002/05/08. eng.

300. Shenaq JM, Shenaq SM, Spira M. Reliability of sciatic function index in assessing nerve regeneration across a 1 cm gap. Microsurgery. 1989;10(3):214-9. PubMed PMID: 2796717. Epub 1989/01/01. eng.

301. Urbanchek MS, Chung KC, Asato H, Washington LN, Kuzon WM, Jr. Rat walking tracks do not reflect maximal muscle force capacity. Journal of reconstructive microsurgery. 1999 Feb;15(2):143-9. PubMed PMID: 10088927. Epub 1999/03/24. eng.

302. Gramsbergen A, J IJ-P, Meek MF. Sciatic nerve transection in the adult rat: abnormal EMG patterns during locomotion by aberrant innervation of hindleg muscles. Experimental neurology. 2000 Jan;161(1):183-93. PubMed PMID: 10683284. Epub 2000/02/23. eng.

303. Meek MF, Den Dunnen WF, Schakenraad JM, Robinson PH. Long-term evaluation of functional nerve recovery after reconstruction with a thin-walled biodegradable poly (DL-lactide-epsilon-caprolactone) nerve guide, using walking track analysis and electrostimulation tests. Microsurgery. 1999;19(5):247-53. PubMed PMID: 10413791. Epub 1999/07/22. eng.

304. Walker JL, Evans JM, Meade P, Resig P, Sisken BF. Gait-stance duration as a measure of injury and recovery in the rat sciatic nerve model. Journal of neuroscience methods. 1994 Apr;52(1):47-52. PubMed PMID: 8090016. Epub 1994/04/01. eng.

305. Dellon AL, Mackinnon SE. Sciatic nerve regeneration in the rat. Validity of walking track assessment in the presence of chronic contractures. Microsurgery. 1989;10(3):220-5. PubMed PMID: 2796718. Epub 1989/01/01. eng.

306. Madison RD, da Silva C, Dikkes P, Sidman RL, Chiu TH. Peripheral nerve regeneration with entubulation repair: comparison of biodegradeable nerve guides versus polyethylene tubes and the effects of a laminin-containing gel. Experimental neurology. 1987 Feb;95(2):378-90. PubMed PMID: 3803518. Epub 1987/02/01. eng.

307. Verter EE, Gisel TE, Yang P, Johnson AJ, Redmond RW, Kochevar IE. Light-initiated bonding of amniotic membrane to cornea. Investigative ophthalmology & visual science. 2011;52(13):9470-7. PubMed PMID: 22058339. Epub 2011/11/08. eng.

308. Zeev MS, Miller DD, Latkany R. Diagnosis of dry eye disease and emerging technologies. Clinical ophthalmology (Auckland, NZ). 2014;8:581-90. PubMed PMID: 24672224. Pubmed Central PMCID: PMC3964175. Epub 2014/03/29. eng.

309. Kim J, Foulks GN. Evaluation of the effect of lissamine green and rose bengal on human corneal epithelial cells. Cornea. 1999 May;18(3):328-32. PubMed PMID: 10336037. Epub 1999/05/21. eng.

310. Braeuninger S, Kleinschnitz C. Rodent models of focal cerebral ischemia: procedural pitfalls and translational problems. Experimental & translational stroke medicine. 2009;1:8. PubMed PMID: 20150986. Pubmed Central PMCID: PMC2820446. Epub 2010/02/13. eng.

311. Watson BD, Dietrich WD, Busto R, Wachtel MS, Ginsberg MD. Induction of reproducible brain infarction by photochemically initiated thrombosis. Annals of neurology. 1985 May;17(5):497-504. PubMed PMID: 4004172. Epub 1985/05/01. eng.

312. Schroeter M, Jander S, Stoll G. Non-invasive induction of focal cerebral ischemia in mice by photothrombosis of cortical microvessels: characterization of inflammatory responses. Journal of neuroscience methods. 2002 May 30;117(1):43-9. PubMed PMID: 12084563. Epub 2002/06/27. eng.

313. Wachter E, Dees C, Harkins J, Scott T, Petersen M, Rush RE, et al. Topical rose bengal: pre-clinical evaluation of pharmacokinetics and safety. Lasers in surgery and medicine. 2003;32(2):101-10. PubMed PMID: 12561042. Epub 2003/02/01. eng.

314. Yao M, Yaroslavsky A, Henry FP, Redmond RW, Kochevar IE. Phototoxicity is not associated with photochemical tissue bonding of skin. Lasers in surgery and medicine. 2010 Feb;42(2):123-31. PubMed PMID: 20166159. Epub 2010/02/19. eng.

315. Barton M, Piller SC, Mahns DA, Morley JW, Mawad D, Longo L, et al. In vitro cell compatibility study of rose bengal-chitosan adhesives. Lasers in surgery and medicine. 2012 Nov;44(9):762-8. PubMed PMID: 23001619. Epub 2012/09/25. eng.

316. Terenghi G, Hart A, Wiberg M. The nerve injury and the dying neurons: diagnosis and prevention. The Journal of hand surgery, European volume. 2011 Nov;36(9):730-4. PubMed PMID: 22058229. Epub 2011/11/08. eng.

317. Lundborg G. Intraneural microcirculation. The Orthopedic clinics of North America. 1988 Jan;19(1):1-12. PubMed PMID: 3275919. Epub 1988/01/01. eng.

318. Almgren KG. Revascularization of free pheripheral nerve grafts. An experimental study in the rabbit. Acta orthopaedica Scandinavica Supplementum. 1975;154:1-104. PubMed PMID: 46686. Epub 1975/01/01. eng.

319. Lind R, Wood MB. Comparison of the pattern of early revascularization of conventional versus vascularized nerve grafts in the canine. Journal of reconstructive microsurgery. 1986 Jul;2(4):229-34. PubMed PMID: 3761243. Epub 1986/07/01. eng.

320. Penkert G, Bini W, Samii M. Revascularization of nerve grafts: an experimental study. Journal of reconstructive microsurgery. 1988 Jul;4(4):319-25. PubMed PMID: 2459380. Epub 1988/07/01. eng.

321. Settergren CR, Wood MB. Comparison of blood flow in free vascularized versus nonvascularized nerve grafts. Journal of reconstructive microsurgery. 1984 Oct;1(2):95-101. PubMed PMID: 6544354. Epub 1984/10/01. eng.

322. Weiss P, Taylor AC. The viability of isolated nerve fragments and its modification by methylene blue. Journal of cellular physiology. 1946 Apr;27:87-103. PubMed PMID: 20982963. Epub 1946/04/01. eng.

323. Best TJ, Mackinnon SE, Midha R, Hunter DA, Evans PJ. Revascularization of peripheral nerve autografts and allografts. Plastic and reconstructive surgery. 1999 Jul;104(1):152-60. PubMed PMID: 10597688. Epub 1999/12/22. eng.

324. Sanders FK, Young JZ. The degeneration and re-innervation of grafted nerves. Journal of anatomy. 1942 Jan;76(Pt 2):143-66 7. PubMed PMID: 17104885. Pubmed Central PMCID: PMC1252699. Epub 1942/01/01. eng.

325. Chalfoun C, Scholz T, Cole MD, Steward E, Vanderkam V, Evans GR. Primary nerve grafting: A study of revascularization. Microsurgery. 2003;23(1):60-5. PubMed PMID: 12616521. Epub 2003/03/05. eng.

326. Walther J, Gaertner M, Cimalla P, Burkhardt A, Kirsten L, Meissner S, et al. Optical coherence tomography in biomedical research. Analytical and bioanalytical chemistry. 2011 Jul;400(9):2721-43. PubMed PMID: 21562739. Epub 2011/05/13. eng.

327. Fujimoto JG. Optical coherence tomography for ultrahigh resolution in vivo imaging. Nature biotechnology. 2003 Nov;21(11):1361-7. PubMed PMID: 14595364. Epub 2003/11/05. eng.

328. Yun S, Tearney G, de Boer J, Iftimia N, Bouma B. High-speed optical frequency-domain imaging. Optics express. 2003 Nov 3;11(22):2953-63. PubMed PMID: 19471415. Pubmed Central PMCID: PMC2758565. Epub 2003/11/03. eng.

329. Vakoc BJ, Lanning RM, Tyrrell JA, Padera TP, Bartlett LA, Stylianopoulos T, et al. Three-dimensional microscopy of the tumor microenvironment in vivo using optical frequency domain imaging. Nature medicine. 2009 Oct;15(10):1219-23. PubMed PMID: 19749772. Pubmed Central PMCID: PMC2759417. Epub 2009/09/15. eng.

330. van den Berg ME, Castellote JM, Mahillo-Fernandez I, de Pedro-Cuesta J. Incidence of spinal cord injury worldwide: a systematic review. Neuroepidemiology. 2010;34(3):184-92; discussion 92. PubMed PMID: 20130419. Epub 2010/02/05. eng.

331. Schoenfeld AJ, McCriskin B, Hsiao M, Burks R. Incidence and epidemiology of spinal cord injury within a closed American population: the United States military (2000-2009). Spinal cord. 2011 Aug;49(8):874-9. PubMed PMID: 21383763. Epub 2011/03/09. eng.

332. Schoenfeld AJ, Laughlin MD, McCriskin BJ, Bader JO, Waterman BR, Belmont PJ, Jr. Spinal injuries in United States military personnel deployed to Iraq and Afghanistan: an epidemiological investigation involving 7877 combat casualties from 2005 to 2009. Spine. 2013 Sep 15;38(20):1770-8. PubMed PMID: 23759821. Epub 2013/06/14. eng.

333. Blair JA, Patzkowski JC, Schoenfeld AJ, Cross Rivera JD, Grenier ES, Lehman RA, Jr., et al. Spinal column injuries among Americans in the global war on terrorism. The

Journal of bone and joint surgery American volume. 2012 Sep 19;94(18):e135(1-9). PubMed PMID: 22992883. Epub 2012/09/21. eng.

334. Schoenfeld AJ, Sielski B, Rivera KP, Bader JO, Harris MB. Epidemiology of cervical spine fractures in the US military. The spine journal : official journal of the North American Spine Society. 2012 Sep;12(9):777-83. PubMed PMID: 21393068. Epub 2011/03/12. eng.

335. Werginz P, Rattay F. Past, present, future: a review on visual prostheses. Minerva medica. 2015 Feb;106(1):65-77. PubMed PMID: 25300894. Epub 2014/10/11. eng.

336. Wilson BS, Dorman MF. Cochlear implants: a remarkable past and a brilliant future. Hearing research. 2008 Aug;242(1-2):3-21. PubMed PMID: 18616994. Pubmed Central PMCID: PMC3707130. Epub 2008/07/12. eng.

337. Serruya MD, Hatsopoulos NG, Paninski L, Fellows MR, Donoghue JP. Instant neural control of a movement signal. Nature. 2002 Mar 14;416(6877):141-2. PubMed PMID: 11894084. Epub 2002/03/15. eng.

338. Taylor DM, Tillery SI, Schwartz AB. Direct cortical control of 3D neuroprosthetic devices. Science. 2002 Jun 7;296(5574):1829-32. PubMed PMID: 12052948. Epub 2002/06/08. eng.

339. Velliste M, Perel S, Spalding MC, Whitford AS, Schwartz AB. Cortical control of a prosthetic arm for self-feeding. Nature. 2008 Jun 19;453(7198):1098-101. PubMed PMID: 18509337. Epub 2008/05/30. eng.

340. Hochberg LR, Bacher D, Jarosiewicz B, Masse NY, Simeral JD, Vogel J, et al. Reach and grasp by people with tetraplegia using a neurally controlled robotic arm. Nature. 2012 May 17;485(7398):372-5. PubMed PMID: 22596161. Pubmed Central PMCID: PMC3640850. Epub 2012/05/19. eng.

341. Hochberg LR, Serruya MD, Friehs GM, Mukand JA, Saleh M, Caplan AH, et al. Neuronal ensemble control of prosthetic devices by a human with tetraplegia. Nature. 2006 Jul 13;442(7099):164-71. PubMed PMID: 16838014. Epub 2006/07/14. eng.

342. Kubler A, Nijboer F, Mellinger J, Vaughan TM, Pawelzik H, Schalk G, et al. Patients with ALS can use sensorimotor rhythms to operate a brain-computer interface. Neurology. 2005 May 24;64(10):1775-7. PubMed PMID: 15911809. Epub 2005/05/25. eng.

343. McFarland DJ, Krusienski DJ, Sarnacki WA, Wolpaw JR. Emulation of computer mouse control with a noninvasive brain-computer interface. Journal of neural engineering. 2008 Jun;5(2):101-10. PubMed PMID: 18367779. Pubmed Central PMCID: PMC2757111. Epub 2008/03/28. eng.

344. Wolpaw JR, Birbaumer N, McFarland DJ, Pfurtscheller G, Vaughan TM. Brain-computer interfaces for communication and control. Clinical neurophysiology : official journal of the International Federation of Clinical Neurophysiology. 2002 Jun;113(6):767-91. PubMed PMID: 12048038. Epub 2002/06/06. eng.

345. Donoghue JP. Bridging the brain to the world: a perspective on neural interface systems. Neuron. 2008 Nov 6;60(3):511-21. PubMed PMID: 18995827. Epub 2008/11/11. eng.

346. Bullock TH. Signals and signs in the nervous system: the dynamic anatomy of electrical activity is probably information-rich. Proceedings of the National Academy of Sciences of the United States of America. 1997 Jan 7;94(1):1-6. PubMed PMID: 8990149. Pubmed Central PMCID: PMC33648. Epub 1997/01/07. eng.

347. Birbaumer N, Weber C, Neuper C, Buch E, Haapen K, Cohen L. Physiological regulation of thinking: brain-computer interface (BCI) research. Progress in brain research. 2006;159:369-91. PubMed PMID: 17071243. Epub 2006/10/31. eng.

348. Cohen O, Koppel M, Malach R, Friedman D. Controlling an avatar by thought using real-time fMRI. Journal of neural engineering. 2014 Jun;11(3):035006. PubMed PMID: 24834973. Epub 2014/05/20. eng.

349. Ajemian R, Green A, Bullock D, Sergio L, Kalaska J, Grossberg S. Assessing the function of motor cortex: single-neuron models of how neural response is modulated by limb biomechanics. Neuron. 2008 May 8;58(3):414-28. PubMed PMID: 18466751. Epub 2008/05/10. eng.

350. Ragnarsson KT. Functional electrical stimulation after spinal cord injury: current use, therapeutic effects and future directions. Spinal cord. 2008 Apr;46(4):255-74. PubMed PMID: 17846639. Epub 2007/09/12. eng.

351. Peckham PH, Knutson JS. Functional electrical stimulation for neuromuscular applications. Annual review of biomedical engineering. 2005;7:327-60. PubMed PMID: 16004574. Epub 2005/07/12. eng.

352. Kilgore KL, Hoyen HA, Bryden AM, Hart RL, Keith MW, Peckham PH. An implanted upper-extremity neuroprosthesis using myoelectric control. The Journal of hand surgery. 2008 Apr;33(4):539-50. PubMed PMID: 18406958. Pubmed Central PMCID: PMC2743484. Epub 2008/04/15. eng.

353. Memberg WD, Polasek KH, Hart RL, Bryden AM, Kilgore KL, Nemunaitis GA, et al. Implanted neuroprosthesis for restoring arm and hand function in people with high level tetraplegia. Archives of physical medicine and rehabilitation. 2014 Jun;95(6):1201-11 e1. PubMed PMID: 24561055. Epub 2014/02/25. eng.

354. Peckham PH, Kilgore KL, Keith MW, Bryden AM, Bhadra N, Montague FW. An advanced neuroprosthesis for restoration of hand and upper arm control using an implantable controller. The Journal of hand surgery. 2002 Mar;27(2):265-76. PubMed PMID: 11901386. Epub 2002/03/20. eng.

355. Fang ZP, Mortimer JT. A method to effect physiological recruitment order in electrically activated muscle. IEEE transactions on bio-medical engineering. 1991 Feb;38(2):175-9. PubMed PMID: 2066127. Epub 1991/02/01. eng.

356. Navarro X, Krueger TB, Lago N, Micera S, Stieglitz T, Dario P. A critical review of interfaces with the peripheral nervous system for the control of neuroprostheses and hybrid bionic systems. Journal of the peripheral nervous system : JPNS. 2005 Sep;10(3):229-58. PubMed PMID: 16221284. Epub 2005/10/14. eng.

357. Larsen JO, Thomsen M, Haugland M, Sinkjaer T. Degeneration and regeneration in rabbit peripheral nerve with long-term nerve cuff electrode implant: a stereological study of

myelinated and unmyelinated axons. Acta neuropathologica. 1998 Oct;96(4):365-78. PubMed PMID: 9797001. Epub 1998/10/31. eng.

358. Rodriguez FJ, Ceballos D, Schuttler M, Valero A, Valderrama E, Stieglitz T, et al. Polyimide cuff electrodes for peripheral nerve stimulation. Journal of neuroscience methods. 2000 Jun 1;98(2):105-18. PubMed PMID: 10880824. Epub 2000/07/06. eng.

359. Stieglitz T. Considerations on surface and structural biocompatibility as prerequisite for long-term stability of neural prostheses. Journal of nanoscience and nanotechnology. 2004 May;4(5):496-503. PubMed PMID: 15503435. Epub 2004/10/27. eng.

360. Ohsawa I, Inui K. Use of tripolar electrodes for minimization of current spread in uncut peripheral nerve stimulation. Neuroscience research. 2009 May;64(1):63-6. PubMed PMID: 19321132. Epub 2009/03/27. eng.

Section 8: Appendix